1. REPORT NO. NASA CR 168081	2. GOVERNMENT AGENCY	3. RECIPIENT'S CATALOG NO.
4. TITLE AND SUBTITLE AN ASSESSMENT OF THE USE OF ANTIMISTING FUEL IN TURBOFAN ENGINES		5. REPORT DATE October 1983 6. PERFORMING ORG. CODE
7. AUTHOR(S) A.J. Fiorentino and J.R. Planell		8. PERFORMING ORG. REPT. NO. PWA-5697-65
9. PERFORMING ORG. NAME AND ADDRESS UNITED TECHNOLOGIES CORPORATION Pratt & Whitney Aircraft Group Pratt & Whitney Engineering		10. WORK UNIT NO. 11. CONTRACT OR GRANT NO. NAS3-22045
12. SPONSORING AGENCY NAME AND ADDRESS National Aeronautics and Space Administration Washington D.C. 20546 and Federal Aviation Administration Technical Center, Atlantic City Airport, N.J. 08405		13. TYPE REPT./PERIOD COVERED Contractor Report 9/79 - 3/82 14. SPONSORING AGENCY CODE

15. SUPPLEMENTARY NOTES

Project Manager, Harold Schmidt, NASA Lewis Research Center, Cleveland, Ohio 44135 and Gary Frings, ACT-320, Atlantic City Airport, N.J. 08405

16. ABSTRACT

An evaluation was made on the effects of using antimisting kerosene (AMK) on the performance of the components from the fuel system and the combustor of current in-service JT8D aircraft engines. The objectives were to identify if there were any problems associated with using antimisting kerosene and to determine the extent of shearing or degradation required to allow the engine components to achieve satisfactory operation. The program consisted of a literature survey and a test program which evaluated the antimisting kerosene fuel in laboratory and bench component testing, and assessed the performance of the combustor in a high pressure facility and in an altitude relight/cold ignition facility.

17. KEY WORDS (SUGGESTED BY AUTHOR(S))	18. DISTRIBUTION STATEMENT
Antimisting kerosene Safety fuels	Document is available to the U.S. public through the National Technical Information Service, Springfield, Virginia 22161

19. SECURITY CLASS (THIS REPT)	20. SECURITY CLASS (THIS PAGE)	21. NO. PGS	22. PRICE *
Unclassified	Unclassified		

* For sale by the National Technical Information Service, Springfield, VA 22161

NASA CR-168081
PWA 5897-65

AN ASSESSMENT OF THE USE OF ANTIMISTING FUEL IN TURBOFAN ENGINES

by

A.J. FIORENTINO
J.R. PLANELL

UNITED TECHNOLOGIES CORPORATION
Pratt & Whitney Whitney Aircraft Group
Commercial Engineering

October 1983

Prepared for
National Aeronautics and Space Administration
NASA Lewis Research Center
Cleveland, Ohio 44135
and
U.S. Department of Transportation
Federal Aviation Administration
Technical Center
Atlantic City, Airport, N.J. 08405

Contract NAS3-22045

FOREWORD

This document report describes the work conducted by the Pratt & Whitney Aircraft Group and the United Technologies Research Center (UTRC) of United Technologies Corporation to evaluate the effect of using antimisting fuel on components of an aircraft engine. The work was supported in part by the Federal Aviation Administration Technical Center, Atlantic City Airport, New Jersey. This final report was prepared for the National Aeronautics and Space Administration Lewis Research Center in compliance with the requirements of Contract NAS3-32045.

The authors of this report wish to acknowledge the guidance and assistance of Harold Schmidt, NASA Manager of the Antimisting Kerosene program, and FAA personnel at the Technical Center in Atlantic City Airport, New Jersey, for their on-going efforts to keep all interested parties informed. The authors would also like to thank J. Marks of Pratt & Whitney Aircraft and and E. Szetela of United Technologies Research Center for their contributions to this program.

TABLE OF CONTENTS

TABLE OF CONTENTS (Cont'd)

TABLE OF CONTENTS (Cont'd)

LIST OF ILLUSTRATIONS

LIST OF ILLUSTRATIONS (Cont'd)

LIST OF ILLUSTRATIONS (Cont'd)

LIST OF ILLUSTRATIONS (Cont'd)

LIST OF ILLUSTRATIONS (Cont'd)

LIST OF TABLES

LIST OF TABLES (Cont'd)

SUMMARY

This report presents the results of a two year technical effort to evaluate the effects of using FM 9 antimisting additive on the performance of the components from the fuel system and the combustor of a current in-service JT8D aircraft engine which was selected as the reference engine for this program. The major objectives of this program were to evaluate the effects of using this additive on the performance of engine fuel system components. determine the extent of fuel processing required to achieve satisfactory operation of the engine components, and identify promising concepts for accomplishing this fuel degradation.

This report briefly describes the physical and chemical characteristics of Jet A and antimisting fuels including: 1) effect of degradation on fuel system flow characteristics, 2) effect of water contamination of AMK, 3) effect of the additive on thermal stability, corrosion, heat transfer and materials compatibility. It also describes various fuel processing techniques and requirements on the performance of the combustor of the JT8D engine. Finally a discussion of the feasibility of using anitmisting fuels in existing in-service engines is presented.

The test program was organized into three phases. In the first phase, antimisting kerosene fuel was evaluated in laboratory and short duration "bench" type component tests. These included the analysis of the physical and chemical properties of the fuel antimist additive mixture, the evaluation of fuel injector atomization characteristics, and the performance of fuel filters. In the second phase, more comprehensive component and system tests were conducted to assess the performance of the combustor in both a high pressure combustion facility and an altitude relight/ cold ignition facility. The third phase was devoted to ambient and low temperature filterability tests, de-icing tests, a fuel degrader design study and fuel injector performance tests.

Summary of Results

Significant technical results were obtained from this program which are pertinent to safe engine implementation:

- The very high molecular weight of the additive which produces the antimisting results in a tendency to clog filters in fuel systems. This tendency increases as the fuel temperature is reduced.

- The combination of transition velocity (a filter characterization test) measurements, and Gel Permeation Chromatography, quantified the degradation levels of antimisting kerosene.

- The level of AMK degradation to satisfy ambient and low temperature short duration filterability requirements was identified.

- Water/antimisting kerosene compatibility tests at concentration levels of water found typically in aircraft fuel tanks (~200 ppm) resulted in the formation of white precipitates at ambient temperatures. Excessive water contamination resulted in precipitation of the additive forming a gum like residue.

- Degraded mixtures of antimisting kerosene with small concentrations of water (~200 ppm) failed the de-icing experiment.

- Poor fuel atomization and filterability preclude the use of AMK in commercial aircraft engines or fuel systems until an acceptable means of restoring the necessary fuel properties is developed.

- A promising and unique technique of degradation, using the principle of cavitation, was identified which may reduce the horsepower requirements relative to those of the multipass JT8D fuel pump. Further experimental testing and development are necessary to achieve a viable flight worthy design.

- Combustor/fuel injectors have the potential of operating satisfactorily on antimisting kerosene if sufficient degradation or shearing (degradation) of the high molecular weight additive has been achieved.

1.0 INTRODUCTION

Approximately 30% of the fatalities in impact-survivable aircraft crashes are fire related. In a typical aircraft crash, fuel spilled from ruptured fuel tanks typically forms a fine mist which can be ignited by a number of sources present at the crash site. Supression of the tendency of the turbine fuel to form this fine mist by addition to or modification of the fuels can reduce the fire hazard and save lives.

Tests conducted by the U.S. Federal Aviation Administration (FAA) have demonstrated the post-crash fire resistance of antimisting kerosene (AMK), a Jet A fuel containing high molecular weight, long chain polymers. The antimisting additive, FM-9, when blended in Jet A fuel in concentrations of about .3% by weight, alters the flow characteristics of the fuel causing non-newtonion behavior, thus suppressing atomization and mist formation. At the same time the additive produces undesirable flow characteristics, such as poor fuel atomization and filterability in an aircraft fuel system. The antimisting additive, FM-9, selected for testing in this program was developed by the Imperial Chemical Industries (ICI) and the Royal Aircraft Establishment of the United Kingdom.

2.0 TECHNICAL PROGRAM OVERVIEW

The objectives of this program were to assess the effect of using FM-9 antimisting additive on the performance of the components of a JT8D engine and establish the feasibility of designing a modified or new engine component that would be capable of degrading the fuel additive. To accomplish these objectives, the activities depicted in the flow chart of Figure 1 were accomplished in the program.

The JT8D was selected as the reference engine for this program. A detailed description of the engine and its fuel system and combustor that were influenced by the use of antimisting fuel is provided in the following section.

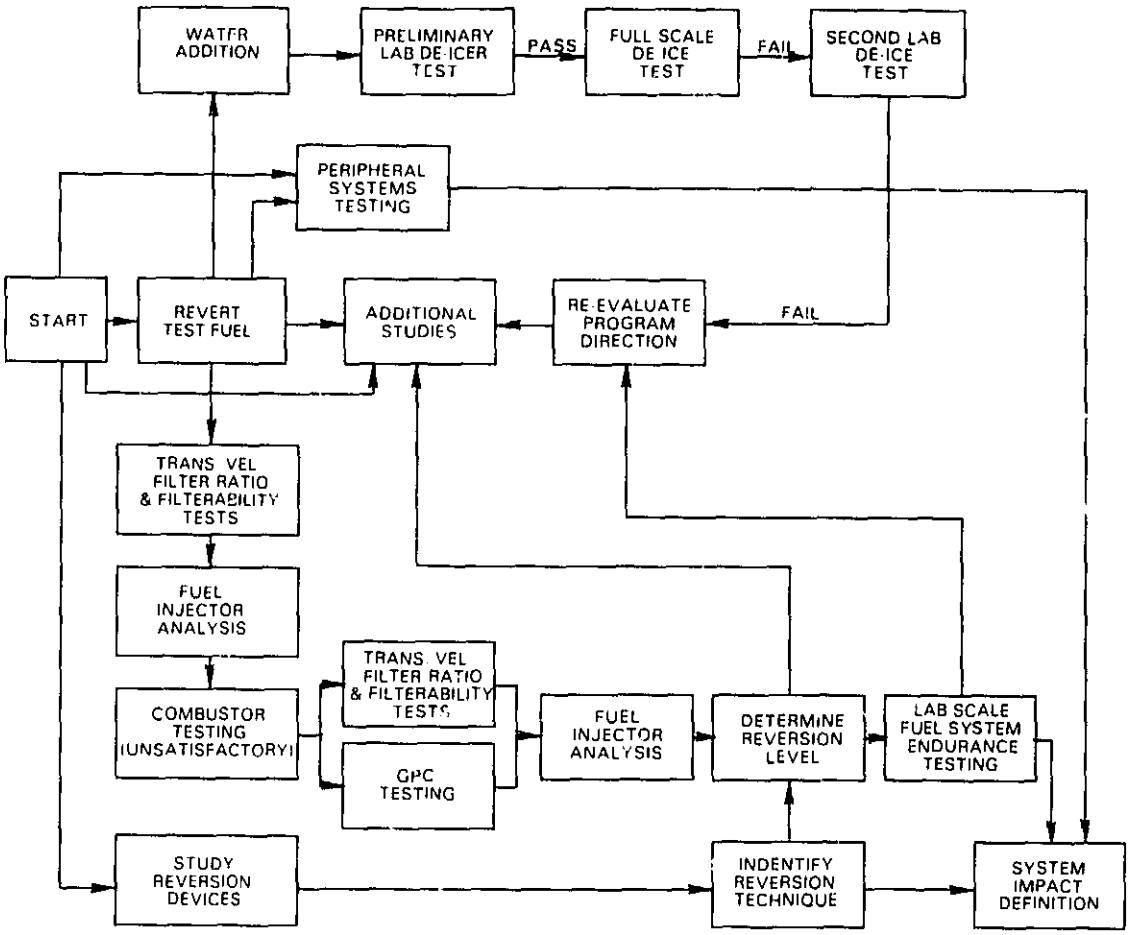

Figure 1 Antimisting Kerosene Program Flow Chart

3.0 JT8D-17 ENGINE DESCRIPTION

The JT8D-17 engine model, selected as the baseline for this program, is the current production version of the JT8D engine which is in widespread use throughout the commercial transport fleet. It also represents current production gas turbines in that its clearances, filter sizes, pumps and fuel flow paths are typical. A cross section of the JT8D-17 is shown in Figure 2 and key specifications for this engine are listed in Table I.

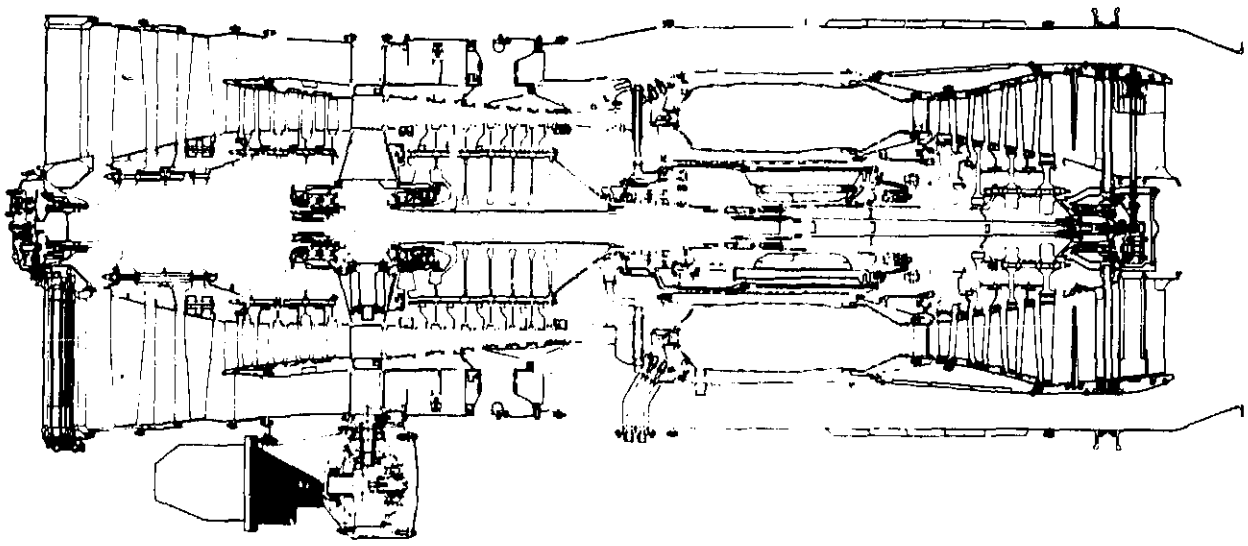

Figure 2 Cross-Section of JT8D Turbofan Engine

TABLE I
KEY SPECIFICATIONS OF THE JT8D-17 ENGINE

Weight (kg)	1510.5
Length (m)	3.045
Maximum Diameter, cold (m)	1.080
Pressure Ratio	16.9
Airflow Rate (kg/s)	148.3
Maximum Sea Level Static Thrust (kN)	71.2
Cruise Performance	
Mach Number	0.8
Altitude (m)	9140
Thrust (kN)	18.9
Specific Fuel Consumption (kg/Ns)	2.273×10^{-5}

3.1 Engine Fuel System

The function of the fuel system is to supply clean liquid fuel, free from vapor, at the required pressure and flow rate to the engine at all operating conditions. Figure 3 shows a schematic of the basic JT8D engine fuel system.

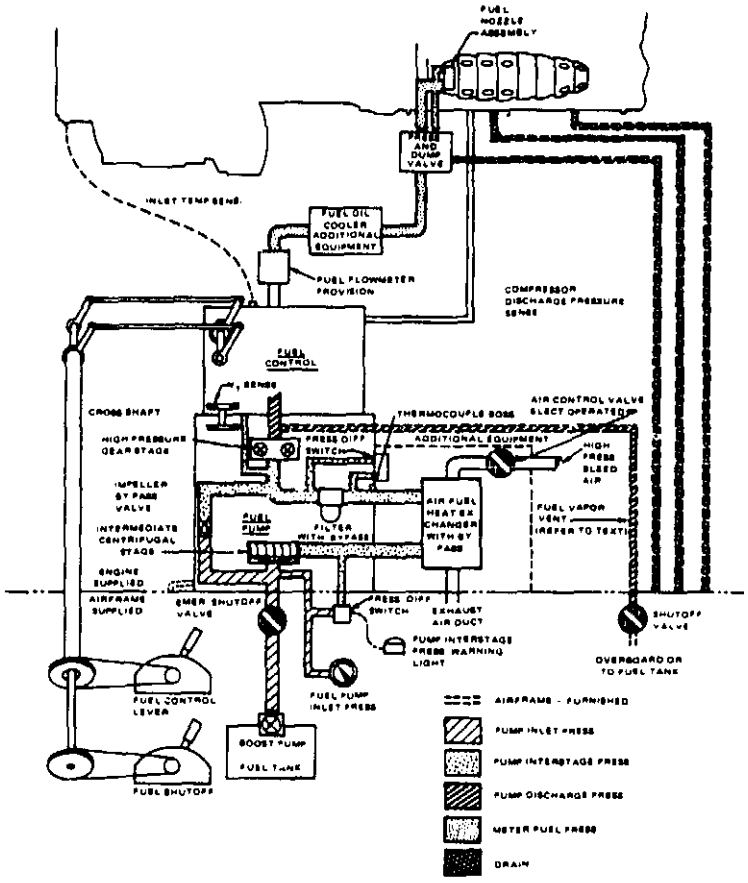

Figure 3 JT8D Turbofan Engine Fuel System Diagram

Fuel is supplied from the aircraft tanks to the engine driven fuel pump inlet. The fuel is pressurized to an intermediate pressure level by the fuel pump centrifugal stage and is passed through the air-fuel, de-icing heat exchanger to the main fuel inlet filter. The filtered fuel is supplied to the high pressure gear stage and after pressurization is passed to the fuel control through a coarse mesh inlet filter. Excess fuel passes through the throttle differential pressure regulating valve and is returned to the fuel pump upstream of the high pressure gear stage. The metered fuel passes through the

throttle valve which is controlled by the fuel control that senses, computes and positions the valve as a function of power lever position, engine speed, engine compressor discharge pressure, and engine low compressor inlet temperature. The metered fuel passes out of the fuel control via the control minimum pressure and shut off valve, through the airframe supplied fuel flow meter and the fuel oil cooler to the pressurizing and dump valve. The pressurizing valve schedules flow to the fuel nozzle secondary manifold as a function of primary fuel nozzle pressure drop. The two position dump valve is hydraulically actuated by primary fuel pressure during engine operation. The dump valve has a checking feature that actuates at engine shutdown when the primary fuel pressure is reduced. The check valve closes and prevents draining of upstream fuel lines into the engine.

3.1.1 Fuel Pump

The main fuel pump consists of a single element gear stage with a high speed centrifugal boost stage (see Figure 4). A cartridge type relief valve limits the pressure rise across the gear stage. The unit provides a rigid mounting pad arrangement and a rotational splined drive for the fuel control. An integral fuel filter containing a replaceable paper barrier filter element is located between the discharge of the centrifugal stage and the inlet of the gear stage. In the event of a malfunction of the boost stage, a bypass valve opens into the inlet passage of the pump to direct flow in the gear stage. This is normally held closed by a light spring force and remains closed due to boost stage pressure. Outlet and return ports are provided between the boost stage discharge and the filter inlet for installation of an external fuel deicing heater. A drive shaft seal drain is located in the lower extremity of the mounting flange.

3.1.2 Fuel Control

The fuel control consists of a metering and a biasing system. The metering system selects the rate of fuel flow upon demand but is subject to the engine operating limitations imposed by the biasing system which monitors the engine parameters i.e., power lever angle, burner pressure, engine high compressor speed and engine inlet temperature to control the output of the metering section of the control during all regimes of engine operation.

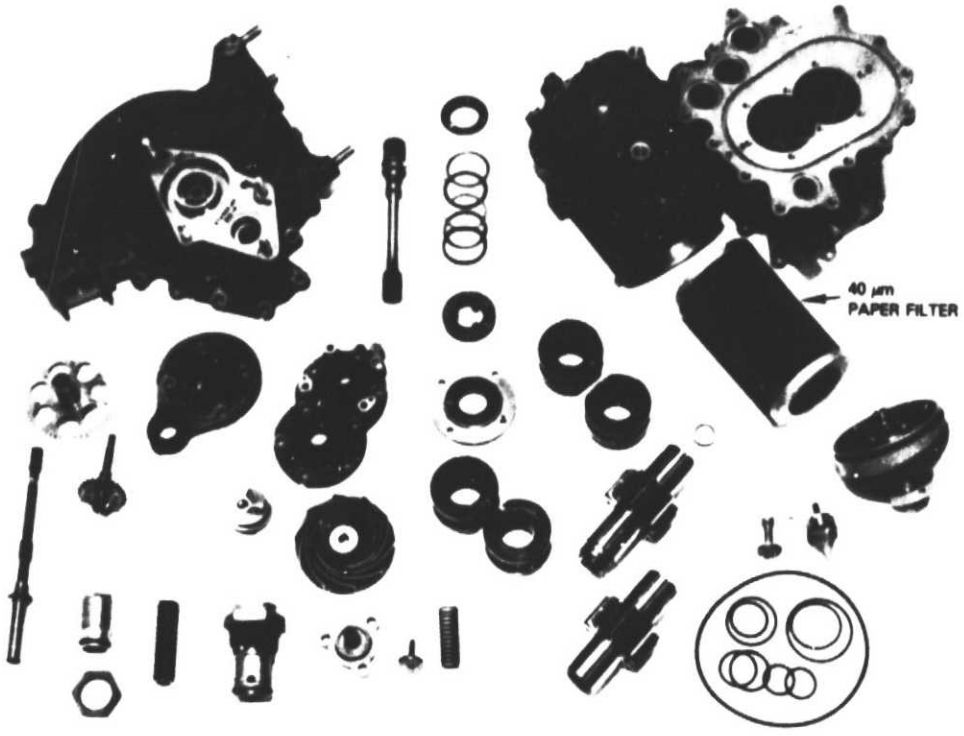

Figure 4 JT8D Engine Fuel Pump

3.1.3 Fuel Filter System

The JT8D engine fuel system incorporates several fuel filters differing in construction, filtration quality and filtration characteristic depending on the subsystem component protection requirements. The main inlet 40 μm paper cartridge filter, incorporated within the fuel pump, provides the primary protection for all subsystem components. This inlet filter provides protection against solid particulate matter and, in addition, collects fuel borne ice crystals at fuel temperatures below freezing. Periodically, the fuel deicing heater system is activated by a pressure transducer to increase fuel filter inlet temperature above the water freeze point and thereby clear the filter of collected ice.

The remaining filters are coarser and with the exception of the control inlet filter have significantly smaller flow rate capacity. These filters vary from 50-325 mesh, are either barrier or wash flow type and are constructed of stainless steel.

3.2 Combustor Description

The JT8D-17 combustor section consists of nine tubular combustion chambers in a can annular arrangement. Each chamber contains one centrally located duplex fuel nozzle. Two of the chambers are equipped with spark igniters. The nine combustion chambers are interconnected by tubes for flame propagation during starting. A cross-sectional schematic of the JT8D-17 combustor is shown in Figure 5.

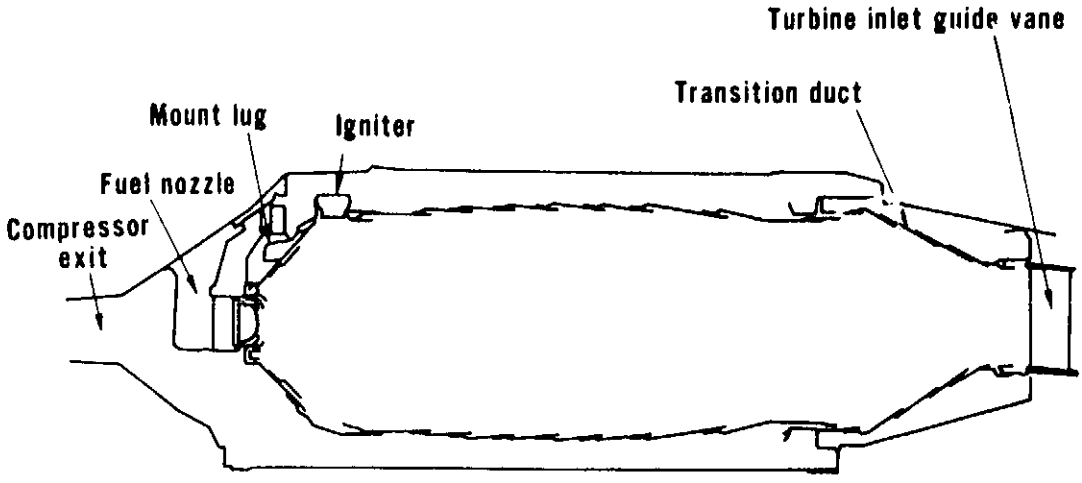

Figure 5 Cross-Sectional Schematic of the Production JT8D-17 Combustor

The combustor employs a dual passage fuel injection system to obtain the required turn down ratio (ratio of maximum to minimum fuel flow) for a reasonable range of fuel pressure. The relationship between fuel flow and nozzle pressure drop for a typical engine is shown in Figure 6. The break in the curve indicates the staging point where transition is made from the primary metering system to the primary plus secondary metering system. Staging is controlled by a spring loaded pintle valve near the fuel control, which is sensitive to the difference between fuel pressure and air chamber pressure. The staging point is independent of the combustor fuel-air ratio for a particular engine operating condition.

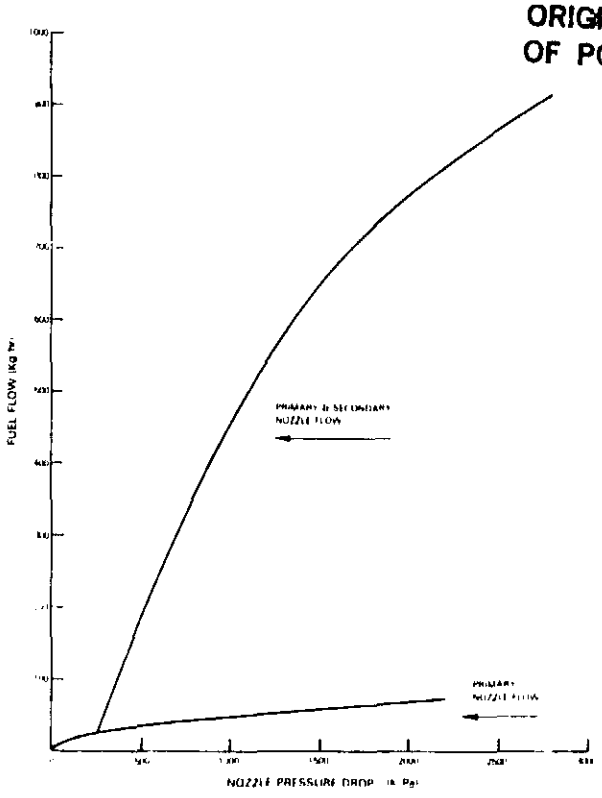

Figure 6 JT8D Dual Orifice Fuel Flow Schedule

3.3 Combustor Performance Requirements

Table II lists the critical operating parameters for the JT8D-17 combustor at the four operating conditions of the Environmental Protection Agency landing and takeoff cycle and at the cruise operating condition. Other key operating parameters of the JT8D combustor at sea-level takeoff conditions are:

Compressor Exit Axial Mach Number	0.42
Combustor Section Total Pressure Loss	8.2%
Combustor Exit Temperature Pattern Factor*	0.39

Figure 7 shows the design flight envelope of the JT8D-17 engine. The engine must be capable of self starting with the combustor driven only by a windmilling fan and compressor over a substantial fraction of the flight envelope as

---

*Pattern factor is the ratio of the difference between the maximum gas temperature and the average combustor exit temperature to the difference between the average combustor exit temperature and the combustor inlet temperature.

TABLE II
JT8D-17 ENGINE COMBUSTOR OPERATING PARAMETERS

Operating Condition	Inlet Total Pressure (ATM)	Inlet Total Temperature (°C)	Combustor Airflow (kg/sec)	Combustor Fuel Flow (kg/sec)	Combustor Fuel/Air Ratio
Idle (with bleeds)	2.4	120	12	0.14	0.0123
Takeoff	16.9	438	66	1.24	0.0188
Climb	13.2	406	53	0.90	0.0169
Approach	9.7	321	42	0.56	0.0133
Cruise	6.3	340	29	0.43	0.0148

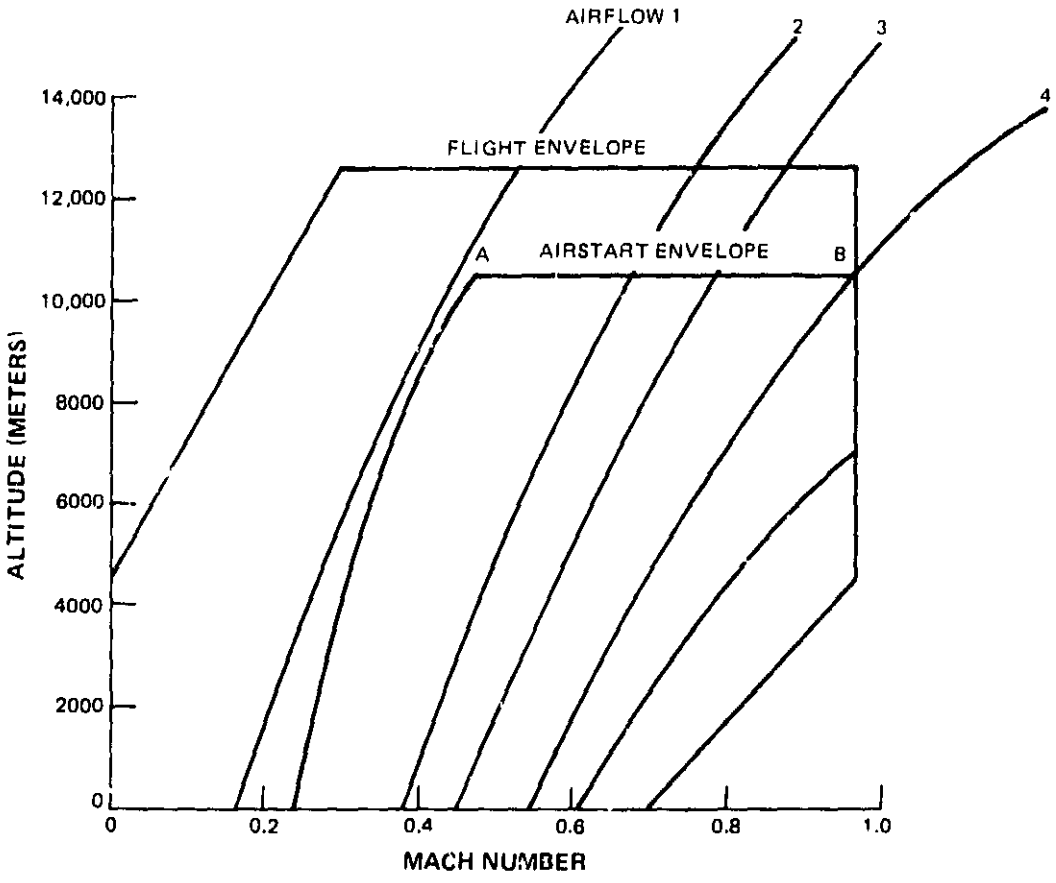

Figure 7 JT8D-17 Airstart Envelope

shown in the figure. Table III lists the combustor operating conditions at the lettered points on the upper boundary of the relight envelope as defined from the windmilling performance characteristics of the JT8D-17 compressor.

TABLE III
COMBUSTOR INLET CONDITIONS AT ALTITUDE RELIGHT

Point on Figure 7	A	B
Altitude (Meters)	10,668	10,668
Flight Mach Number	0.475	0.57
Combustor Inlet Total Pressure (ATM)	0.30	0.66
Combustor Inlet Total Temperature (°C)	32	21
Engine Airflow (kg/sec)	0.20	6.1
Fuel Flow* (kg/sec)	0.076	0.076

*Minimum fuel flow of JT8D engine control schedule

4.0 PHYSICAL AND CHEMICAL CHARACTERISTICS OF FUELS

4.1 Fuel Analysis

Fuel analysis and quality control experiments were conducted to monitor the physical and chemical properties of the antimisting kerosene and its parent fuel.

Table IV lists the different fuel analyses that were conducted on fuel samples. The specific analyses conducted on a particular sample depended on the intended use of the fuel lot, and in general, consisted of not more than five or six of the analyses listed in Table IV. For example, a sample from a fuel batch that was used in a combustor or smoke test was analyzed primarily for hydrocarbon characterization (ASTM Methods D1319 and D1840) and smoke point (ASTM Method D1322), while a sample that was used in combustor ignition tests was analyzed primarily for the distillation temperature distribution and viscosity.

TABLE IV
FUEL PROPERTIES MEASURED AND TEST METHODS

Property	Test Method
Hydrogen and Carbon, wt. %	Perkin Elmer Model 240 Analyzer
Aromatics, vol. %	ASTM D1319
Sulfur, wt. %	Dohrmann Combustion/Titration
Specific Gravity, 288/288°K	ASTM D1298
Flash Point, °C	ASTM D56
Freezing Point, °C	ASTM D2386
Carbon Residue, 10 Vol. % Bottoms, wt. %	ASTM D524
Net Heat of Combustion, cal./gm	ASTM D2382
Smoke Point, mm	ASTM D1322
Viscosity, 25°C, cs	ASTM D445
Water Content, ppm	Karl Fisher Titration
Surface Tension, Dynes/ cm^2	ASTM D971
Thermal Stability	ASTM D3241
Distillation Curve	ASTM D86
Naphthalenes, Vol. %	ASTM D1840
Nitrogen, ppm	Kjeldahl Method
Mercaptan Sulfur, ppm	ASTM D1323
Metallic Trace Elements	Atomic Absorption

Four batches of antimisting kerosene and the parent fuel from which the antimisting kerosene was blended were measured to determine certain physical properties. In addition, an abbreviated characterization was made of a fifth batch of antimisting kerosene and parent fuel. The results of these measurements are given in Table V. Properties of the parent fuels in all cases appeared typical of Jet A fuel used for most commercial jet aviation.

Sample lots of the antimisting fuel contained sodium levels that were unexpectedly high (Table VI). Antimisting kerosene received early in the program contained a minimum level of 0.3 ppm or less sodium. Because a sustained high level of Na may accelerate hot corrosion, six additional blend lots of antimisting kerosene and two additional parent fuels were analyzed. The six additional blend lots include RMH Nos. 1-141, 142, 153, 154, 157, 158 and the two parent fuels were RMH 10720 and 10608. Table VII shows the sodium levels for these additional lots of fuel ranged from 3.4 to 3.7 ppm. Long time exposure to these high levels of sodium in the fuel would appreciably accelerate corrosion of the engine hot section.

TABLE VI
CHARACTERIZATION RESULTS FOR ANTIMISTING KEROSENE
Lot RMH - 139 and Parent Lot RMH-01105

	RMH 1-139 AMK	RMH-01105 Jet A
Filter Ratio	Drum 1 = 60.4 Drum 2 = 50.7	1 by Definition
Additive Content (% wt)	0.33	
Hydrogen Content (% wt)	13.7	13.73
Hydrogen/Carbon Ratio	1.89:1	1.89:1
Specific Gravity, 60/60F	0.8128	0.8123
Viscosity, 27°C	3.09	1.87
Water Content, ppm	31	41
Aromatics Content, Vol. %	20.8	21.1
Napthalenes, Vol. %	1.78	1.78
Copper Content, ppm	0.12	0.03
Sodium Content, ppm	3.2	.01

TABLE V
ANTIMISTING KEROSENE FUEL CHARACTERIZATION

	RMH 1-45		RMH 1-64		RMH 1-65		RMH 1-86		RMH 1-90	
	Neat Fuel	AMK	Neat Fuel	AMK	Neat Fuel	AMK	Neat Fuel	AMK	Neat Fuel	AMK
Hydrogen Content, Wt. %	13.58	13.61	13.93	13.82	13.82	13.80	14.18	13.91	13.91	
Hydrogen-to-Carbon Ratio	1.90:1	1.89:1	1.92:1	1.92:1	1.92:1	1.92:1	1.96:1	1.92:1	1.92:1	
Aromatics Content, Vol. %	22.6	21.3	19.8	20.5	20.0	19.9	18.9	21.1	20.9	
Sulfur Content, Wt. %	0.04	0.04	0.02	0.02	0.02	0.02	0.02	0.02		
Specific Gravity, 60/60F	0.8146	0.8156	0.8085	0.8100	0.8100	0.8109	0.8058	0.8090	0.8063	0.8072
Flash Point, °C	53	53	53	53	52	53	54	53		
Freezing Point, °C	-49	-49	-45	-46	-46	-47	-49	-46		
Carbon Residue, 10 Vol. % Bottoms, Wt. %	0.09	--	0.05	--	0.10	--	0.06	--		
Heat of Combustion, net, KJ/kg	43,124	43,008	43,171	43,124	43,124	43,031	43,194	43,147	43,194	43,171
Smoke Point, mm	20	20	21	21	21	21	22	22		
Viscosity, 77F, cs	1.96	3.28	1.87	3.08	1.89	3.14	1.85	3.07	1.77*	2.91*
Additive Content, Wt. %	--	0.29	--	0.31	--	0.31	--	0.32		
Water Content, ppm	34	54	34	42	34	42	22	32		
Surface Tension, dynes/cm	29.7	30.1	29.3	29.5	29.6	29.7	29.5	29.6		
Thermal Stability, JFTOT, 260C										
P, cm Hg	5	11	>25	0	>25	7	>25	3.5		
Deposit Code	1	1	1	1	1	1	1	1		
Distillation, F										
IBP	320	322	324	322	326	322	316	316		
10 Vol. %	369	368	365	362	367	366	361	363		
20	384	384	385	377	380	381	381	377		
30	396	397	396	395	392	393	393	391		
40	407	409	406	405	407	403	404	401		
50	418	419	416	416	418	414	413	411		
60	430	431	426	427	429	426	425	423		
70	443	443	438	440	441	439	437	436		
80	459	459	452	455	457	455	453	452		
90	480	480	473	476	478	474	476	472		
EP	530	517	531	522	532	512	529	509		
Recovery, Vol. %	98.9	98.8	99.0	99.0	98.5	99.0	99.0	99.0		
Residue	1.1	1.2	0.8	0.7	1.3	0.7	0.4	0.9		
Naphthalenes Content, Vol. %	2.1	2.1	1.8	1.6	1.9	1.6			1.69	
Nitrogen Content, ppm	11	27	10	28	4	26	4	21		
Mercaptan Sulfur, ppm	<10		<10	--	<10	--	<10	--		
Metallic Element Content, ppm										
Sodium	<0.02	0.3	<0.1	0.4	<0.1	0.4	<0.1	0.4		
Copper	<0.02	<0.02	<0.02	<0.02	<0.02	0.02	<0.02	0.02		
Calcium	<0.02	0.1	<0.1	<0.1	<0.1	<0.1	<0.1	<0.1		
Lead	0.03	0.06	<0.1	<0.1	<0.1	<0.1	<0.1	<0.1		

*Measured at 26°C

TABLE VII
SODIUM CONTENTS OF ANTIMISTING KEROSENE FUEL

Sample	ppm Sodium
RMH 141	3.5
RMH 142	3.7
RMH 153	3.5
RMH 154	3.4
RMH 157	3.4
RMH 158	3.5
Parent 10720	0.04
Parent 10608	0.02

Naphthalene, aromatics, water and hydrogen content levels measured on shipments of AMK and the parent fuels showed them to be typical of that for Jet A fuel. The additive content, specific gravity and viscosity show the expected deviations on addition of FM-9 polymer to the Jet A fuel.

4.1.1 Filter Ratio of Undegraded Antimisting Kerosene

The antimisting kerosene was blended in lots of four hundred gallons by ICI before shipment to Pratt & Whitney Aircraft. Filter ratio measurements made on as-received, undegraded antimisting kerosene samples are shown in Table VIII. Filter ratio (defined in section 5.2.1.1) was measured by both Pratt & Whitney Aircraft and ICI before shipment and overall, the agreement was fairly good considering the nature of the measurement and differences in samples. However, three blend lots of AMK fuel produced quite high and nonreproducible filter ratios as shown in Table IX. Limited testing revealed the solids content for these blended lots was approximately 0.3% by weight as expected. The viscosity of the parent fuel from which the AMK fuels were blended was somewhat higher than previous parent fuels. Other parameters measured for both parent and AMK fuel appeared normal. Initially, there was no apparent explanation for these high and nonreproducible filter ratios on the three blend lots of AMK. Additional analysis reported later in section 9.4 offers a plausible explanation for this phenomenon.

TABLE VIII
FILTER RATIO MEASUREMENTS ON UNDEGRADED ANTIMISTI'G KEROSENE SAMPLES

Shipment Date	Blend Lot	Filter Ratio Pratt & Whitney Aircraft (As Received)	ICI (As Shipped)
10-25-79	1-45	54	34
01-09-80	1-64	53	52
01-17-80	1-65	49	42
03-04-80	1-83	34	32
04-16-80	1-90	28	41
	1-91	42	44
	1-92 Drum 1	45	51
	2	37	51
	1-93	33	60
	1-94	55	38
	1-95	59	62
07-02-80	1-112	16	27
	1-113	18	24
	1-114	21	26
	1-115 Drum 1	25	24
	1-115 2	21	
	1-115 3	21	
	1-115 4	23	
	1-115 5	21	
	1-115 6	21	
	1-115 7	19	
	1-115 8	22	

TABLE IX
FILTER RATIO MEASUREMENTS ON NEW SHIPMENT OF AMK

Blend Lot	Filter Ratio P&WA	ICI
177	146	59
178	166, 130, 116	63
179	210, 115	69

5.0 FUEL DEGRADATION MEASUREMENTS

5.1 Fuel Degradation

Degradation of antimisting kerosene requires that large polymer bonds be broken to reduce the effective viscosity of the blended fuel toward that of the reference Jet A fuel. Early in the program, the fuel was degraded by passing AMK through the JT8D fuel pump at the P&WA engine control systems laboratory. The test stand was modified to allow operation in either open or closed loop mode (Figure 8). In the open loop mode all the fuel flowed through the fuel pump systems to the collection tank. In the closed loop mode the flow from the discharge valve returned to the supply tank via a cooler for continued operation. Figure 9 shows the specific test setup, instrumentation locations and fuel sampling locations for the JT8D fuel pump.

The JT8D engine fuel pump was a reasonable laboratory method for processing undegraded antimisting kerosene. Fuel degradation was accomplished by passing the antimisting kerosene through the JT8D fuel pump system N times; three-pass antimisting kerosene is antimisting kerosene passed through the fuel pump system three times

To ensure that all antimisting kerosene within a batch was subjected to the degradation process for each pass, the first three passes were operated open loop. Subsequent passes were accomplished at closed loop and agitated to enhance homogeneous tank mixing. One pass for a 1514 liter (400 gallon) antimisting kerosene batch at the 24.6 liters/minute (6.5 gpm) processing rate took approximately one hour. Antimisting kerosene samples were obtained at various system locations and operating conditions and tested for filter ratio (defined in section 5.2.1.1).

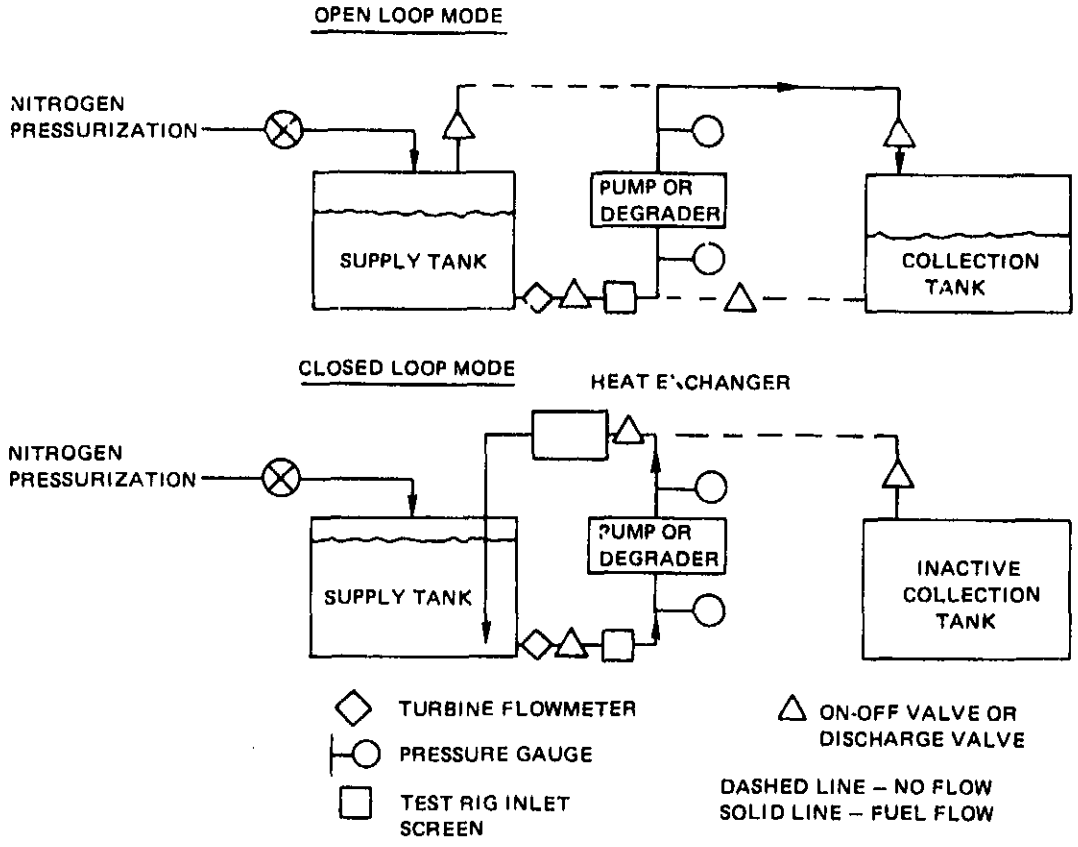

Figure 8 Schematic Arrangement of Fuel Degrading Test Rig

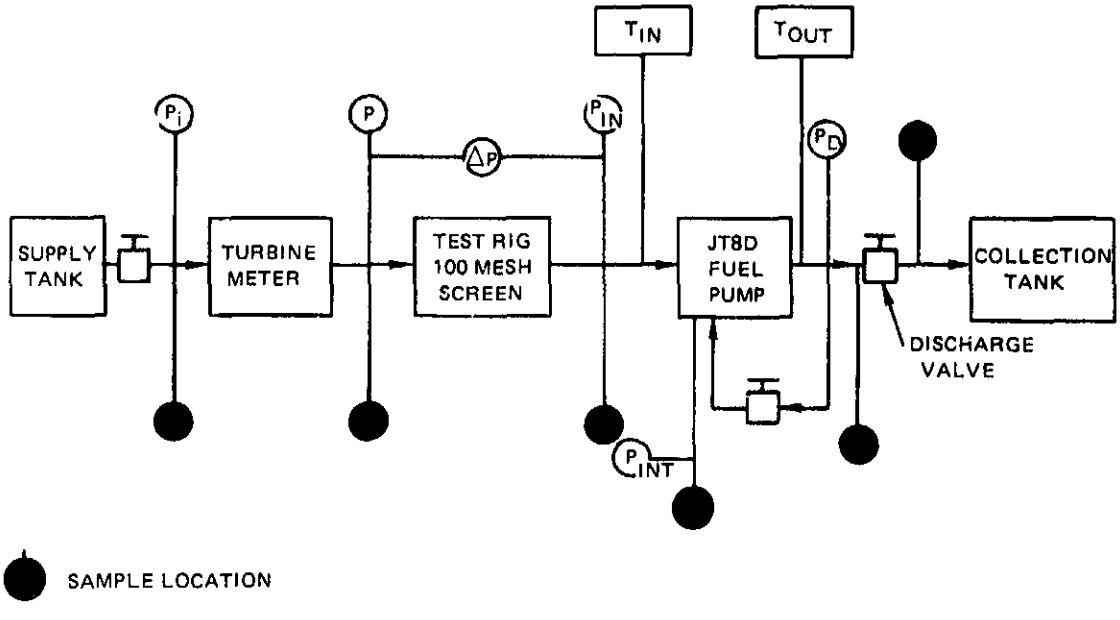

Figure 9 Instrumentation Fuel Sampling Locations

Later in the program, there was a need to acquire highly degraded fuel in large quantities. It was found that plausible methods for degrading the fuel fell into three categories:

1. Cavitation produced by high velocity flow
2 Shear produced mechanically by passing the fuel between stages of multi-bladed rotors and stators.
3 Cavitation produced by ultrasonic vibration

Samples of AMK processed by suppliers of equipment using the methods of Category 1 and 2 showed cavitation to be more effective. The results are summarized in Table X.

TABLE X
SUMMARY OF RESULTS WITH COMMERCIAL UNITS

	Transition Velocity* cm/sec	Filter Ratio
AMK Undegraded	0.19	23
Jet-A Without Additive	9-10	1.00
Gaulin Disperser (Cavitation)		
20.7 MPa	1.0	1.30
34.5 MPa	2.5	1.12
55/2 MPa	5.2	1.15
Sonic Sonolator (Cavitation)		
13.8 MPa 1 pass	1.1	1.41
10.3 MPa 3 pass	2.4	2.60
13.8 MPa 3 pass	3.9	1.30
Speco (Mechanical)	0.37	8.0
Tekmar (Mechanical)	1.1	2.6

It was found that when the pressure consumed by the Sonic Sonolator was multiplied by the number of passes, the Gaulin and Sonic results could be combined as shown in Figure 10*. Also shown for comparison are results obtained with the JT8D fuel pump operating in a 16-pass mode. It can be concluded from Table X and Figure 10 that cavitation is a promising method for

---

*See Section 5.2.2 for definition of transition velocity

degrading AMK fuel. Based on these results and the available equipment, the Gaulin Disperser was selected as the prime workhorse device for the program. In this device the degree of degradation increases as the pressure across the valve becomes greater or as the number of passes through the device increases. Although this device performed well in degrading AMK, its size and power requirements preclude its use in aircraft applications.

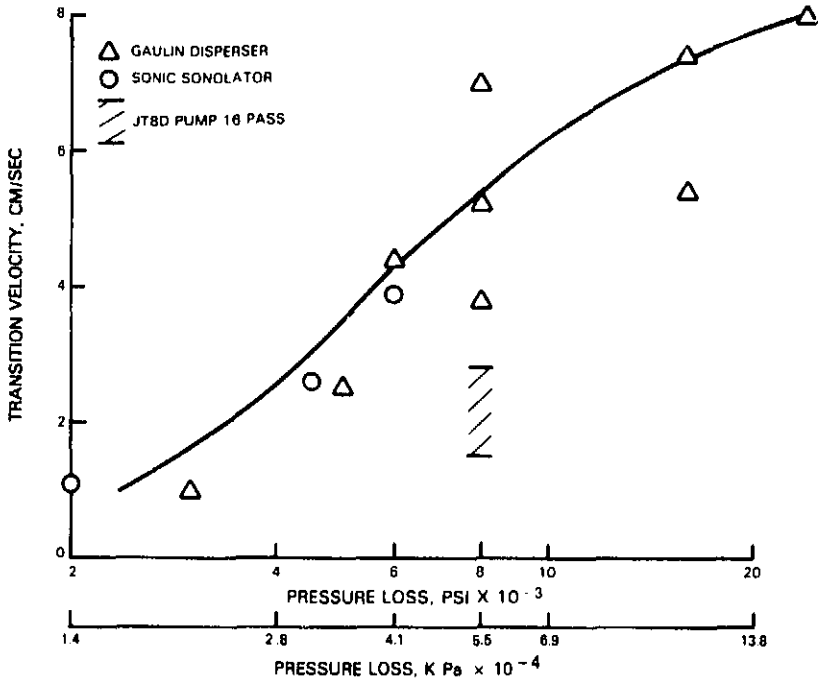

Figure 10 Degrader Performance

5.2 Measurement Techniques

U. S. Navy tests (Ref. 1) indicated that the excess viscosity of an antimisting mixture relative to the reference JP-5 fuel was reduced by about 50 percent in one pass through the engine fuel pump and control. Continuous recirculation of the fuel mixture through the pump and control for a period of 4 to 12 hours led to reductions in the viscosity excess of about 70 percent. This asymptotic behavior suggested that, if the magnitude of the viscosity excess relative to the reference fuel was used as a measure of degradation, it would not be possible to achieve a completely degraded state in which the viscosity was reduced to the level of the parent fuel. Consequently, the 100 percent degraded state was defined as that achieved when additional processing of a batch of fuel would not produce an additional five percent reduction in the viscosity in an hour of closed loop operation of the degrading system.

Early in the program it was learned that antimisting kerosene measured as 100 percent degraded by the above definition or characterized by the filter ratio method (see Section 5.2.1.1)required considerably more processing in order to achieve levels acceptable to system components. Therefore it became necessary to utilize and develop additional measurement techniques to distinguish relative levels of processed antimisting kerosene. The various techniques are described, discussed, and compared below.

5.2.1 Viscosity Measurements

The addition of the antimist additive is known to increase the effective viscosity of the blended fuel. Therefore, techniques which measure viscosity or effective viscosity can be used to measure the extent to which the fuel has been degraded from its initial state. The different apparatus and methods used to measure the effective viscosity of antimist fuels are described in the following paragraphs and the results are listed in Table XI.

TABLE XI
ANTIMISTING KEROSENE VISCOSITY MEASUREMENT TECHNIQUES

Method	Measurement	Result
Screen Mesh Filter	Filter Ratio	Adequate Up to 120 min. in Blender
British Orifice Cup	Flow Rate Ratio	Beyond 2 min. in Blender, too insensitive
ASTM Viscometer	Viscosity Ratio	Too insensitive
Glass Bead	--	Unsuccessful

5.2.1.1 Screen Mesh (Filter Ratio)

The filter screen device shown in Figure 11 (Standardized by U.S./United Kingdom AMK Technical Committee) was utilized to measure effective viscosity. This filter ratio procedure measured the time required for a predetermined volume of fuel to flow through a 17 μm size screen at 20°C.

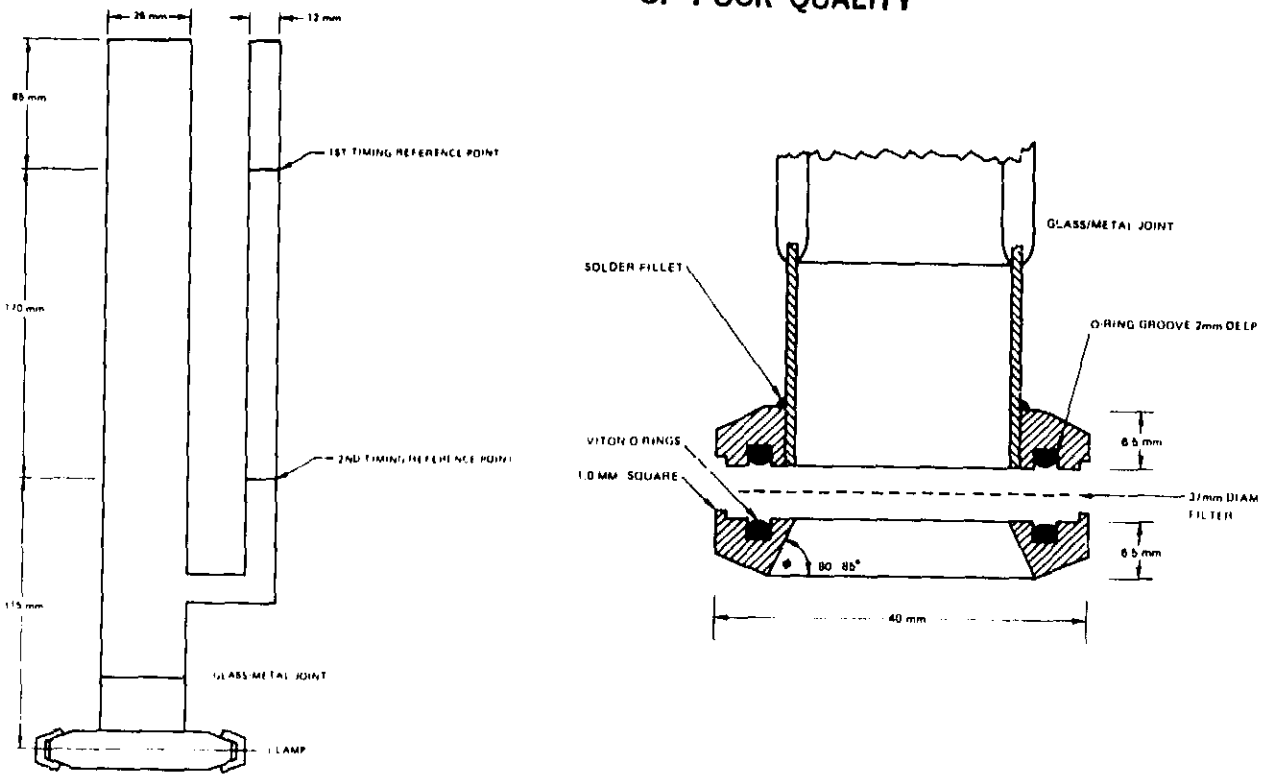

Figure 11 Filter Screen Device

Effective viscosity was measured by filling the tube of the filter device with the reference fuel to the uppermost reference mark then allowing the fuel to drain out of the tube. The time required for the meniscus of the fuel to pass between the two reference marks on the tube was recorded. This procedure was repeated with the antimisting kerosene test fuel. The ratio of the time required for the antimising kerosene and the reference fuel to flow between marks is defined as the filter ratio (FR).

5.2.1.2 Orifice Flow Cup (Flow Rate Ratio)

This procedure is similar to the Screen Mesh (FR) method in that it measures the time a predetermined volume of fuel flows through an orifice in the container. Viscosity is defined from a correlation derived from calibration of the apparatus. The apparatus consists of a flow cup constructed of brass with an orifice diameter of 6.6mm $\pm$0.0127mm, and a 10 ml graduated cylinder with a glass funnel to collect fuel from the cup.

In this procedure, the cup was filled with the reference fuel until it overflowed. The fuel was released and allowed to drain into a beaker for 30 seconds, after which time the graduated cylinder replaced the beaker and the fuel was allowed to flow for an additional 30 seconds. The amount of fuel collected in the cylinder was recorded. If it failed to reach a range of 7.7 to 8.3 ml, clogging is indicated and the test is invalid. This procedure was repeated with antimisting kerosene fuel. Replicate tests with antimisting kerosene were carried out until volumes collected agreed within 0.1 ml. The results were expressed as the ratio of flow rates of antimisting kerosene fuel to the reference fuel.

5.2.1.3 Standard ASTM Capillary Viscometer (Viscosity Ratio)

Viscosity of the antimisting kerosene fuel and parent fuel was also measured by standard capillary viscometers according to ASTM D445 procedure. A Cannon Fenske reverse flow viscometer was used for the antimisting kerosene fuel and a Cannon Fenske routine viscometer for the parent fuel. The test is based on the time required for a given volume of fuel to flow through a capillary tube. A viscosity ratio was obtained by dividing the viscosity measured for the antimisting kerosene fuel by that of the parent jet fuel.

5.2.1.4 Glass Bead Bed

This apparatus consisted of a bed of 210 μm glass beads packed in a 35 mm section of a 0.64 cm inside diameter tube. The fuel sample was forced through the bed at differential pressures up to 1 atm and the flow rate measured. In laminar flow, the flow rate is inversely proportional to the viscosity of the fluid. Thus after calibration of the device with a sample of known viscosity, the viscosity of AMK samples can be determined by measuring the flow rate.

5.2.1.5 Comparison of Laboratory Methods for Viscosity Measurements

An initial comparison of the techniques for measuring viscosity was made by degrading small quantities of antimisting kerosene fuel with a laboratory blender for varying times from 1 minute to 120 minutes. Viscosity measurements with the glass bead bed proved impractical due to plugging of the bed under the suggested test conditions. The responsiveness of the remaining three techniques to changes in fuel properties is illustrated in Figure 12 where filter

ratio, viscosity ratio and flow rate ratio are plotted for the flow-through screen mesh, the ASTM viscometer, and the orifice cup, respectively, versus time of agitation in the blender. Data from two different lots of antimisting kerosene are shown and indicate good repeatability. The flow-through screen test and the orifice cup measurements are seen to be more definitive than the standard ASTM viscometer in establishing the degree of degradation of the antimisting kerosene. The responsiveness of the orifice cup falls off rapidly after approximately two minutes, whereas the flow-through screen test shows changes in filter ratio for times up to 120 minutes. The results are summarized in Table XI.

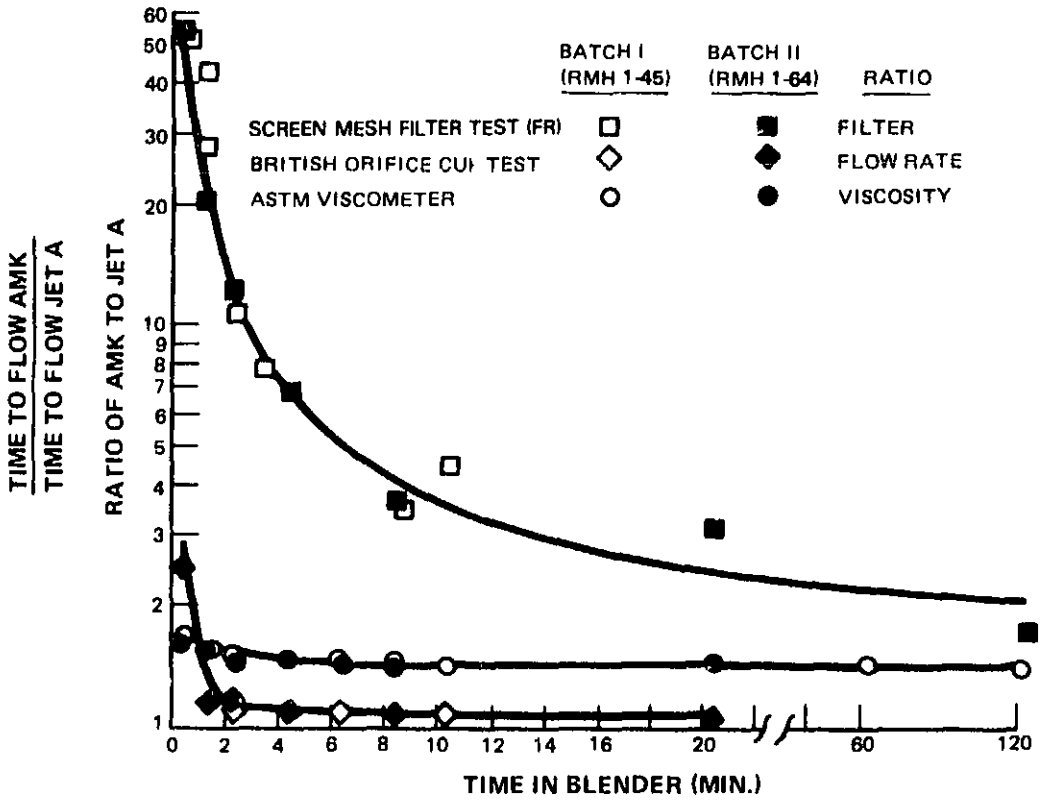

Figure 12 Comparison of Three Viscosity Measuring Devices

Early in the program, the fuel was degraded by passing the antimisting kerosene through a JT8D engine fuel pump system. The sensitivity of filter ratio to number of passes can be seen in Figure 13. The measurement is adequate to about two or three passes. From 3 to 16-passes, using filter ratio measurement as a means of discriminating degradation levels was unacceptable due to lack of resolution. Most of the tests early in the program were run with a degradation level of 3-pass or less and are, hence, reported in terms of both number of passes and filter ratio.

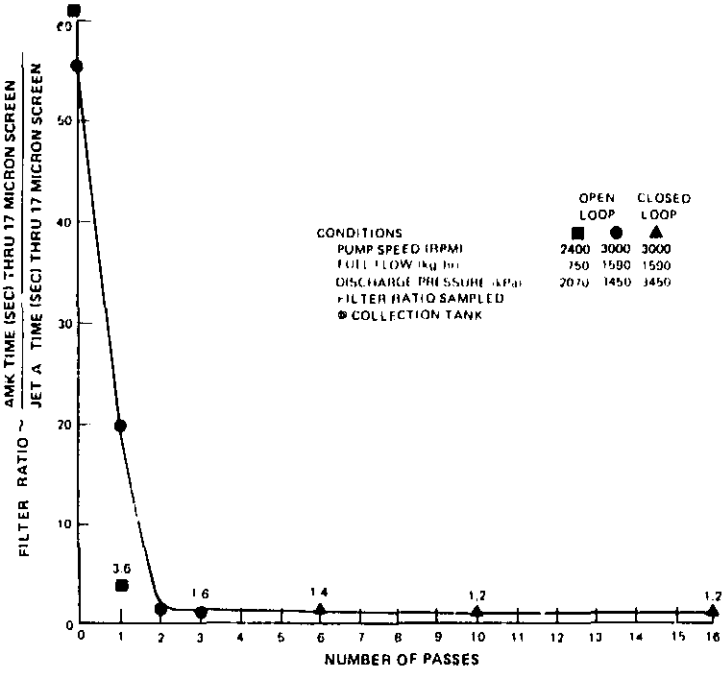

Figure 13 JT8D Fuel Pump System Filter Ratio

5.2.1.5 Effect of Temperature Variations on the Filter Ratio Test

The effects of temperature variations on the filter ratio test were evaluated by measuring the time for the fuel to flow between two reference marks at varying temperatures. Undegraded, 1-pass, and 3-pass antimisting kerosene and Jet A were tested. The results are shown in Figure 14. Temperature affected the antimisting kerosene flow times to a greater degree than for the parent fuel. The slope of the time vs. temperature curve for the undegraded fuel showed a large shift at a temperature of approximately 25°C. Table XII shows

the filter ratio as calculated from Figure 14. As temperature increased, the filter ratio showed a corresponding decrease. Also shown in Table XII is viscosity ratio using a Cannon Fenske viscometer. Over the temperature range of -35°C to 99°C the viscosity ratio of antimisting kerosene to parent jet fuel increased by a factor of 1.5.

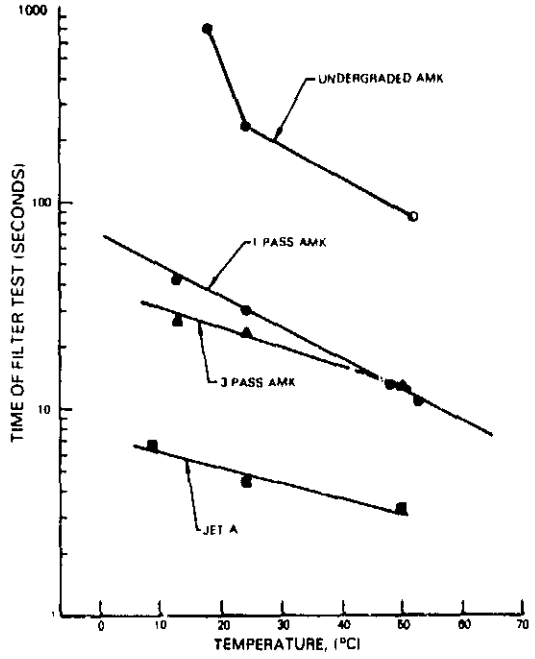

Figure 14 Screen Viscosity Temperature Chart

TABLE XII
EFFECT OF TEMPERATURE ON MEASURED FILTER AND VISCOSITY RATIO

Temperature (°C)	Filter Ratio Undegraded	Filter Ratio 1-Pass	Filter Ratio 3-Pass
18	126	7.0	4.8
25	49	6.4	4.6
53	28	4.2	3.9

Temperature (°C)	Viscosity Parent Fuel (cp)	Viscosity Antimisting Kerosene Fuel (cp)	Viscosity Ratio
-35	8.78	10.71	1.21
0	2.75	4.16	1.51
25	1.58	2.65	1.68
38	1.27	2.17	1.71
99	0.59	1.10	1.86

5.2.1.7 Effect of Filter Type and Pore Size on Filter Ratio

An attempt was made to determine whether changing the pore size or filter type would increase the sensitivity of the filter ratio measurement to degradation level. A 10 μm metal screen and a 40 μm paper filter were used in the standard filter ratio test instead of the usual 17 μm metal screen. The results are shown in Table XIII. Filter ratios were tabulated for undegraded fuel, 1-pass, 3-pass, 7-pass and 16-pass antimisting kerosene. Filter ratio resolution between 7 and 16-pass was at best 20 percent. Filter ratio resolution from 16-pass to the highest possible level of degradation (antimisting kerosene properties identical to Jet A) was 30 percent at best.

TABLE XIII
EFFECT OF DIFFERENT FILTERS ON FILTER RATIO (FR)

	Filter Ratio and Filter Flow					
	17 μm Metal Screen		10 μm Metal Screen		40 μm Paper Filter	
Degradation Level	FR	Avg. Flow (cm^3/sec)	FR	Avg. Flow (cm^3/sec)	FR	Avg. Flow (cm^3/sec)
AMK						
Undegraded	43	0.53	28.6	0.22	133	0.19
1-Pass	8.0	3.0	6.8	0.74	86	0.28
3-Pass	3.0	7.6	7.0	0.85	79	0.31
7-Pass	1.17	18	--	--	1.44	18
16-Pass	1.17	20	1.28	4.7	1.20	21
Jet A		23.8	1.28			25

Filter ratios recorded for the nominal 40 μm paper filter were much higher than either of the metal filters at levels of degradation less than 16-pass. The permeability of the paper filter to Jet A was approximately the same as that of the the 17 μm metal screen as illustrated by the flow through the two filters. The measured filter ratio of undegraded antimisting kerosene for the 10 μm screen (29) was significantly less than that measured with the 17 μm screen (43). The flow rate of Jet A through the 10 μm metal screen was

approximately one-fourth the rate through either of the other two filters. Perhaps the lower flow rate allowed additional time for deformation of the antimisting kerosene additive aiding passage through the filter pores. The degree of tortuosity of the paper filter is considerably greater than either of the metal filters resulting in the greatest requirement for deformation. This factor may account for the resulting high filter ratios measured for the 40μm paper filter.

5.2.2 Transition Flow Rate (Transition Velocity)

An evaluation of transition flow rate or transition velocity, V_T as a method for measuring antimisting kerosene degradation, was conducted because of the need for a more sensitive technique than those discussed above.

It is found that when antimisting kerosene flow through a filter is plotted as a function of increasing ΔP across the filter, there is an increase in the flow resistance occurring at a defined flow rate or velocity as shown in Figure 15. This flow rate is termed the critical flow rate or transition flow rate and is a function of the fuel's level of degradation. The velocity associated with this flow rate is termed the transition velocity (or superficial transition velocity), V_T, and is based on the total filter cross-sectional area.

The theory of the flow of fluids through a porous media was applied to Jet A data from the transition flowrate experiments in an attempt to lend some physical meaning to the results (AMK data were not analyzed in this manner due to the complication of its non-newtonian nature). A Reynold's number was calculated for the flow corresponding to the transition velocity (the intersection of the two lines through the Jet A data in Figure 15). The characteristic dimension selected for the calculation was based on the ratio of the wetted surface area of the flow channels within the Nuclepore filter to the total filter solid volume, following the analysis described in Reference 2. As shown in Figure 16, this Reynold's Number correlates well with the point at which the experimental data begin to deviate from laminar behavior in making the transition to turbulent flow. It can be concluded from this that

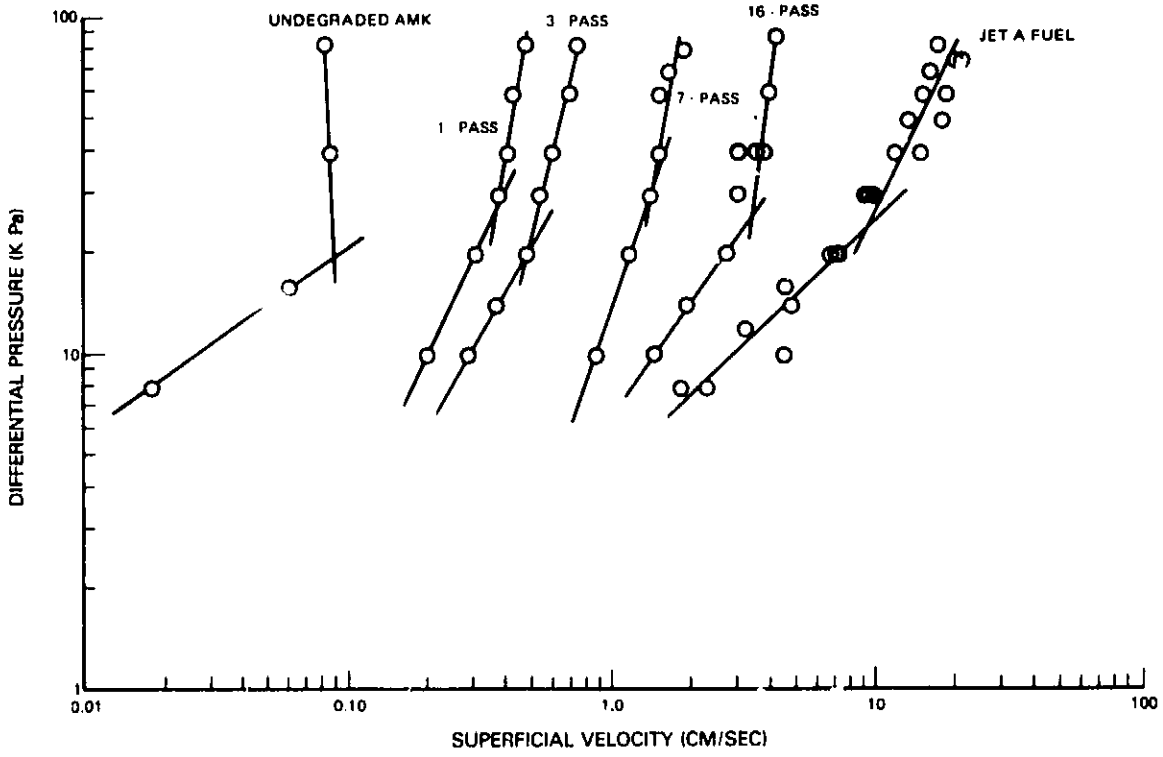

Figure 15 Transition Velocity Comparison

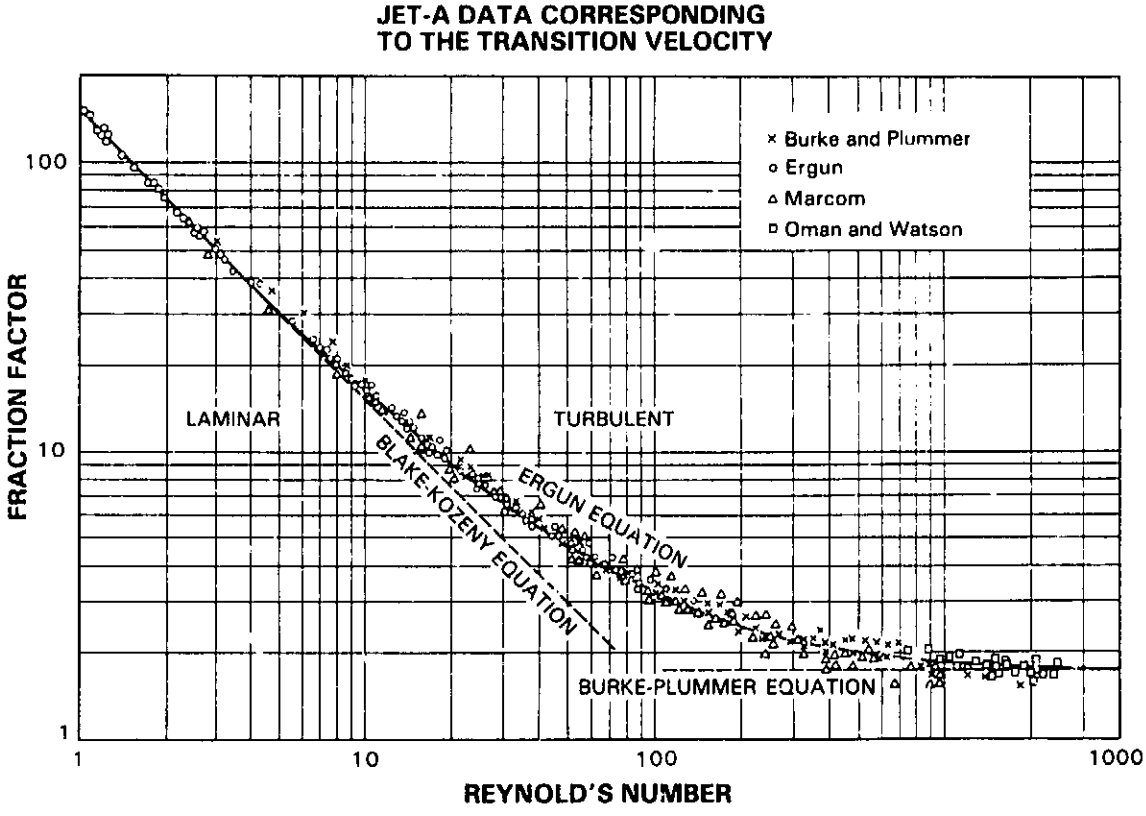

Figure 16 Friction Factor vs Reynold's Number for Porous Media Flow (reproduced from Ref. 2)

the transition velocity is related to some aspect of the transition from laminar to turbulent flow within the filter element. Additional credence to this hypothesis can be shown by considering the pressure drop/superficial velocity relationships of the Jet A data.

For low values of superficial velocity (9.5 cm/sec), the data show that

$$\Delta P \propto \text{superficial velocity}^{.8}$$

while porous media flow theory shows that the exponent should be unity. At higher flows (>9.5 cm/sec), the data show that

$$\Delta P \propto \text{superficial velocity}^{1.75}$$

while the theoretical result for turbulent flow indicates a second power relationship. However, laminar to turbulent transition occurs over a transition range, where pressure drop is a somewhat weaker function of superficial velocity. As it is likely that the Jet A data come from this transition range, the 1.75 power observed relationship is probably a good approximation of the data in Figure 16. A second point is that the transition flow rate experiment was envisioned as an expedient means of producing repeatable indications of the degradation level of AMK fuel. As such, it was not intended to incorporate a high degree of precision. Based on these arguments, it seems that the porous media flow theory can be employed to decribe the transition flow rate experiment, and that the transition velocity as defined as used in this report is a real phenomena and can be supported through a consideration of basic fluid mechanical principles.

Although porous media flow theory is not directly applicable to non-newtonian fluids such as AMK, the theory may be employed to explain the general trend of lower transition velocity with reduced degradation level. It is noted in Figure 15 that the transition velocity always seems to occur near a constant pressure drop level. In Reference 2, it is shown that

$$\Delta P \cong \text{constant } (\mu)(\text{superficial velocity})$$

in the laminar and initial transition regions, where the transition flow rate experiments were performed. Since the apparent viscosity of AMK increases with reduced levels of degradation (corresponding to fewer passes through the JT8D fuel pump), the above equation makes clear that the superficial velocity must decrease for a given pressure drop. This trend is evident in Figure 15.

Tests were conducted using a standard Millipore filtration apparatus and filters made of polycarbonate, metal screen and paper. The polycarbonate filters were manufactured by Nuclepore Corp. and had a pore diameter of 8 μm, pore density of 1 x 10^5 pores/cm^2 and a nominal filter thickness of 10 μm. The filters were unique in that the pores were regular circular openings. The percent open area which was calculated from the nominal pore diameter and density was 5.0%. The characteristics of the wire screen filters are tabulated in Table XIV. The percent open areas of screens 316L and T304L were calculated from the difference in apparent density and the nominal density of stainless steel (7.8 g/cm^3) (calculated from measurements of screen diameter thickness). Fiber paper filters with 40 μm nominal pore size were cut directly from a JT8D fuel filter.

TABLE XIV
DUTCH TWILL WEAVE SCREEN CHARACTERISTICS

Screen Designation	Diameter of Wires (cm)	Mesh	Pore Size (μm) Absolute	Nominal	Screen Thickness (cm)	Percent Open Area
316L	0.0071x0.0041	165x1400	17	9-12	0.0142	39.4
T304L	0.0038x0.0030	325x1900	10	2-3	0.0084	25.9

The test for each type of filter was conducted by pouring a measured quantity of antimisting kerosene into the reservoir over the filter and measuring the time for the fuel to flow through the filter. The test was repeated at different vacuum settings from 8 x 10^4 to 87.5 x 10^4 Dynes/cm^2. A detailed laboratory procedure for measuring transition velocity is included in Appendix A.

5.2.2.1 8 μm Nuclepore Paper Filter

Flow through Nuclepore filter papers in a standard millipore filtration apparatus was chosen for study because of the ready availability of equipment and the well defined characteristics of the Nuclepore filters with respect to pore size, geometry and pore density. Figure 15 shows the flow characteristics

through a 8 μm Nuclepore paper filter for Jet A. The superficial velocity (based on total cross sectional filter area) linearly increased with ΔP. At 9 - 10 cm/sec there was an abrupt change in the slope in which the flow rose at a slower rate with increasing pressure. Figure 15 also shows the flow characteristics for 1-pass, 3-pass, 7-pass, 16-pass and undegraded antimisting kerosene. These curves are qualitatively similar to the curve for Jet A; however, the superficial transition zone occurred at lower velocities and were related to the AMK test fuel's degree of degradation. In addition, a transitional flow velocity was calculated based on the actual filter flow area (true transition velocity). Table XV compares the superficial transition velocity, true transition velocity and filter ratio. The superficial transition velocity and the true transition velocity change quite significantly from 7-pass antimisting kerosene to 16-pass antimisting kerosene, while the filter ratio results show very little difference.

TABLE XV

FLOW PROPERTIES OF JET FUEL AND ANTIMISTING KEROSENE THROUGH 8 μm NUCLEPORE PAPER FILTER

Fuel Sample	Superficial Transition Vel. (cm/sec)	True[1] Transition Vel. (cm/sec)	Filter Ratio (Standard 17 μm Screen)
Undegraded AMK	0.09	1.8	40
1-Pass AMK	0.4	8	8
3-Pass AMK	0.5	10	3
7-Pass AMK	1.5	30	1.2
16-Pass AMK	3-4	56	1.17
Jet A	9-10	200-240	1.00

[1]Based on actual flow area.

5.2.2.2 40μm Engine Fuel Pump Paper Filter

Tests were conducted with filters cut from a 40μm paper engine fuel pump filter. The flow rate of the undegraded antimisting kerosene through the filter was low due to severe clogging necessitating a reduction in fuel volume used in the flow measurement from 300 (used in all other tests) to 25 cc. Results with the 40μm paper filter are shown in Figure 17. Transition velocities based on the superficial filter area (total filter cross sectional area)* were 0.7 and 20 cm/sec for 3-pass and 16-pass respectively.

---

*Actual flow area is unknown.

An indication of filter clogging was obtained by running the test at a fixed ΔP and recording the flow rate at two different times. This is shown in Figure 17 as "first test" and "second test". The rate of clogging appeared to decrease as the level of degradation increased. The clogging tendency of 16-pass antimisting kerosene was much lower than for the 3-pass. This small scale filter test predicted that during the full scale tests, 3-pass antimisting kerosene would clog faster than 16-pass.

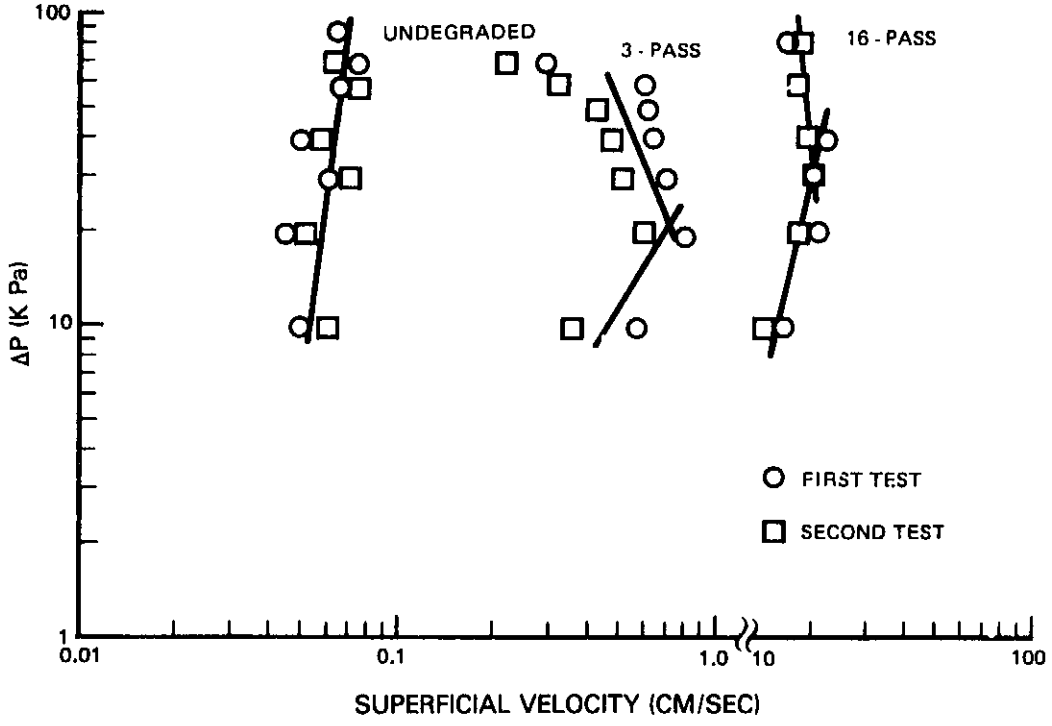

Figure 17 AMK Flow Through 40 μm Paper Filter

5.2.2.3 10 μm Woven Metal Filter

Velocity curves for antimisting kerosene through 10 m woven metal filter are plotted in Figure 18 at levels of degradation corresponding to 1-pass, 3-pass, 7-pass and 16-pass. Superficial transition velocities are identifiable for the 3, 7 and 16-pass but not for the 1-pass. The lack of an apparent transition for 1-pass antimisting kerosene and the steep slope of the flow curve indicate that the transition may occur at flow rates below the lowest measured for this filter.

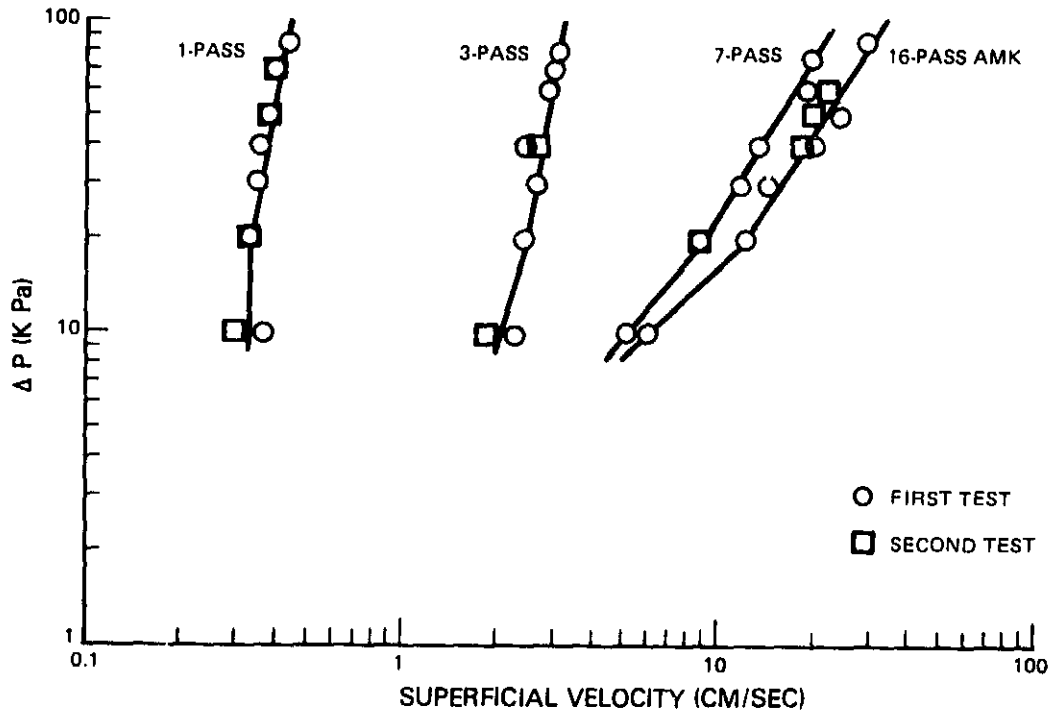

Figure 18 AMK Flow Through 10 μm Metal Screen

The effect of lowered temperature on flow properties of 3-pass AMK through 10 μm woven metal filter is shown in Figure 19. The antimisting kerosene demonstrated a tendency for clogging at lower temperatures. This may introduce nonreproducibility and procedure dependence into the measurements. The very viscous gel formed on the downstream side of the filter in the -26^{o}C experiment is shown in Figure 20.

5.2.2.4 17 μm Woven Metal Screen

Flow data for 1-pass and 16-pass antimisting kerosene, and Jet A through a 17 μm woven metal screen is shown in Figure 21. Very high velocities through the screen required the use of an aperture to reduce the filter area to 0.5 cm^2. The screen showed a well defined transition for 16-pass antimisting kerosene at a superficial velocity of 20 cm/sec. The transition for Jet A occurred at 55 cm/sec.

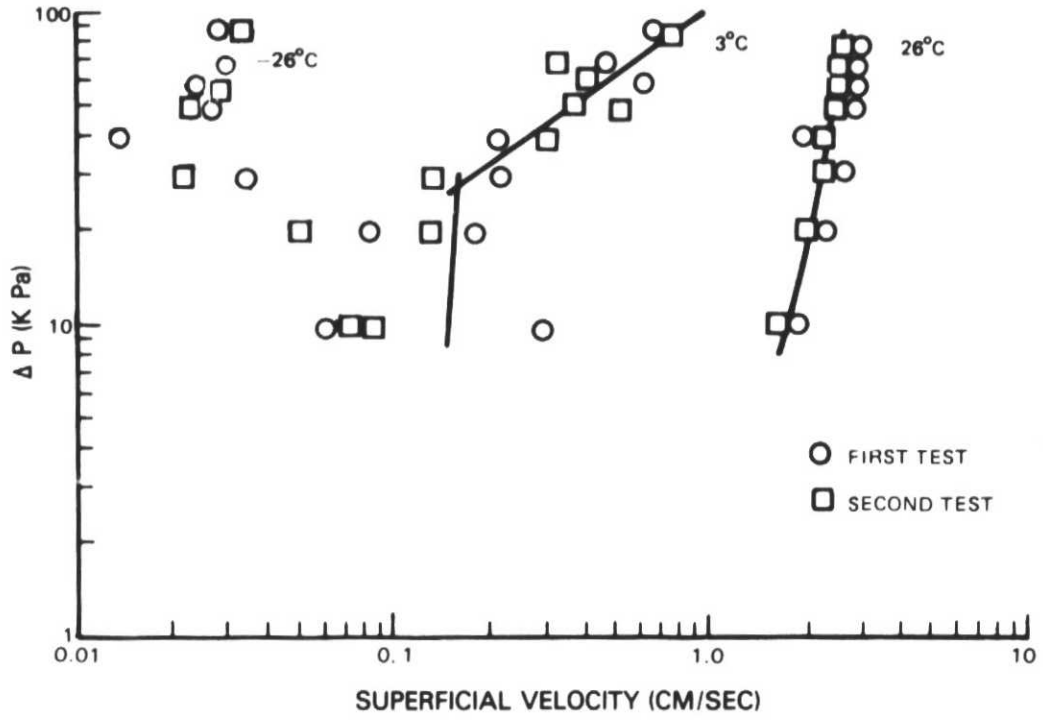

Figure 19 Effect of Reduced Temperature on Flow Properties of 3-Pass, (F_R = 1.28) AMK Through 10 μm Metal Screen

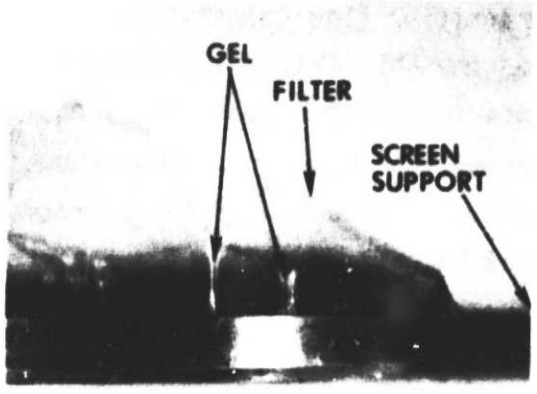

Figure 20 Gel Formed on Downstream Side of 10 μm Metal Filter After Flow at -26°C

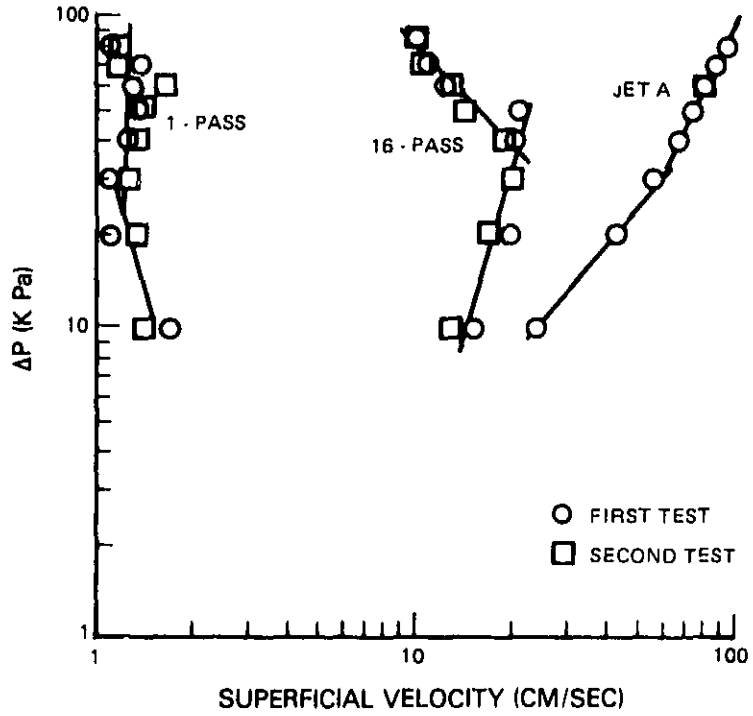

Figure 21 AMK Flow Through 17 μm Metal Screen

5.2.2.5 Summary of Transition Flow Rates

The true (normalized) transition flow velocities, based on the actual filter flow area, are summarized in Table XVI. Transition velocities through the 40 μm paper filter are not tabulated because the actual flow area is not known. Given the wide range of actual flow rates among the three filters, the agreement in flow velocities is good. The 8 μm Nuclepore paper filter was selected for continued use because of its well defined characteristics of pore size, geometry and pore density. The transition velocity measurement has been found to be capable of detecting changes at high levels of degradation.

TABLE XVI
TRUE TRANSITION FLOW VELOCITY OF ANTIMISTING KEROSENE THROUGH FILTERS

Sample	True Transition Velocity (cm/sec) 8 μm Nuclepore	10 μm Screen	17 μm Screen
Undegraded AMK	1.8	-	-
1-Pass AMK	8	-	-
3-Pass AMK	10	10	-
7-Pass AMK	30	38	-
16-Pass AMK	56	47	53
Jet A	200 - 240	-	147

5.2.3 Gel Permeation Chromatography

Gel Permeation Chromatography (GPC) was studied as an indicator of AMK fuel degradation and as having an additional benefit of showing the distribution of molecular weights after the fuel has undergone degradation. The GPC technique appears to be particularly applicable at higher levels of degradation where the filter ratio method loses resolution (see Figure 22).

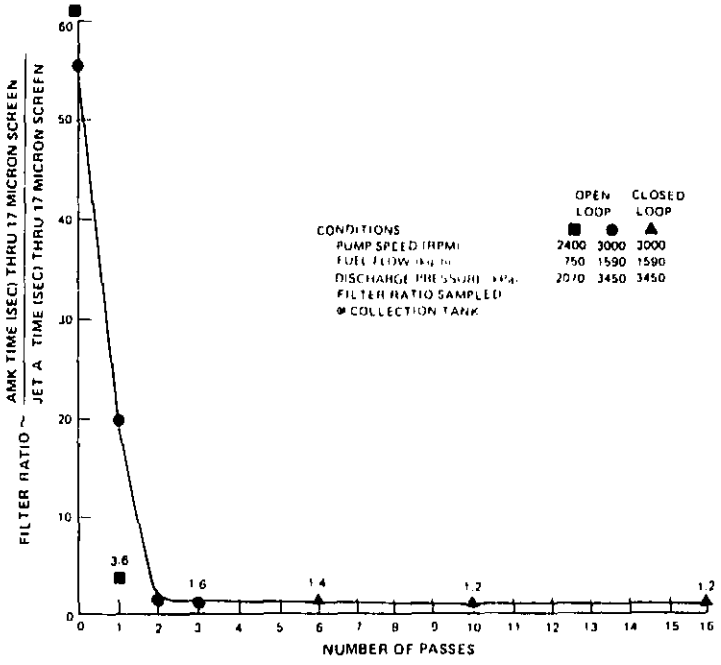

Figure 22 JT8D Fuel Pump System Filter Ratio

Degradation of AMK results in a reduction in the molecular weight of the polymer additive. By using the GPC technique to measure the molecular weight and molecular weight distribution of the polymer, this technique becomes a viable tool for monitoring the degradation process. The principle of gel permeation chromatography is separation by size of the molecules in solution. This separation is accomplished by means of the pore size distribution in the chromatograph column packing material. Molecules too large to penetrate any of the pores are totally excluded by the column packing and elute first. Smaller molecules penetrate some of the pores and are retained somewhat longer on the column before elution. Molecules small enough to penetrate all of the pores in the column packing are retained longest and elute last. The result is a chromatogram which is a recording of relative molecular size (or weight) of the molecular species versus elution time.

The instruments used in the Pratt & Whitney Aircraft measurements include the Water Associates Model 6000 solvent delivery system, the Model R401 Differential Refractometer, and a Chromatronix Dual Wavelength Detector. Gel permeation chromatography columns were 10^3Å, 10^5Å and 10^6Å microstyragel, each with a retained volume of approximately 12 ml. The combination of 10^3, 10^5 and 10^6 Å columns appears to be effective in analyzing the FM-9 polymer and Jet A fuel and in giving insight into the degradation process. The measurements were made at ambient temperature and at a solvent flow rate of 1 ml/min, maintained at a pressure of 1.4 MPa (200 psi).

Initial testing, using the GPC technique, showed that the apparent average molecular weight of undegraded AMK was approximately three million. This value is subject to a low bias error because preanalysis sample handling (prefiltration) sheared the polymer to some degree. A single pass through multiple stage screens with openings ranging from 400 μm to 10 μm at 8.3 MPa (1200 psi) reduced the molecular weight to two million. AMK fuel reverted during the first phase of the program by pumping through the JT8D pump 16 passes gave a molecular weight of 700,000. Finally, 100 ml of AMK fuel subjected to a 300 watt ultrasonic probe for ten minutes gave a molecular weight of 300,000.

Figure 23 shows GPC chromatograms for antimisting kerosene fuel degraded by sequential passes through the Gaulin disperser operated at 55.2 MPa (8000 psi) The X-axis is linear in time, and since the flow is constant, represents the volume of solvent eluted. The X-axis may also be directly interpreted as the molecular weight of the FM-9 polymer relative to polystyrene standards which has been generally accepted as a standard for GPC measurements. It is important to note that molecular weights measured by GPC are not absolute, but are relative to polystyrene weights. The absolute molecular weight of the FM-9 additive in AMK fuel is not as important as the relative changes in weight and distribution of molecular weights.

The molecular weight scale is logarithmic with the highest molecular weights being held up in the shortest time and eluting first. The Y-axis is the output of an ultraviolet absorption detector and is directly proportional to the concentration of the particular molecular weight species giving rise to the absorption. Thus, the GPC chromatograms may be interpreted directly as a

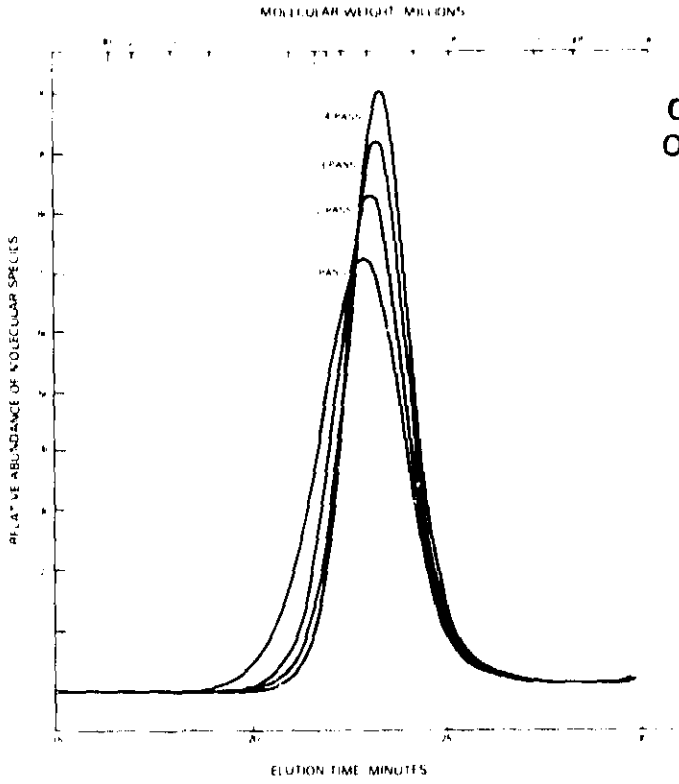

Figure 23 Effect of Successive Passes Through the Gaulin Dispenser on Molecular Weight Distribution of AMK

logarithm of FM-9 molecular weight, relative to polystyrene standards, decreasing left to right, versus concentration, or relative abundance of molecular weight species.

All three of the samples in Figure 23 were highly degraded as measured by normal techniques such as the filter ratio (FR). Using this method, one pass antimisting kerosene had a filter ratio of 1.15 while subsequent passes through the Gaulin device produced no measurable difference in this parameter.

Further degradation occurred, however, as evidenced from the changing peak molecular weights of the four samples and from transition velocity measurements which were recommended to determine degree of degradation whenever the filter ratio was less than 2.0. Transition velocities for one, two and three pass antimisting kerosene were 7.0, 7.4 and 8.0 cm/sec, respectively.

It is interesting to note that there is a regular shift in the peak of the curve of the GPC chromatograms. A tabulation of molecular weights for the three samples is shown in Table XVII. Peak molecular weights varied from

255,000 for one pass antimisting kerosene to 205,000 for three passes through the Gaulin disperser. There was still a more dramatic effect on the molecular weight of components which had a relative abundance of 1% and 5% of the peak molecular weight. After one pass through the Gaulin device when the peak molecular weight was 255,000, molecular weight components of 4.4×10^6 were still present. Even after three passes through the Gaulin disperser when the peak molecular weight was reduced to 195,000, components were present with molecular weights of 1.7×10^6.

TABLE XVII
MOLECULAR WEIGHT DATA FOR DEGRADED ANTIMISTING KEROSENE

Degradation Method	Transition Velocity	Peak Molecular Weight	0.05 Peak Molecular Weight	0.01 Peak Molecular Weight
Gaulin Disperser 1 pass, 55.2 MPa	7.0	255,000	2.5×10^6	4.4×10^6
Gaulin Disperser 2 passes, 55.2 MPa	7.4	225,000	1.3×10^6	2.3×10^6
Gaulin Disperser 3 passes, 55.2 MPa	8.0	205,000	0.95×10^6	1.7×10^6
16 pass through JT8D pump plus 12 test hours	4	500,000	2.9×10^6	3.7×10^6

The filter ratio after even one pass was 1.15. A comparison of the three curves showed that the peak rose and the width narrowed as the number of passes increased from one to three. This indicated that the distribution of molecular weight became closer with a larger percentage of the FM-9 polymer in the peak molecular weight area. Examination of the three curves showed also that where the curves reduced most rapidly was the high molecular weight, lowest elution volume portion of the chromatogram. The presence of small amounts of high molecular weight components, even in highly degraded antimisting kerosene samples, indicated that filtration problems which may not be immediately evident may occur over extended times.

To better understand the mechanism of flow velocity as related to gel formation on filters, an experiment was carried out in which AMK fuel was ultrasonically degraded to successively higher levels. Fuels were degraded to

transition velocities of 0.8, 2.1 and 6.7 cm/sec. These fuels were passed through the filters at a fast flow rate to induce gel formation. The filters were then treated in a chemical solvent, tetrahydrofuran, to remove the gel. Chromatograms were measured at an exclusion range from 70,000 to 50 million at a flow rate of 1 ml/min.

Figure 24(A) shows chromatograms for the undegraded AMK (I), transition velocity 2.1 AMK (II), and transition velocity 6.7 AMK (III). In addition, Figure 24(B) shows chromatograms of gel formed from transition velocity 0.8 AMK (IV), as well as the V_T = 2.1 cm/sec (V) and 6.7 cm/sec AMK (VI) samples. The chromatograms for the parent AMK samples show single peaks with increasing elution volumes (decreasing molecular weight) as levels of degradation increased. The undegraded AMK sample shows a broad peak from approximately 1 to 4 million, the intermediate V_T = 2.1 cm/sec peaks at approximately 600,000 and the highly degraded V_T = 6.7 cm/sec sample peaks at approximately 300,000. Several peaks appeared unexpectedly in the chromatograms of the gel (Figure 24B). The highest molecular weight peak occurs at about 5 million and appeared only as a shoulder on the V_T = 2.1 cm/sec AMK gel chromatogram. On the V_T = 6.7 cm/sec AMK gel chromatogram, the peak was fully developed. In both chromatograms, a second peak appeared at approximately 3 million, one-half the molecular weight of the first peak. The third and lowest molecular weight peak was at the same molecular weight as the degraded parent AMK. This peak may be due to the parent fuel being absorbed in the gel and may not be a part of the gel. The chromatogram of the gel from V_T = 0.8 cm/sec AMK did not show the presence of multiple peaks which may be due to the following explanation.

Gel that forms on filters may result from only the highest molecular weight constituents from the undegraded AMK which escaped degradation. The bimodal distribution of molecular weights may be present in the undegraded AMK parent sample but is masked due to the abundance of constituents with molecular weights centering around the peak molecular weight. Therefore, the composition of the gel would be relatively independent of the overall degree of degradation of the parent AMK, and only the concentration of the high molecular weight constituents would change as the degree of degradation increased. Thus, the rate of clogging would decrease with increasing levels of degradation.

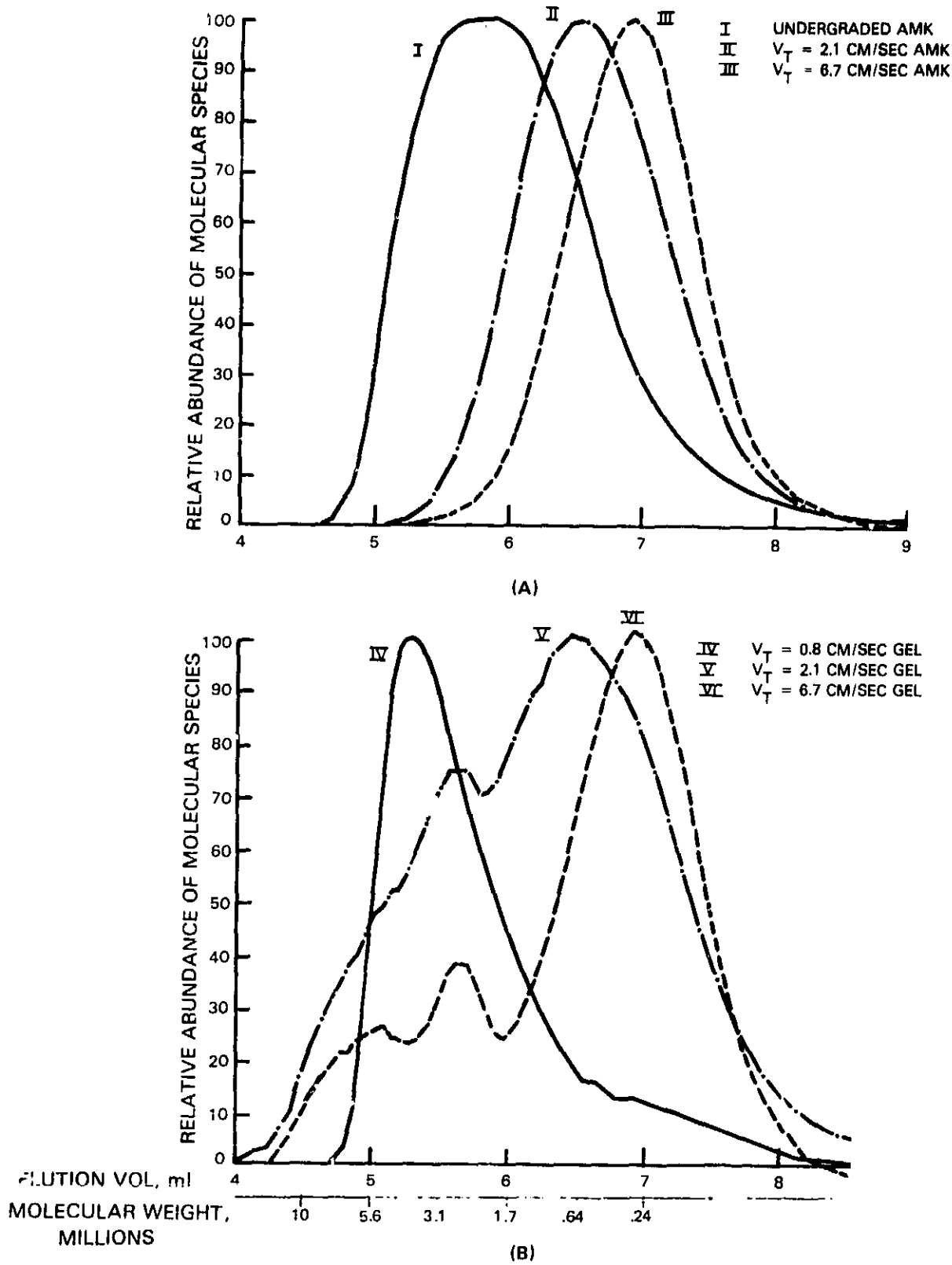

Figure 24 Gel Permeation Chromatograms of AMK and Flow Induced Gel

Figure 25 summarizes and compares the three degradation level measurement techniques; filter ratio (FR), Transition Velocity (V_T), and Gel Permeation Chromatography (GPC).

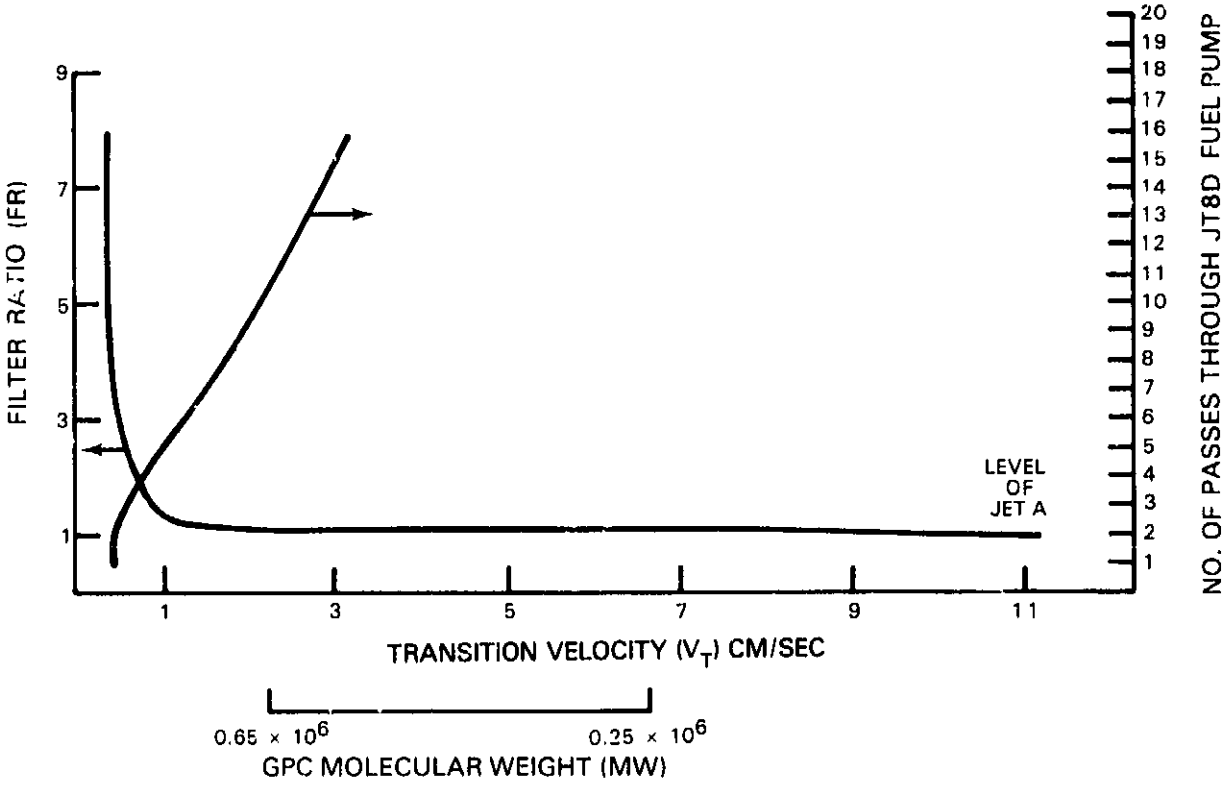

Figure 25 Comparison of Degradation Level Measurement Techniques

6.0 PERIPHERAL FUEL SYSTEM REQUIREMENTS

The use of antimisting additives may significantly impact the operation of the engine fuel system because of the changes in the physical and chemical characteristics of the fuel. Studies documented in this section include thermal stability, i.e., the propensity to form solids in the presence of elevated temperatures, heat transfer characteristics as related to the performance of oil coolers, corrosion in copper piping, and compatibility with fuel system component materials, in particular, nonmetallic seals. The following paragraphs discusses the results in these areas.

6.1 Thermal Stability

Thermal stability of jet fuel is important in preventing coking problems in the fuel delivery systems of the engine. To determine the effect of antimisting kerosene additive on fuel thermal stability, the Jet Fuel Thermal Oxidation Tester (JFTOT) was used, as summarized in ASTM D3241. A schematic diagram of the fuel flow scheme is shown in Figure 26. The fuel was pumped at a fixed flow rate of 3 ml/min. through an annular passage where the fuel was heated as it flowed around an electrically heated aluminum tube. After exiting the heating chamber, the fuel entered a stainless steel filter (17 μm nominal porosity) where fuel deposits were trapped. The test was run for 150 minutes and the pressure drop (ΔP) across the stainless steel filter was recorded every 30 minutes. During the 150-minute test, when the ΔP reached 25mm Hg, the filter was bypassed to complete the test. At the end of the test, deposits formed on the aluminum heater tube were compared with the ASTM Color Standard. The test failure criteria was a ΔP equal or greater than 25mm Hg or a deposit code of 3 or greater. To determine the thermal stability breakpoint (the temperature at which a failure occurs), tests were run at successively higher temperatures until failure occurred. Breakpoint tests were run with parent jet fuel, 3-pass (filter ratio = 1.6) and 16-pass (filter ratio = 1.2).

Data from these studies are shown in Table XVIII. A substantial increase in breakpoint is seen from the parent fuel to antimisting kerosene at all levels of degradation. The failure mode for antimisting kerosene is deposit code, failure due to deposits forming on the heated tube, while the failure mode for Jet A is pressure buildup on the metal filter.

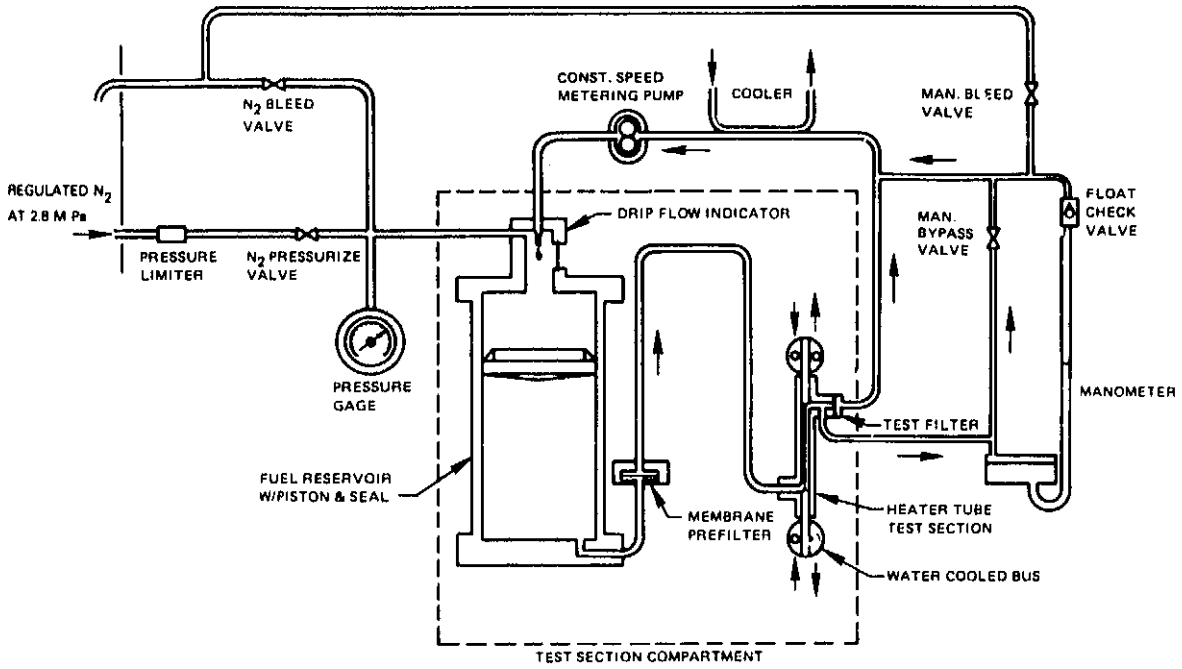

Figure 26 Thermal Stability Tester

TABLE XVIII
THERMAL STABILITY MEASUREMENTS ON ANTIMISTING KEROSENE

Sample	Test Temperature (°C)	ΔP (mm Hg)	Deposit Code
Parent Fuel	260	184	1
	245	55	1
	230	4	1
Undegraded Antimisting Kerosene	290	1	4
	275	1	4
	260	2	1
3-Pass Antimisting Kerosene	275	1	4
	260	0.5	1
16-Pass Antimisting Kerosene	290	0.5	4
	275	0.5	1

Sample	Breakpoint Range (°C)	Failure Mode
Parent Fuel	230-245	ΔP
Undegraded Antimisting Kerosene	260-275	Deposit Code
3-Pass Antimisting Kerosene	260-275	Deposit Code
16-Pass Antimisting Kerosene	275-290	Deposit Code

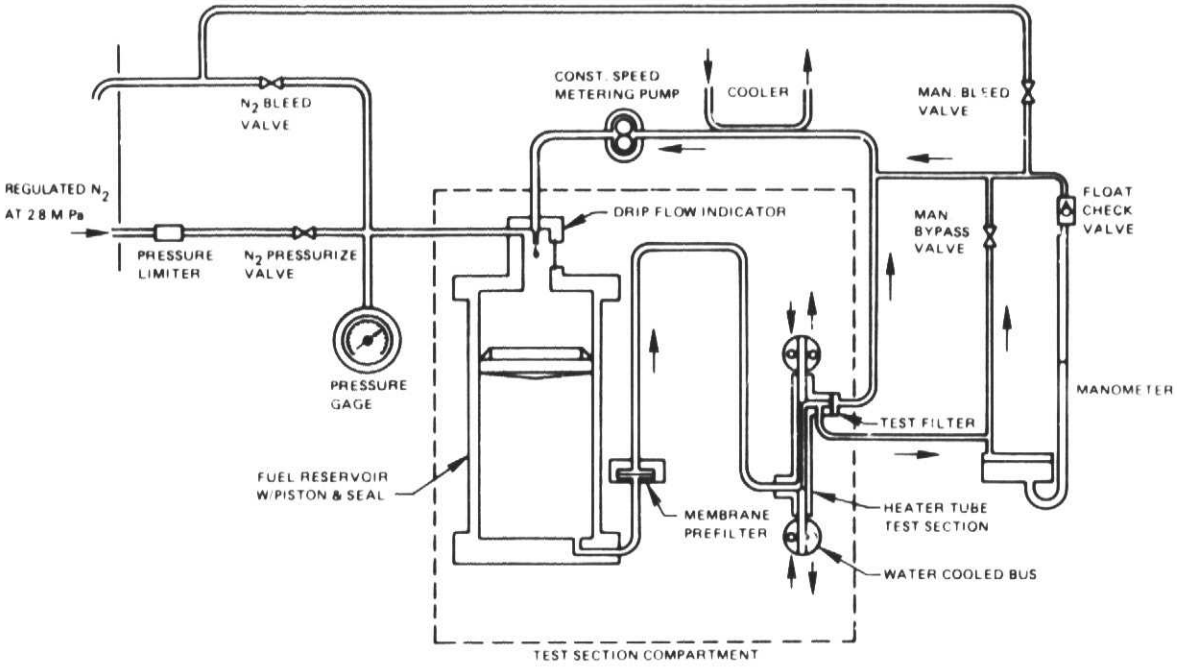

Figure 26 Thermal Stability Tester

TABLE XVIII
THERMAL STABILITY MEASUREMENTS ON ANTIMISTING KEROSENE

Sample	Test Temperature (°C)	ΔP (mm Hg)	Deposit Code
Parent Fuel	260	184	1
	245	55	1
	230	4	1
Undegraded Antimisting Kerosene	290	1	4
	275	1	4
	260	2	1
3-Pass Antimisting Kerosene	275	1	4
	260	0.5	1
16-Pass Antimisting Kerosene	290	0.5	4
	275	0.5	1

Sample	Breakpoint Range (°C)	Failure Mode
Parent Fuel	230-245	ΔP
Undegraded Antimisting Kerosene	260-275	Deposit Code
3-Pass Antimisting Kerosene	260-275	Deposit Code
16-Pass Antimisting Kerosene	275-290	Deposit Code

6.2 Copper Corrosion

It is suspected that copper corrosion may be a potential problem since some fuel system components are composed of alloys containing copper. Traces of copper in fuel at levels of less than .02 ppm have been responsible for degraded thermal stability. Also, some increases in wear rates at long time exposure might be expected on hardware components containing brass or copper. To determine if antimisting kerosene produced accelerated corrosion rates with copper, approximately 400 ml of antimisting kerosene fuel and parent fuel were equilibrated with light copper turnings for 48 hours. Samples of fuel were withdrawn from both parent and antimisting kerosene samples after 2, 24 and 48 hours and analyzed for dissolved copper directly by atomic absorption spectrophotometry using Conostan standards.

Measurements on the corrosion rate of copper in antimisting kerosene are tabulated in Table XIX. Copper dissolution was enhanced in antimisting kerosene. Some copper dissolved in the parent fuel; however, the rate appeared to slowdown after 24-hour exposure. Copper concentrations increased in the antimisting kerosene fuel throughout the period of the study.

TABLE XIX
COPPER CORROSION STUDY

Hours	PPM Cu	
	Antimisting Kerosene	Parent Fuel
2	0.05	0.02
24	0.64	0.05
48	1.5	0.05

6.3 Oil Cooler Heat Transfer

It is necessary to determine the effect antimisting kerosene has on the fuel heat transfer coefficient (h) in order to evaluate the fuel-oil cooler efficiency. Typical fuel-oil coolers used in aircraft gas turbine engines are shell and tube heat exchangers in which the fuel flows inside the tubes and the oil flows across the tubes. Because the fuel side is usually single pass, and the velocity is somewhat low, the fuel is usually turbulated to produce enhanced heat transfer coefficients. Pratt & Whitney Aircraft oil coolers are

typically constructed from tubes which are dimpled at frequent intervals to increase heat transfer coefficients. The heat transfer tests were conducted by flowing ambient temperature fuel through an aluminum tube surrounded by a 5 cm diameter shell (See Figure 27). The inner tube is 33 cm long with an outer diameter of 0.23 cm and an inner diameter of 0.17 cm. The fuel pressure was maintained above its thermodynamic critical pressure, 22 atm, throughout the tests. Saturated steam, at 5 atm, flowed through the shell. Due to the saturated nature of the steam and the large shell to tube volume ratio, the inner tube could be considered to be surrounded by a constant temperature reservoir.

A heat transfer test consisted of setting a fuel flow, adjusting the fuel pressure, turning on the steam, and allowing sufficient time for thermal equilibrium. Heat transfer coefficients were derived from an energy balance (conduction terms were neglected).

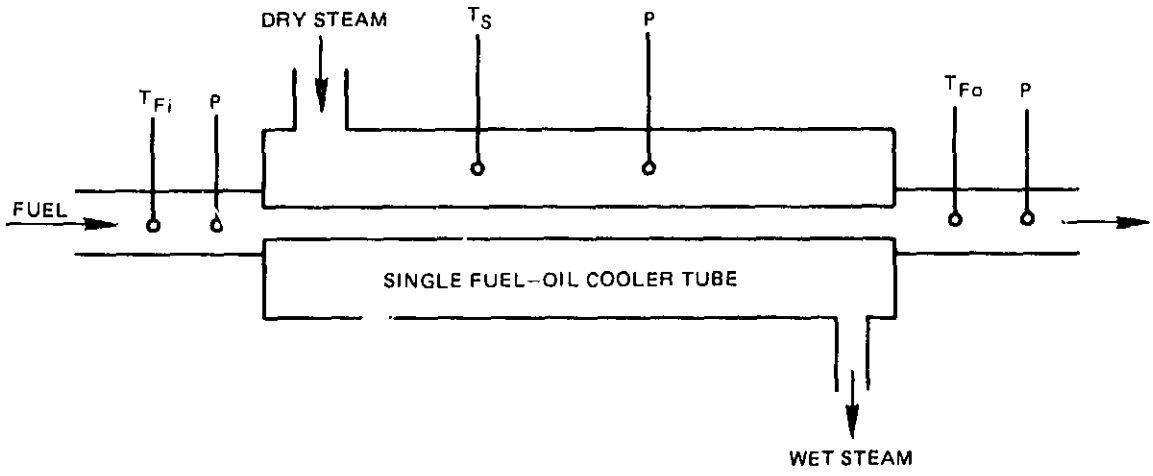

Figure 27 Heat Transfer Test Section

The results for Jet A, 3 and 1-pass degraded antimisting kerosene and unsheared antimisting kerosene are shown in Figure 28. The h of the Jet A increased with fuel flow rate as expected. This is consistent with results previously obtained at Pratt & Whitney Aircraft. Above 3.4 Kg/hr, the h of the undegraded antimisting kerosene was considerably different from that of the Jet A. Approximately between 4.5 and 10 Kg/hr, the h of the undegraded

antimisting kerosene leveled out and increased again beyond 10 Kg/hr. Similar qualitative behavior between AVTUR and FM-4 additive was reported by Medani and Hayes (3). The h of the 1-pass antimisting kerosene increased with fuel flow rate less rapidly than either the 3-pass antimisting kerosene or the Jet A and at about 19 kg/hr crossed over and remained below the undegraded h. The 3-pass degraded antimisting kerosene (~3 FR) was very similar to the reference Jet A. At low flow rates they were nearly identical, and at higher flow rates the 3-pass was about 10 percent lower than the Jet A.

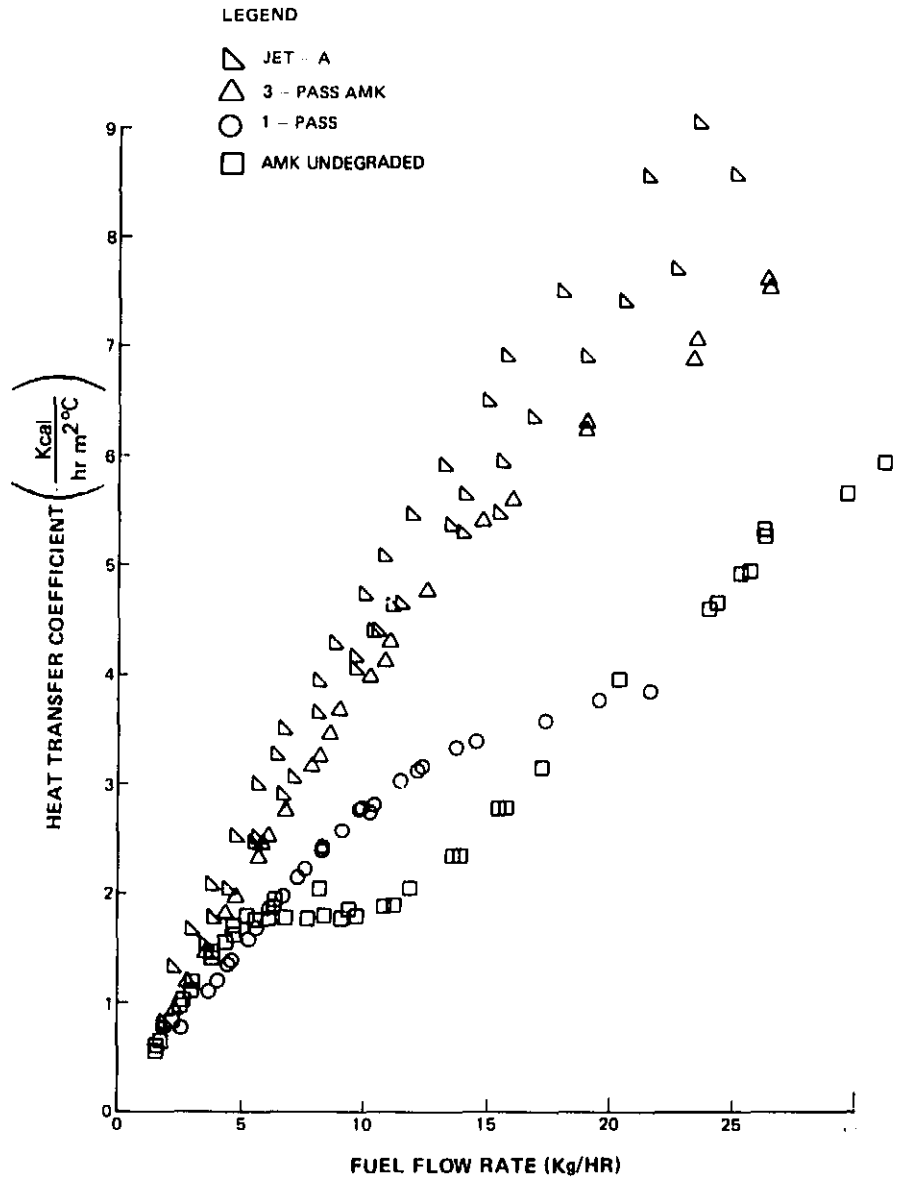

Figure 28 Effect of Antimisting Additive on Heat Transfer in Fuel-Oil Cooling Tubes

The performance of the 3-pass or FR 3 AMK was deemed acceptable, although marginally so, at the higher fuel flow rates. The 1-pass and undegraded antimisting kerosene were not acceptable for use in the existing engine component.

6.4 Materials Compatibility - Elastomers

During engine operation, fuel system components are continuously soaked by fuel. To evaluate the compatibility of the materials with antimisting kerosene three typical fuel system elastomers were tested in accordance with ASTM D1414-72. The materials were soaked in antimisting kerosene for 6 months and periodically inspected for changes in mechanical properties. Table XX lists the test variables.

TABLE XX
TEST VARIABLES FOR MATERIAL COMPATIBILITY TESTS

Common Name	AMS Specification	Military Specification	Part
Butadiene Rubber	7271	MS 9021	O-ring
Fluorosilicone Rubber	7273	MS 9967	O-ring
Fluorosilicone Rubber/ Fiberglass	-	-	Diaphragm (P&WA P/N 442375)
Fuels:			
Undegraded antimisting kerosene			
3-pass degraded antimisting kerosene			
Inspection Times:			
1 week; 1,2,3,4,5,6 months			
Fuel Temperatures:			
22°C			
67°C			
Measurements:			
Tensile strength			
Elongation			
Volume Change			
Hardness			

Butadiene rubber and fluorosilicone rubber are used in gas turbines at severe operating temperatures; up to 122°C and 177°C respectively. Results are presented as plots of elastomer immersion time in AMK versus volume change, tensile strength, elongation, and hardness in Figures 29 through 32 respectively. In all the tests minor differences were observed between the 1-pass and 3-pass antimisting kerosene. Therefore, the test data is reported as an average of the results obtained for each of the two fuels. Three samples were run for each test point resulting in an average of 6 tests for each point. Within experimental accuracy, little change occurred beyond 1 week for any of the measured properties.

The fluorosilicone exhibited a volume change (Figure 29) of less than 15 percent and was insensitive to temperature. The other two elastomers have volume changes in excess of 50 percent with the fluorosilicone/fiberglass elastomer displaying appreciable temperature dependence.

Reduction in tensile strength for both the fluorosilicone and Butadiene (Figure 30) was significant. Tensile strength of the fluorosilicone and butadiene was re duced by one-third. Elongation of the fluorosilicone (Figure 31) was negligible while the Butadiene decreased by about 1/3.

Hardness (Figure 32) of the butadiene and fluorosilicone was unchanged at practically both 22°C and 67°C. Inspection of the elastomers at the conclusion of the 6 month testing showed no cracks or material crazing in any of the test specimens. Also, as mentioned earlier, the measured mechanical properties stabilized after one week of soak- ing. Based on these results and from test results obtained with Jet A, it was concluded that the materials tested are compatible with antimisting kerosene.

Inspection of the elastomers at the conclusion of the 6 month testing showed no cracks or material crazing in any of the test specimens. Also, as mentioned earlier, the measured mechanical properties stabilized after one week of soaking. Based on these results and from test results obtained with Jet A, it was concluded that the materials tested are compatible with antimisting kerosene.

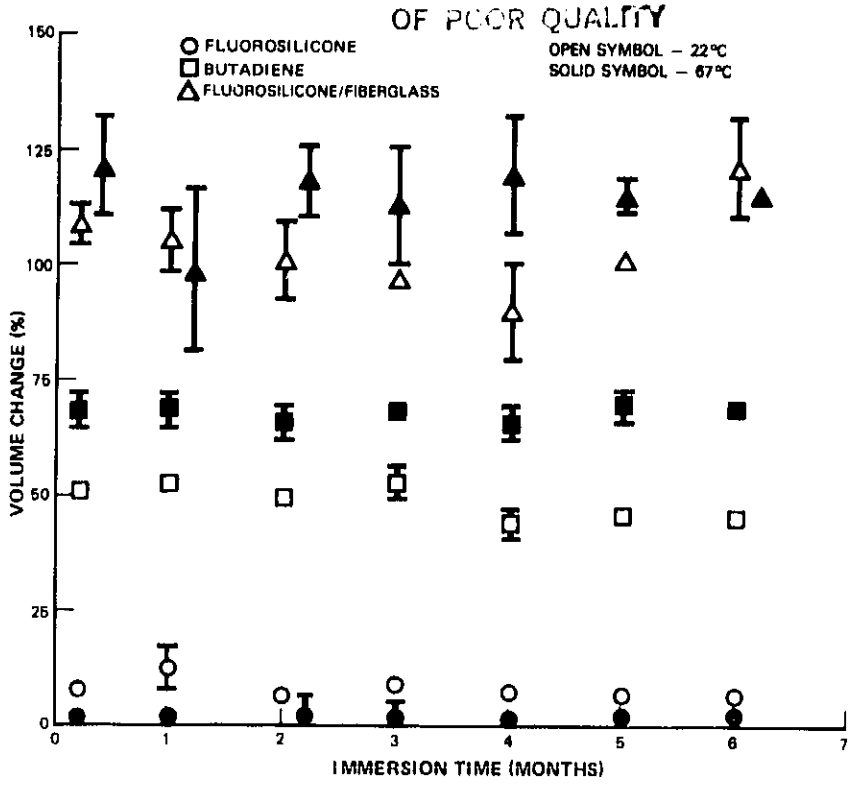

Figure 29 Effect of Volume Change on Elastomers Immersed in AMK

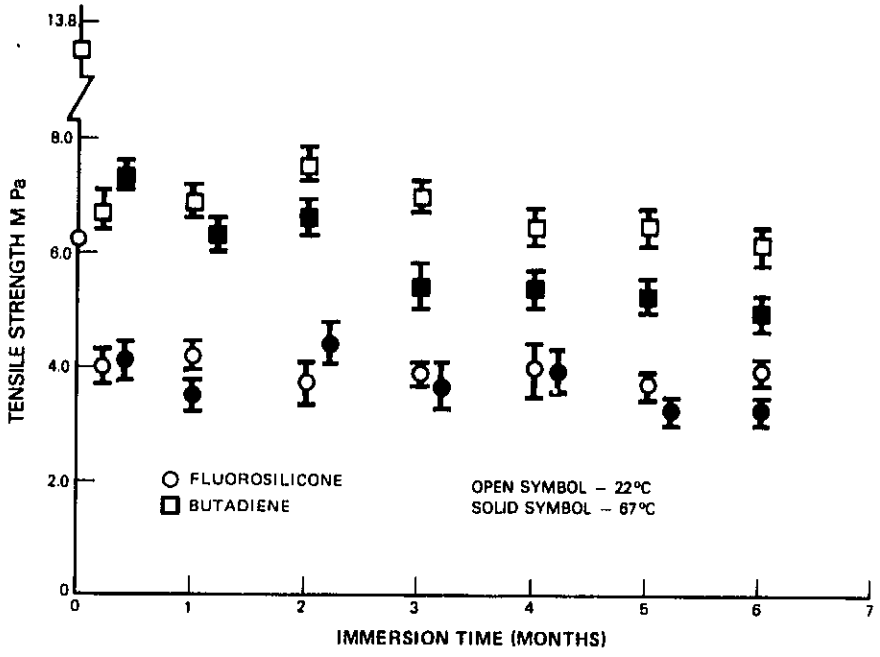

Figure 30 Effect of Tensile Strength on Elastomers Immersed in AMK

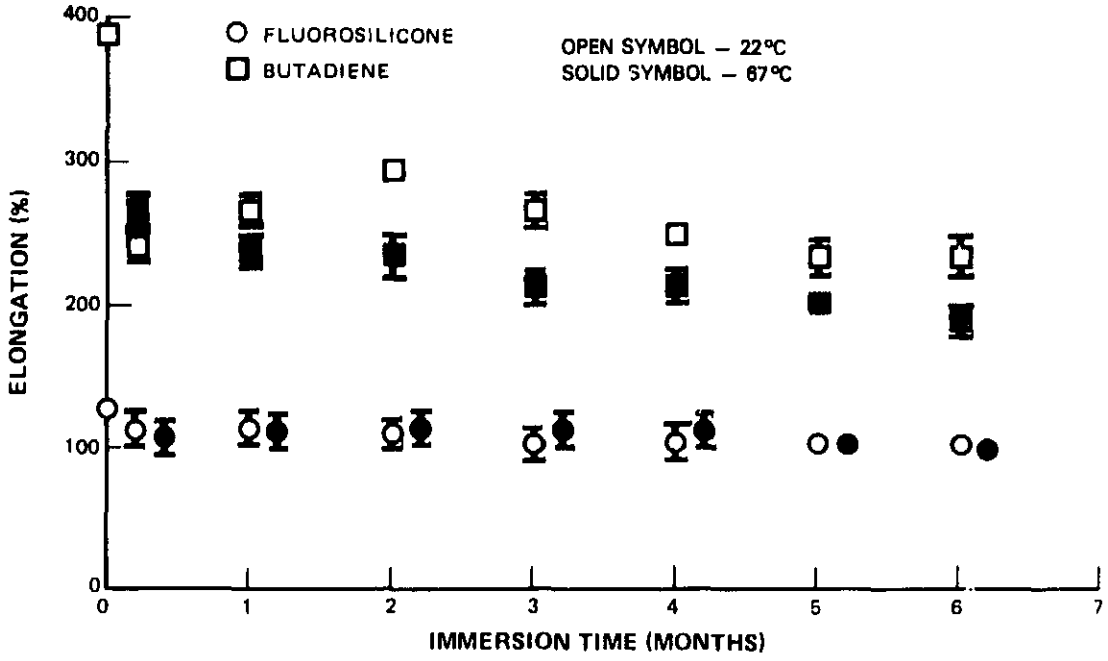

Figure 31 Effect or Elongation on Elastomers Immersed in AMK

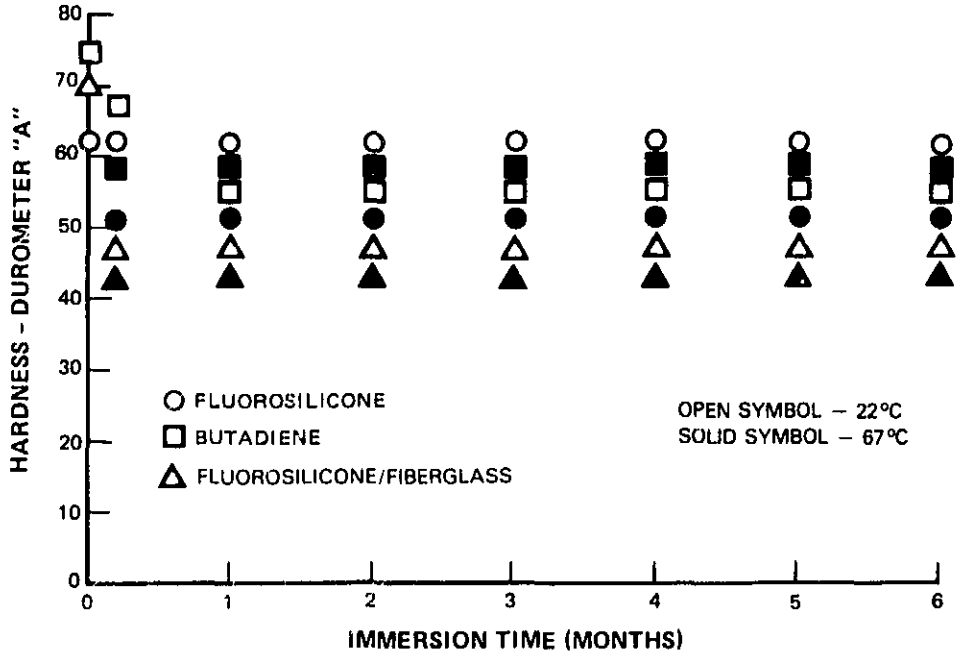

Figure 32 Effect of Hardness on Elastomers Immersed in AMK

7.0 FILTERABILITY EXPERIMENTS

Since filter construction and size is determined concurrent with the upstream system pressure capability, filter bypass valves and requirements of downstream components, the normal flow pressure drop characteristics of the filter must be maintained. Therefore, it was essential to determine the effect of the FM-9 additive on filters as related to fluid viscosity, accumulation or buildup of deposits on the filter elements, and interaction with water or fuel borne ice crystals which would affect the fuel de-icing operation.

It was found earlier that gelling, a clogging phenomenon, is velocity sensitive regardless of the fuel degradation level. Therefore, the test filters were selected where the combination of mass flow and flow area yielded the highest velocities in the fuel system. Typical flow requirements for critical filters in Pratt & Whitney current engines are tabulated below. Although the JT9D engine was the reference engine of the program, the worst case condition was found to exist for the JT9D engine ph filter (pressure/ hydraulic fuel loop), and it was therefore included in the testing. During the program, filtration data was also tabulated for 8 μm Nuclepore membrane and 17 and 26 μm Dutch weave screen.

	Superficial Velocity -34°C (cm/sec)	Jet A Normalized (True) Vel.(cm/sec) 239°K	293°K Ambient	322°K
8D Wash Flow 325 Mesh (45 μm)	11	300	140	110
8D 40 μm Paper	0.4	210	100	70
9D PH 325 Mesh Screen (45 μm)	25	450	250	190

Fuel flow velocity was defined as: 1) superficial velocity which is based on the pipe cross-sectional area in which the filter is placed and 2) true or normal velocity which is based on a flow coefficient corrected flow area (AC_D).

7.1 Short Term Filterability Testing

Tests were conducted to measure the pressure drop across the filters as a function of fuel flow rate using Jet A and AMK.

A schematic diagram of the short term filterability test is shown in Figure 33. This rig allows filterability measurements to be made as a function of degree of AMK degradation, pressure, temperature and filter type. Fuel is driven from a piston-type accumulator (capacity 9.5 ℓ) by high pressure nitrogen through a heat exchanger to control temperature. Sub-ambient fuel was achieved by the use of the Neslab ULT-80 cooler while above ambient temperatures are controlled with a heated oil bath. The fuel then passes through the filter holder which is instrumented for temperature and pressure drop across the filter. The fuel then flows to a catch vessel suspended from a load cell which produces a signal proportional to the weight of fuel it contains. The weight of fuel and pressure are continuously recorded throughout the test. System pressure and temperature are recorded at regular intervals.

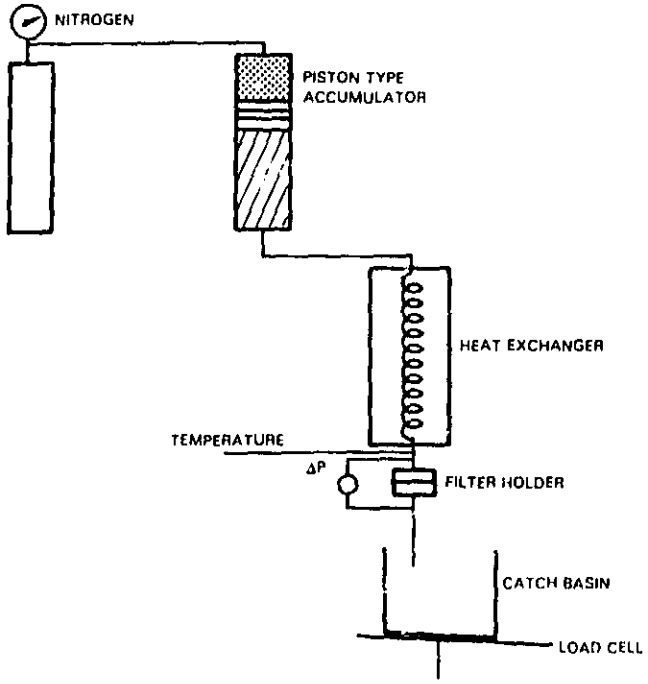

Figure 33 Short Term Filterability Apparatus

Two filter-holding chambers were constructed for use with the device. The first assembly, shown in Figure 34, was machined from aluminum and was designed primarily for wire screen filters. The flow area of the first assembly (.32 cm^2) was designed smaller than the second assembly to accommodate the higher flow velocities normally encountered through wire mesh screens and to give a test of reasonable duration. The second assembly, shown in Figure 35, is a modification of a standard Millipore filter holder with a flow area of 3.90 cm^2. Care must be exercised when using small filter areas to prevent bias results due to clogging with debris that may be present in the test fuel. A large surface area, 10 μm paper filter was placed upstream of the test filter in all the filter experiments.

The 325 mesh screen shown in Figures 36 and 37 was used in the JT8D wash flow filter. The filter consisted of two metal screens in a sandwich construction with the finer 325 mesh (45 μm openings) on the downstream side of the larger mesh screen. It was assumed the 40 μm paper filter would be the limiting filter because of the finer distribution of pores. AMK fuel was degraded ultrasonically to a transition velocity of 5.2 cm/sec and filterability tests were run first with the 325 mesh wash filter, and, subsequently, with a 40 μm paper filter. The tests were run at -35°C because filterability problems are more apt to occur at lower temperatures. Results of the study are shown in Table XXI. The paper filter allowed a flow rate of up to five times the maximum flow rate of the JT9D engine at takeoff with no indication of clogging. The 325 mesh wire screen filter showed no clogging until a flow rate of 19 cc/sec-cm^2 where clogging was noted at a rate of approximately .83 KPa/min (.12 psid/min). A flow rate of 19 cc/sec-cm^2 is well in excess of the rate the wash flow filter would be expected to operate in a JT8D engine; however, the same screen is used in a JT9D filter component where the flow rate must reach 25 cc/sec-cm^2. This test showed that the most severe filterability application is through wire screen filters for P&WA JT8D and JT9D engines because of the very high flow rate per unit area during normal operation.

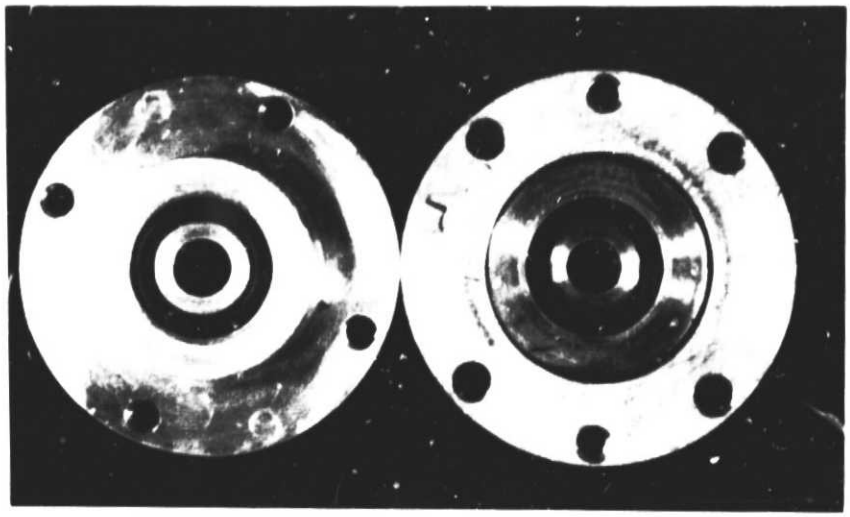

TOP VIEW

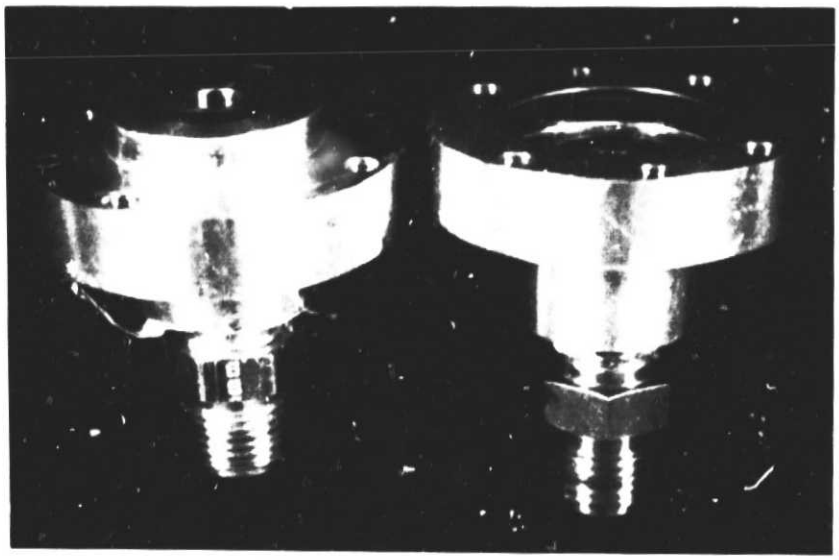

SIDE VIEW

Figure 34 Filter Holder (Flow Area, .32 cm^2)

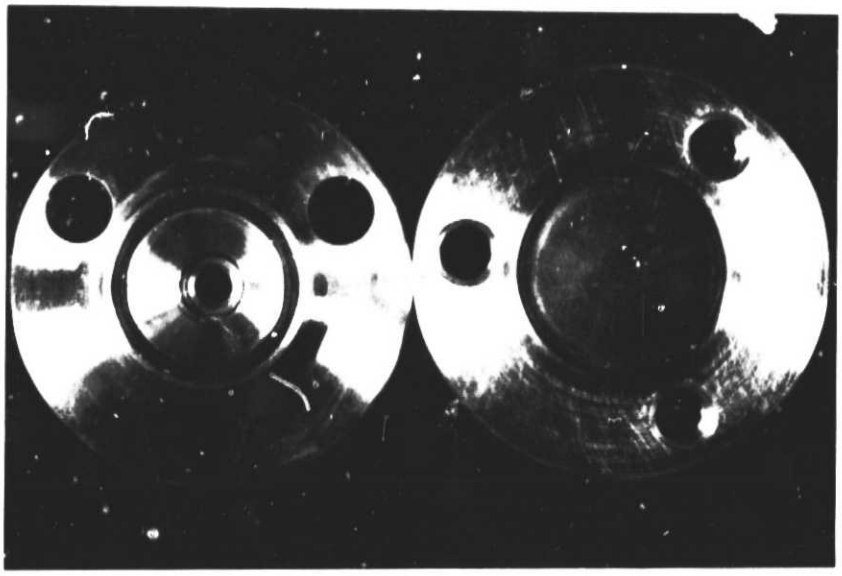

TOP VIEW

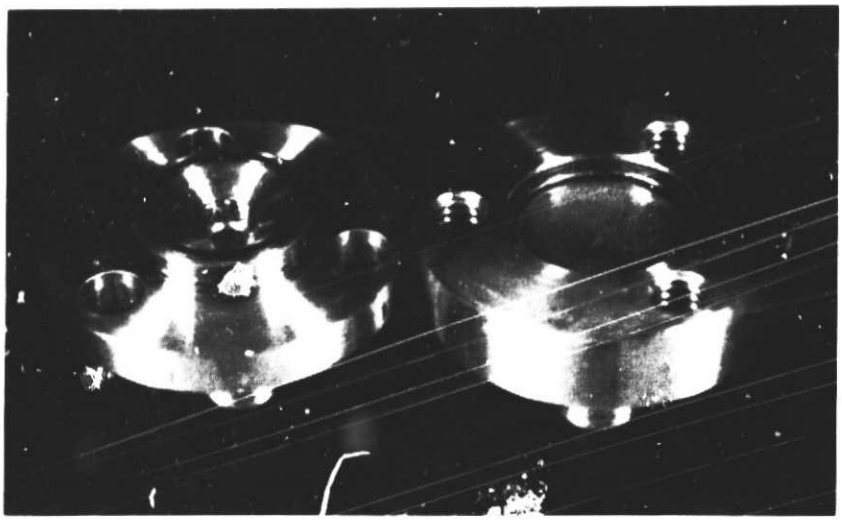

SIDE VIEW

Figure 35 Filter Holder (Flow Area, 3.90 cm^2)

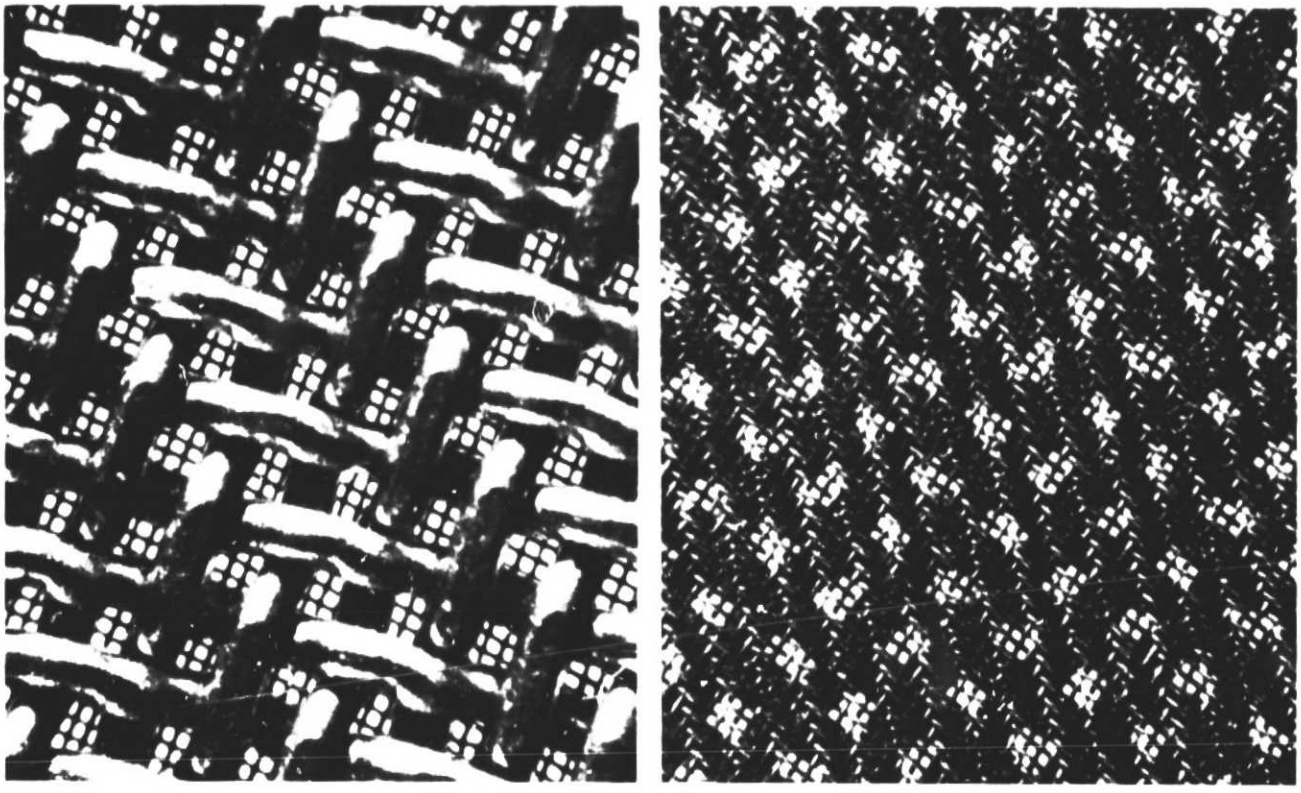

Figure 36 325 Mesh Screen Used in the JT8D Wash Flow Filter

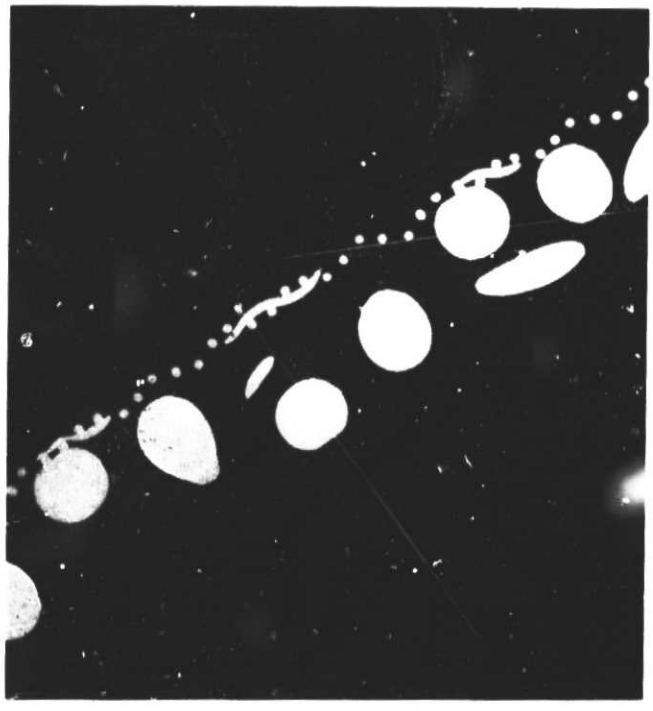

Figure 37 Wash Flow Filter Cross-Section

TABLE XXI
CLOGGING BEHAVIOR OF DEGPADED AMK (V_T = 5.2 cm/sec)
THROUGH 325 MESH SCREEN AND 40 μm PAPER FILTERS AT -35°C

Filter Type	Flow Rate (cc/sec-cm^2)	ΔP (KPa)	Clogging Rate (KPa/Min)
325 Mesh Screen	3	6.9	ND
	9	13.8	ND
	16	13.8	ND
	19	13.8-20.7	.83 (.12 psi/Min)
40 μm Paper	.26	6.9	ND
	.51	6.9	ND
	.90	13.8	ND
	2.3	13.8	.28 (.04 psi/Min)

Note: ND = Not detected

The effect of changing filter media and pore size on superficial flow-pressure characteristics of antimisting kerosene degraded by one pass through the Gaulin disperser at 41.4 MPa (6000 psi) is shown in Figure 38 (V_T=4.4 cm/sec). Clogging is indicated by two points at the same superficial velocity connected by a vertical line. The data indicated clogging behavior and pressure versus superficial velocity depended on the type of filter and pore size. The clogging appeared highly dependent on pore size with the smallest pore size filters clogging at the lowest velocities.

The data were again analyzed by plotting true velocity versus pressure for the different filter types. True velocity is defined utilizing a flow coefficient corrected area. Flow coefficients were determined for each filter as a function of flow rate during Jet A calibrations. In Figure 39, the flow behavior of the antimisting kerosene formed a single curve with some scatter for all types of filter materials and pore sizes. This indicated relative independence of velocity-pressure characteristics for different filters with antimisting kerosene and that the behavior of antimisting kerosene degraded to some particular level might be predicted in any filter.

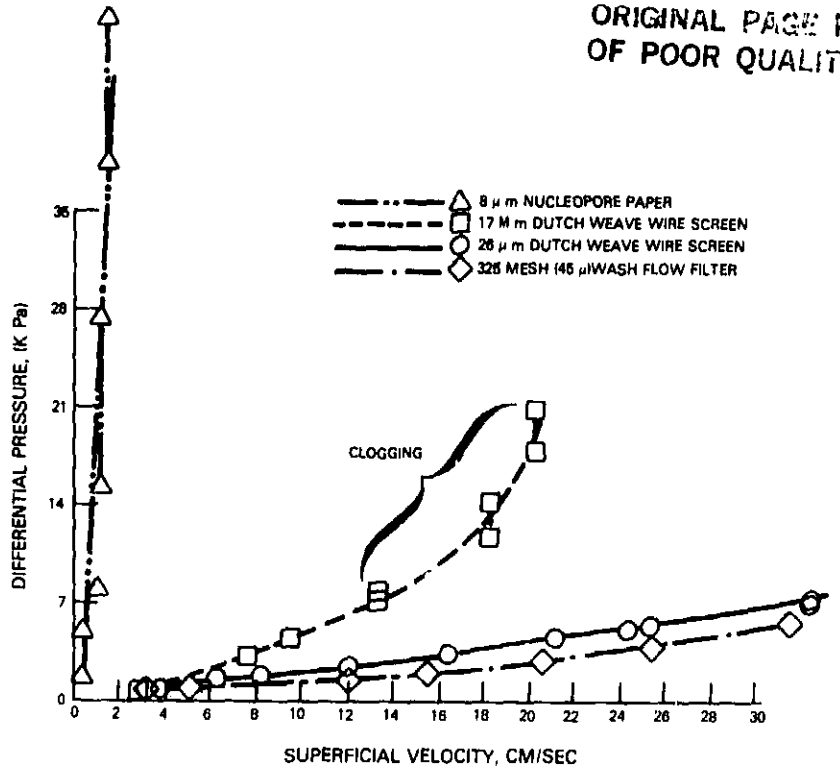

Figure 38 Effect of Changing Pore Size on Flow Characteristics of AMK Through Filters at Room Temperature, V_T=4.4

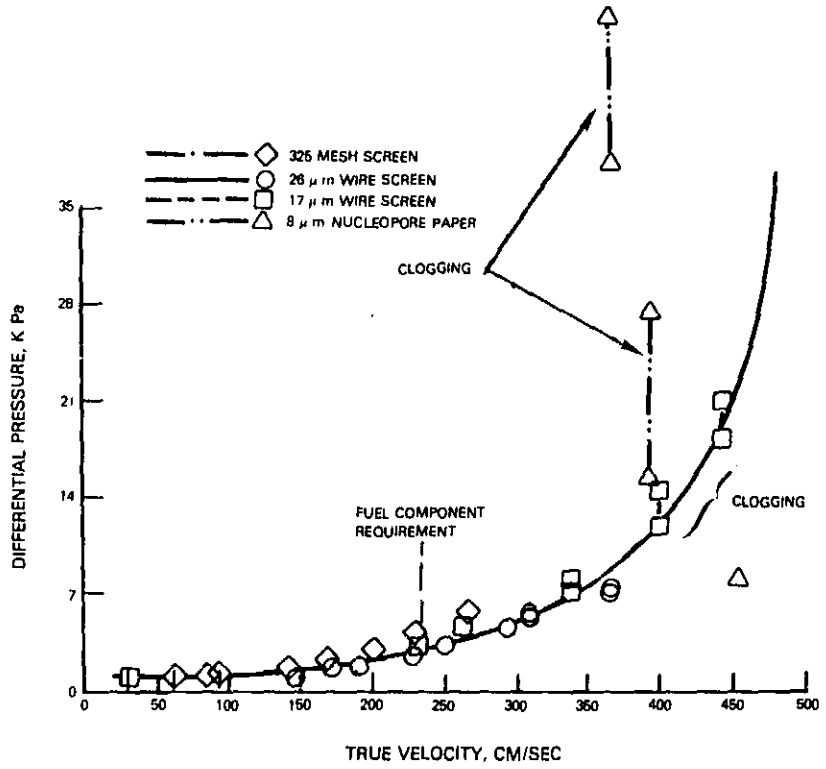

Figure 39 Effect of True Velocity on Flow Characteristics of AMK Through Filters at Room Temperature, V_T=4.4 cm/sec

7.2 Additional Short Duration Testing (325 Mesh Wash Flow Filter)

There was concern that filter clogging, not detected in short term tests (approximately 1 to 2 minutes), might occur after the filter operated at longer times which were more typical of normal flight operation. In short term laboratory testing, antimisting kerosene degraded by one pass through the Gaulin disperser at 55.2 MPa (8000 psi) did not clog the 325 mesh wash flow filter at JT8D normal flow rates (12 cc/sec-cm^2) at -35°C. To investigate the effect of extended operation, a five hour laboratory test was devised using these same conditions of flow and temperature. Because of the longer time for the test and the small filter area, .32 cm^2, a baseline test was first run with neat Jet A followed by the test with antimisting kerosene to ensure that small amounts of debris from handling and the test apparatus would not produce some filter clogging. The results of the extended duration test are shown in Figure 40.

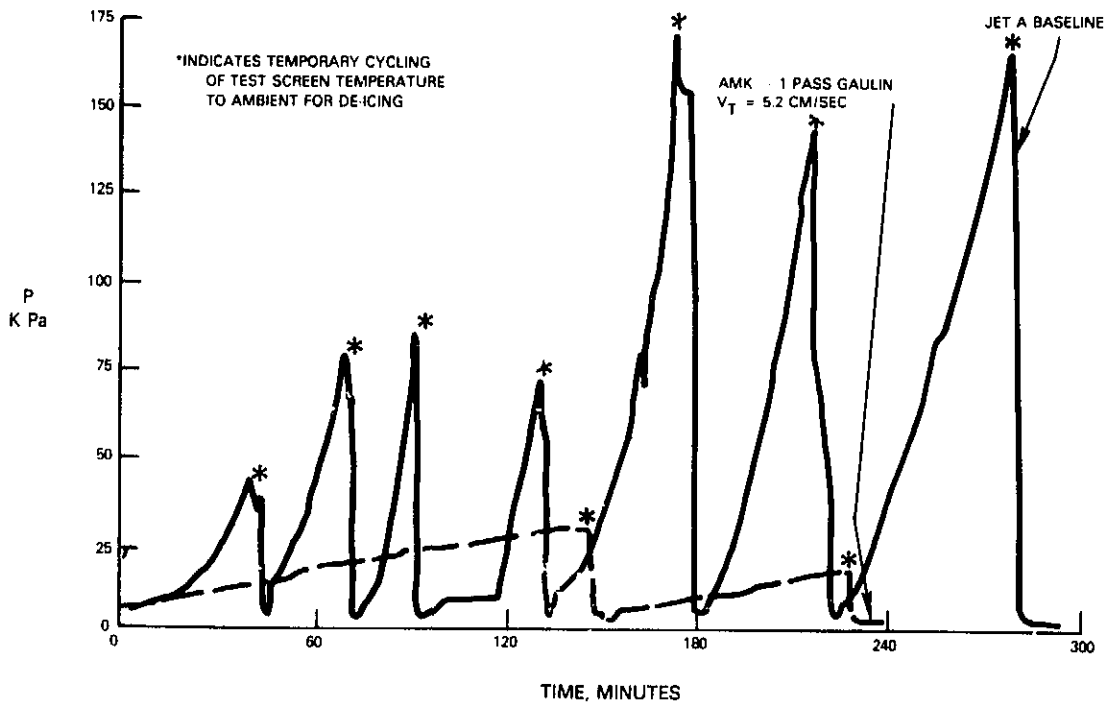

Figure 40 Duration Comparison of Jet A and AMK Through a 325 Mesh Wash Flow Filter Screen at 12 cc/sec-cm^2 and a Temperature of -35°C(-30°F)

After running the baseline Jet A test for approximately 15 minutes, some clogging was indicated by a pressure increase across the filter. The pressure increased to about 34.5 KPa (5 psi) after approximately 30 minutes. This pressure increase might be due to ice formation on the filter. To confirm the presence of ice, the filter housing was removed from the -35°C bath and allowed to reach a temperature greater than 0°C. At this point the starting pressure was recovered, confirming the presence of ice.

Over the five hour period, a total of seven de-icing cycles were run. At the end of the five hours there was no detectable pressure increase across the 325 mesh wash flow filter. The test was repeated with antimisting kerosene at the same conditions of temperature and flow. The AMK was tested on a single pass basis; it was not recirculated. Again, clogging was seen but at a much reduced rate relative to the neat Jet A. After 150 minutes the pressure differential across the filter increased to only 27.6 KPa (4 psi). To determine if the pressure buildup was due to ice or gel formation, the filter housing was removed from the bath and allowed to reach 0°C. The pressure at that point had returned to its original value. The filter housing was returned to the bath and the test continued for a total time of approximately 240 minutes. At this point the filter housing was again removed from the bath and allowed to come to room temperature. No pressure differential from that at the beginning of the test was observed. The remaining fuel was used to record the ambient pressure-velocity relationship for the test fuel. The results are shown in Figure 41. Clogging due to antimisting kerosene gel was observed at a true velocity of approximately 450 cm/sec.

The reduced rate of pressure buildup on the antimisting kerosene test relative to the neat Jet A test may be due to several factors. If one assumed that the pressure increase in both cases was entirely due to ice formation, the water content of the net Jet A may have been higher than that for the antimisting kerosene fuel. Secondly, it was reported that a small amount of glycol is part of a chemical carrier that aids in FM-9 dispersion in jet fuel. This glycol may influence the icing behavior of the antimisting kerosene. Finally, the FM-9/carrier combination may affect the wetting or sticking behavior of ice to the filter. The tests indicated that for periods as long as four hours there

was no indication of gel-induced filter clogging with antimisting kerosene degraded by one pass through the Gaulin disperser under flow conditions typical of the JT8D wash flow filter at -35°C.

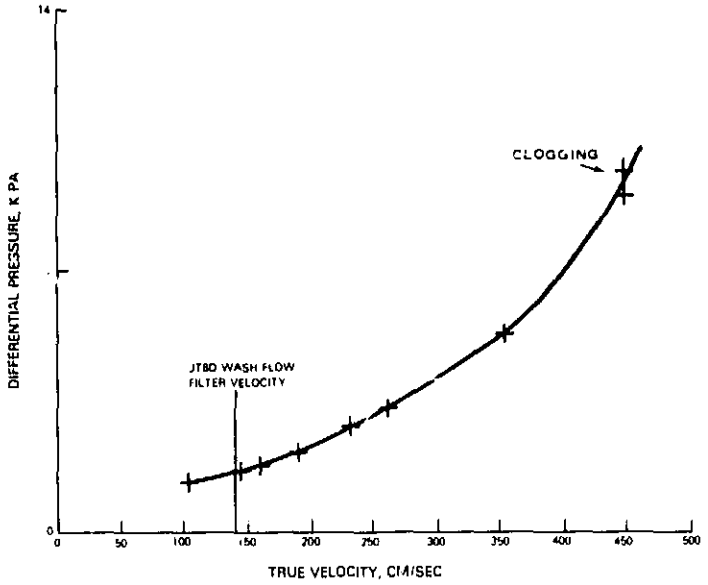

Figure 41 Velocity-Pressure Curve for Duration Test Fuel Through 325 Mesh Wash Flow Filter, T_f=20°C(70°F), V_T=5.2 cm/sec

7.3 Effect of Changing Temperature On Filter Flow Characteristics

The effect of changing temperature on flow characteristics of antimisting kerosene degraded by one pass through the Gaulin disperser at 55.2 KPa (8000 psi) through the 325 mesh wash flow filter is shown in Figure 42. The transition velocity of the test fuel was 5.2 cm/sec. Flow-pressure curves were measured for the test fuel at temperatures of 22°C, 0°C and -35°C. No filter clogging was observed at either 22°C or 0°C throughout the range of flow rates normally encountered in JT8D or JT9D engines. At -35°C clogging was observed at a superficial velocity of approximately 15 cm/sec. Experience gained in the extended duration test showed that the clogging noted at -35°C may be due to icing rather than gelling.

Results of filterability experiments for various levels of degradation at temperatures of -35°C, ambient and 50°C and with various filters are summarized in Tables XXII through XXIV. Because of the point by point nature of data measurement, the last point at which no filter clogging was noted is given as well as the first point where filter clogging was seen.

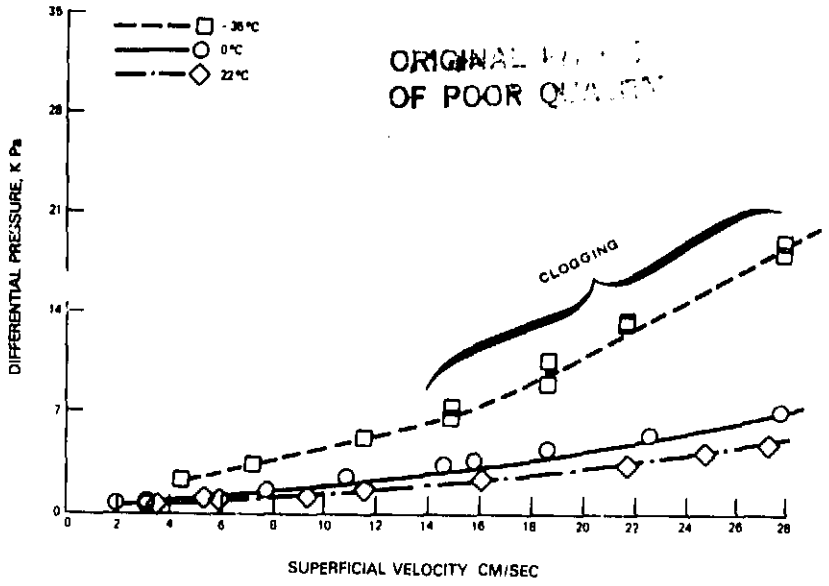

Figure 42 Effect of Changing Temperature on Flow Characteristics of AMK Through 325 Mesh Wash Flow Filter, V_T=5.2cm/sec

TABLE XXII
FLOW BEHAVIOR OF AMK THROUGH FILTERS AT -35°C

Degradation Level V_T(cm/sec)	Filter Type	Superficial Velocity (cm/sec) No Indication of Filter Clogging	Superficial Velocity (cm/sec) First Indication of Filter Clogging	Jet A Normalized (True) Vel. (cm/sec) No Indication of Filter Clogging	Jet A Normalized (True) Vel. (cm/sec) First Indication of Filter Clogging
0.8	17 μm screen	-	2.3	-	270
1.9	↓	6.6	7.8	440	460 - 17 μm
4.4	↓	9.7	13.1	510	600
0.8	325 mesh screen 45 μm	2.8	3.1	160	180
1.9	↓	12	13.4	240	370 - 45 μm
5.2	↓	12	15	340	530
7.0	↓	26	-	530	-
1.9	40 μm paper	0.46	0.64	230	260 - 40 μm
5.2		0.9	2.3	300	480

TABLE XXIII
FLOW BEHAVIOR OF AMK THROUGH FILTERS AT AMBIENT TEMPERATURES

Degradation Level VT	Filter Type	Superficial Velocity (cm/sec) No Indication Filter Clogging	Superficial Velocity (cm/sec) First Indication of Filter Clogging	Jet A Normalized (True) Vel. (cm/sec) No Indication Filter Clogging	Jet A Normalized (True) Vel. (cm/sec) First Indication of Filter Clogging
0.8	17μm screen	7.5	14	270	390
1.9	↓	9.4	12	300	350
2.5	↓	17	19	420	450
4.4	↓	9.4	13	300	360
2.5	26μm screen	30	44	370	460
4.4	↓	25	32	330	390
5.2	↓	56	-	560	-
7.0	↓	14	-	240	-
4.4	325 mesh screen 45 μm	31	-	280	-
5.2	↓	28	-	250	-
7.0	↓	26	-	260	-

TABLE XXIV
FLOW BEHAVIOR OF AMK THROUGH FILTERS AT 50°C

Degradation Level V_T(cm/sec)	Filter Type	Superficial Velocity (cm/sec)		Jet A Normalized (True) Vel. (cm/sec)	
		No Indication of Filter Clogging	First Indication of Filter Clogging	No Indication of Filter Clogging	First Indication of Filter Clogging
1.0	17 μm screen	4.4	6.2	170	210
1.9		10	13	260	310
3.5		9.1	13	250	310
3.7		12	14	300	330
1.0	325 mesh screen 45 μm	22	30	180	230

The highest velocity requirement for Pratt & Whitney Aircraft engine filters is that for a hydraulic fuel filter (325 mesh screen), the PH filter, which is required to flow at a superficial velocity of 25 cm/sec at takeoff or 450 cm/sec normalized velocity at -35°C. To meet this requirement, AMK must be degraded to very high levels (V_T=7 cm/sec) as shown in Table XXII. Maximum flow requirements for the 40 μm paper filter are met at much lower levels of degradation. While the superficial velocity required to cause clogging varies greatly with the type of filter and pore size, the normalized velocity or true velocity does not vary over nearly as great a range. At the lowest levels of degradation (V_T = 0.8 and 1.0 cm/sec), there is much scatter in the experimental data, and this trend is not clearly seen. These observations may result in the ability to predict the clogging behavior of untested filters if the pressure-flow characterstics of the filter are known with Jet A fuel.

Fuel Temperature	Range of Superficial Velocity Where Clogging Was First Noted (cm/sec)	Range of Jet A True (Normalized) Velocities Where Clogging Was First Noted (cm/sec)
-30°F	0.64 to 15	260 to 600
Ambient	12 to 44	350 to 460

Additional short duration filter tests were run. Fuel for the tests was prepared by degrading AMK with the Gaulin Disperser at 13.8, 41.4 and 55.2 MPa for one pass. Transition velocities of 1, 5.3 and 6.4 cm/sec were recorded for the three test fuels, respectively. Test filters included the 17 μm and 26 μm

Dutch weave metal screens, and the 325 mesh wire screen used in fuel control applications (Tables XXV - XXVII). Clogging tests with transition velocity 2.7 cm/sec AMK were run at 21°C and -33°C with the 40μm paper filter used as the fuel pump filter in Pratt & Whitney engines (Table XXVIII). The data again confirm that the AMK flow rate, where clogging is initiated, varies with filter pore size. Larger pores allow higher flow rates before clogging occurs. When flow rates are normalized to true velocities, the variation in clogging velocity is much less dependent on filter pore size or filter material. Figure 43 summarizes the short term filter data measured in the current test program, including types of filters and test temperatures varying from -35°C to +49°C.

A filtration experiment was conducted to determine if complete clogging could occur at flow velocity conditions known to produce a significant clogging rate such as those listed in Table XXV and illustrated in Figure 43. AMK fuel was degraded by one pass through the Gaulin Disperser at 2000 psi to produce a transition velocity of 1 cm/sec which corresponds to a filter ratio of less than 2. The degraded fuel was passed through a 17 m Dutch weave screen at a flow rate of 8 cc/sec-cm^2 at -35°C (-30°F) which results in a Jet A normalized velocity greater than 500 cm/sec. At these conditions, filter clogging occurred within several minutes and the flow rate decreased as the initial differential pressure of approximately 10 psi across the filter was maintained. The pressure across the filter was gradually increased in order to maintain 8cc/sec/cm^2 flow up to a total pressure drop of approximately 95 psi. Within minutes, the flow rate dropped significantly and soon stopped completely. Thereupon the temperature of the filter and housing was increased to approximately 45°C(114°F) and in approximately 20 minutes, the original flow was reset at a corresponding differential pressure of 25 psi. This test sequence was repeated twice more with nearly identical results.

TABLE XXV
CLOGGING CHARACTERISTICS OF TRANSITION VELOCITY 1 cm/sec AMK

Temperature (°C)	Filter	Flow Rate (cc/sec-cm^2)	Jet A Normalized Velocity (cm/s	Clogging Rate (KPa/sec)
21	17 μm	3.8	190	--
		6.2	248	24.8
		8.4		51.7
		12.88		41.4
		15.9		93.1
		18.8		120.7
		21.9		107.6
21	26 μm	10.0	224	--
		14.1	243	49.0
		20.6		39.3
		26.6		74.5
22	325 mesh	20.0	370	331.0
		25.0		1110.3
		35.6		2700.3
-33	17 μm	1.2		--
		2.2		--
		4.4	400	--
		7.5	507	161.4
		10.0		703.4
		12.5		1262.1
-33	325 mesh	4.0		--
		8.3		--
		10.6	392	--
		12.8	400	34.5
		14.7		75.9
		15.6		133.8
		18.4		254.5
		22.2		377.9
		28.8		617.9

TABLE XXVI

CLOGGING CHARACTERISTICS OF TRANSITION VELOCITY 5.3 cm/sec AMK

Temperature (°C)	Filter	Flow Rate (cc/sec-cm^2)	Jet A Normalized Velocity (cm/sec)	Clogging Rate (KPa/sec)
23	17 μm	2.8	-	--
		4.1	195	--
		6.6	254	22.8
		9.4	-	91.7
		10.9	-	248.3
		15.0	-	405.5
		20.0	-	737.9
23	26 μm	11.2	-	-
		21.2	424	--
		30.6	443	5.3
		40.0	-	69.0
		50.0	-	46.2
		60.0	-	57.2
23	325 mesh	19.1	367	--
		35.0	407	26.2
		42.5	-	22.8
		50.0	-	34.5
		55.2	-	34.5
		68.8	-	46.2
-33	17 μm	5.6	-	--
		7.8	-	--
		10.9	605	--
		14.1	671	17.2
		18.8	--	63.4
		22.5	--	184.1
		27.5	--	264.
-33	325 mesh	23.1	469	--
		33.1	532	11.7
		41.9	--	60.7
		52.5	--	126.2
		56.2	--	155.2
		75.0	--	215.9

TABLE XXVII
CLOGGING CHARACTERISTICS OF TRANSITION VELOCITY 6.4 AMK

Temperature (°C)	Filter	Flow Rate (cc/sec-cm^2)	Jet A Normalized Velocity (cm/sec)	Clogging Rate (KPa/sec
22	17 μm	12.5	--	--
↓	↓	16.9	420	--
		25.0	520	29.0
		28.8	--	55.2
		32.8	--	57.2
		47.5	--	80.7
22	26μm screen	18.1	--	--
↓	↓	21.2	--	--
		25.6	--	--
		32.5	--	--
		36.2	--	--
		40.0	--	--
		52.5	--	--
		56.2	--	--
		81.2	419	--
22	325μmesh	50.0	--	--
↓	↓	58.4	--	--
		65.6	--	--
		98.1	393	--
-33	17 μm	9.4	--	--
↓	↓	14.4	--	--
		19.4	--	--
		25.6	--	--
		30.6	987	--
		41.2	1144	34.5
		50.0	--	57.2
-33	325 mesh	30.0	--	--
↓	↓	38.8	--	--
		45.6	--	--
		62.5	694	--
		93.1	780	29.2
		150	--	51.0

TABLE XXVIII
CLOGGING CHARACTERISTICS OF TRANSITION VELOCITY
2.7 cm/sec AMK IN THE 40 μm PAPER FILTER

Temperature (°C)	Flow Rate ($cc/sec-cm^2$)	Jet A Normalized (True) Velocity (cm/sec)	Clogging Rate (KPa/sec)
21	0.51	--	--
	.87	131	9.0
	1.1	149	46.2
	1.3	--	51.7
	1.7	--	251-1379.3
-33	0.46	--	--
	.67	--	--
	.82	293	--
	1.0	322	17.2
	1.2	--	149.7
	1.5	--	1034-1496.6

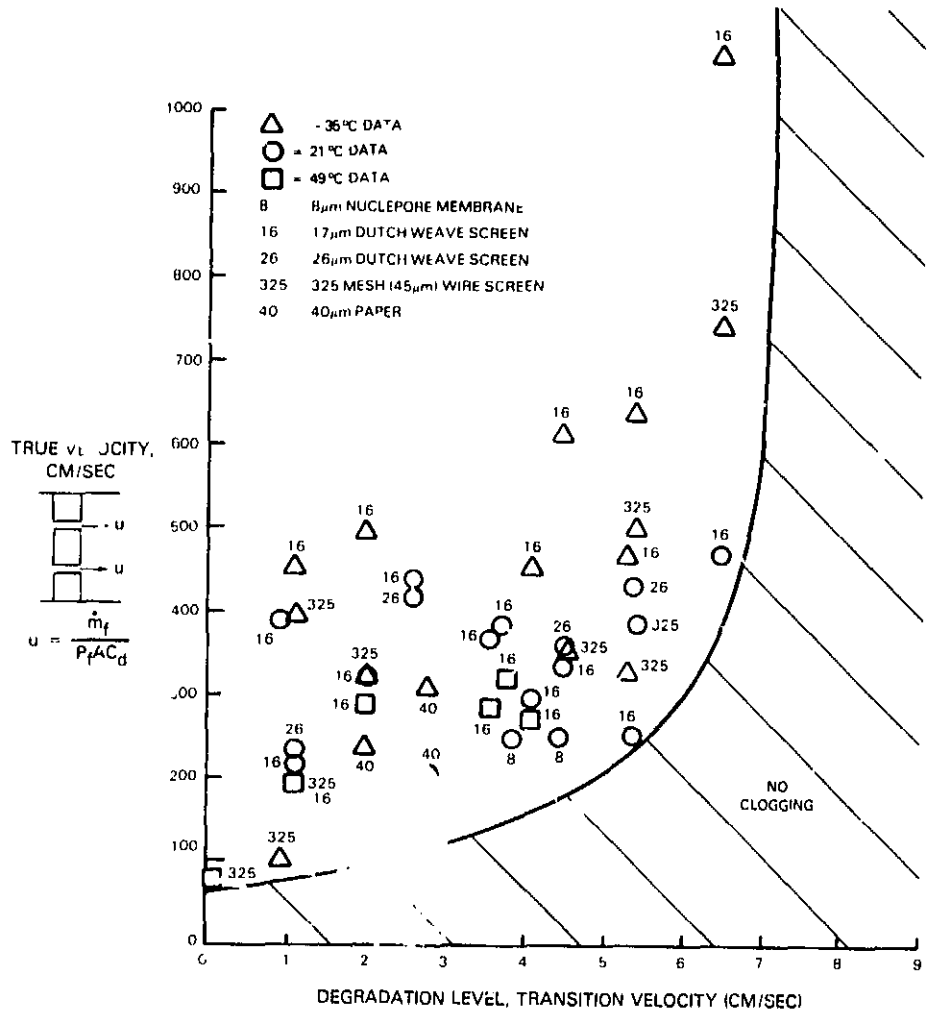

Figure 43 Short Term Clogging

7.4 Long Term Filter Life Evaluation Rig

A laboratory-scale apparatus shown in Figure 44 was constructed to evaluate the effects of AMK on gas turbine filters during longer duration flow tests. Fuel is pumped by a gear pump through a 10 micron filter element to remove any debris from the fuel. After leaving the filter, the fuel passes through four parallel independently adjustable loops. The flow rate in one loop can be adjusted to simulate the flow through the main paper filter element typically seen in the JT8D and JT9D engines. The second and third flow loops contain 325 wire mesh filter screens. One of those loops can be adjusted to give a flow rate of approximately 11 cc/sec-cm^2, which is seen in wash flow application in the JT8D and JT9D. The other loop can be adjusted to give a flow rate of approximately 25 cc/sec-cm^2, typical of that used in the hydraulic flow loop of the JT9D engine under takeoff conditions. The fourth flow loop is a bypass flow loop which carries the excess flow from the pump. The fuel from all four flow loops passes into a reservoir, having a capacity of approximately 6 liters, which acts as a supply vessel for the pump. A 0-69 KPa differential pressure gauge is mounted across each of the filters in the three flow loops containing filters. Through a valving arrangement, these flow loops can be isolated to measure flow rate. At the start of the test, flow rates are adjusted to the proper levels and the pressure is then recorded as a function of time.

Several initial tests were conducted with anti-misting fuel circulating in the apparatus for periods up to 15 hours. The fuels used in these tests were AMK degraded by one pass through the Gaulin disperser at 41.4 MPa (6000 psi), one pass at 55.2 MPa (8000 psi), and two passes at 55.2 MPa (8000 psi). No filter clogging was noted in previous short term filter tests with fuel degraded to these levels in ambient filter tests. During the extended filter test, small changes in filter pressure were noted (less than 6.9 KPa total).

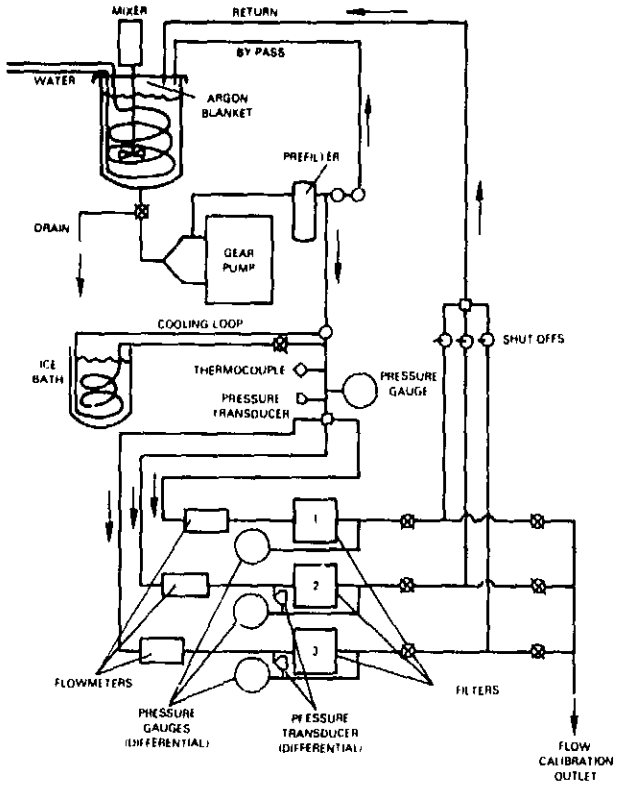

Figure 44 Schematic of Extended Duration Filter Test Apparatus

7.5 Extended Duration Filterability Tests

Results have shown that AMK degraded to a transition velocity of 5.4 cm/sec did not plug filters while another batch of less degraded AMK (transition velocity of 1.6 cm/sec) did show filter clogging. The present test being discussed was run to determine the clogging tendencies of AMK degraded to an intermediate level. A transition velocity of 4 cm/sec was achieved by passing the fuel through the Gaulin disperser twice at 13.8 MPa (2000 psi). The extended duration test was run with a 40 μm paper filter section and two 325 mesh wire screens arranged in parallel flow paths. The pressure was monitored as a function of flow time. One-half of the total fuel volume was replaced eight times without interrupting the tests. The degradation level of the fuel was measured at various times throughout the test to determine if recirculation substantially increased the degradation level of the fuel. Gel permeation chromatograms were also made as a further check on degradation level throughout the test and are shown in Figure 45. Both the transition velocity measurements and the chromatograms indicate the fuel remained at a relatively constant state of degradation throughout the test.

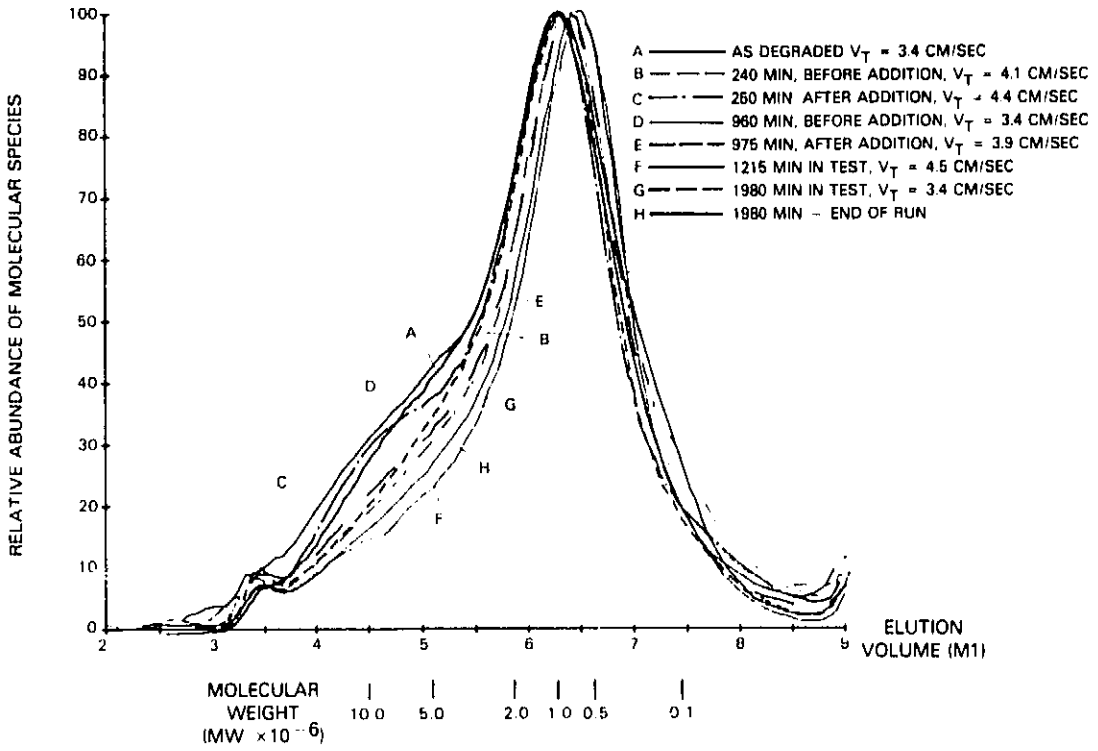

Figure 45 Molecular Weight Distributions for AMK Degraded by Two Passes Through the Gaulin Disperser @13.8 MPa During Extended Filter Test

Pressure-time data shown in Table XXIX indicate no significant pressure buildup throughout the first 24 hours of test. When the fuel temperature was reduced to -15°C, a pressure buildup was noted in both the 11 cc/sec-cm^2 and 25 cc/sec-cm^2 filters. No pressure increase was noted across the paper filter throughout the entire test. As the fuel temperature decreased, the rate of pressure buildup increased in both wire screen flow loops. After a total test time of 32 hours, flow was stopped and the temperature allowed to come to 20°C. After approximately 15 hours with no flow, the flow was restarted at 20°C. The pressure differential across the filters had returned to their initial values.

TABLE XXIX
EXTENDED DURATION FILTER TEST
(TRANSITION VELOCITY = 4 cm/sec) WITH AMK
DEGRADED BY 2 PASSES THROUGH THE GAULIN DISPERSER AT 13.8 MPa

Time (min.)	Temperature (°C)	ΔP (KPa) 11.0 cc/sec-cm²	ΔP (KPa) 25 cc/sec-cm²	Transition Velocity (cm/sec)
31	Ambient	.69	2.75	3.4
67			2.06	--
190			2.75	--
240				4.1
*				
360				--
477				--
**				
482	4 ± 2		2.06	3.9
515			3.4	4.0
590			3.4	--
720			4.1	3.9
*				
787		1.3		--
853				--
960				--
**				
963	Ambient	.69	2.06	--
975			2.75	3.9
1113				--
*				
1215				4.3
1430				4.2
**				
1444	-15°C		3.4	--
1455		1.3	4.1	3.8
1481		1.3	6.89	--
1560		2.75	10.3	--
1680		4.1	15.2	3.7
*				
1760		6.89	22.1	--
1780	-19	6.89	25.5	--
1800	-26	9.0	31.7	--
1826	-29	12.4	41.4	--
1850	-30	15.2	53.8	--
1877	-30	19.3	61.4	--
1920		20.7	69.7	3.4
**				
1935	Ambient	.69	2.06	--
1980			2.06	4.4

* Replaced one-half of test fuel with new fuel

** Flow discontinued, apparatus allowed to equilibrate to ambient temperature for approximately 15 hours, one-half of test fuel replaced and test resumed.

7.5.1 Gel Permeation Chromatography Results of Fuels From Extended Duration Tests

Fuel used in the extended filter test described above and the metal screens from the extended flow apparatus were evaluated by gel permeation chromatography using techniques described earlier.

The gel permeation chromatograms from these studies are shown in Figures 46 through 49. In all the chromatography results, the largest peak in the chromatogram was normalized to 100 intensity units. The intensity of the chromatogram at any given elution volume point is directly proportional to the concentration of the particular molecular species eluting at that point. Figure 46 shows gel permeation chromatograms during extended duration testing for AMK degraded by one pass at 41.4 MPa (6000 psi) through the Gaulin disperser at the beginning of the test, after 15 hours into the test, and at the end of the test at 15 hours. Also, gels extracted from the metal screen filters after 15 hours of test at flow rates of approximately 11 cc/sec-cm^2 and 25 cc/ sec-cm^2 are shown.

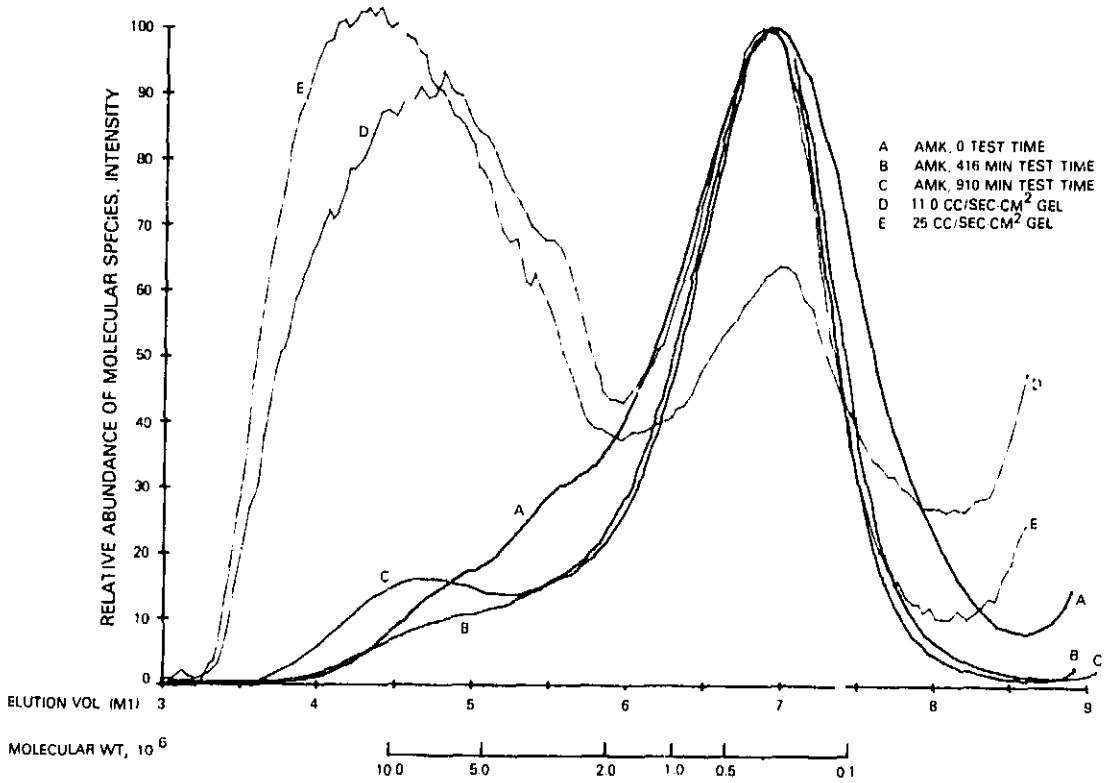

Figure 46 GPC Results for AMK and Gel From Filters Formed From 1 Pass, 41.4 MPa Gaulin Disperser Degraded AMK (V_T=3.5 cm/sec)

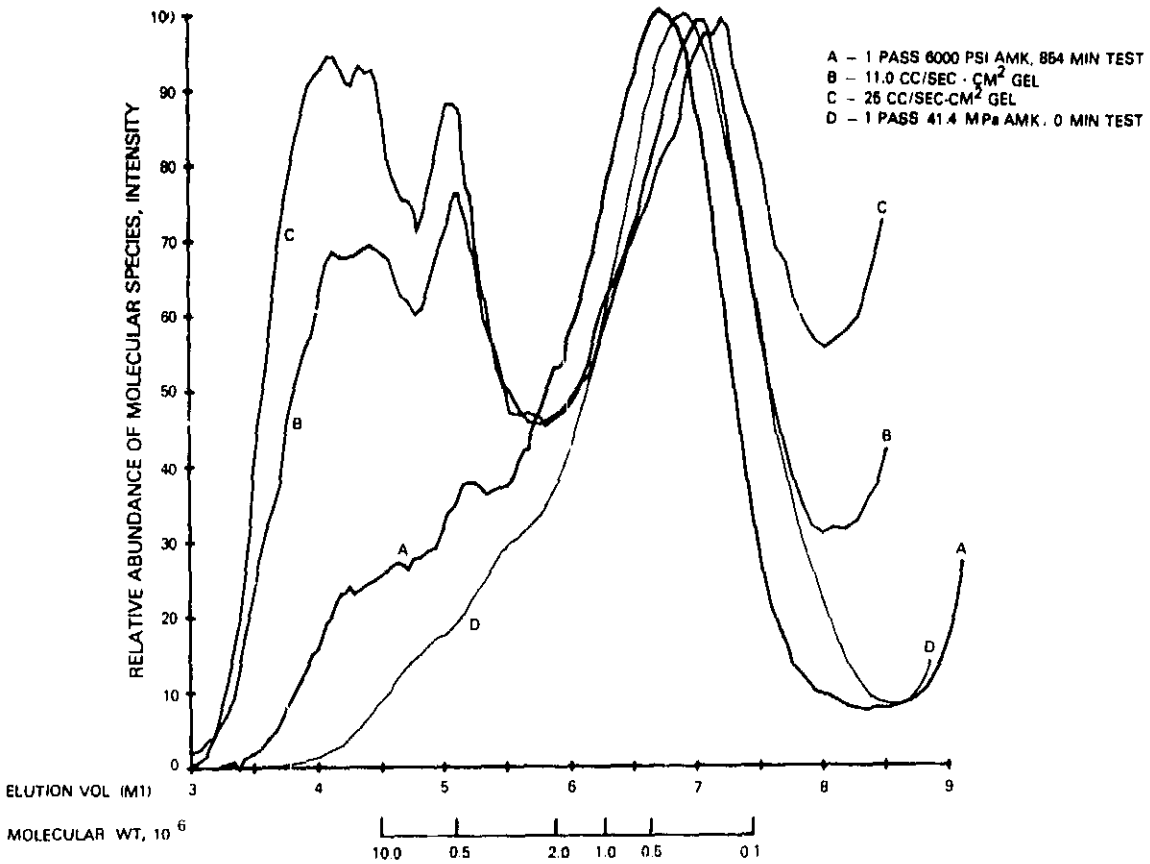

Figure 47 Repeat of Extended Duration Filter Test With 1 Pass, 41.4 MPa Gaulin Disperser Fuel (V_T=3.5 cm/sec)

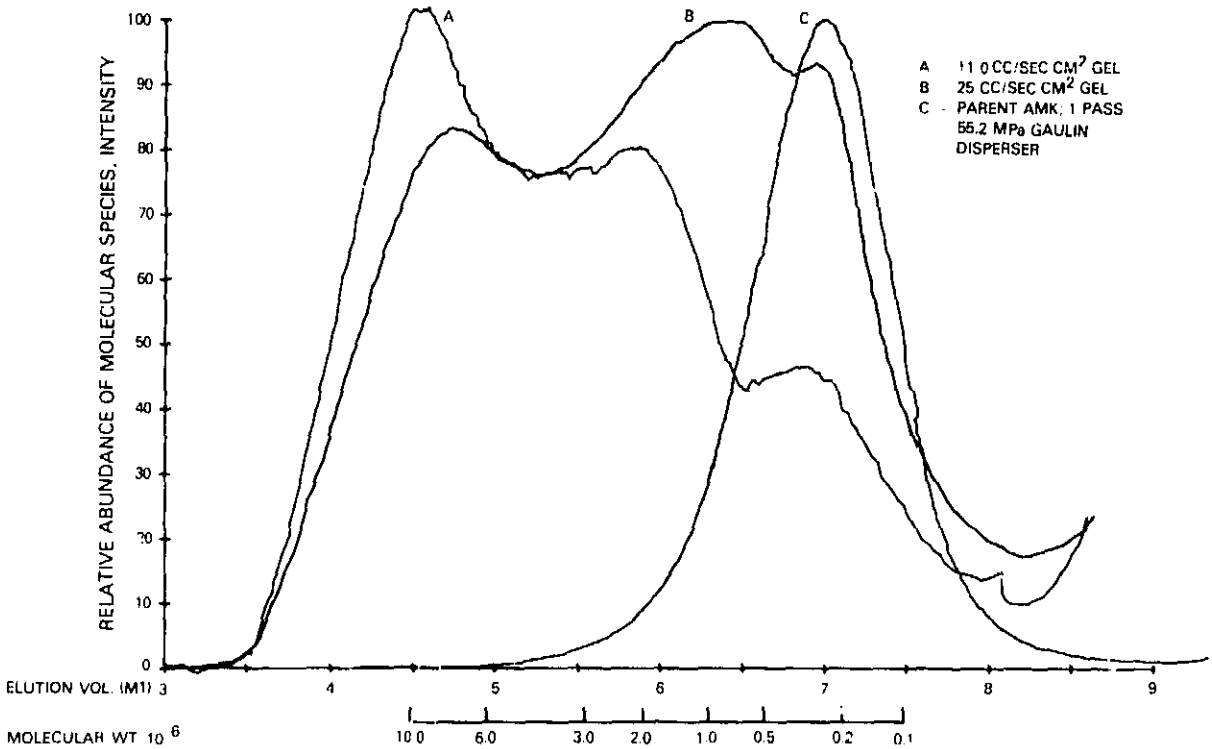

Figure 48 GPC Results Extended Filterability Test With 1 Pass, 55.2 MPa Gaulin Disperser Fuel

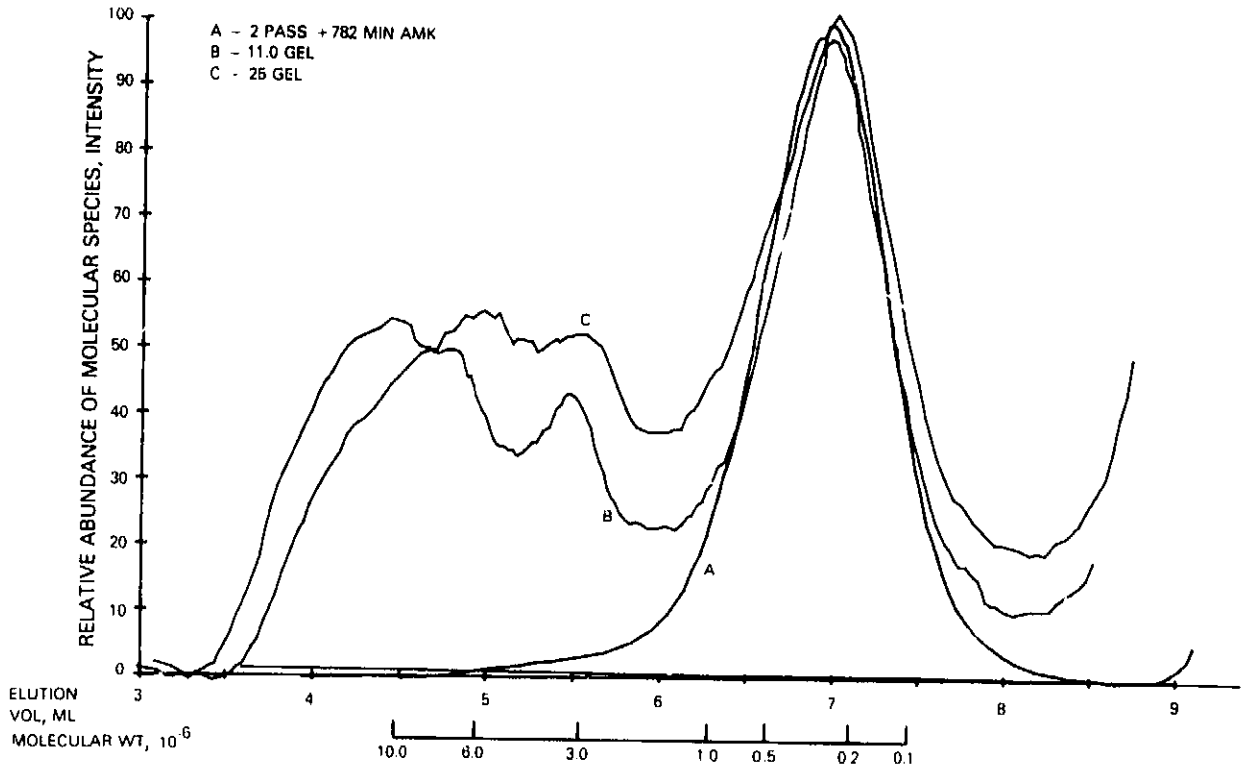

Figure 49 GPC Results for Extended Duration Test with 2 Pass, 55.2 MPa Gaulin Disperser Fuel (V_T=9.2 cm/sec)

In the chromatogram of the parent AMK fuel, a species of a high molecular weight formed with increasing test time. This particular component eluted at a volume of approximately 4.5 ml and had a molecular weight of approximately ten million. The gel formed on the metal filters and while an appreciable pressure increase did not result during the test period, the gel was apparent in the chromatograms. The major part of the gel consisted of material with molecular weight much greater than the characteristic molecular weight of the parent AMK fuel. In Figure 46, the gel appeared to have a peak molecular weight of approximately ten million. Because of the high molecular weight component in the chromatogram of the parent AMK fuel, another test was run to reproduce this component. Figure 47 shows that once again, a higher concentration of high molecular weight components appeared in AMK fuel after 14 hours of test than at the start of the test. The chromatograms of the gel extracted from the metal screens are similar to those of Figure 46; however, the bimodal distribution of molecular weights in the gel with peaks at elution volumes of approximately 4.2 ml and 5.1 ml is much more pronounced. Figure 48 shows the

chromatogram of AMK fuel degraded by one pass at 55.2 MPa (8000 psi) through the Gaulin disperser. In addition, the figure shows the chromatograms for gel formed by flowing the AMK fuel at flow rates of approximately 11 cc/sec-cm^2 and 25 cc/sec-cm^2 through the 325 mesh metal screens for approximately 5 hours. The chromatograms of gel once again show a major constituent at a molecular weight of approximately ten million. Figure 49 shows the chromatogram of fuel degraded by two passes through the Gaulin disperser at 55.2 MPa (8000 psi) at the beginning of the test period and after approximately 13 hours of test. Chromatograms of the gel formed on the metal screens at flow rates of 11 and 25 cc/sec-cm^2 are also shown. Once again, the chromatograms show the familiar bimodal distribution of molecular weights.

All of the test fuels were degraded by the Gaulin Disperser. The transition velocity of the least degraded test fuel, 41.4 MPa (6000 psi) degraded fuel, was approximately 3.5 cm/sec, and that of the most degraded sample, two-pass Gaulin at 55.2 MPa (8000 psi), was 9.2 cm/sec. Once more, this indicates the inability of a filter ratio measurement to define differences with moderately and/or highly degraded fuel. Several features appeared to be common to all the chromatograms of gels examined in these studies. Two major peaks were present on the chromatograms in addition to the peak of the parent fuel. The highest molecular weight of these two peaks appeared at an elution volume corresponding to a molecular weight of approximately ten million. The position of the second peak appeared at lower molecular weights and was not as constant as the position of the first peak. The ratio of the areas under the curves for the gel having high molecular weight components and of the parent fuel was generally greater for the filter exposed to the higher flow rate. This is probably indicative of a greater amount of gel formed on the filter exposed to the higher flow rate. In addition, preliminary results seemed to indicate that the lower molecular weight constituent of the gel that formed on the filter flowing at the higher flow rate made up a larger fraction of the overall gel than in the case of the filter exposed to the lower flow rate. These formations may result from the polymer being subjected to extensional forces which were proportional to the flow rate through the filter as the AMK fuel flowed through the metal screen filters.

A long term filter test was carried out with AMK fuel degraded by one pass at 55.2 MPa (8,000 psi) through the Gaulin disperser. The results of this test are reported in Table XXX. The degree of degradation of the fuel was monitored throughout the test by gel permeation chromatography and by approximate measurement of the transition velocity. The transition velocity was obtained by measuring a single flow rate point versus pressure utilizing the transition velocity apparatus at a pressure differential of 12.7 cm of mercury. Previous experience has shown that the transition velocity occurred at approximately 15.7 cm of mercury pressure within variation limits of $\pm$ 2.5 cm of mercury. For purposes of monitoring changes in level of degradation, this procedure was considered to be adequate. The test was conducted at ambient temperatures for a period of approximately six hours. No pressure buildup was noted on any of the three filters in the recirculation loop. The fuel temperature was then lowered to approximately 4°C and the test continued for another six hours. Once again, no pressure buildup was noted on any of the three filters. Testing was conducted at ambient temperatures for another six hours, and again, no pressure buildup was noted on any of the filters. The transition velocity was monitored throughout the test and showed no substantial changes.

Gel permeation chromatograms of fuel samples shown in Figure 50 and the gel collected from the filter screens indicate no substantial change in the level of degradation. Because of the lack of additional degradation, the fuel was not changed during the test. The results of the long term filter test with the fuel degraded by one pass at 55.2 MPa (8000 psi) through the Gaulin disperser were similar to the results of the short term filter clogging test performed earlier in the program where no clogging was found at ambient temperature. No data was collected previously at 4°C. Due to the lack of clogging in the initial test with fuel degraded at 55.2 MPa (8000 psi), an additional test was run with fuel degraded by one pass through the Gaulin disperser at 13.8 MPa (2000 psi). The results of this test are shown in Table XXXI. The level of degradation of the fuel throughout the test again was monitored by measuring the transition velocity at a single point, and by measuring the molecular weight distribution utilizing gel permeation chromatography. Chromatograms for AMK and gel removed from the filter screens are shown in Figure 51 where some degradation is seen in the chromatograms of the fuel.

TABLE XXX
LONG TERM FILTER TEST WITH AMK FULL DEGRADED BY ONE PASS
AT 55.2 KPa THROUGH THE GAULIN DISPERSER

Time (min.)	Temperature (°C)	ΔP (KPa) 11 cc/sec-cm²	ΔP (KPa) 25 cc/sec-cm²	Transition Velocity (cm/sec)
22	Ambient (20°C)	1.4	1.4	--
36		0.69		--
62				5.8
103				--
178				5.4
220			2.8	--
268				--
337				5.
360				5.2
375	4 ± 2°C		3.4	
420			3.4	5.2
448			4.1	--
493				--
532				--
590				--
625				--
697				--
720				--
738	Ambient (20°C)		2.8	--
759				--
782				6.4
793				--
827				--
1081				6.2

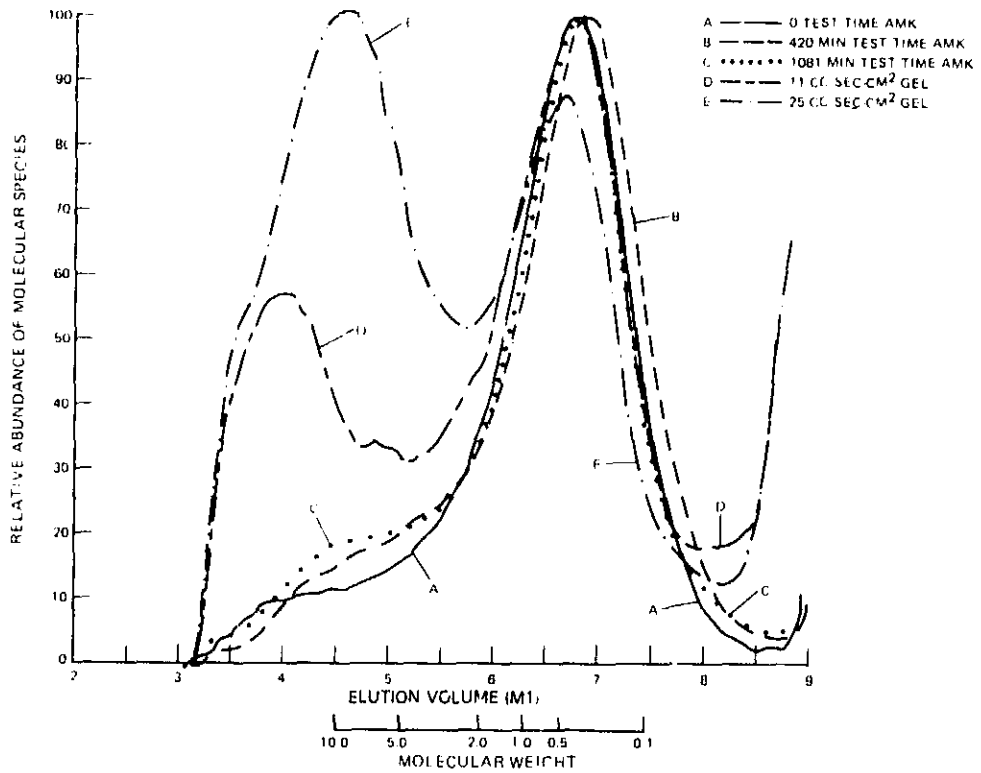

Figure 50 Molecular Weight Distributions for AMK Fuel and Gel Formed in Long Term Filter Test With AMK Degraded by 1 Pass, 55.2 MPa Through the Gaulin Disperser

TABLE XXXI
LONG TERM FILTER TEST WITH AMK FUEL DEGRADED BY ONE PASS
AT 2000 PSI THROUGH THE GAULIN DISPERSER

Time (min.)	Temperature (°C)	ΔP (kPa) 11 cc/sec-cm²	ΔP (kPa) 25 cc/sec-cm²	Transition Velocity (cm/sec)
18	Ambient (25 °C)	1.4	3.4	--
27		2.1	4.1	1.20
54		0.69	3.4	--
94			2.1	1.60
126				--
218				--
275				--
420	▼			1.87
422	4 [illegible]			--
456			2.8	--
464			2.8	--
480			3.4	2.07
520		1.4	4.1	--
560				--
[illegible]				--
649		2.1	4.8	--
703		2.1	5.5	--
764		2.8	6.2	--
800		2.8	6.2	--
843		1.4	6.9	--
890				--
900				2.51
934			2.1	--
927		0.69	2.8	--
964			3.4	--
973			[illegible]	--
1041				--
1060				--
1103		1.4	4.8	--
1130				--
1226	▼			--
1304			5.5	2.56

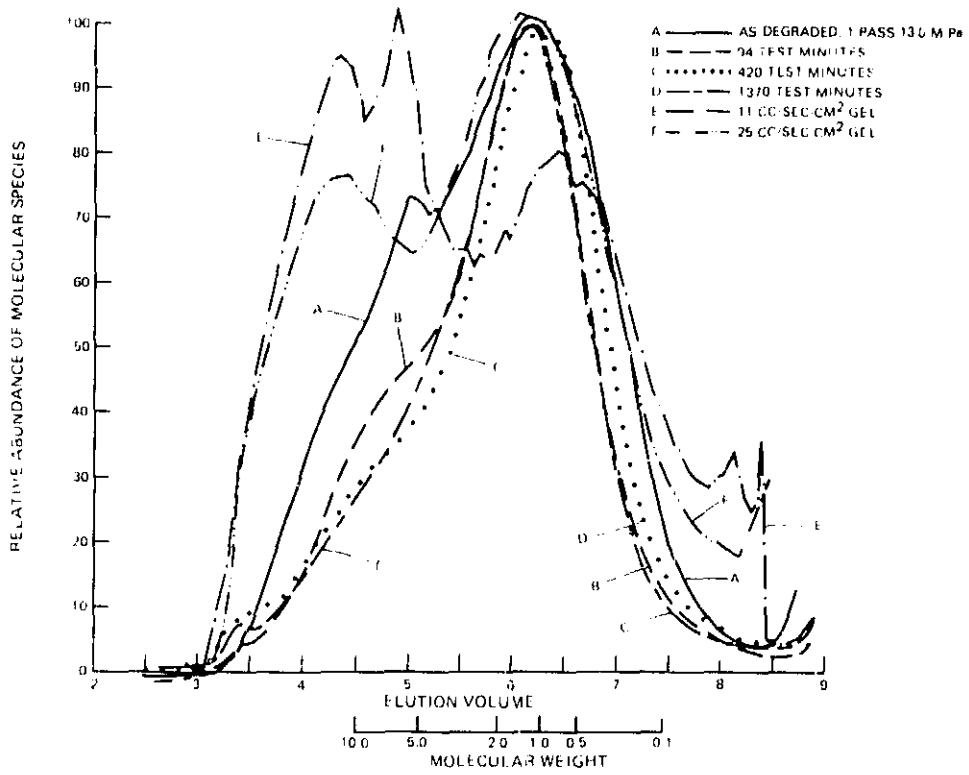

Figure 51 Molecular Weight Distributions of AMK Fuel and Gel Formed in Long Term Filter Test With AMK Degraded by 1 Pass, 13.8 MPa Through the Gaulin Disperser

Approximately seven hours of ambient temperature testing was conducted. No pressure buildup was noted on any of the three filters during this test period after which time the fuel temperature was lowered to 4°C and an additional eight hours of testing performed. During this portion of the test, a slow, but significant increase in pressure was noted for both of the 325 mesh screens operating at flows of approximately 11 cc/sec-cm^2 and 25 cc/sec-cm^2. There was no detectable pressure increase across the paper filter. The apparatus was then turned off, the flows discontinued, and the temperature allowed to come to ambient. Approximately 15 hours later, the fuel was cooled to 4°C and the test continued. An additional eight hours of testing was conducted to confirm the result previously recorded at 4°C. Once again, a slow, but significant rise in pressure across both of the 325 mesh wire screen filters occurred with no apparent increase in pressure across the paper filter. The rate of pressure buildup across the metal filter screens was slower during the second testing of the fuel at 4°C. However, this may be due to a slight increase in the level of degradation of the fuel which was noted from the transition velocity measurements and which was later confirmed in the gel chromatography molecular weight distribution measurement.

7.6 Additional Extended Duration Filterability Tests

Additional extended duration filterability tests were run in a manner similar to that described earlier, however, an automated data recording system was added so that the test could be run continuously for periods longer than one day without shutdown. The system utilized a Hewlett Packard Model 85 calculator and Hewlett Packard Model 3497A digital voltmeter to record temperature and differential pressures from the transducers. As before, the three flows were run with flows of 25 cc/sec-cm^2 (High Flow-HF) and 11 cc/sec-cm^2 (Low Flow-LF) through the two 325 mesh wire screens and 0.4 cc/sec-cm^2 through the 40 μm paper filter. In addition to the pressure transducers, gauges monitored the differential pressure across each filter. Figure 52 shows the results for differential pressures as a function of time and temperature for the 25 cc/sec-cm^2 flow loop in an extended duration test with fuel degraded by the Gaulin disperser (transition velocity = 10 cm/sec).

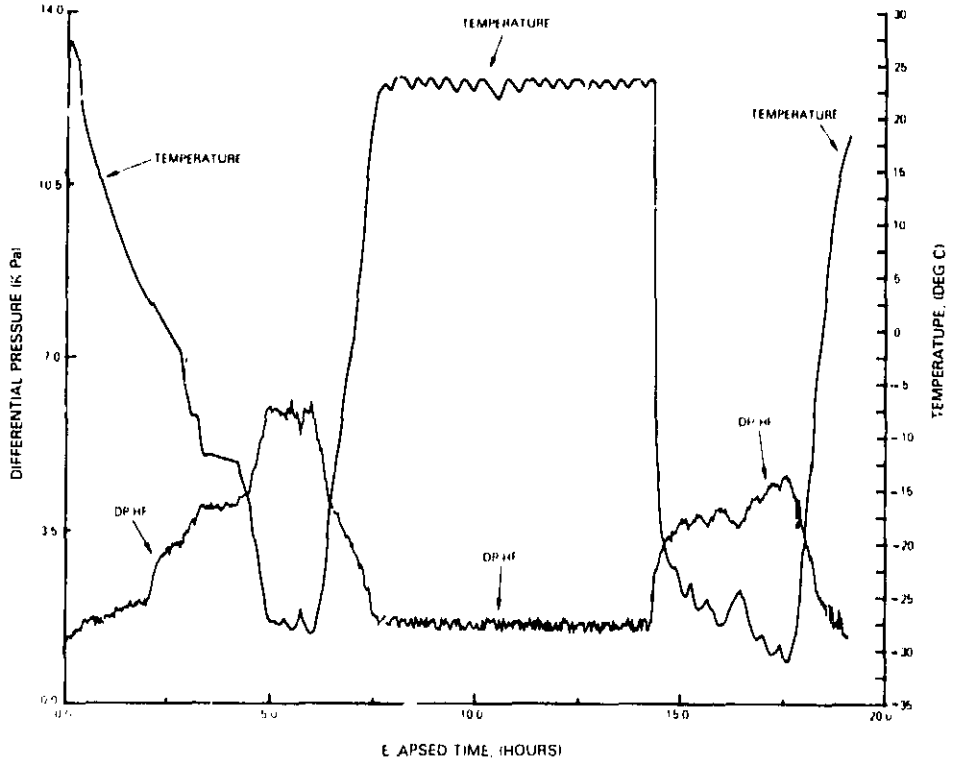

Figure 52 AMK Characterization - Transition Velocity 10 cm/sec

After approximately 20 hours of continuous running at temperatures ranging from +25°C to -30°C, no evidence of filter clogging was seen. The differential pressure across the filter showed small changes in response to the changing temperature; however, at the end of the test, the pressure was within the measurement error of the starting pressure. The same trend was noted for the 11 cc/sec-cm^2 flow loop. No measurable pressure changes were seen in the 40 μm paper filter loop.

After replacing the filters, another extended duration filter test was run for approximately 60 hours of continuous testing with AMK degraded by the Gaulin disperser to a transition velocity of 8 cm/sec. The results are shown in Figure 53 where pressure data as well as the fuel temperature for both the 25 cc/sec-cm^2 and the 11 cc/sec-cm^2 filters are shown . Once again, the pressure in both flow loops varied, as expected, with the fuel temperature. However, clogging was evident in the 25 cc/sec-cm^2 flow loop during periods when constant, cold temperatures occurred. Such periods were noted from

C-2

approximately 28 hours to 35 hours and again from approximately 40 hours to 50 hours. For the most part, it appears that unclogging occurs with increased temperature. The pressure at the end of the test period (when the temperature reached approximately 22°C) was equivalent to approximately 25 hours of testing.

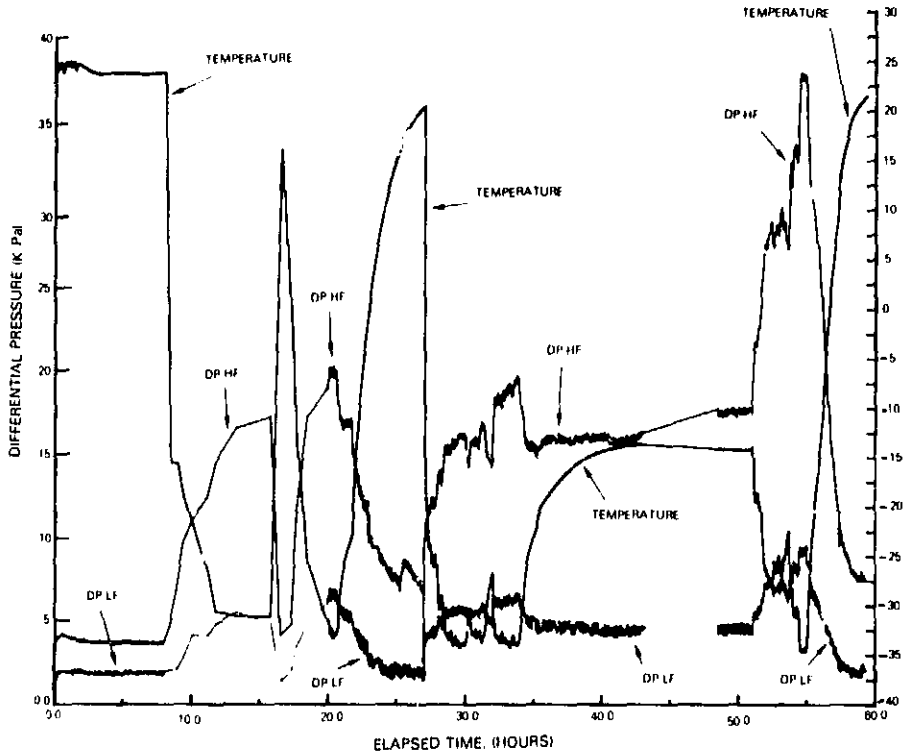

Figure 53 AMK Characterization - Transition Velocity 8 cm/sec

The tendency of the AMK fuel to unclog was recorded in another extended duration test shown in Figure 54. The test was run with AMK degraded in the Gaulin disperser to a transition velocity of 7 cm/sec. As the temperature was reduced, the pressure across the 25 cc/sec-cm^2 filter increased to 138 KPa (20 psi); however, when the temperature was brought back to ambient, the pressure returned approximately to the starting value. After 7.5 hours the flow was stopped and the rig allowed to sit overnight. At start-up, the pressure for the 25 cc/sec-cm^2 flow loop was lower than when the test was terminated after the initial 7.5 hours.

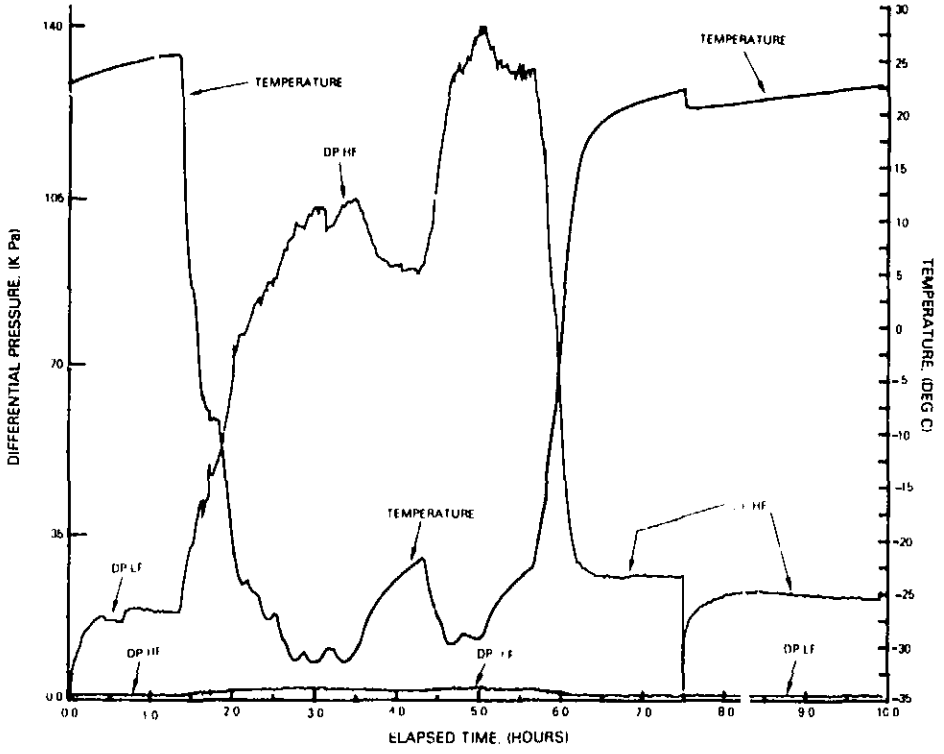

Figure 54 AMK Characterization - Transition Velocity 7 cm/sec

To ensure the measured phenomena were due to properties peculiar to AMK, a control test was run with neat Jet A fuel for approximately 25 hours. Results shown in Figure 55 indicate that the pressure changes across the filters were minor and were only a function of temperature. No time-dependent pressure changes at constant temperature were noted as was in the case with AMK fuel.

Figure 56 summarizes the clogging characteristics for the worst case engine fuel system filters as a function of fuel temperature and degradation level. The data shown in this figure were accumulated from the extended duration (periods of several hours) bench scale tests described in Sections 7.4, 7.5 and 7.6 and one full scale filter test performed early in the program (reported in NASA CR-165258). Figure 56 also represents the total accumulated experience gained from this contract on filter clogging for systems that were exposed for several hours, and as such, should be used to establish minimum degradation requirements (transition velocity) until further information is acquired.

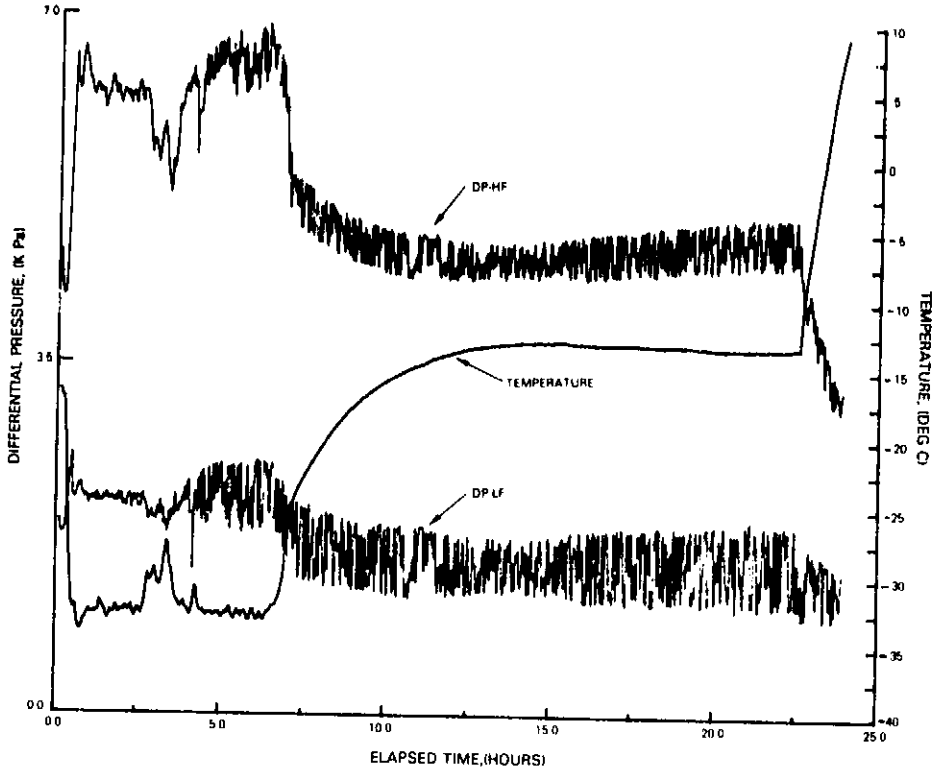

Figure 55 AMK Characterization - Transition Velocity Jet A

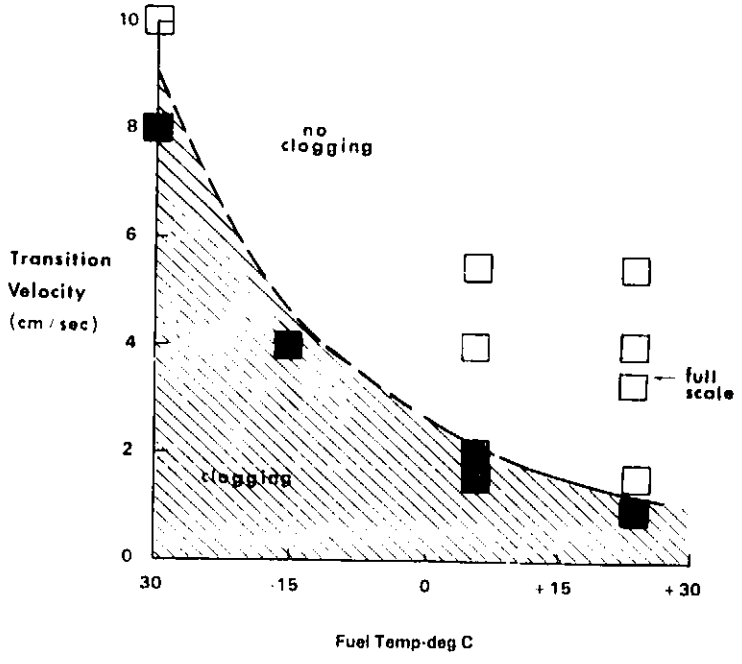

Figure 56 Long Term Clogging Characteristics

8.0 WATER COMPATIBILITY

8.1 Water Solubility

Early in the program, a simple test was made to determine the effect of the antimisting kerosene additive on water solubility in fuel. 100 ml of parent fuel and 100 ml of undegraded antimisting kerosene were equilibrated with 10 ml water by shaking, then centrifuged to separate the water from fuel. Fuel samples were drawn from the fuel layers and titrated by the Karl Fisher technique for water content. The procedure is included in Appendix B.

A white precipitate formed on contact of the antimisting fuel with free water and did not return to solution upon standing. The white precipitate was concentrated at the water-fuel interface. When the parent fuel was saturated with water, the water content of the fuel layer increased from 22 ppm to 62 ppm. The water content of the antimisting kerosene fuel layer after contact with free water increased by a smaller amount rising from 32 ppm to 38 ppm.

8.2 First Laboratory De-icing Test

A laboratory scale deicing test was run prior to the full scale test to determine the deicing behavior of the AMK fuel. Water was added to undegraded AMK to produce a mixture containing 210 ppm water and subsequently degraded by the Gaulin Disperser at 55.2 MPa (8000 psi). A fuel sample drawn for testing displayed no turbidity and gave a transition velocity of 8 cm/sec. The fuel was loaded into the accumulator at room temperature with no stirring, and then passed through a heat exchanger to bring the fuel to test temperatures of -35°C, -18°C and 9°C. The fuel was passed through a 40 μm paper filter and the pressure differential across the filter was recorded. Icing was noted at all three test temperatures as evidenced by a pressure buildup at flow rates where previously no pressure buildup was noted. At all three test temperatures the pressure differential across the filter was allowed to reach 69 KPa (10 psi). The filter was removed from the cold bath and the heat exchanger flow loop was bypassed allowing warm fuel to pass through the filter. In all cases the pressure differential that developed was eliminated when the filter reached room temperature.

8.3 Fuel System De-icing Performance

In normal engine operation, ice crystals that form from fuel borne water accumulates on the surface of the paper cartridge filter. When this accumulation becomes sufficient to increase the pressure drop across this filter, a de-icing heater is either manually or automatically actuated. This heater is upstream of the filter and operates from the high pressure compressor bleed air and momentarily increases the inlet fuel temperature to melt the ice crystals permitting them to pass through the filter and remainder of the fuel system. This program attempted to evaluate the de-icing performance of the filter and the fuel system in the presence of the antimisting additive.

The components of the JT8D fuel system that were to be evaluated consisted of a calibrated pressurizing and dump valve, fuel heater and fuel control. The AMK fuel was prepared by adding the approximate FAA specification of 210 ppm of water to the as-received AMK fuel and degraded by one pass at 55.2 KPa (8000 psi) in the Gaulin Disperser. Prior to its use, eleven barrels of the degraded fuel were stored in a vented facility tank which had cooling coils to reduce the fuel temperature to approximately -29°C.

During the testing, a white precipitate thought to be ice formed on the paper filter. The white precipitate restricted the fuel flow and was deposited on several fuel system filters and tank walls as well as the piping surfaces. Attempts to dissolve the precipitate by heat were unsuccessful. Based on the inspection of inlet and system filters it was postulated that some precipitate formed during storage and increased when humid air came in contact with the cooling coils and the fuel through the vented tank. Analysis of the fuel samples taken prior to the test during continuous tank stirring showed the presence of an average of 1000 ppm water. Although the de-icing characterization was not completed, it was learned that the formation of a precipitate occurred.

Testing was suspended to remove the white precipitate from the JT8D fuel system and additional laboratory scale water compatibility experiments were subsequently conducted.

8.4 Second Laboratory De-icing Test

In the first laboratory test, the fuel was blended to approximately 210 ppm water concentration. This concentration was later found to have increased to approximately 1000 ppm prior to the full-scale deicing rig test. Therefore, the laboratory-scale de-icing test was repeated to determine with certainty the effect of the water content in the fuel on the deicing characteristics of AMK.

For the repeat laboratory test, approximately 10 liters of undegraded AMK and water were blended to obtain fuel containing 245 ppm water. After measurements of the fuel showed water concentrations of 254 ppm and 168 ppm (Avg. = 211 ppm), the blended fuel was then immediately degraded by passing it through the Gaulin Disperser once at 55.2 KPa (8000 psi). The fuel was then measured again. Water concentrations after degradation of 130 ppm, 110 ppm and 113 ppm (Avg. = 118 ppm) were recorded. The transition velocity of the fuel blend was found to be 5.4 cm/sec, a value typical of degrading AMK one pass at 55.2 KPa (8000 psi) through the Gaulin device. The reduction in water content, due perhaps to an elevation in fuel temperature during the degradation process made the test fuel unsuitable for the deicing test. A second batch of fuel was blended using the following procedure: First, a batch of the AMK fuel containing approximately 750 ppm water was degraded by one pass through the Gaulin Disperser once at 55.2 KPa (8000 psi). This degradation step reduced the turbidity considerably, leaving only a slight milky appearance in the fuel. Secondly the degraded, water concentrated fuel was blended with previously degraded fuel. Replicate water measurements on the final test fuel showed water contents of 230 ppm, 138 ppm, 180 ppm, 240 ppm and 297 ppm (Avg. = 197 ppm) making it acceptable as a final test fuel for the deicing experiment.

One reason for the lack of reproducibility in water content readings is the nonhomogeneous nature of the AMK fuel sample containing the water. Only a small amount of the fuel is removed for the test and the reading obtained depends to some degree on the amount of precipitate removed in the aliquot for analysis.

Deicing tests were run at fuel temperatures of -30°C, -18°C and -9°C. The fuel flow rate through the 40 μm paper test filter section was maintained at 0.2 cc/sec-cm^2, a typical flow condition during normal icing flow was maintained by adjusting a needle valve downstream of the test filter. Changes in flow conditions during this period would have produced changes in pressure, thus complicating the interpretation of the icing results. When the differential pressure across the filter reached approximately 82.8 KPa (12 psi), the filter was deiced by immersing the entire filter assembly in hot water to approximately 43°C; the typical deicing temperature in the engine. When the fuel temperature reached 43°C, the assembly was placed in the controlled temperature cold bath for next icing cycle

In the first three deicing cycles, pressure increase due to icing was completely eliminated when the filter assembly was heated to 43°C as shown in Figure 57. On subsequent cycles, the pressure did not return to the initial value before icing. On the eighth deicing cycle, when the filter was removed from the cold bath and heated to 43°C, the pressure initially fell to approximately 13.8 KPa (2 psi) but showed rapid clogging even though the temperature was maintained at 43°C. On the final deicing cycle there was a rapid increase in pressure at an elevated temperature which was probably due to flow-induced gel formation resulting from the increase in fluid velocity required to maintain the 0.2cc/sec-cm^2 fuel flow rate through the partially clogged filter.

8.5 Effect of Free Water Addition to AMK Fuel

Laboratory tests were conducted to understand the formation of gross amounts of white precipitate in the antimisting fuel during the preparation for full-scale de-icing test. Water was added to approximately 500 ml of undegraded AMK to give the equivalent of 0.75, 1.5, 3.0, 6.0, and 10 cc/gal of free water. Samples were prepared for each level of water; one-half being undegraded, and the other one-half degraded ultrasonically for 20 minutes at room temperature.

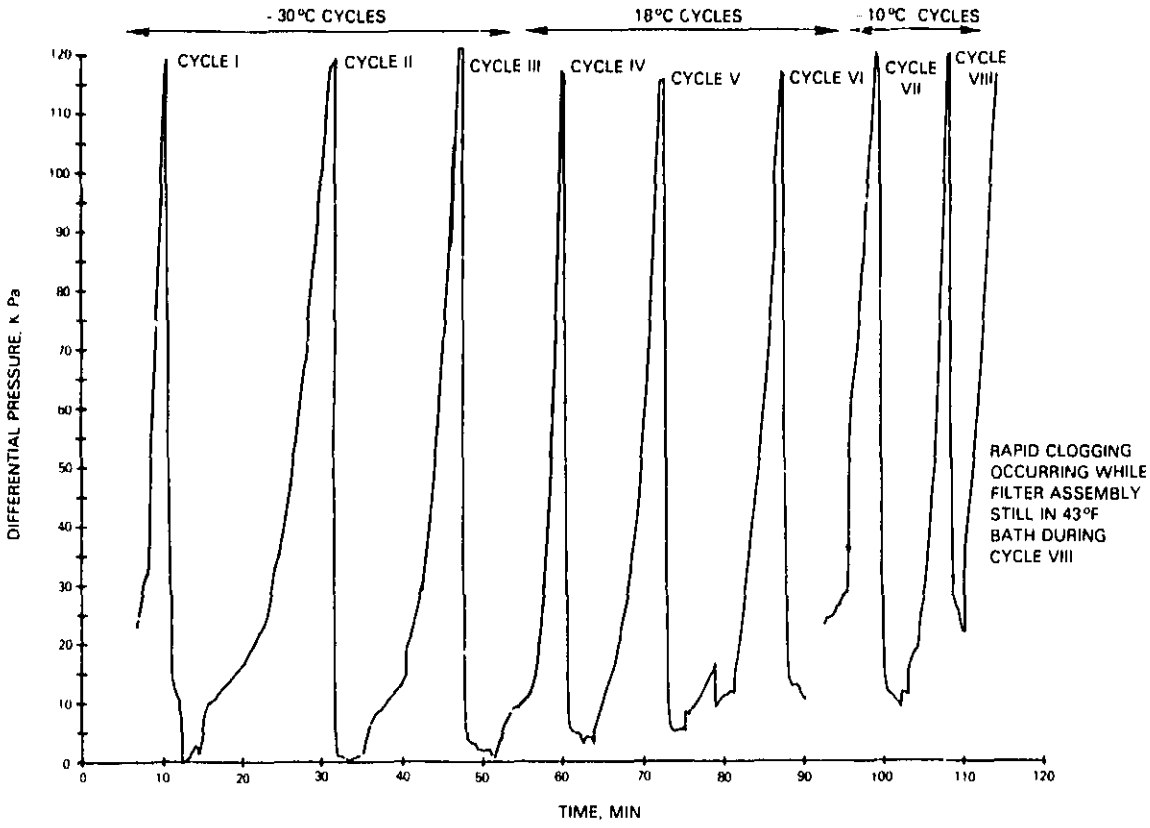

Figure 57 Laboratory De-Icing Test at -30°C, -18°C, and -10°C

Additional samples were prepared containing 0.75 cc/gal and 10 cc/gal water, respectively, and were stored at -10°C. All of the samples were then observed for a period of approximately two weeks. Degraded samples immediately formed a white precipiate at the interface between the water and fuel. The undegraded samples showed a similar precipitate which was limited to the interface between the water and fuel after standing for approximately 24 hours. Because the samples were placed in the same size containers and had nearly the same total volumes, it was concluded that the volume of precipitate was proportional to the amount of water that was in the fuel. The samples that were placed in a freezer showed a similar appearance; however, the water precipitate layer was semi-solid with a soft consistency. There was no apparent additional change in the appearance of any of the samples after two weeks of observation. While this investigation further clarified the behavior of free water in AMK, it did not provide sufficient explanation for the existence of gross amounts of precipitate encountered during the full-scale de-icing test.

8.6 Rate of Water Adsorption into AMK and Jet A Fuel from Surface Contact with Humid Air

It was theorized that part of the precipitate which was identified during the full-scale de-icing test may have formed when humid air, entering the tank through vents, came in contact with cold AMK. The Karl Fischer titration method was used to determine the rate of water absorption into AMK fuel at ambient temperature and -35°C. This method measured the water content after exposing the surface of the fuel to water saturated air at ambient temperature. The fuel was ultrasonically degraded to give a transition velocity of 2.4 cm/sec before exposure to the water saturated air. As shown in Figure 58, the rate of water absorption in the cold AMK fuel was considerably more rapid than that of the ambient temperature AMK fuel. After approximately eight hours exposure of -35°C AMK to saturated air, the water content of the AMK increased to approximately 2600 ppm. A similar exposure of ambient temperature AMK to saturated air increased the water content of the AMK fuel to only approximately 550 ppm. The rate of water adsorption in ambient AMK was also greater than that for Jet A fuel.

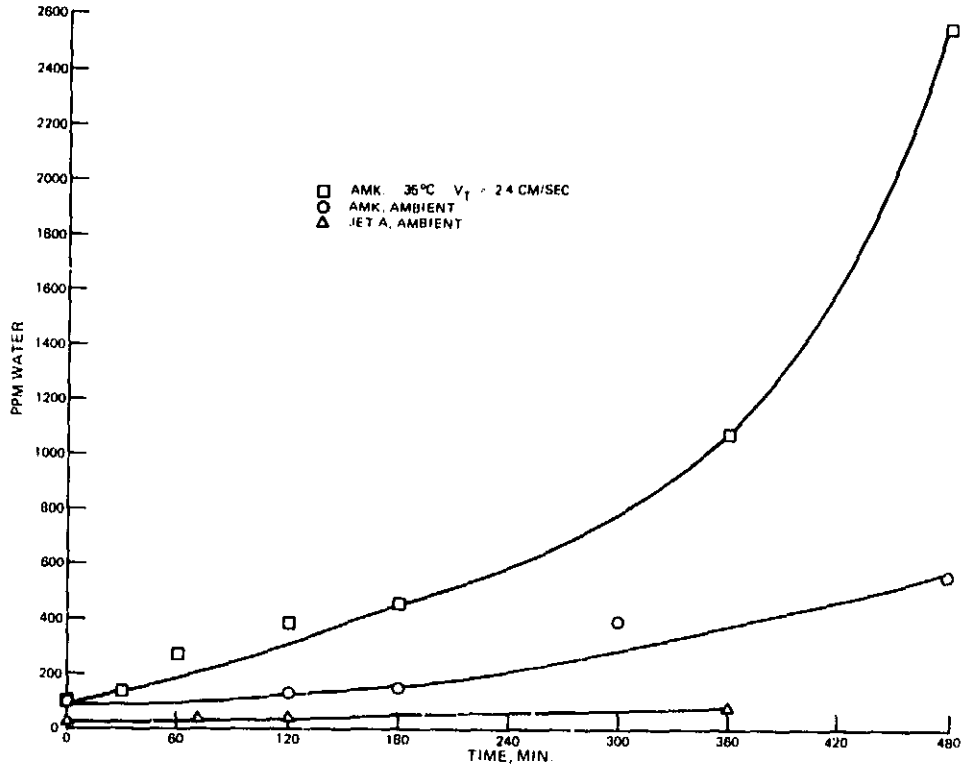

Figure 58 Rate of Water Adsorption of AMK and Jet A Fuel From Surface Contact With Humid Air

8.7 Rate of Water Uptake in Undegraded AMK

The rate of water uptake in undegraded AMK was studied by bubbling air, saturated with water at room temperature, through AMK. Care was taken to avoid water droplets from getting into the AMK by inserting a glass wool filter plug in the line. Tests were run at AMK temperatures of 24°C and 2°C. The air temperature was constant at 24°C. The 2°C fuel temperature condition is representative of an aircraft that had been at altitude for some time and had landed in an a warm, humid environment. The results of these two tests are shown in Figure 59. In the ambient AMK, there was a small increase in the water content of the fuel after water was bubbled through for six days and no precipitate formed in the fuel throughout the test period. In contrast, the water content in the 2°C AMK fuel rapidly increased from 59 ppm to a high as 670 ppm after approximately 70 hours. A white precipitate was evident after about 25 hours exposure and a water concentration of 150 ppm. The water concentration levels in the 2°C AMK fuel were quite variable after 40 hours test due to the lack of homogeneity of the sample caused by the precipitate. Samples containing larger amounts of precipitate had higher water content levels than samples with less precipitate. When the results of this study are evaluated collectively with those of Section 8.6, it appears that water absorption in AMK is not a strong function of degradation level.

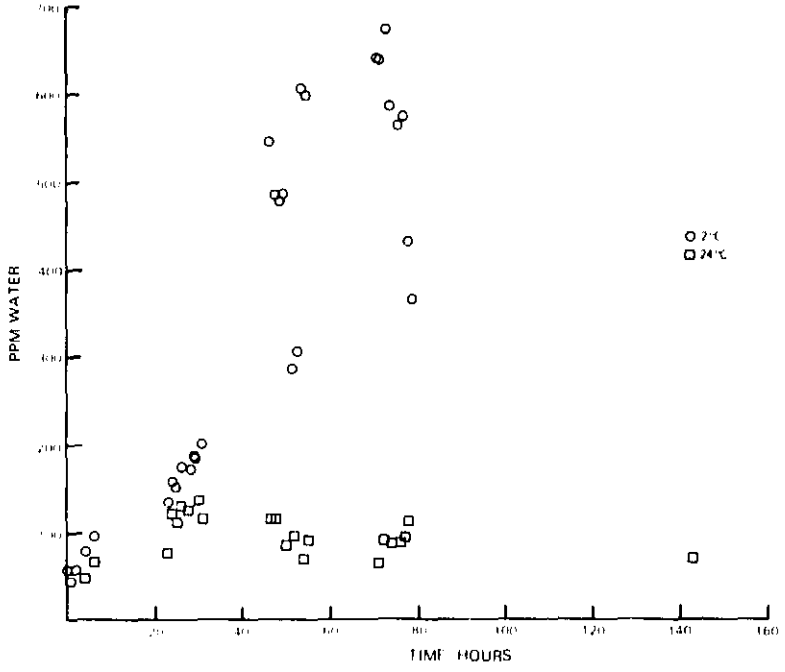

Figure 59 Water Uptake Rate From Water Saturated Air Into Undegraded AMK

9.0 ADDITONAL AMK STUDIES

9.1 Compatibility of AMK with Approved Jet Fuel Additives

An investigation was conducted to determine the effect of several additives used in Jet A fuel on AMK properties. In particular, visual as well as filter ratio changes were recorded. A listing of the additives tested for compatibility with AMK is given in Table XXXII. To accentuate potential subtle effects, all additives, except the anti-icing additive, were blended into undegraded AMK fuel (FR = 45) at ten times the amount normally used and were observed for five days. During this period only the metal deactivator showed no observable reaction. The Hitec E515, added in some cases to increase lubricity and in other cases to act as an anticorrosion agent when fuel is sent through pipelines, produced a slight turbidity after standing for one day. Turbidity was not observed in the control sample of Jet A fuel containing no FM-9. The JFA-5 thermal stability additive produced a small amount of particulate precipitate in the AMK fuel after four days. The control sample showed similar results after five days. The anti-icing additive gave an immediate lacy deposit in the AMK fuel at the normally recommended concentration, while no reaction was observed in the control sample. The lacy deposit remained for the entire five-days test period. The Biobar additive, utilized to prevent microbial growth in fuel in warm, moist atmospheres, showed no apparent reaction for four days, after which time a filmy deposit on the walls of the test vessel appeared.

TABLE XXXII
ADDITIVES TESTED FOR COMPATIBILITY WITH AMK

Additive	Recommended Concentration or Maximum Allowable	Test Concentration	Additive Purpose
Cooper Hitec E515	7.27 kg/1000 bbl	72.7 kg/1000 bbl	Corrosion Preventative, Lubricity
duPont JFA-5	13.64 kg/1000 bbl	136.4 kg/1000 bbl	Thermal stability improver
N,N'-disalicylidene 1,2-propane-diamine	.91 kg/1000 bbl	9.1kg/1000 bbl	Metal deactivator
Ethylene Glycol Monomethyl ether	0.15%	0.15%	Anti-icing additive
U.S. Borax Biobor JF	270 ppm	2700 ppm	Biocide

The rheological effect of the additives on the AMK fuels was determined by measurement of the filter ratio. Substantial changes were noted for some of the fuel additives (Table XXXIII). The metal deactivator increased the filter ratio by a factor of approximately two (45 92), whereas the Hitec E515 anti-corrosion additive decreased the filter ratio by almost a factor of two (45 28). These tests indicated that rheological effects existed with the FM-9/AMK fuel and various additives approved for use in Jet A fuel and suggests that more work is justified.

TABLE XXXIII
FILTER RATIO OF AMK FUELS WITH APPROVED ADDITIVES

Additive	Filter Ratio After Blending	Filter Ratio After Five Days
No Additive, Neat AMK	45	51
Anti-icing Additive	39	40
Metal Deactivator	92	110
Hitec E515	28	25
Biobor JF	39	29

In a second test, all the additives were blended at the recommended or maximum allowable concentration for that additive. The results of this test are shown in Table XXXIV and they supported the rheological effects noted in the earlier test. The anti-icing additive was the only additive in the second test that produced a precipitate.

9.2 Comparison of Filterability Properties of AMK Degraded by the Ultrasonic Technique and by the Gaulin Disperser

An experiment was devised to determine if AMK fuels degraded by different techniques to the same level of degradation resulted in similar filterability properties through metal screens. One sample of AMK fuel was degraded by a single pass through the Gaulin Disperser at 41.4 MPa (6000 psi) and the other sample degraded ultrasonically. The transition velocity of the sample degraded with the Gaulin Disperser was determined to be 3.5 cm/sec and the sample degraded ultrasonically was adjusted to a transition velocity of 3.6 cm/sec. This adjustment is accomplished by sequential steps of ultransonic degradation followed by measurements of the transition velocity. As the transition velocity of 3.5 cm/sec was approached, smaller and smaller time intervals of ultrasonic agitation were applied to the fuel in order to closely match the

degradation level of the sample degraded by the Gaulin Disperser. Gel permeation chromatograms shown in Figure 60 for both of the samples show a substantial difference in peak molecular weights. The sample degraded with the Gaulin device has a peak molecular weight of approximately 370,000 while the sample degraded ultrasonically has a peak molecular weight of approximately 840,000. The distribution of molecular weights in both cases was similar. The results of the filterability test with the two fuels through 17 μm steel screen filters are also shown in Figure 60. The point at which clogging is first observed is approximately the same for both fuels. The substantial difference in peak molecular weights for two samples showing similar filterability properties was unexpected; however, chromatograms of gel formed from AMK fuel discussed earlier showed that the concentration of molecular species having weights much higher than that of the peak molecular weight may be most important in determining the flow rate at which clogging first occurred.

TABLE XXXIV

EFFECT OF APPROVED FUEL ADDITIVES
ON AMK FUEL AT RECOMMENDED CONCENTRATIONS

Additive	Test Concentration	Filter Ratio		
		Immediately After Blending	After 48 Hours	After 96 Hours
None, Neat AMK Lot 1-158	-	105	88	80
Anti-Icing[1]	0.15%	51	61	50
Metal Deactivator[2]	.91 kg/1000 bbl	104	124	94
Hitec E515	7.27 kg/1000 bbl	77	76	71
Biobar JF[3]	270 ppm	64	79	61
JFA-5 Thermal Stability Improver	13.64 kg/1000 bbl	115	112	99

[1]Lacy deposit formed on addition of anti-icing additive which remained throughout the test.

[2]A few particles formed in the control sample of Jet A fuel containing no FM-9 after 3 days; however, no deposits formed in the AMK sample.

[3]A few particles formed in the AMK sample after 4 days; however, no deposit was visible in the Jet A control sample.

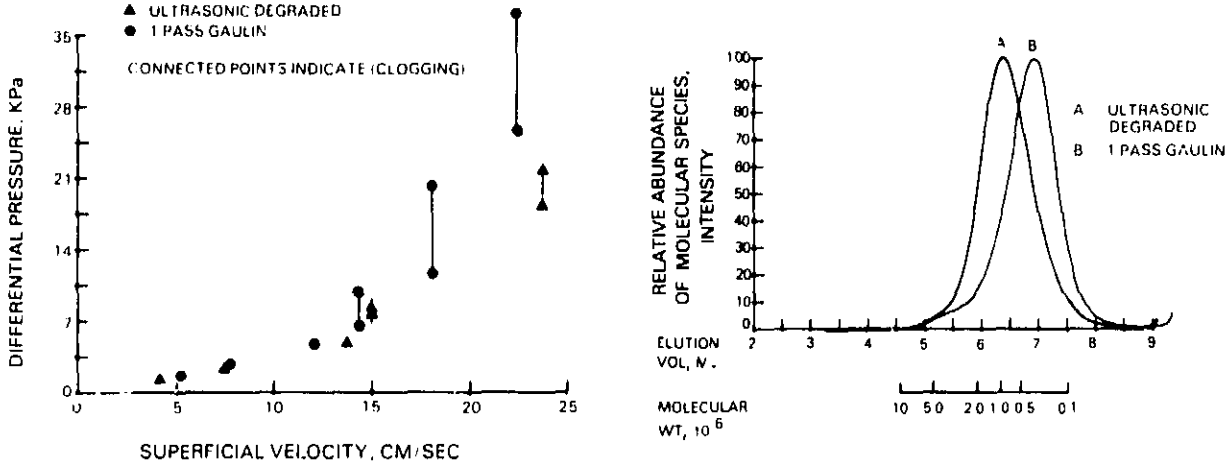

Figure 60 Filter Test With 17 μm Wire Screen and Molecular Weight Distributions of AMK Degraded Different Methods

9.3 Capillary Flow Tests

A test using stainless steel capillary tubing, 10 cm long with a diameter of 0.0254 cm, to simulate fuel control passages was conducted to determine the flow characterstics of AMK fuel. The AMK fuel was prepared by ultrasonically degrading the fuel to a transition velocity of 2.6 cm/sec. The flow characteristics of the capillary tube were determined by passing Jet A fuel through the capillary tube at pressures ranging from 0 - 690 KPa (0-100 psi). Similar to the calibrations performed with the filter media, the capillaries were calibrated with Jet A to obtain their apparent area so that the true velocity of the AMK through the tube could be calculated. Testing was performed at room temperature.

The flow characteristics of Jet A and AMK fuels were determined by the same method. The capillary was allowed to flow for approximately one minute after each pressure increment. The flow rate was measured immediately before and after adjusting the pressure for the one minute cycle. The results of the test are shown in Figure 61. No clogging was apparent over the entire range of pressures and flows investigated.

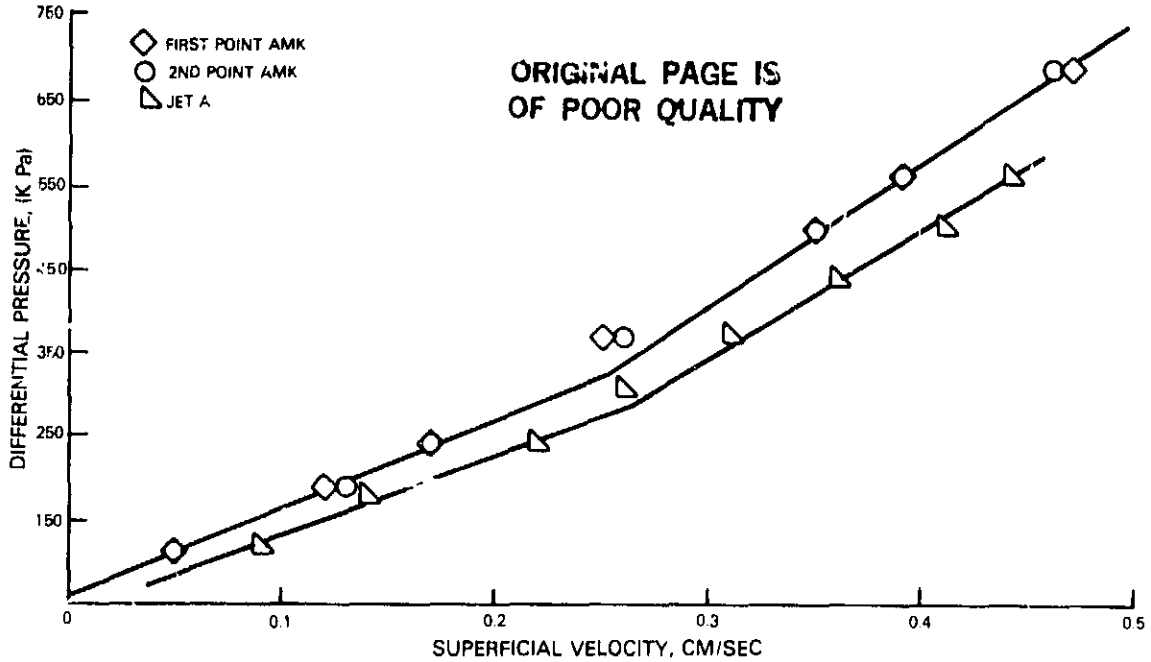

Figure 61 Capillary Flow Test With AMK

In a second experiment, the effect of reduced temperature on the flow properties of AMK with transition velocity of 2.6 cm/sec and AMK with degradation levels having a transition velocity less than 2.6 cm/sec through the capillary tube was studied. The results of the reduced temperature capillary tube flow test with AMK fuel degraded to transition velocity 2.6 cm/sec is shown in Table XXXV. As in the earlier study, the difference in flow rates, measured through the capillary tube before and after approximately one minute of flow time would be compared in order to indicate possible clogging . Because of the very low flow rates involved in capillary testing, it was difficult to maintain a constant cold fuel temperature through the length of the tube. As the pressure on the capillary tube increased, the flow rate through the capillary increased allowing lower temperatures to be achieved. As can be seen from the table, no clogging was observed at differential pressures up to 690 KPa (100 psi).

TABLE XXXV
REDUCED TEMPERATURE CAPILLARY FLOW TEST WITH AMK,
TRANSITION VELOCITY = 2.6 cm/sec

ΔP (KPa)	Temperature (°C)	Volume Flow Rate (cc/sec) Initial	Final
138	-19	0.10	0.09
207	-24	0.11	0.11
276	-28	0.13	0.13
414	-28	0.16	0.16
552	-30	0.19	0.19
690	-31	0.22	0.21

An additional capillary flow test was conducted with fuel degraded by one pass at 13.8 MPa (2000 psi) through the Gaulin Disperser. The measured transition velocity of this fuel was 1.0 cm/sec. The results of this study are shown in Figure 62A along with the results for a capillary flow test with undegraded AMK fuel in Figure 62B. It can be seen that no clogging was observed for the transition velocity of 1.0 cm/sec AMK fuel at differential pressures up to 3.4 MPa (500 psi) at ambient temperature. However, when the capillary flow test was run with undegraded AMK fuel, clogging was observed at a differential pressure of 310 KPa (45 psi) as evidenced by the reduced flow rate with time. When the pressure increased to 414 KPa (60 psi), the flow rate increased from the previous value measured at 310 KPa (45 psi). At 414 KPa (60 psi), within one minute after the initial measurement, the flow rate dropped to zero, indicating complete clogging of the capillary. In conclusion, no clogging was observed in flow tests with a a 0.0254 cm diameter capillary except with undegraded AMK.

9.4 Effect of Storage Temperature on Filter Ratio of Undegraded AMK

Preliminary laboratory data suggested that the storage temperature of undegraded AMK after blending may markedly affect the rheology of the undegraded fuel as determined by filter ratio measurements. This may be why one shipment of AMK fuel received at Pratt & Whitney Aircraft produced filter ratios ranging from 146 to 210 while measurements at ICI on the same fuels recorded filter ratios varying from 59 to 69.

Undegraded AMK stored in a freezer at -8°C for 87 days recorded a filter ratio increase from 57 to 424. Therefore a study was conducted to evaluate the effect of storage temperature on the fuel. After three days of storage at room temperature, it was found that the filter ratio of the fuel decreased to 161. When warmed to 71°C for 4.5 hours, the filter ratio decreased to 45. In another study, undegraded AMK was warmed and maintained at 71°C for periods up to 6 hours. Before warming, the filter ratio was 125 and after 3 hours at room temperature, the filter ratio decreased to 39. After an additional 3 hours at 71°C, the filter ratio showed only a minor change to 31.

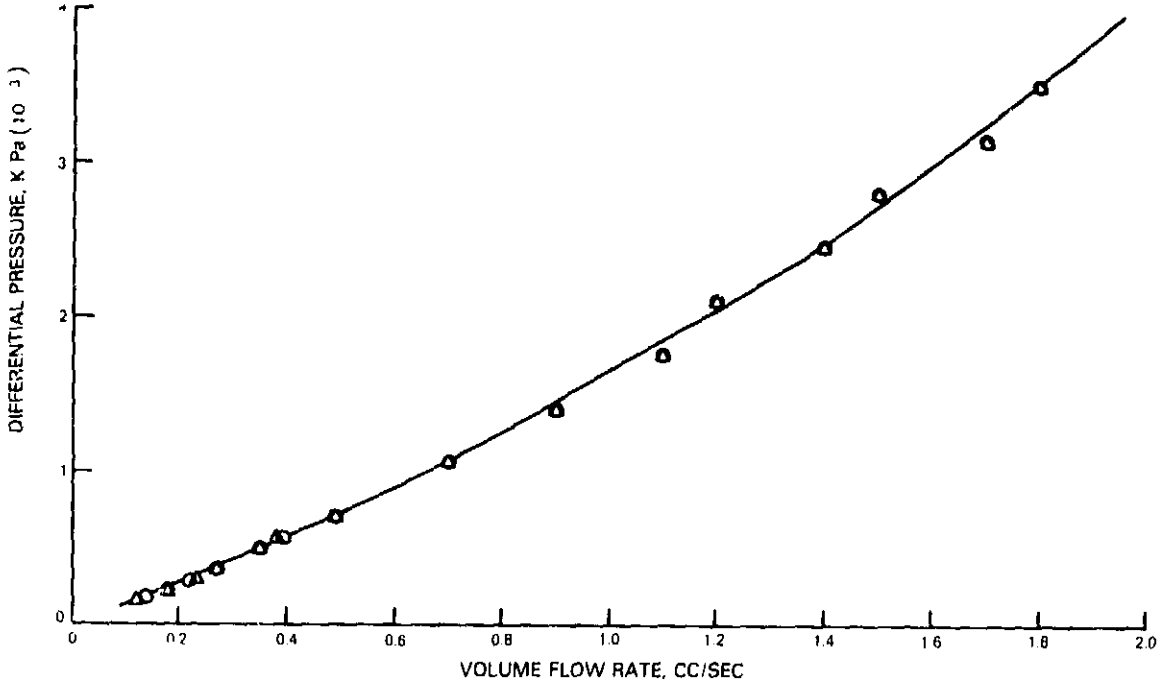

Figure 62A Capillary Flow Test With Transition Velocity 1.0 cm/sec AMK at Ambient Temperature

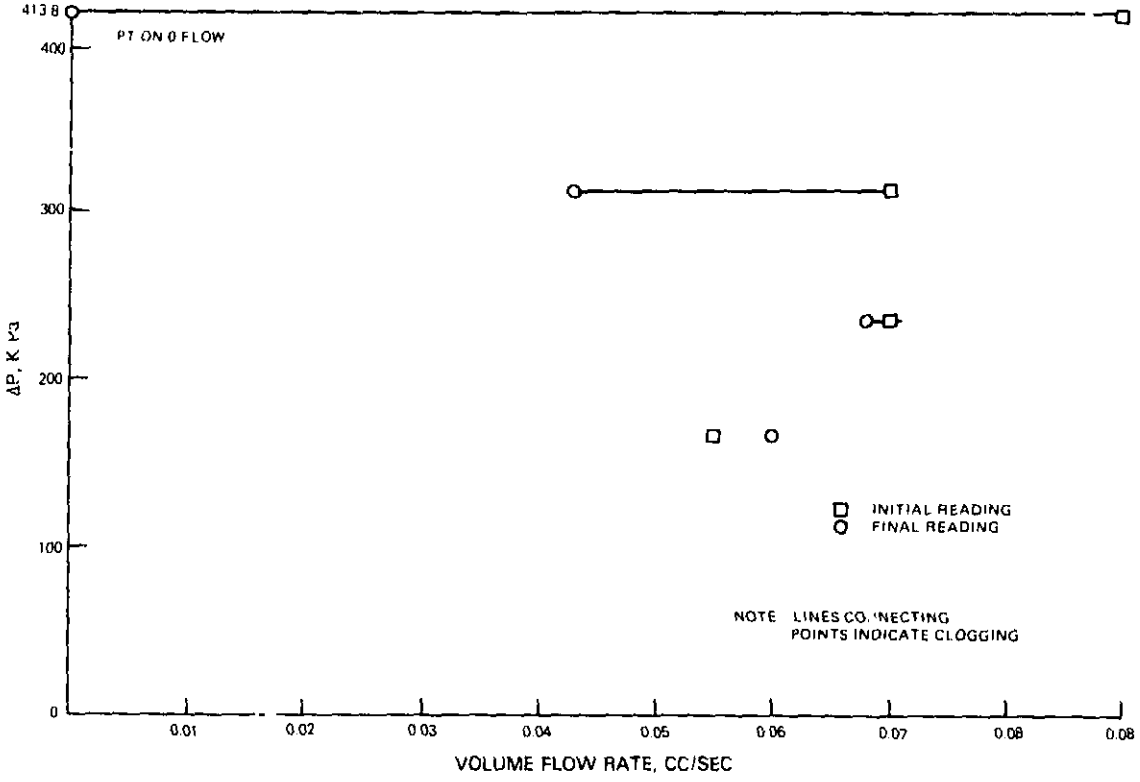

Figure 62B Capillary Flow Test with Undegraded AMK at Ambient Temperature

A second study focused on a single batch of AMK which had been stored in drums at outside temperatures ranging from -23°C to 38°C between July 1981 and February 1982. One-half of the fuel was stored at ambient and the other one-half heated at 71°F for three hours. One-half of each of the divided samples was then cooled and stored at -8°C while the rest of the samples were stored at ambient. Filter ratio measurements were taken at intervals after bringing the fuel to room temperature. Results of these tests are shown in Table XXXVI.

These studies revealed that at storage temperature, significant changes in the filter ratio of AMK can occur. The studies indicate that initial lower filter levels may be regained if the fuel is heated. The studies also showed that the filter ratio levels were low and relatively steady even after storing the heated fuel at cold temperatures. It is possible, therefore, that nine days of storage at -8°C is not severe enough to have a measurable impact. It also appears that continued storage at ambient will lower filter ratios to their original values.

TABLE XXXVI

FILTER RATIO RESULTS OF AMK STORAGE TEMPERATURE TESTS

	Ambient AMK		AMK Heated for 3 Hours at 71°C	
# Days	Stored Ambient	Stored at -8°C	Stored Ambient	Stored at -8°C
0	261	261	64	64
1	158	105	77	56
2	116	265	74	75
3	81	212	78	53
9	69	42	77	58

10.0 FUEL SHEARING APPARATUS DESIGN STUDY

The objective of this investigation was to evaluate candidate shearing methods and devices and to develop degrader design criteria. The study focused on three areas: 1) current techniques of degrading AMK, 2) evaluation of selected AMK degrader candidates and 3) conceptual application of a degrader to engine requirements.

Degradation of antimisting kerosene requires that the large polymer bonds which produce the fire safe properties be broken in order to satisfy fuel system and engine performance requirements. Devices that can apply molecular stresses to achieve this were investigated and their principles of operation fell into two general categories: mechanically or cavitation based energy input.

Shear produced mechanically by passing AMK between stages of multibladed rotors and stators of through axial flow gear of centrifigal flow impeller-diffuser systems can impart significant degradation. Examples of these are the Royal Aircraft Establishment's (RAE) degrader, P&WA's JT8D fuel pump, and General Electric's F101 afterburner fuel pump, respectively.

Cavitation produced by high velocity flow or by ultrasonic vibration (Ref. 4) has been shown to be an effective technique for degrading AMK. Cavitation in a flowing stream can be produced by accelerating the flow until the static pressure is reduced to the vapor pressure of the liquid. It can also be obtained in a vibrating device that locally produces large variations in liquid pressure. The collapse of cavitating bubbles results in extremely high local pressure and velocity gradients that produce very high levels of shear on the microscopic level. Some dissolved gas is necessary to obtain bubble nucleation sites but extreme amounts of gas leaving the liquid during bubble growth can cushion the ultimate collapse of the bubble. The fundamental physical and mathematical basis for cavitation can be found in References 5 and 6.

Samples of AMK were processed by commercial suppliers of homogenizers, emulsifiers, and dispersers and the results are summarized in Table XXXVII. It was found that when the pressure consumed by the Sonic Sonolator was multiplied by the number of passes, the Gaulin and Sonic results could be combined as shown in Figure 63. Also shown are results obtained with the JT8D fuel pump operating in a 16-pass mode.

TABLE XXXVII
SUMMARY OF RESULTS WITH COMMERCIAL UNITS

	Transition Velocity cm/sec	Filter Ratio
AMK Undegraded	0.19	23
Jet-A Without Additive	9-10	1.00
Gaulin Disperser (Cavitation)		
20.7 MPa	1.0	1.30
34.5 MPa	2.5	1.12
55.2 MPa	5.2	1.15
Sonic Sonolator (Cavitation)		
13.8 MPa 1 pass	1.1	1.41
10.3 MPa 3 pass	2.4	2.60
13.8 MPa 3 pass	3.9	1.30
Speco (Mechanical)	0.37	8.0
Teknar (Mechanical)	1.1	2.6

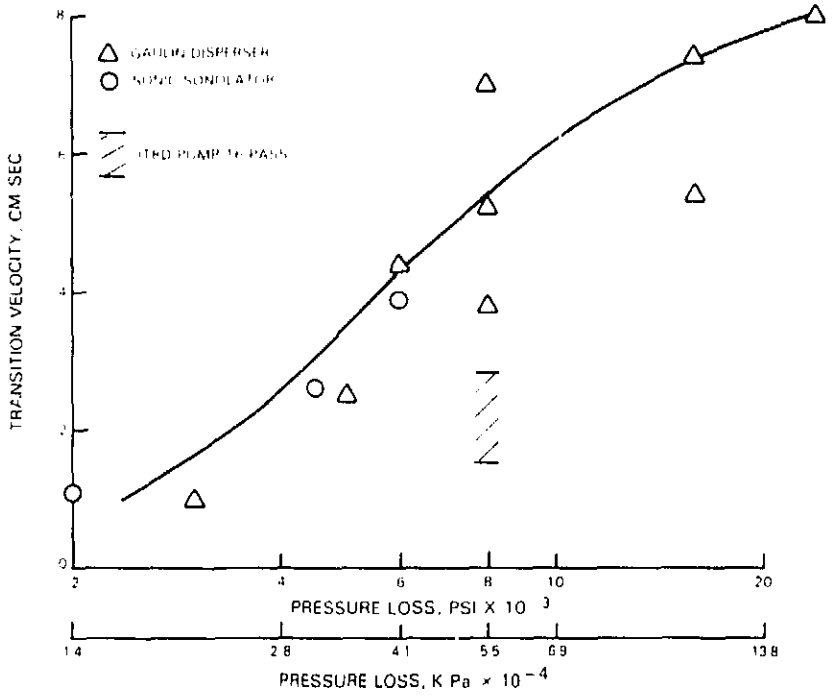

Figure 63 Reverter Performance

The use of ultrasonic energy to degrade polymers was investigated and this mechanism has been described in some detail (Refs. 7,8). In ultrasonic vibration, collapsing bubbles produce eddies with a size distribution. The larger eddies transmit energy to smaller eddies until finally the energy is dissipated through viscosity as heat. When the eddies are large compared to molecule size, the molecule is merely moved from place to place. Eddies smaller than the molecule give motion to various parts of the molecule setting up forces which break up the polymer structure when the force exceeds the bond strength of the molecule.

10.1 Fixed Area Vortex Venturi

In a cavitating venturi inlet static pressure, at the relatively low velocity approach section, is converted to dynamic pressure at the throat where low static pressure causes the formation of vapor bubbles. A diffuser follows the throat section and permits recovery of a considerable portion of the dynamic pressure as exit static pressure. Pressure recovery was important because it economized on the power expended in generating the large pressures used in obtaining the levels of transition velocity shown in Figure 63. Pressure recovery was also desirable because it reduced the fuel temperature rise experienced in converting high static pressure to dynamic pressure while flowing through an orifice, valve, or nozzle, as shown in Figure 64. Cavitation ceased at some point downstream of the throat where the increased static pressure prevented the existence of vapor bubbles.

Only the wall area contained vapor bubbles in an ordinary cavitation venturi. The streamlines near the wall were curved relative to the streamlines near the center resulting in a radial velocity gradient and a low static pressure near the wall. Since a vortex contains a low pressure area in its core, an attempt was made to improve the coverage of bubbles in the throat of a venturi by inducing rotation in the approach section. To accomplish rotation, a swirler made of twisted copper ribbon was placed upstream of the throat.

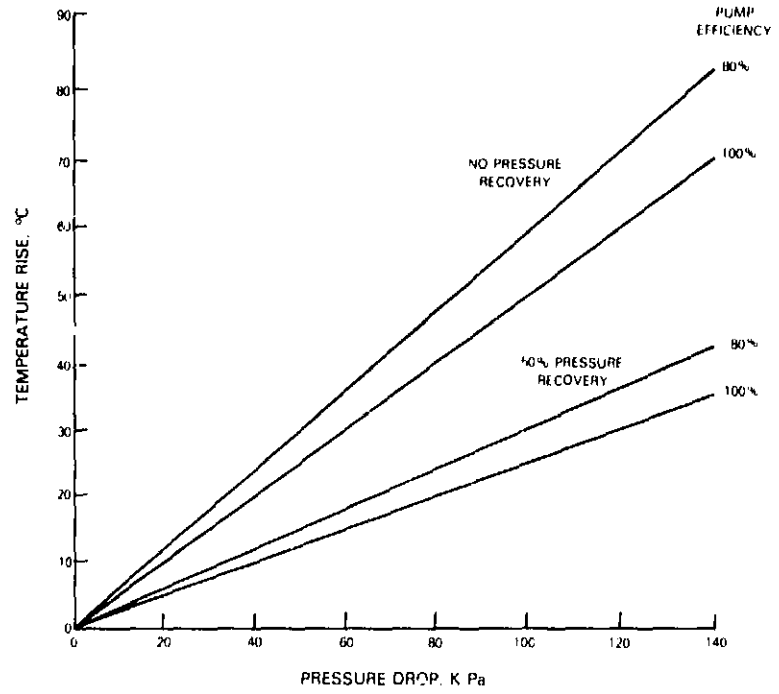

Figure 64 Fuel Temperature Rise

Two plexiglas and one steel venturi were fabricated and tested as fuel degraders. The plexiglas venturis permitted visual observation of the cavitation region; visual observations were recorded in still and motion pictures, examples of which are shown in Figure 65. It can be seen that the length of the cavitating region was reduced as recovery pressure increased. The length of the cavitating region also reduced when the swirler was removed.

The flow rate of the plexiglas venturi was calibrated over a relatively narrow range of pressure (tests ultimately run at 13.8 MPa are described later). The initial results are shown in Figure 66. It can be seen that the removal of the swirler had a negligible effect on flow rate. The throat diameter of the venturi was 0.262 cm.

The performance of the vortex venturi was obtained by operating in a multipass mode in the test apparatus shown in Figure 67. Care was taken to prevent or compensate for the degrading action of the rig components. The fuel was transfered from the supply drum to an accumulator by a peristolic pump that acts as an extrusion device in which a roller passes over a flexible tube. The

accumulator contained a piston which was translated during expulsion by pressurizing the dry side with nitrogen. All valves were 1.3 cm ball valves which in the open position did not restrict the flow except in the case of the back pressure valve. The action of the back pressure valve was compensated by measuring the transition velocity of the fuel in the receiving drum as well as the fuel in the sample container.

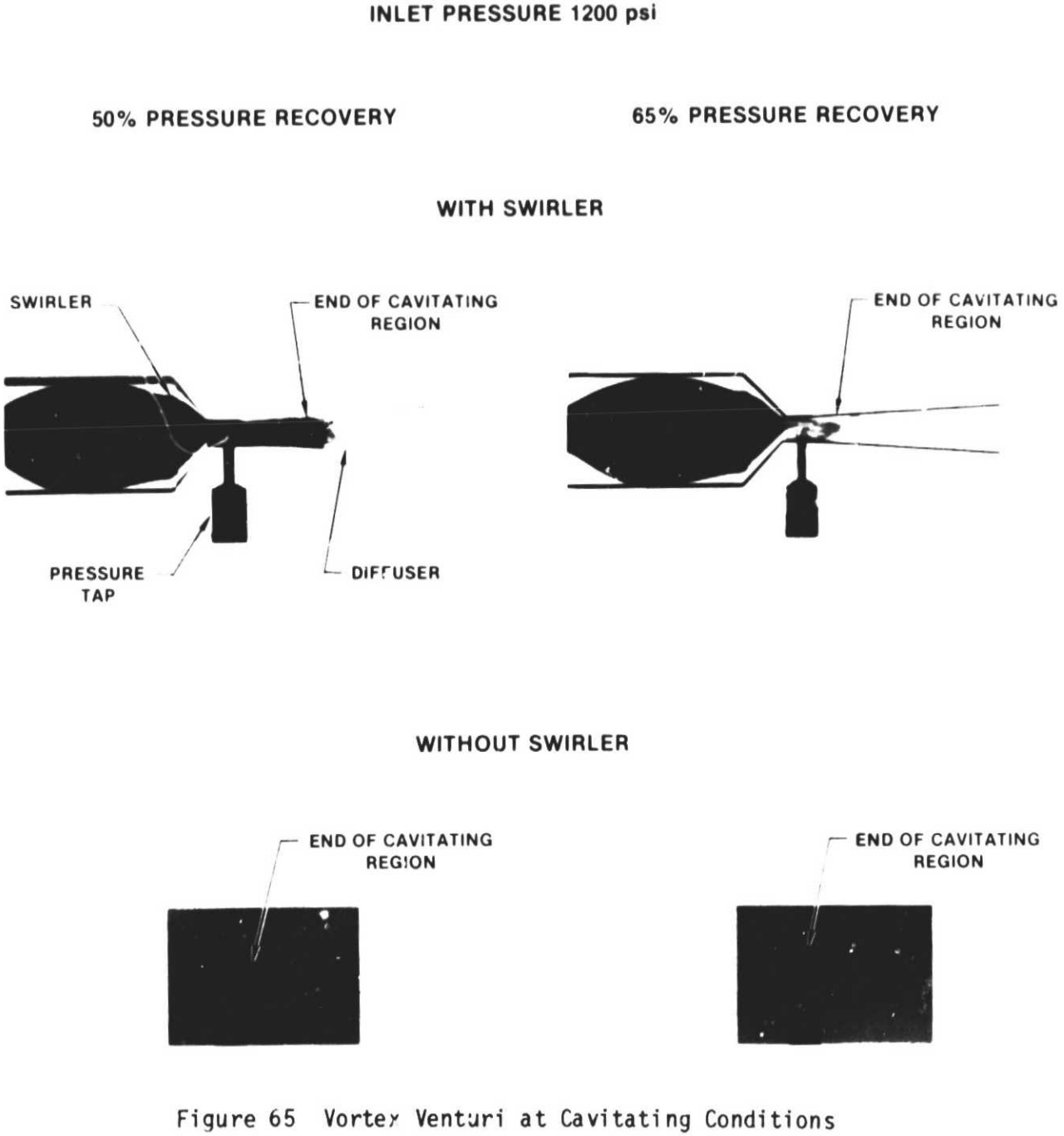

Figure 65 Vortex Venturi at Cavitating Conditions

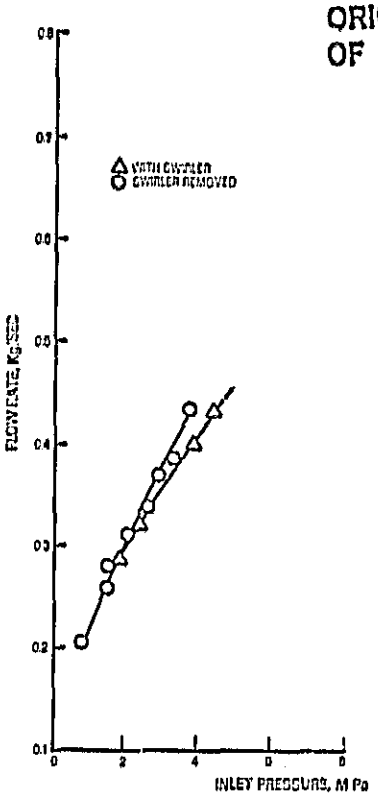

Figure 66 Plexiglas Venturi Flow Calibration

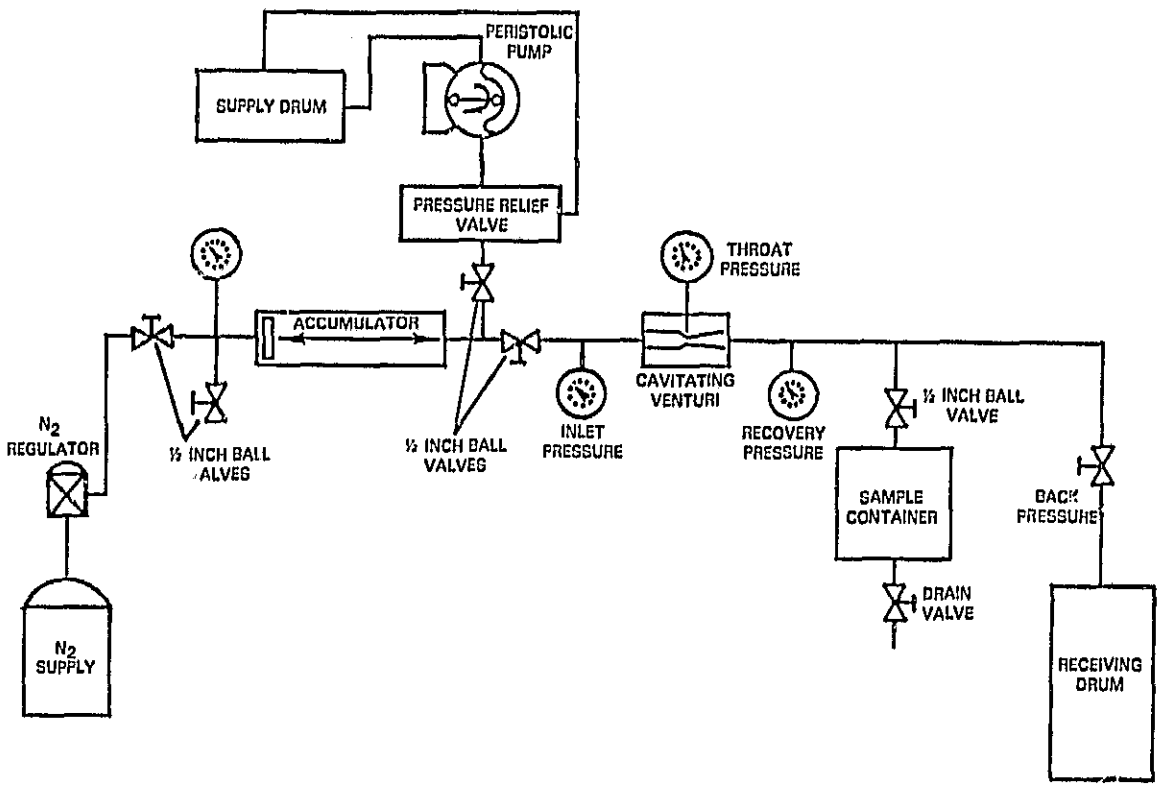

Figure 67 Vortex Venturi Test Apparatus

Sampling was done in two steps. First, the sample container was filled with the rig in operation and the drain valve closed. During the initial filling, a pressure drop occurred between the container supply line and the partially filled container. The pressure dissipated when the container was full, and at that point, the drain valve was reopened. During step two, sample collection was carried out over a period of time sufficient for displacement of a fuel volume greater than the sample container. In the sampling during step two, the container was filled with no pressure drop in the sampling system. After sampling, the sample inlet and drain valves were closed and the fuel remaining in the accumulator was allowed to pass through the venturi. After each pass, the receiving drum became the supply drum for the following pass.

Transition velocity was obtained with an apparatus identical to the one previously described. At least two filtration runs were made after each run on the fuel remaining in the sample container and also an additional sample taken from the receiving drum.

To obtain transition velocity, the flow velocity through the filter was plotted against filter pressure drop and a curve was drawn through the data; transition velocity was considered to be equal to flow velocity at a pressure drop of approximately 12.7cm Hg. It had been established before testing began that in several cases, the transition velocity obtained by the method of intersecting lines previously described corresponded to the velocity measured at 12.7cm Hg on an identical sample. In the revised method, smooth curves were drawn through the data without regard for the exact location of intersecting lines. The accumulated difference between the transition velocity measured for the fuel in the receiving drum was subtracted from the transition velocity for fuel in the sample container to adjust for the small effect of the back pressure valve.

To evaluate the performance of the vortex venturi, the inlet pressure was simply multiplied by the number of passes and the resulting accumulated pressures plotted against transition velocity. The results obtained with the first plexiglas venturi at an inlet pressure of 13.8 cm/sec 2000 psia and a pressure recovery factor of 0.5 (ratio of exit pressure to inlet pressure) are

shown by the open circles in Figure 68. It can be seen that the results are similar to the data obtained from the commercial units that were surveyed. However, pressure expended in commercial units cannot be recovered, while the effective pressure expended in the venturi is equal to the accumulated inlet pressure multiplied by the term (1- recovery factor). The adjusted data shown by the dashed line shows that the vortex venturi is superior to the commercial devices. The half-filled circles show that a reduction in recovered pressure increased the transition velocity and removal of the swirler caused a decrease.

Following this series of tests, a failure of the first unit occurred. The cause of failure was not determined with certainty; however, start of failure appeared to be in the cavitation region where the soft plexiglas surface had been considerably pitted. A second plexiglas venturi was fabricated and tests of the second unit were run at three levels of inlet pressure with a pressure recovery factor of 0.5. After completion of this series, a crack developed at the aft end of the pressure recovery diffuser in the second venturi.

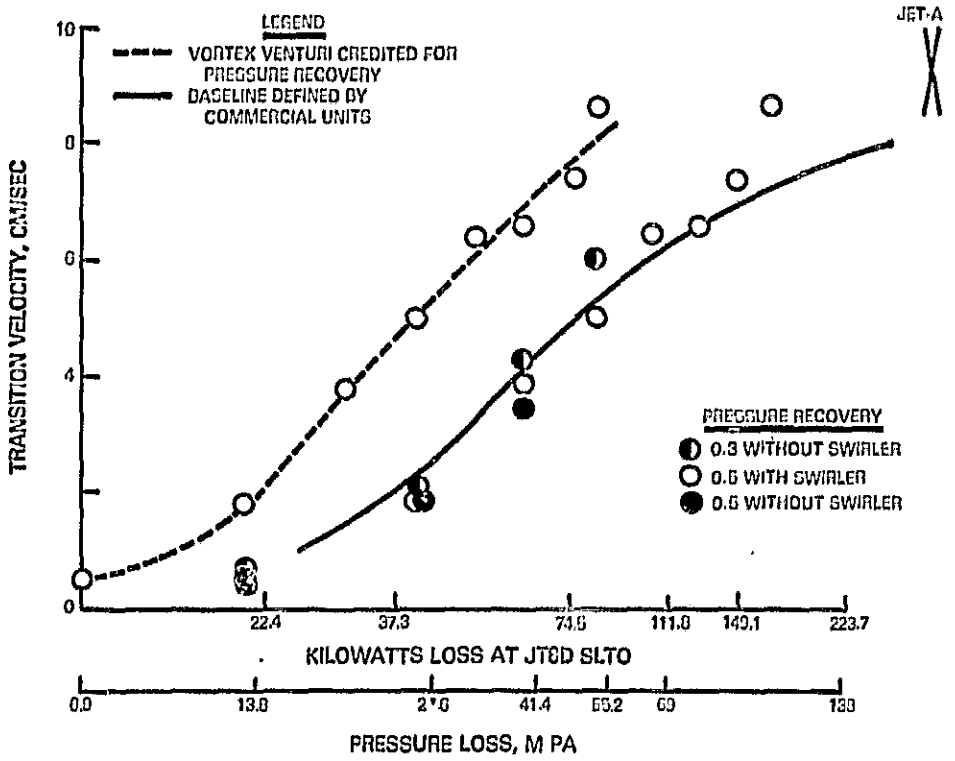

Figure 68 Performance of First Plexiglas Venturi

Two significant factors were found in the data obtained with the second plexiglas venturi as indicated in Figure 69. The data for both units closely followed a single curve. Furthermore, data obtained at inlet pressures of 8.3, 10.3, and 13.8 MPa fell on the same curve when the inlet pressure was multiplied by the number of passes. It appears that where cavitation effects predominate, the accumulated value of inlet pressure is a valid factor for correlating transition velocity.

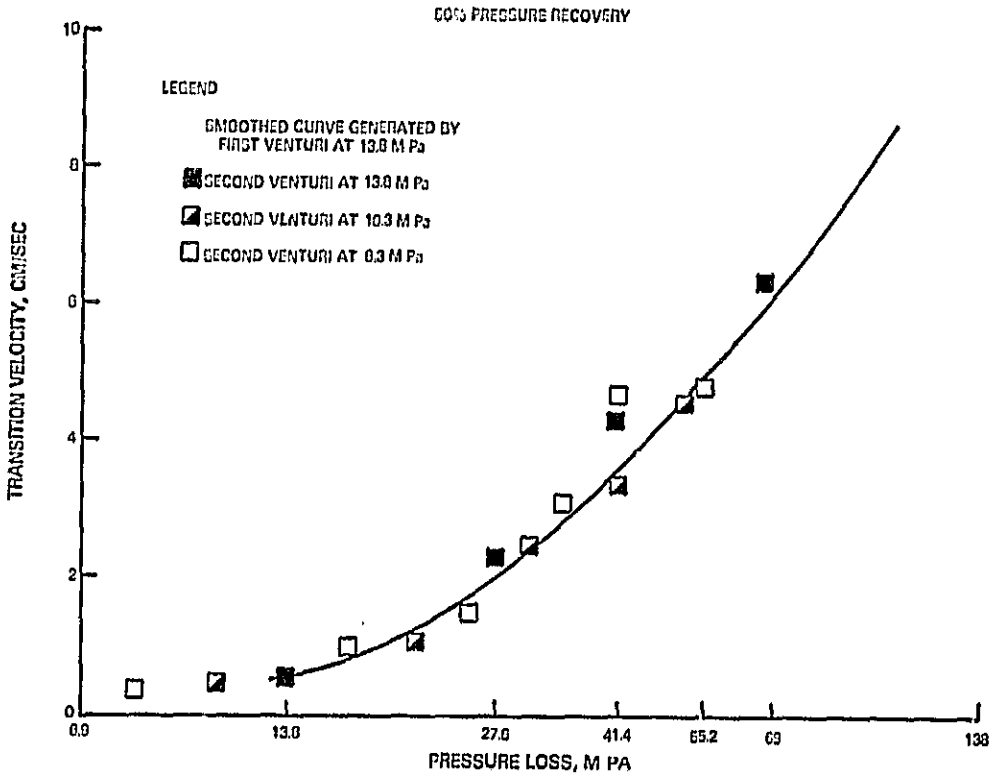

Figure 69 Performance of Second Plexiglas Venturi

A third venturi was fabricated with stainless steel. It was found that the flow calibration with the swirler, as shown in Figure 70, indicated that the effective metering throat area was smaller by approximately 40 percent than the geometric throat area. When the swirler was removed, the effective throat area increased to its anticipated size.

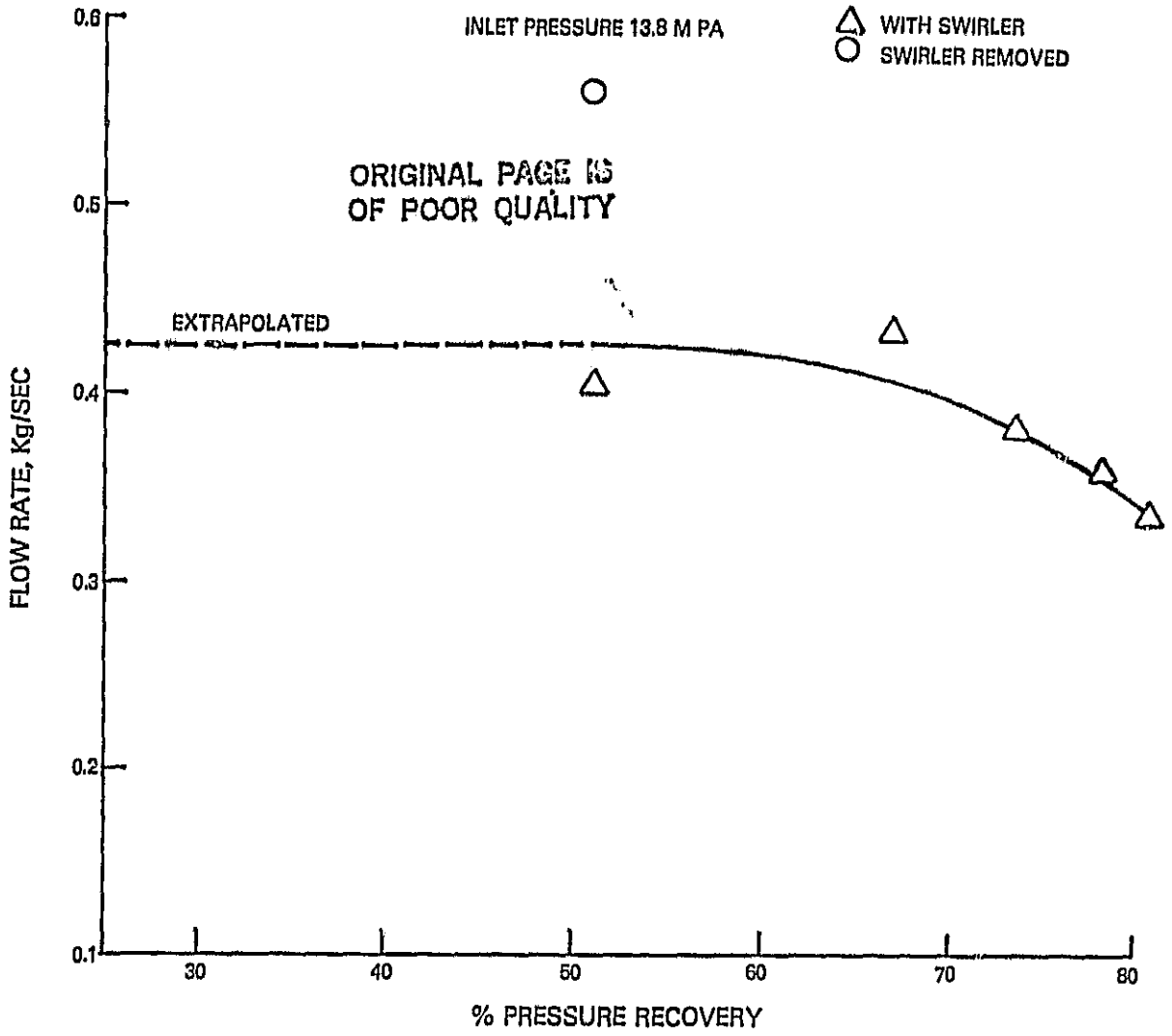

Figure 70 Steel Venturi Calibration

The steel venturi had exceptionally good performance as shown in Figure 71. The transition velocity with an accumulated pressure of 69 MPa (10,000 psia) and a recovery pressure factor of 0.34 to 0.58 was 8-9 cm/sec as compared with the previous value of 6 cm/sec attained at 69 MPa (10,000 psia). The performance was reasonably good at a recovery factor of 0.75. In fact, when accumulated pressure was corrected for pressure recovery for the JT8D at Sea Level Takeoff (SLTO), the theoretical power requirements decreased with pressure recovery over the entire range of test parameters as shown in Figure 72. Theoretical power requirements can only be considered as goals, however, because they cannot be achieved in practical systems with available components.

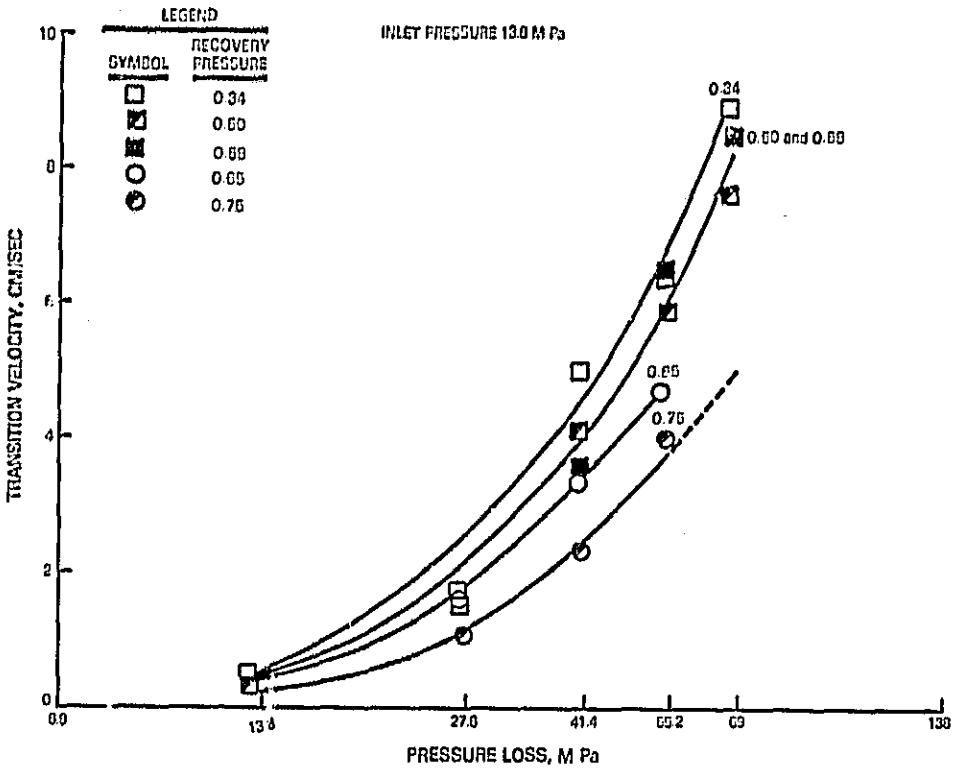

Figure 71 Perfomance of Simple Steel Venturi

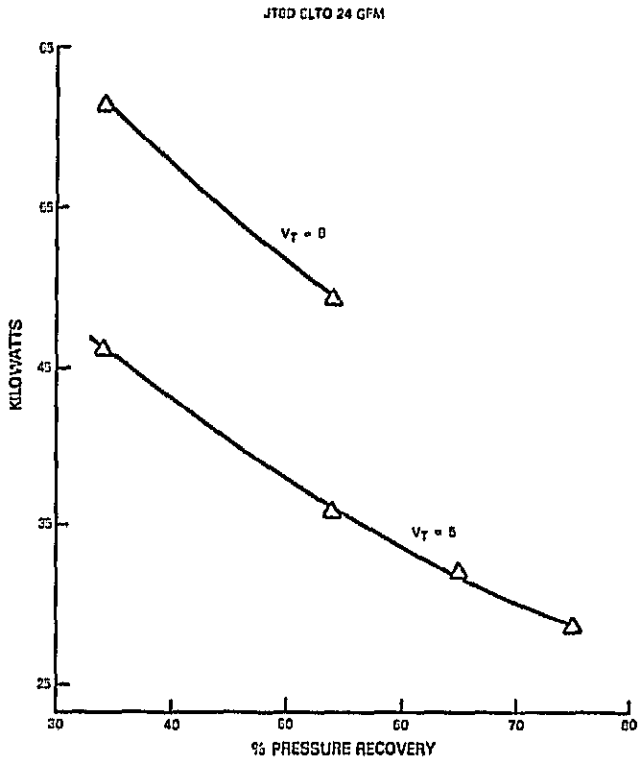

Figure 72 Theoretical Power Requirement Based on Steel Venturi Results

10.2 Variable-Area Vortex Venturi

A fixed area device cannot be used as a degrader in an aircraft gas turbine if performance is based on a pressure drop because the large variation in fuel flow between idle and sea level takeoff results in an even larger variation in pressure drop. Having shown the applicability of a vortex venturi, the performance of a variable-area version was determined. Variable area was accomplished by a pintle in the style shown in Figure 73. It can be seen that for a given area ratio, the use of a pintle reduced the length of the diffuser while increasing its outer wall angle. A flow calibration was made of the venturi with the pintle in two positions as shown in Figure 74. In the aft position with a wide-open throat, the effective metering throat area was close to the geometric throat area. In the forward position, the metering area was reduced by a factor close to 3.

The performance of the steel venturi with pintle in two positions is shown in Figure 75. The square symbols indicate that pressure recovery factor had a drastic effect on the pintle in the aft position while the triangular symbols indicate that pressure recovery did not affect performance when the pintle was moved to the forward position. The difference in behavior at the two positions cannot be explained without additional experimental data. The circular symbols indicate that performance with the swirler was up to 40 percent higher than performance without the swirler.

10.3 Ultrasonic Generator

A continuous flow piezoelectric ultrasonic generator shown conceptually in Figure 76 was fabricated during the program. A total of 16 transducers were mounted on both sides of a shallow channel. The unit was tested but it did not operate successfully even when 10 of the transducers were actuated and approximately 1 Kw of power was dissipated. It was felt that the power was dissipated in the frame of the unit without producing ultrasonic vibration at the walls. Strong audible signals were heard whenever the power was turned on. A redesign of the unit was recommended, however, since the concept was in a developmental stage a reasonable chance of success in the first redesign was not assured. It was decided that at this stage of the degrader program, consideration of the ultrasonic generator should be suspended.

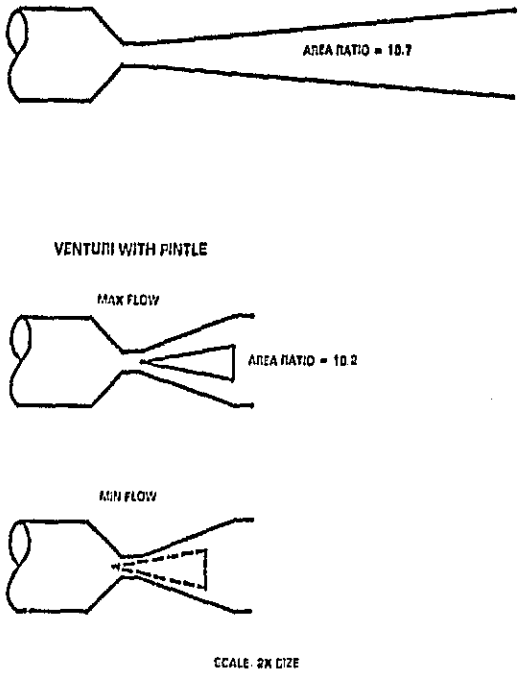

Figure 73 Venturi Without Pintle

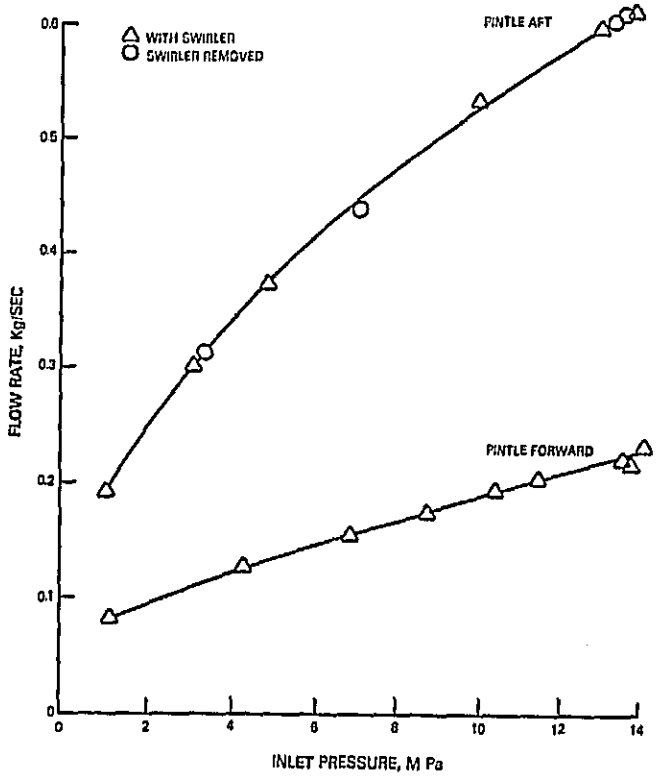

Figure 74 Venturi With Pintle Calibration

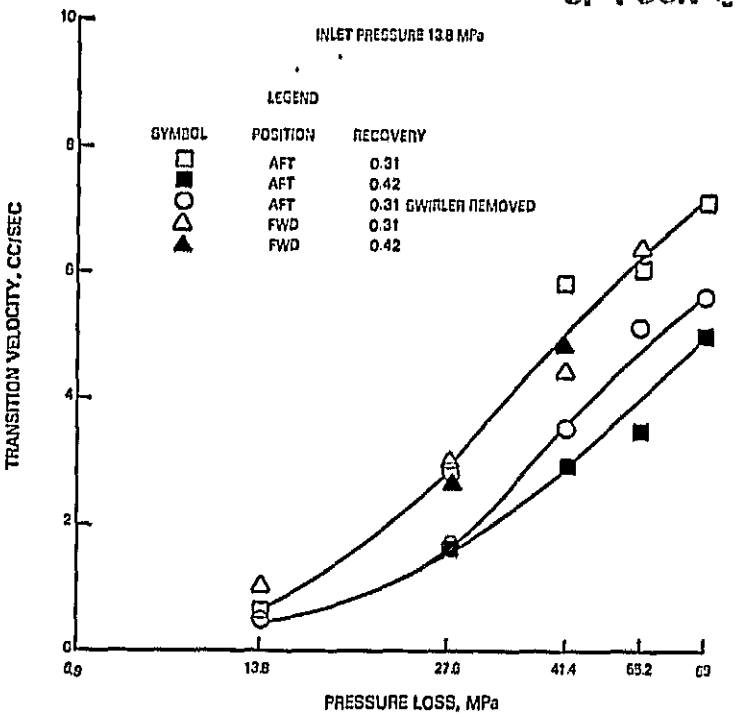

Figure 75 Performance of Steel Venturi with Pintle

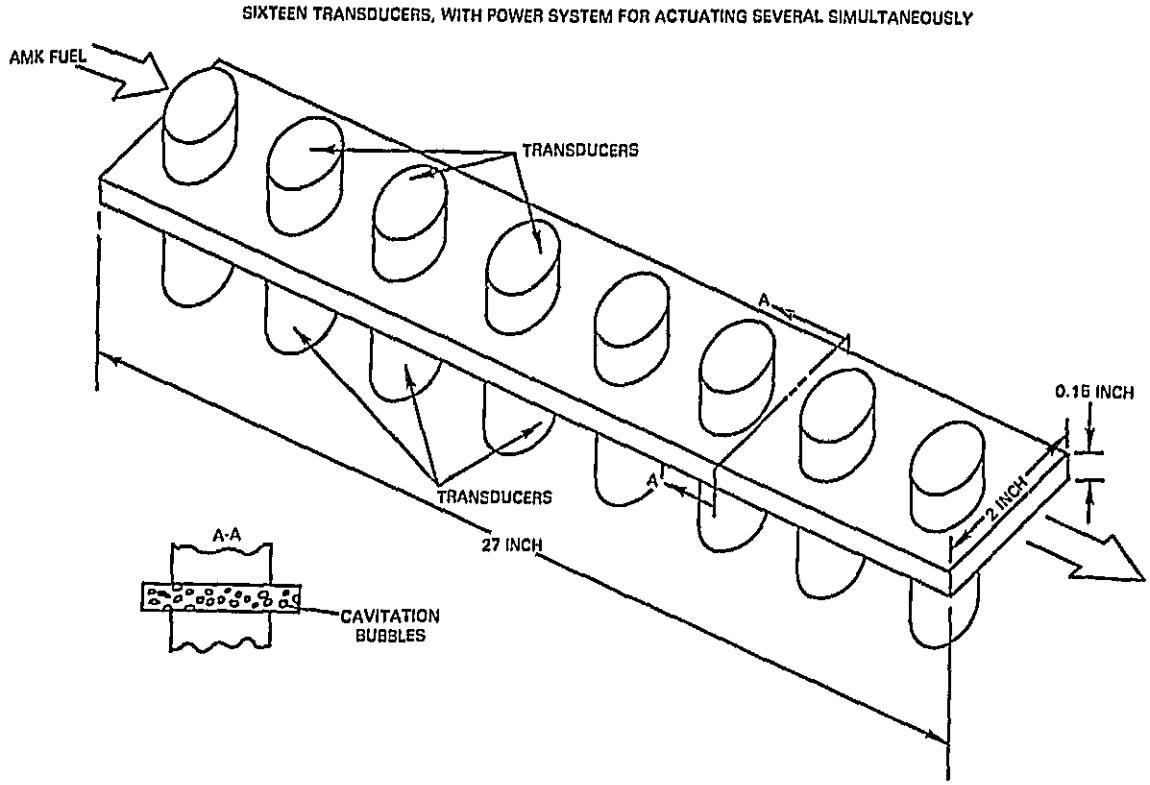

Figure 76 ARTEK Ultrasonic Cavitating Degrader

10.4 Analysis and Application

Using the vortex venturi, it was found that a transition velocity of 8 cm/sec was theoretically possible with considerably less energy cost than that required by the JT8D fuel pump or by the commercial devices that were tested. It can be seen in Figure 77 that the performance of the JT8D pump with 7 passes was approximately equivalent to venturis operating without credit for pressure recovery at an accumulated inlet pressure of approximately 24.1 MPa (3500 psia). Beyond that point, the performance of the pump deviated from the venturi performance. The commercial units were equivalent to the venturis up to a pressure of approximately 41.4 MPa (6000 psia).

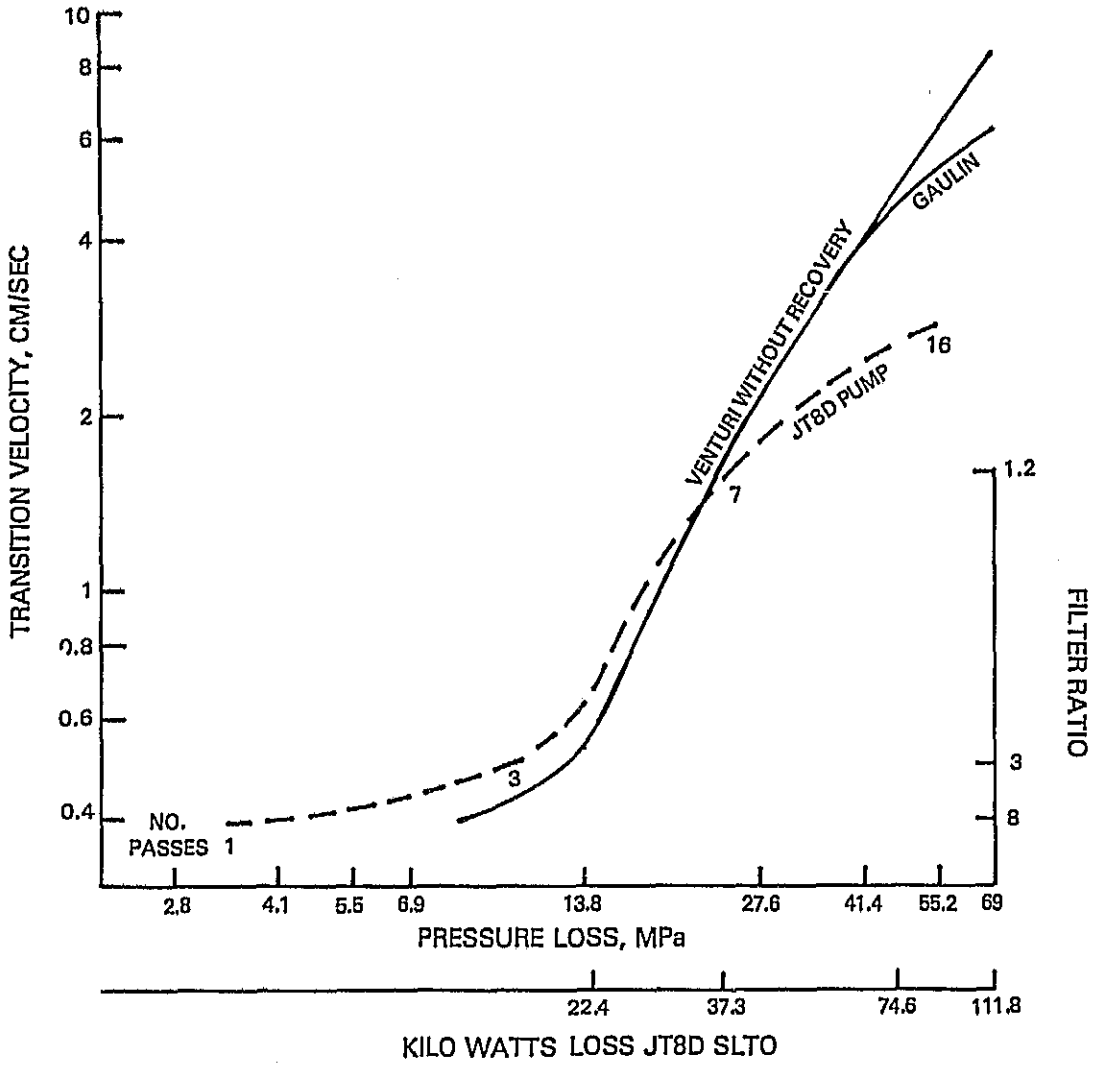

Figure 77 Summary of Degrader Performance

Results of the filtration tests discussed previously indicate that a transition velocity of at least 8 cm/sec will be required to satisfy the requirements of existing engines at low fuel temperatures. This level of performance will be difficult to attain even with the vortex venturi in a staged configuration. Two examples of pump/venturi staging are shown in Figure 78. Three pump stages and 4-5 venturi stages were used, and using the performance data of Figure 70, a transition velocity of 6 cm/sec was achieved at a cost of 48.5 KW at JT8D SLTO conditions. This requirement is higher than the theoretical value shown in Figure 78 and it represents the compromise that must be made in order to set a practical limit on the selected number of pump venturi stages.If the performance of the venturi can be improved at 0.75 pressure recovery, a transition velocity of 8 cm/sec might be attainable with 48.5 KW.

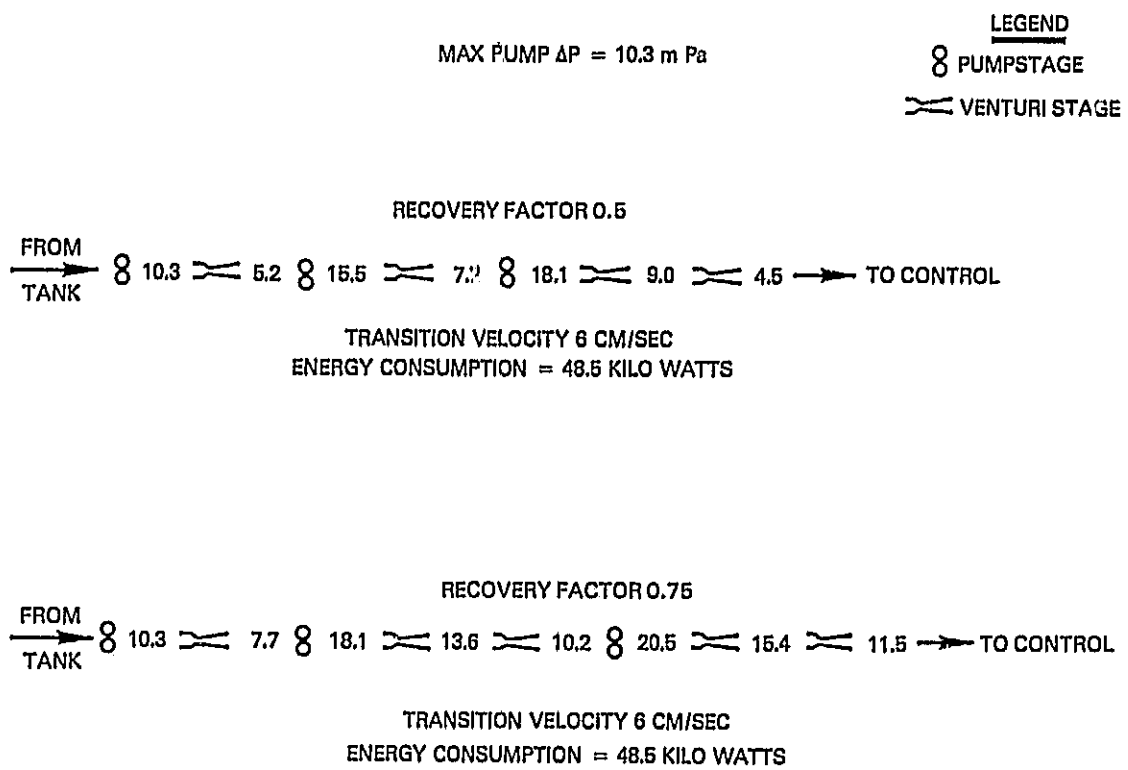

Figure 78 Multiple Venturi Concept

The pump venturi power requirement of 48.5 KW at SLTO translates to approximately 17 KW at JT8D cruise conditions. An estimate was made to determine the effect of power extraction on engine performance and it was found that the 17 KW corresponded to an increase in TSFC of 0.4%. Also a multistage pump/venturi package may require considerable volume and it may be difficult to transmit 48.5 KW to the package. It would be very desirable to reduce the volume and power requirements of the degrader. To miniaturize the degrader it is necessary to supply as many vapor bubble sources as those existing in several venturis. One possible concept of miniaturization is the UTRC rotating cavitating degrader shown in Figure 79. Each of the pin-like projections moves with sufficient velocity to produce cavitation along its sides. It is felt that with a sufficient number of cavitation sources, miniaturization can be accomplished.

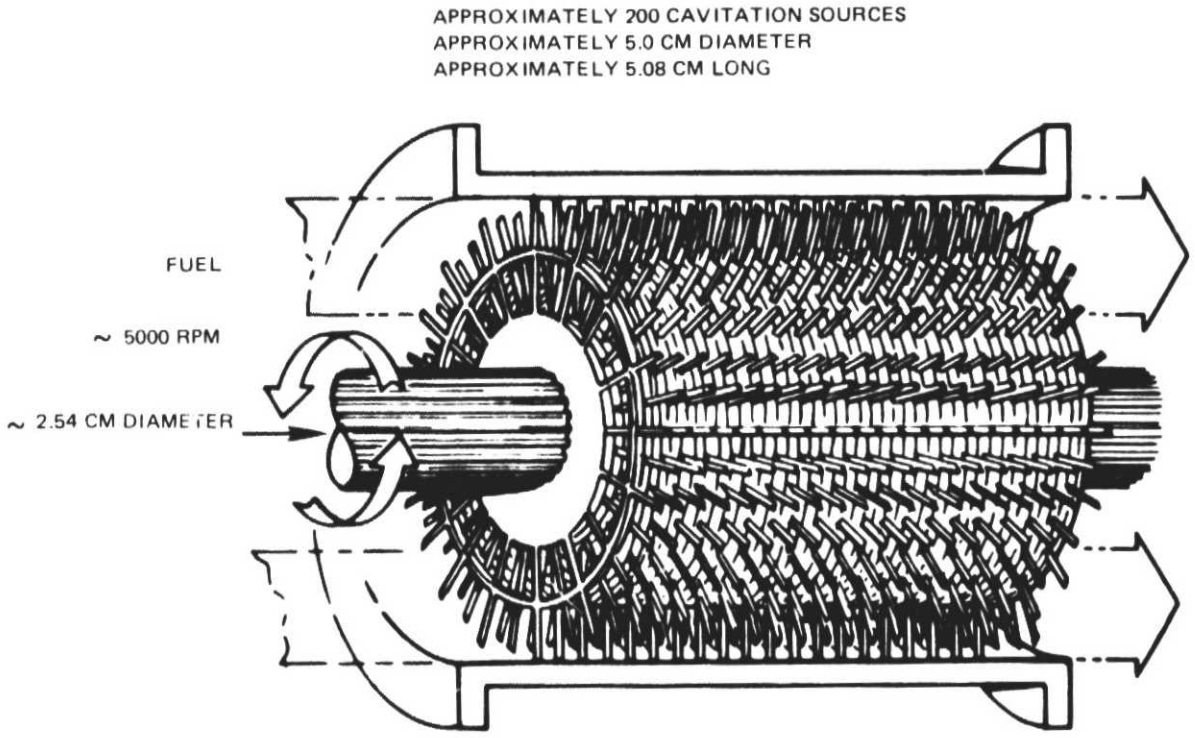

Figure 79 Rotating Cavitating Degrader

There are other practical problems that must be addressed in a degrader development program. Continuous flow variation must be achieved over a very wide range of flow; if multiple venturis are used, they must be carefully matched to achieve the required flow and pressure variation. Special controls will be needed to maintain proper position control of pintles in venturis; controls will also be needed to meter the required engine fuel flow through the venturi/pump system. Cavitation damage is also a problem. Degrader designs must be sufficiently rugged and proper materials must be chosen in order to assure suitable lifetimes. Care must also be taken to avoid excessive temperature rise in the fuel because high temperature can produce varnish and coke deposits in the engine fuel injectors. Special attention must be paid to certain engine operating conditions where there is limited power extraction capability in the engine such as altitude relight conditions. Power requirements for the degrader must be kept to a minimum in order to cope with these special engine conditions.

11.0 FUEL INJECTOR PERFORMANCE TESTS

An existing ambient fuel spray test facility was used to establish the fuel spray spatial distribution and the droplet size distribution produced by the JT8D Bill-of-Material injector, low emission airblast injector, and an air-boost injector. Spray characterization tests were conducted using six fuels; Jet A, one and three-pass JT8D fuel pump degraded, one and two-pass Gaulin degraded, and undegraded antimisting kerosenes.

The objective of this task was to determine if any of the injectors were clearly superior to others in terms of the characteristics of the spray produced with the different fuels, and to determine the extent of degradation required to achieve an acceptable spray. A Malvern Model ST1800 particle size analyzer was used to determine the droplet size distribution. Patternator probes and photographs were used to obtain spatial distribution information.

The spray facility used in the test program is depicted in Figure 80. The facility was equipped with a 20-probe patternator rake used to evaluate the liquid distribution downstream of the injector. In this program, patternator measurements were obtained at a distance of 7.6 cm from the nozzle discharge plane. Still pictures recorded the spray pattern and served as a basis for measuring spray cone angles and to document fuel streaking. The photographs were obtained using a high power General Radio Strobolume to illuminate the spray; the ten microsecond light pulse produced by a strobe substantially stopped the droplet motion.

The particle size analyzer (Figure 81) operated on the basis of the measurement and analysis of the distribution of the diffracted portion of a beam of monochromatic (laser) light which passed through the spray. An analytical program executed within a dedicated minicomputer provided a comparison of the measured light energy distribution with a calculated energy distribution based on a Rosin-Rammler droplet size number distribution. The program operated by continuously modifying the distribution function parameters (the characteristic diameter, PE, and the exponent parameter, W) until a best fit between experiment and prediction was obtained. The Rosin-Rammler distribution function is:

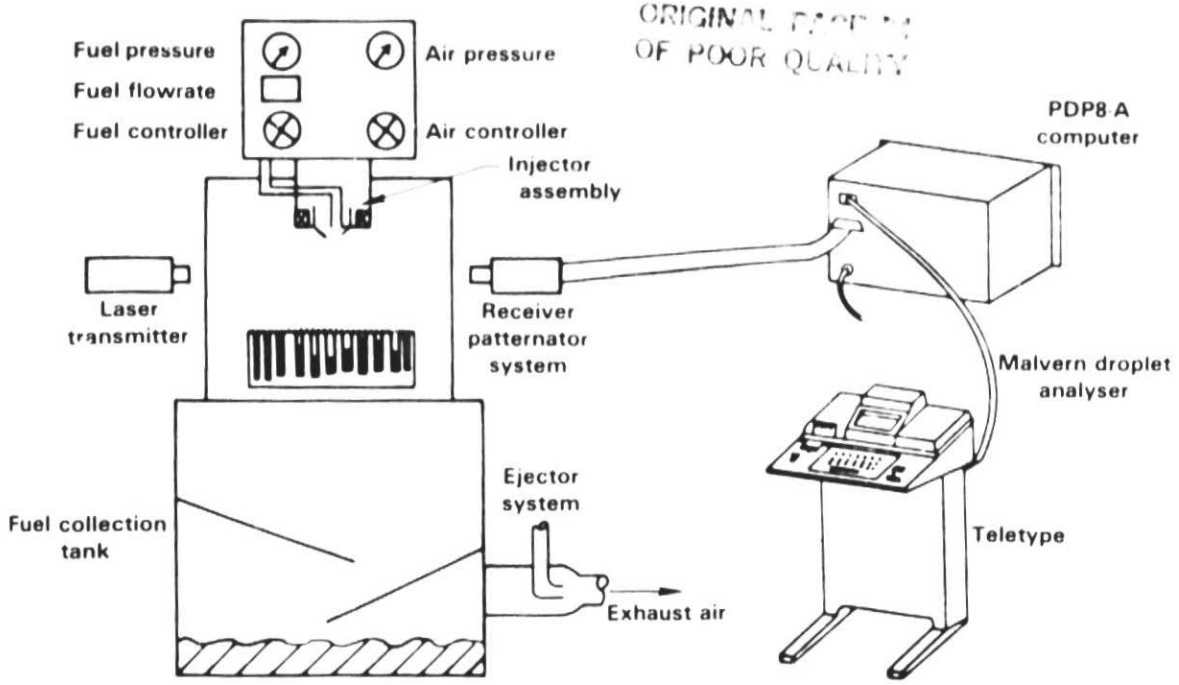

Figure 80 Schematic Diagram of the Ambient Spray Evaluation Facility

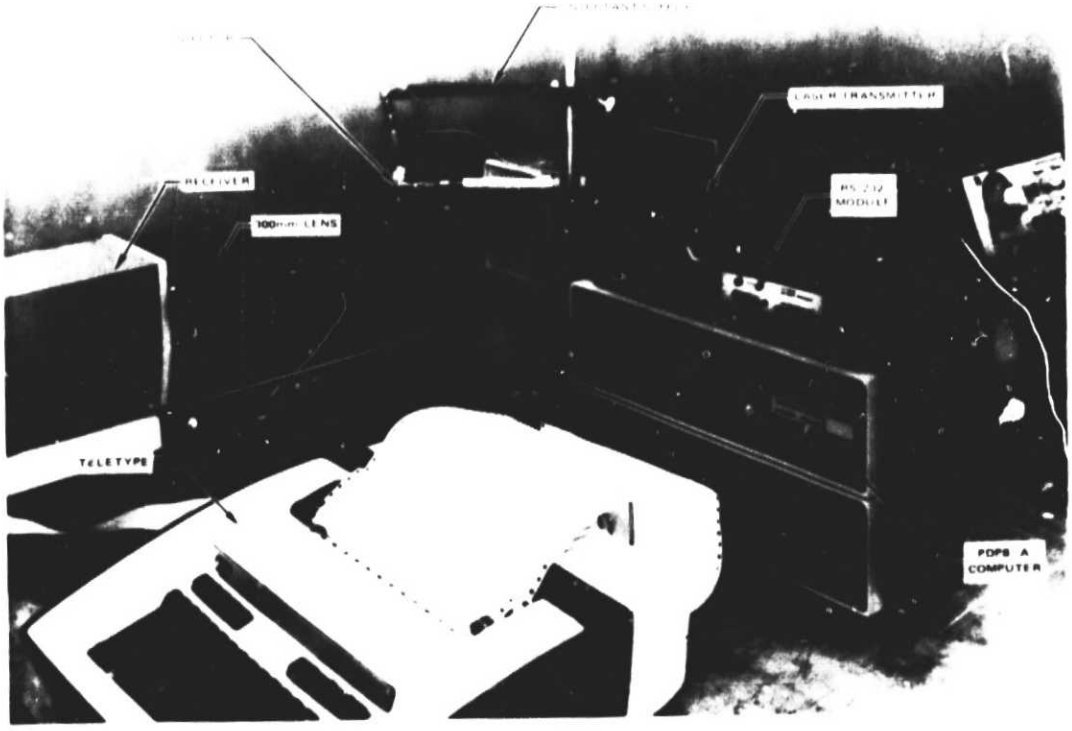

Figure 81 Malvern Droplet Distribution Analyzer

$$1 - v = e^{-\left(\frac{d}{PE}\right)^W}$$

where: v is the volume fraction of droplets with a diameter less than d. The SMD is defined as the diameter of a droplet having the same volume to surface area of the entire spray. It can be calculated from the characteristic diameter and the exponent parameter as:

$$\frac{SMD}{PE} = \frac{1}{\Gamma\left(1 - \frac{1}{W}\right)} = \frac{1 - \left(\frac{1}{W}\right)}{\Gamma\left(2 - \frac{1}{W}\right)}$$

where: $\Gamma(X)$ = Gamma Function.

In this program, measurements were obtained at a location 5 cm. downstream of the nozzle tip. The range of droplet sizes that could be detected by the instrument as configured for use in this program varied from 562 microns to 5.7 microns.

Fuel was delivered to the test apparatus using the delivery system shown schematically in Figure 82. The Jet A fuel was supplied from an underground facility storage tank. The antimisting fuels, which had previously been processed to the desired level of degradation, were stored in a 87 liter accumulator which formed a portion of the fuel temperature conditioning system. Jet A fuel was supplied either directly to the injector being tested (when Jet A was the test fuel) or was delivered to the fuel conditioning system where the Jet A was used to displace the test fuel from the accumulator. The total rate of fuel flow was obtained for all tests by measuring the Jet A flow rate using conventional turbine meters. The fuel conditioning system used a cold acetone bath to chill the test fuel to the desired temperature levels. An electrical resistance fuel heater was used to obtain the elevated fuel temperatures. After temperature conditioning, the fuel was split into the primary and secondary flows. For these tests the secondary flow rate was measured by use of a mass flow meter which was insensitive to the viscosity characteristics of the fuel.

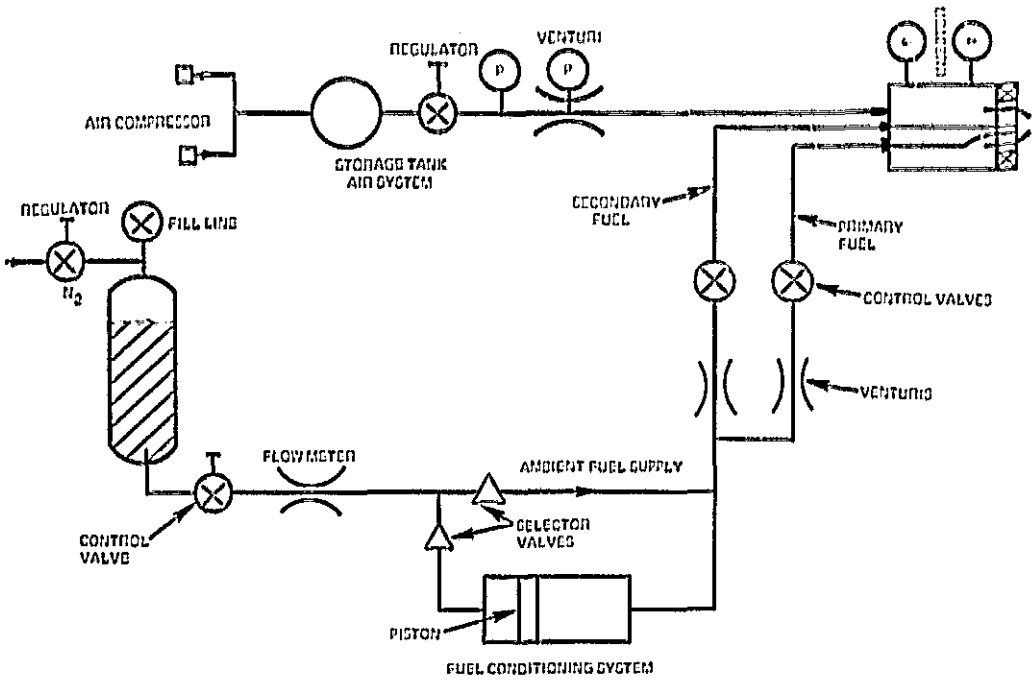

Figure 82 Air and Fuel Delivery System

11.1 Fuel Injectors

The pressure atomizing injector currently used in the JT8D engine is a duplex nozzle in which the primary flow is discharged through a central orifice and the secondary flow issues from a surrounding annular passage (Figure 83). The nozzle was fitted with an air shroud (nut) to prevent carbon from collecting on the nozzle tip. In these tests the nozzles were mounted in a cannister which supplied air to the nozzle nut. In the engine, the nozzle is surrounded by an air swirler which discharges swirler air into the head end of the combustor. The swirl air which may affect the fuel distribution, but not the atomization, was not supplied in these tests.

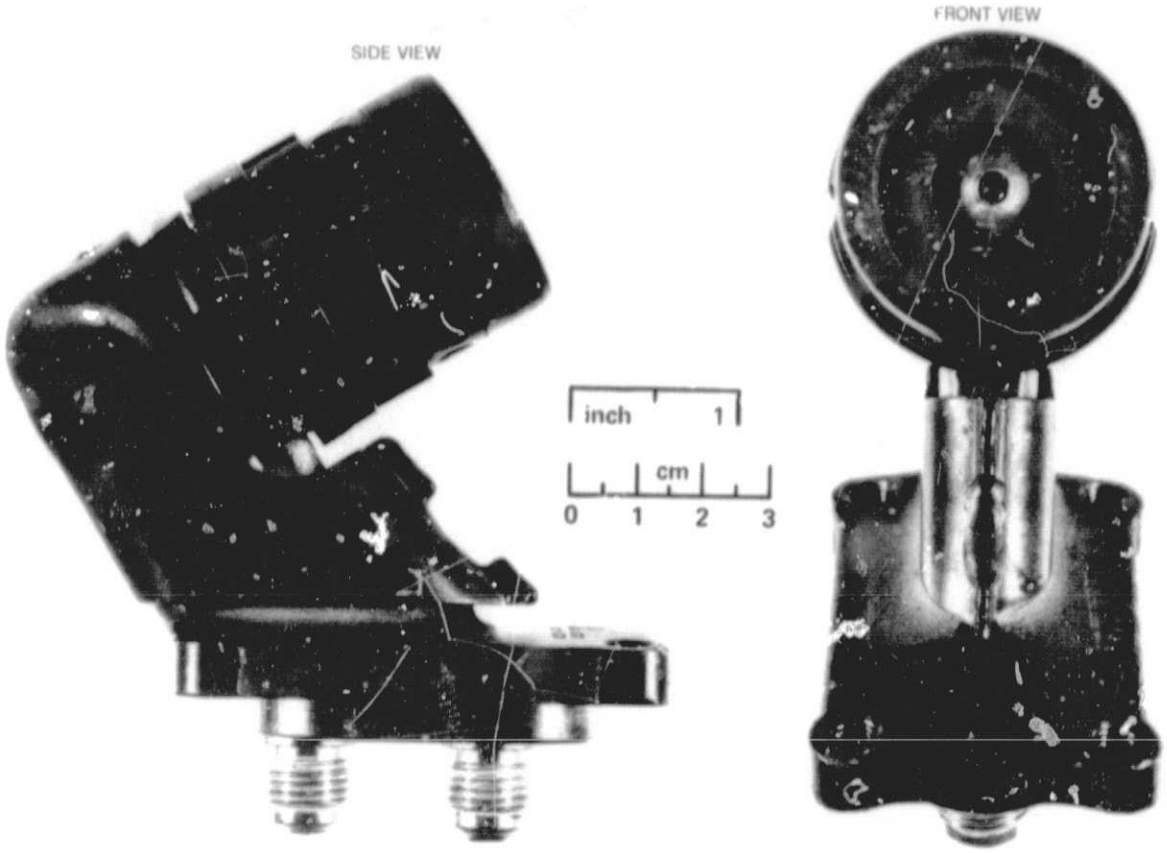

Figure 83 JT8D B/M Injector

The low emission JT8D nozzle (Figure 84) is a hybrid nozzle composed of a pressure atomizing primary nozzle and an airblast (or aerating) secondary nozzle. Fuel is atomized in the secondary passage by shearing the fuel off an annular surface to which a film of fuel is supplied. The high velocity air used to atomize the air is supplied from the engine diffuser; the air velocity is developed by the pressure drop existing across the combustor liner. In the nozzle test program, the injector was mounted in a cannister to which air was supplied at the appropriate condition. Airblast nozzles generally produced a wider range of droplet sizes than pressure atomizers and yielded a large number of small droplets.

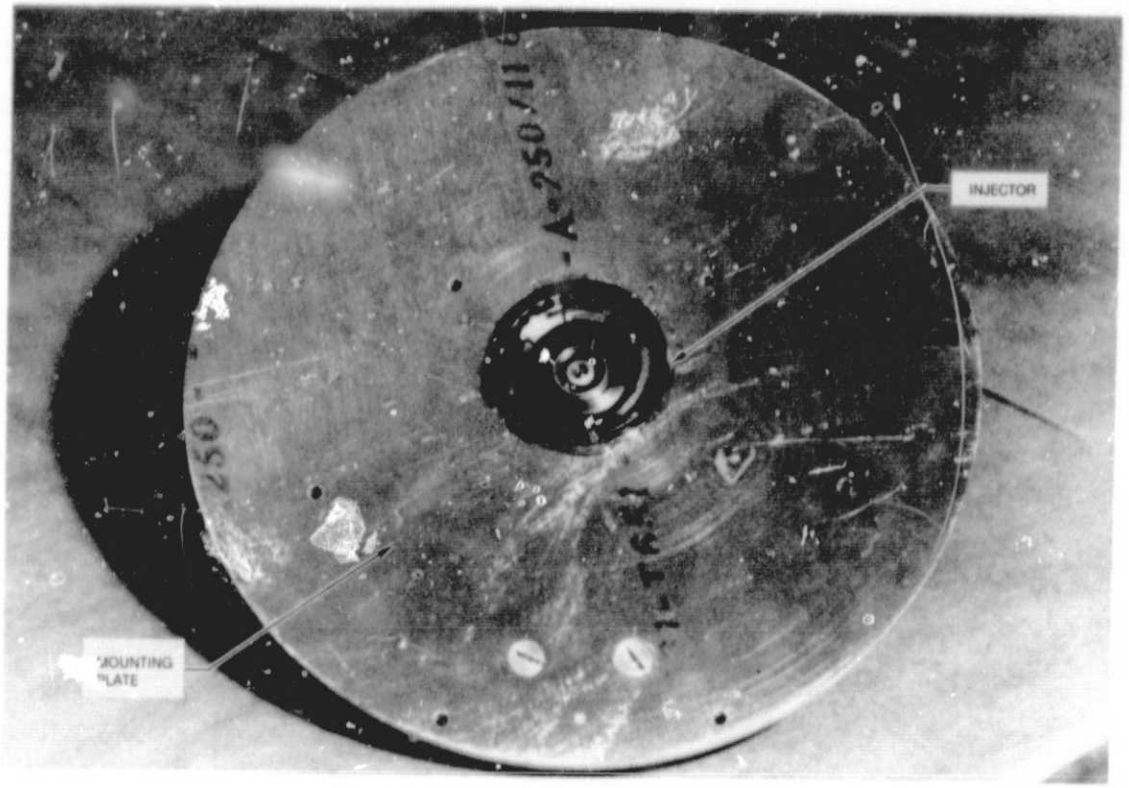

Figure 84 Low Emission JT8D Injector

Because of the poor atomizing characteristics of the antimisting fuel, a nozzle having a high capability for atomizing heavy or viscous fluids was used. An air boost nozzle (Figure 85) which employs an external supply of high pressure air was tested for this purpose. This nozzle, which is not tailored for aircraft engine use, had a somewhat lower flow capacity than the JT8D nozzle. Boost air was supplied to the nozzle at 4 atm for all tests.

11.2 Test Conditions

The fuel flow rates and the fuel temperatures at which the spray characterization tests were conducted are shown in Table XXXVIII. The fuel flow rates correspond to the engine ignition, idle, cruise, and sea-level-takeoff conditions. At each engine condition, tests were conducted at two fuel temperatures which included room temperature and either a low or high temperature condition. Table XXXVIII also shows the air side pressure drops used in the tests. For the pressure atomizing and airblast atomizing nozzles, the air side pressure drop was set to yield the same air velocity that would

exist in the engine burner at the given flight condition due to burner pressure drop. In the case of the air boost nozzle, the pressure drop indicated was the difference between the boost air supply pressure and the ambient pressure and corresponded to the maximum pressure drop recommended by the manufacturer.

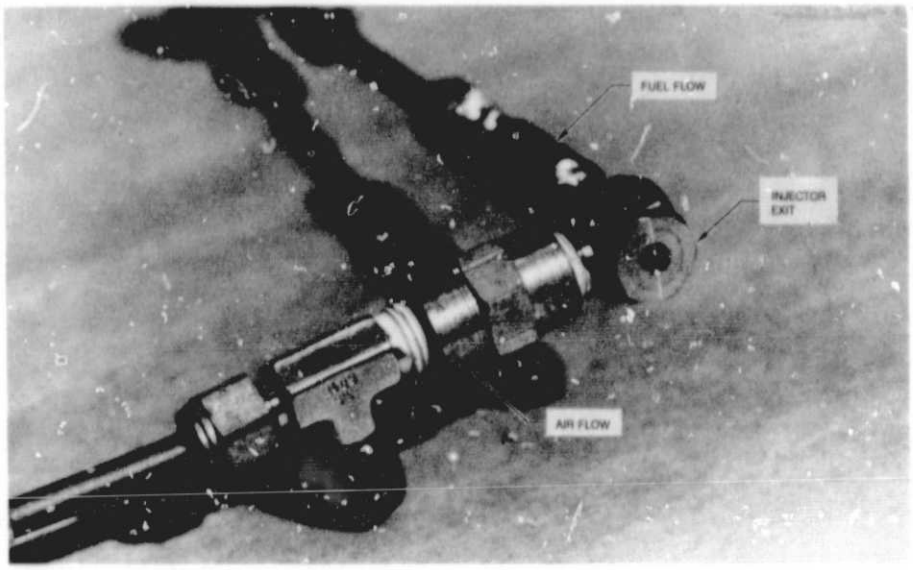

Figure 85 Delavan Air-Boost Injector

TABLE XXXVIII
FUEL NOZZLE SPRAY EVALUATION -- TEST CONDITIONS
Injector: Bill-of-Material (B/M)

Engine Condition	Wpri (Kg/Hr)	Wsec (Kg/Hr)	Tfuel (°C)	ΔPair (KPa)
Ignition	30	--	15 -29	3.4
Idle	58	--	15 46	3.4
Cruise	66	237	15 46	6.6
SLTO	73	930	15 -29	6.9

Injector: Low Emission (LE)

Engine Condition	Wpri (Kg/Hr)	Wsec (Kg/Hr)	Tfuel (°C)	ΔPair (KPa)
Ignition	30	--	15 -29	3.4
Ignition	--	30	15 -29	3.4
Idle	58	--	15	3.4
Idle	--	58	15 46	3.4
Cruise	56	108	15 46	6.6
Cruise	--	174	15 46	6.6
SLTO	73	422	15 -29	6.9
SLTO	--	496	15 -29	6.9

Injector: Air-Boost (DEL)

Engine Condition	W (Kg/Hr)	Tfuel (°C)	ΔPair (KPa)
Ignition	30	15 -29	414
Idle	45	15 46	414
Cruise	159	15 46	414
SLTO	227	15 -29	414

11.3 Test Results

Injector spray tests were performed during the early phases of the program with Jet A, undegraded antimisting fuel and antimisting fuel degraded using a JT8D fuel pump to a filter ratio of approximately three. Results of these tests indicated that the use of antimisting fuels caused a noticeable decline in the quality of the spray produced by all three of the injectors at all conditions tested. Photographs of the sprays produced with three different fuel nozzles are shown in Figures 86, 87, and 88. It is apparent from these photographs that the use of undegraded antimisting fuel resulted in a grossly incomplete atomization of the fuel with the spray being characterized by ligaments of fluid rather than droplets. Processing of the fuel enhanced the quality of the spray; however, the photographs clearly indicate that even the three-pass degraded fuel produced a spray inferior to that of Jet A. A listing of the droplet size information at each of the engine conditions for room temperature fuels is given in Table XXXIX. Shown in the table are the value of the Rosin-Rammler characteristics droplet size (PE) and the Sauter mean diameter (SMD). It is believed that the characteristic size, PE, was a better indicator of the capability for a spray to be consumed when comparing nozzles of different types (pressure atomizers vs. air atomizers), however, the SMD has found more widespread use as a figure-of-merit for spray atomization. Regardless of the parameter inspected, however, the trend of increasing droplet size with decreasing fuel degradation was apparent in the data.

Further indication of the effect of fuel characteristics on spray distribution can be found by examining the patternator data. Typical fuel pattern profiles are shown in Figure 89; the curves show the flowrate of fuel in kilogram per hour entering the tip of the probe located at the indicated radial distance from the injector centerline. The curves shown in the figure indicate the fuel patterns obtained using the low emissions injector at the cruise flow conditions when flowing Jet A, undegraded antimisting fuels, and degraded antimisting fuels. The results indicated that for this injector use of antimisting fuel did not change the basic hollow-cone character of the fuel

Figure 86 Spray Pattern with JT8D B/M - Cruise

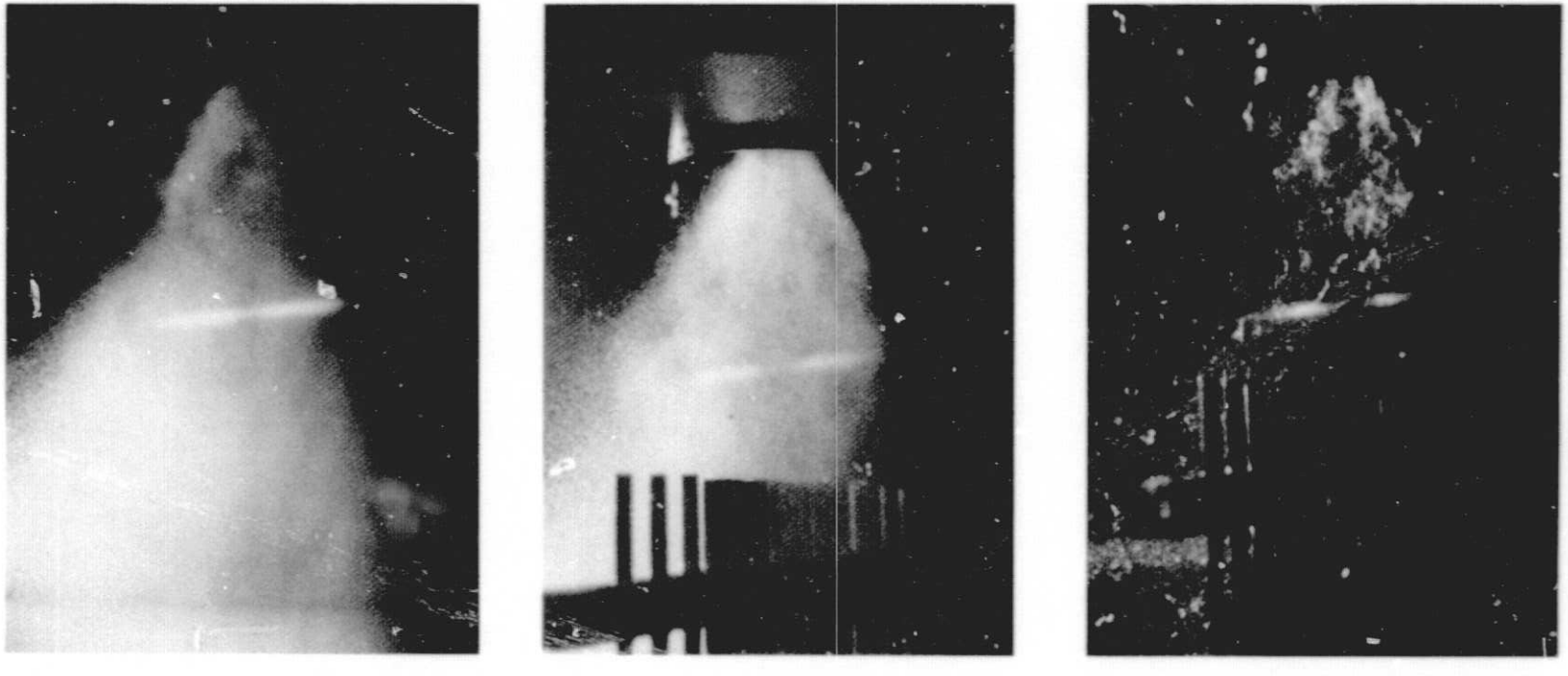

Figure 87 Spray Pattern with JT8D Low Emission Injector - Cruise

Figure 88 Spray Pattern with Air-Boost Injector - Cruise

TABLE XXXIX
MEAN DROPLET SIZE PRODUCED WITH ROOM TEMPERATURE FUELS

		B/H Low Emission				Air-Boost	
		PE	SMD	PE	SMD	PE	SMD
Fuel	Condition	microns	microns	microns	microns	microns	microns
Jet A	Ignition	85	46	97	60	40	20
	Idle	62	33	79	47	34	20
	Cruise	122	57	78	29	45	22
	SLTO	149	47.3	110	41	177	89
Three-Pass Degraded	Ignition	120	48	127	58	64	8
	Idle	110	50	85	31	56	8
	Cruise	171	72	142	45	133	24
	SLTO	151	70	191	61	159	50
One-Pass Degraded	Ignition	180	107	156	92	73	19
	Idle	143	76	111	59	84	15
	Cruise	176	88	139	52	151	38
	SLTO	140	65	152	71	168	71
Undegraded	Ignition	212	158	240	175	80	40
	Idle	137	119	279	210	89	37
	Cruise	251	134	243	144	167	62
	SLTO	150	100	239	164	176	130

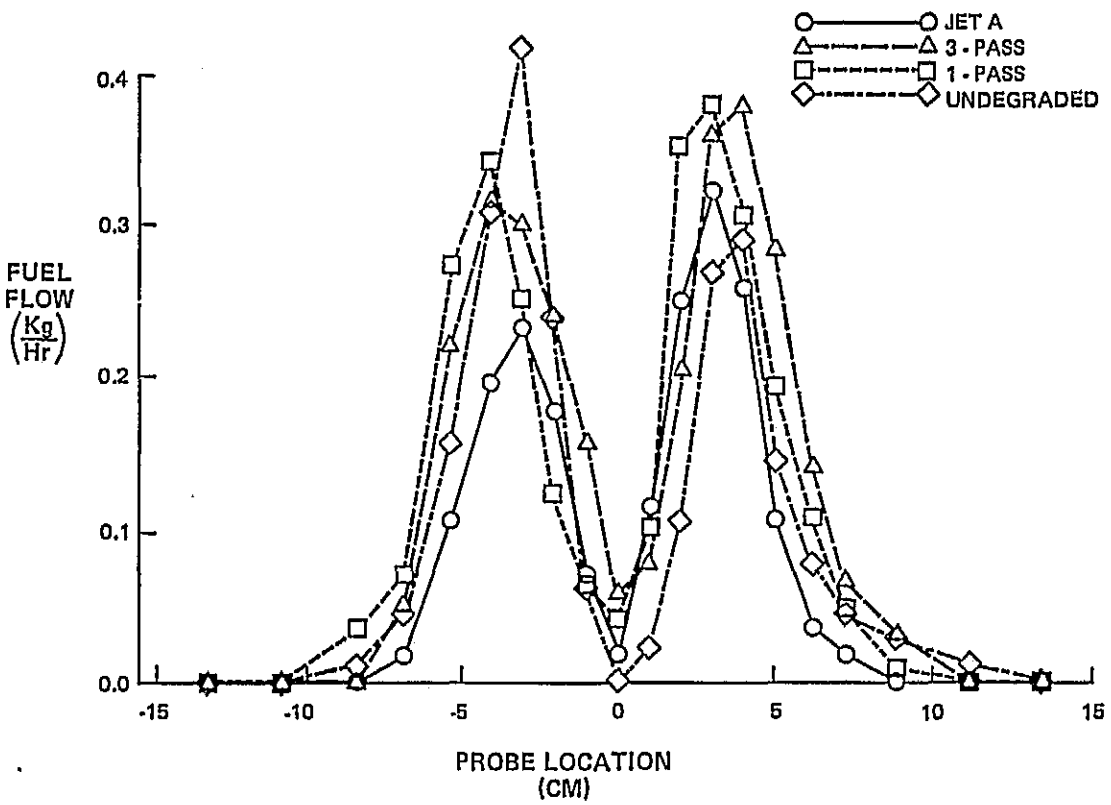

Figure 89 AMK Patternator Data Low Emissions Injector at Cruise

spray. Changes in the detailed features of the curves (shifts in the peak height or a change in the characteristic width of the peaks) were not of the magnitude to cause concern. Examination of the patternator data at the very low flow (ignition) condition indicated that the characteristics of the hollow cone spray produced by the bill-of-material pressure atomizing injector were preserved except in the case in which undegraded antimisting fuel was used. The patterns produced by the low emission injector undergoes significant shifts even for the three-pass degraded antimisting fuels. At the somewhat higher idle flow conditions, the low emissions injector showed less sensitivity to the extent of fuel processing although there was some indication that streaking had occurred with the use of the undegraded fuel.

Only the air boost nozzle was able to produce a distributed spray when utilizing undegraded fuel. The reasonably well atomized spray and minor patternator variations obtained for the bill-of-material nozzle when using three pass degraded fuel suggested that, if improved degradation methods were made available, existing fuel nozzles would be adequate for use with antimisting fuels.

Tests conducted with fuels at temperatures other than room temperature confirmed that the anticipated trends were experienced--droplet size decreased with increasing temperature. The atomization of the antimisting fuel at low temperature (-29°C) revealed no special problems.

At this junction in the program, combustor performance tests were scheduled and conducted with JT8D bill-of-material and low emission combustors. Jet A and antimisting kerosene degraded by a JT8D fuel pump to filter ratio of 8 (1 pass JT8D) and 3 (3 pass JT9D) respectively, were used. An analysis of these combustion test results will be detailed later in section 12.0. However, a summary of these results indicated that the emission levels produced from the antimisting kerosene were excessive and lean blow out, relight and starting characteristics were somewhat deficient.

The results from these spray quality and combustor performance tests coupled with fuel component laboratory evaluations (Section 7.0) pointed out the need for more extensive antimisting fuel degradation. Based on the levels of degradation required for successful cold filter tests and the transitional

velocity measured with Jet A fuel, antimisting kerosene was processed with the Gaulin apparatus to transitional velocities of 5 and 9 cm/sec, respectively. Subsequent spray quality evaluations were conducted with these two levels of degraded antimisting fuels and Jet A with the JT8D airblast (low emissions) fuel injectors. Photographs obtained using 10- microsecond strobe illumination and multi-second-shutter of the sprays produced with Jet A and degraded antimisting fuel are shown in Figures 90 A,B, C. It is evident from these photographs that the gross characteristics of the Jet A and degraded antimisting fuels are similar and the cone angles measured 2.54 and 5.1 cm downstream of the injector are also similar.

The Malvern droplet size data for cold Jet A and degraded AMK are shown in Table XL. Shown in the table are the value of the Rosin-Rammler characteristic droplet diameter (PE) and the Sauter mean diameter (SMD). The SMD has found more widespread use as a figure of merit for spray quality especially when the data evaluated is produced from one nozzle type. A precise comparison between all three fuels listed is not possible because this cold level of fuel temperature could not be maintained any closer than shown. However, both levels of degraded antimisting fuel produced satisfactory droplet sizes quite similar to Jet A.

A 20 probe paternator rake positioned 10 cm from the injector face was used to obtain spray distribution data which needs to be examined along with the droplet size data to give a more meaningful spray quality assessment. The patternator data for fuels tested during this phase of the program, Jet A, and degraded AMK (V_T of 5 and 9 cm/sec) along with 3-pass fuel pump processed AMK from the earlier part of the program are shown in Figures 91 and 92 for idle and SLTO conditions. The curves show the flowrate of fuel entering the top of the probe located at the indicated radial distance from the injector centerline. At idle the 3-pass degraded fuel was very different from the other two degraded fuels and Jet A. At SLTO the data is nearly indistinguishable but the trend at both conditions is that the more degradation performed on the antimisting kerosene the more the fuel resembles Jet A.

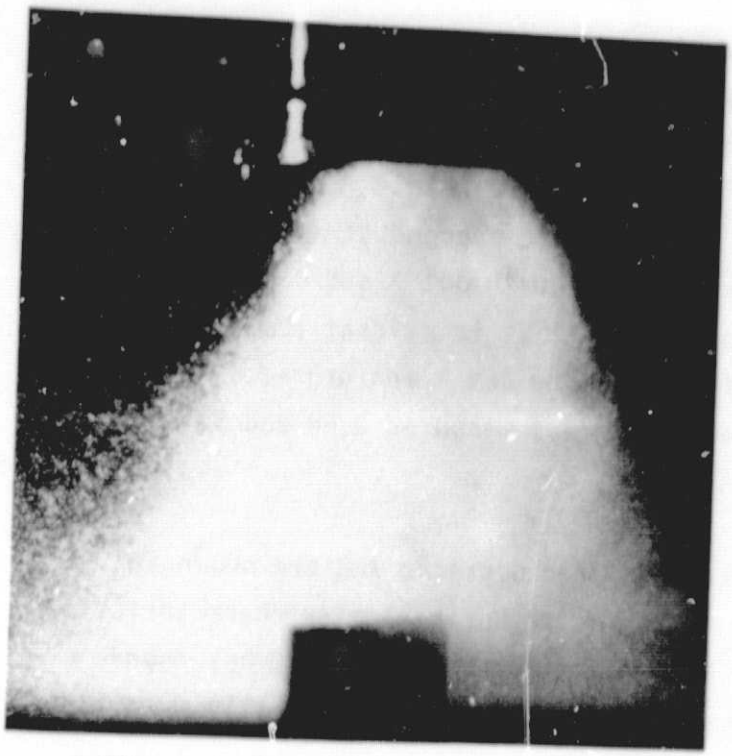

(A)

(B)

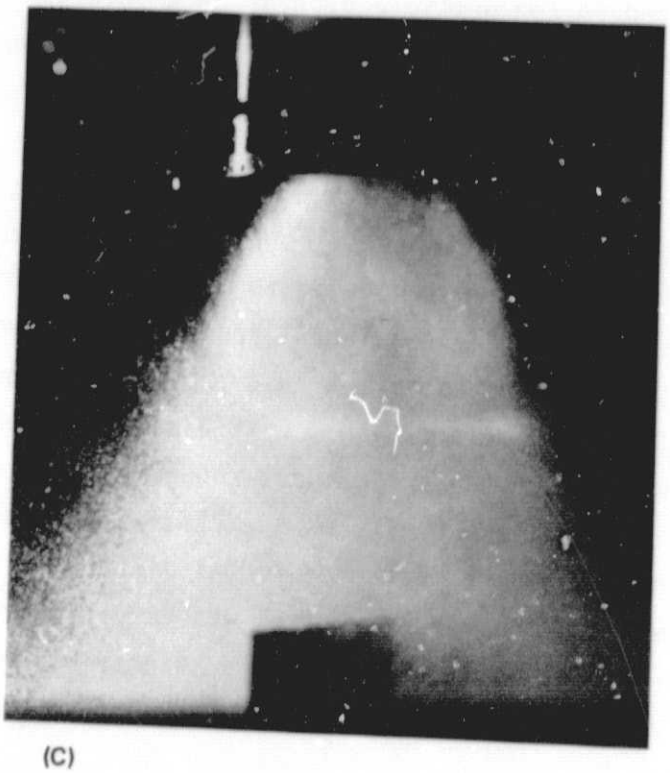

(C)

Figure 90 Nozzle Spray Comparison
(A) JT8D Air Blast (Low Emissions) Jet A, T = -25°C, SLTO
(B) JT8D Air Blast (Low Emissions) V_T = 5 cm/sec, T = 24°C, SLTO
(C) JT8D Air Blast (Low Emissions) V_T = 9 cm/sec, T = -30°C, SLTO

TABLE XL

COMPARISON OF DROPLET DATA

Condition	Jet A			Degraded AMK (V_T = 5 cm/sec)			Degraded AMK (V_T = 9 cm/sec)		
	T(°C)	PE	SMD	T(°C)	PE	SMD	T(°C)	PE	SMD
Ignition	-23	126	71.1	-22	132	74.5	-29	138	81.5
Idle	-25	125	66.9	-26	137	57.0	-30	109	50.6
SLTO	-23	144	36.5	-24	159	50.5	-30	119	44.4

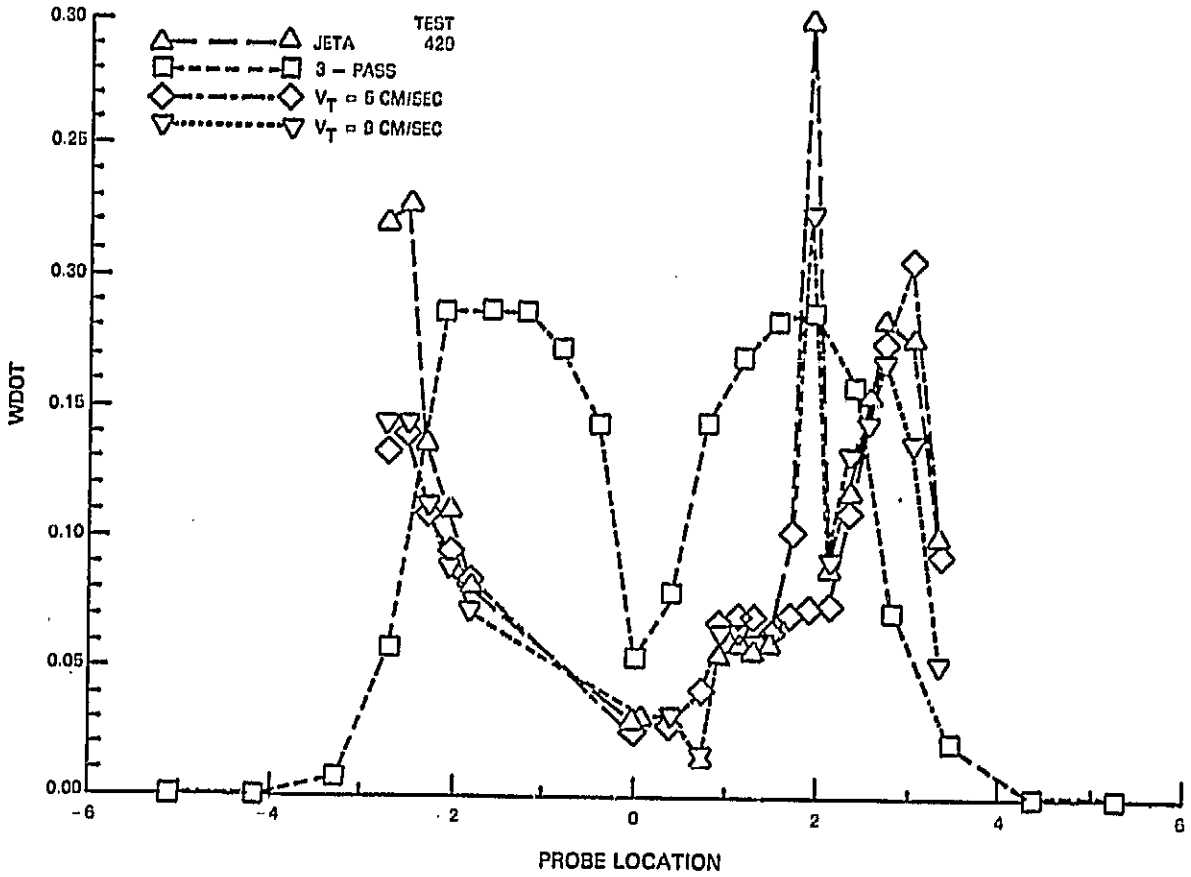

Figure 91 AMK Patternator Data JT8D Low Emissions Injector at Idle

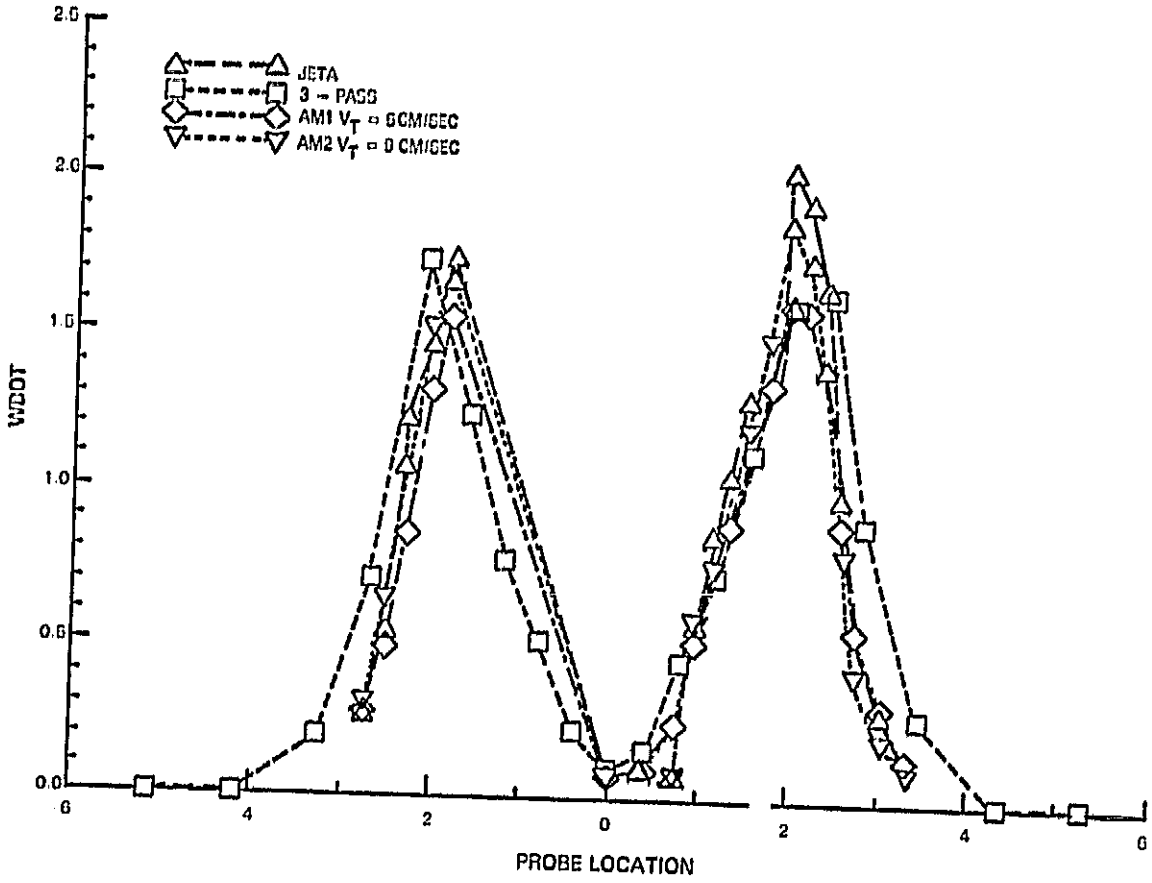

Figure 92 AMK Patternator Data JT8D Low Emissions Injector at SLTO

12.0 COMBUSTOR PERFORMANCE TESTS

12.1 Emissions and Performance Tests

Emissions and performance evaluation, exclusive of the altitude relight tests, were conducted in a high pressure test facility located at Pratt & Whitney Aircraft's Middletown test facility.

A schematic and photograph of the JT8D combustor rig installation are presented in Figures 93 and 94. This rig simulated a 40 degree sector of the JT8D engine including compressor discharge diffuser struts and aircooled turbine entrance transition duct. In addition, provisions were made for extracting inner diameter and outer diameter bleeds in amounts representative of the turbine cooling air requirements of the JT8D-17 engine. This allowed a more precise simulation of the JT8D-17 engine operating conditions.

Instrumentation on this rig included combustor inlet total pressure and total temperature rakes, and airflow measurement in both the inlet and turbine cooling air extraction systems. The combustor inlet temperature and pressure instrumentation consisted of an array of 4 Chromel-Alumel total temperature thermocouples, 5 total pressure rakes each having five measurement ports, and 7 wall static pressure taps. This instrumentation was arranged in a fixed array at the plane simulating the axial position of the last compressor stage.

Sixteen Chromel-Alumel thermocouples were installed on the louvers of each combustion can to observe any differences in liner heat load produced by combustion of antimisting kerosene.

Combustion exit temperatures and pressures were measured by a fixed instrumentation array mounted in an aircooled vane pack. Figure 95 is a photograph of the vane pack which consisted of 7 production JT8D turbine vanes. The five center vanes were each instrumented with five sampling/ pressure ports and two thermocouples. The thermocouples were located near the center of each vane to concentrate temperature measurements in the expected hot areas.

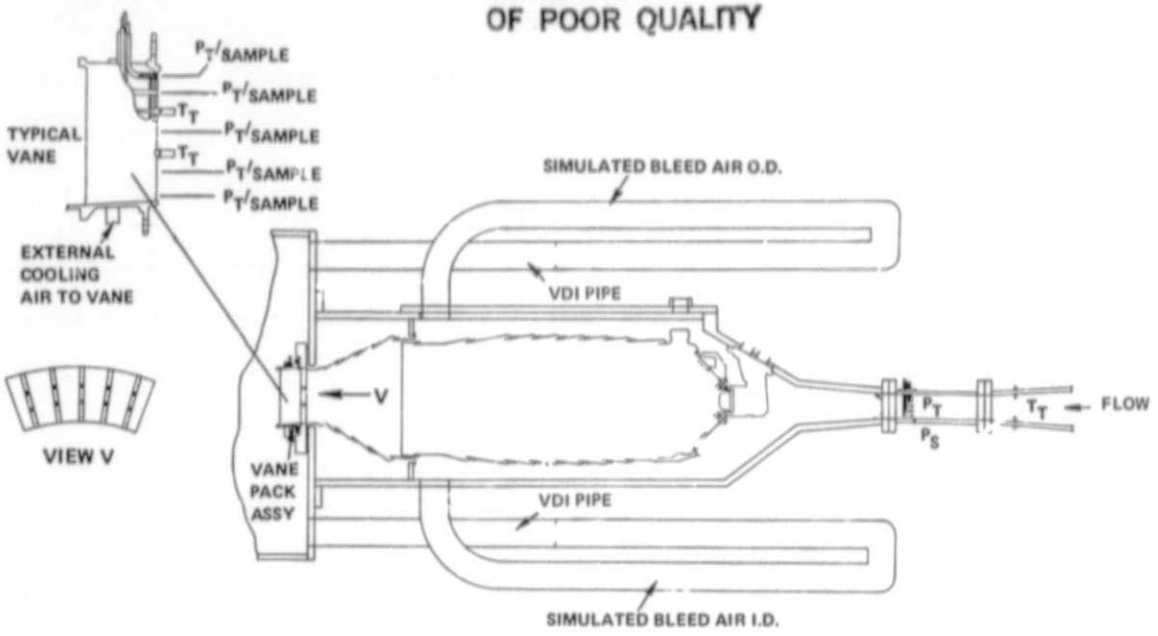

Figure 93 Schematic of JT8D Combustor Rig

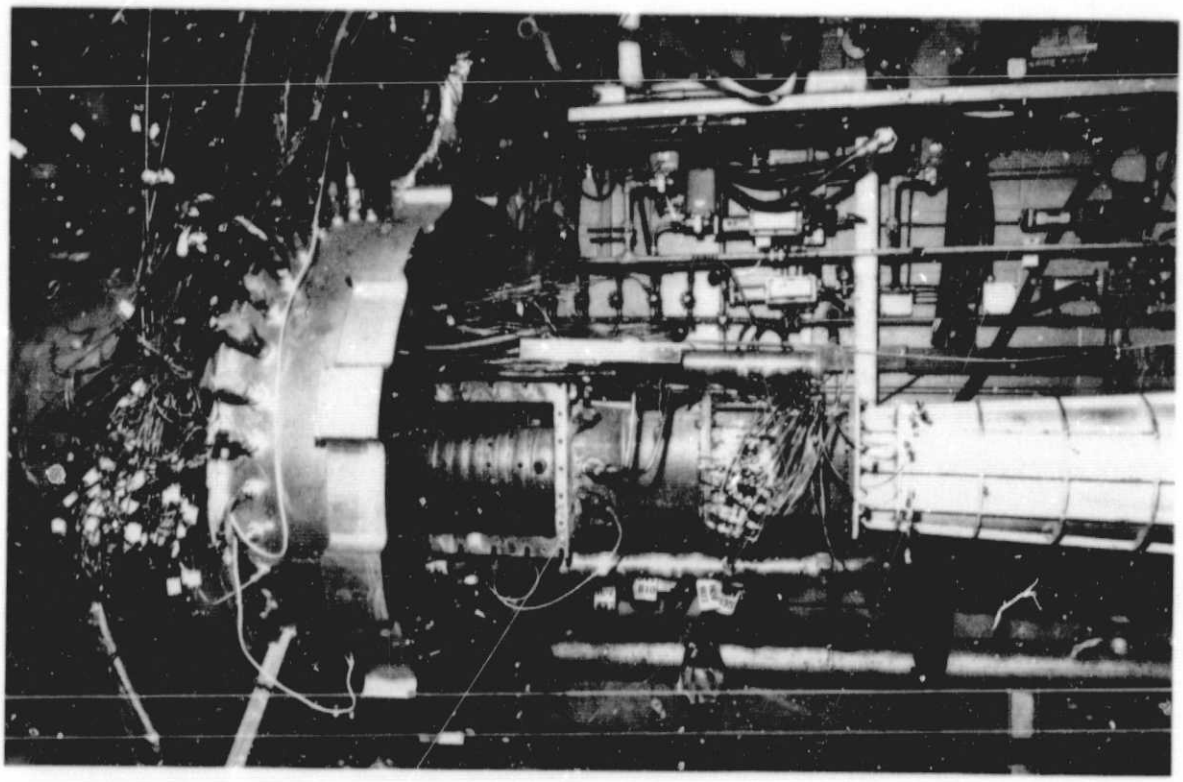

Figure 94 Photograph of 40° Sector Rig

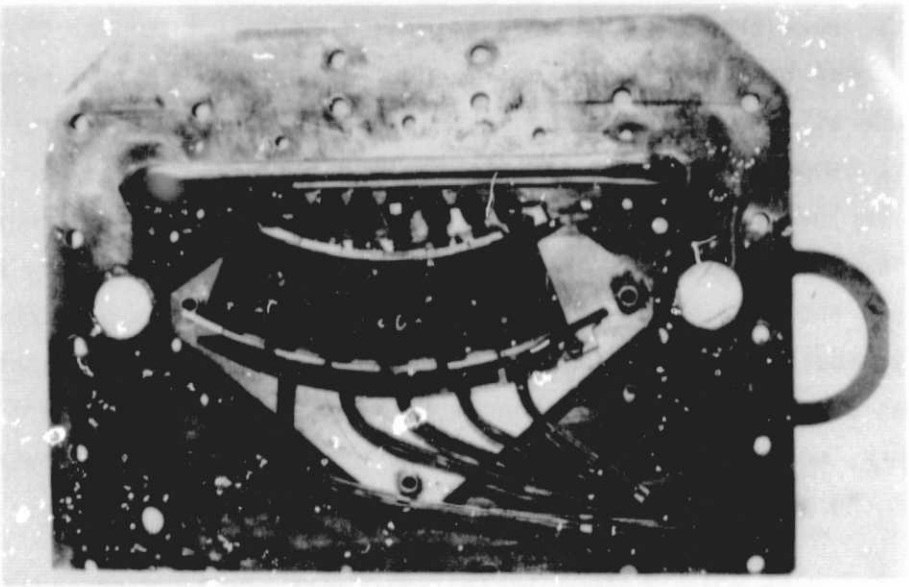

Figure 95 JT8D Combustor Exit Instrumentation Vane Pack

The gas temperature thermocouples in the vane pack employed a grounded immersion type of junction with ISA Type B thermocouple wire. The calibration of this wire is accurate to 1707°C. The gas sampling heads and lines were made from stainless steel tubing. When emissions or smoke were to be measured the samples from all 25 sensors were mixed in a manifold and fed to the analysis equipment. When these sensors were used to measure total pressure the sample lines were dead ended by closing the selector valves and the pressure recorded on a transducer in the automatic data recording system. Temperature measurements on this type of aircooled vane pack have shown that the gas samples were quenched to 147 to 207°C by the cooling air in the vane and the sample lines between the vanes and the analysis equipment were electrically or steam heated to maintain the sample temperature at about 147°C to avoid condensation of hydrocarbons from the sample.

The emissions and smoke analysis equipment in the Middletown Test Facility conformed to the specifications in SAE ARP-1256, SAE ARP-1179 and those of the Federal Register, Vol. 38, No. 1361 July 17, 1973 and in Vol. 43, No. 58, March 24, 1978. The burner test stand complex in the Middletown Test Facility is equipped with a computer controlled automatic data acquisition system. All data from the instrumentation described above with the exception of the smoke

measurements, were processed through an online Sigma 8 computer that provided essentially real time data analysis. The data reduction program computed combustor operating parameters such as diffuser inlet Mach number, fuel air ratio, ideal temperature rise and emission indices. Preselected critical parameters including those derived from emission analysis were presented on a scope in the control room for screening to establish data validity before proceeding to the next point in the test program. Hard copy printout of the entire data reduction program output was made available within minutes after the data was acquired. Data from the smoke measurements, which were processed independently, were related to the computer processed data on a point number basis after the test is completed.

The existing fuel supply systems in this facility employed constant flow gear type pumps sized for the maximum anticipated fuel flow and recirculated unused fuel through a bypass to the pump inlet line. This type of system degraded the antimisting kerosene to unacceptable levels. Consequently, the fuel system was modified to that shown schematically in Figure 96. The existing Jet A fuel system was unaltered but a valve system was employed to permit switching the fuel source from Jet A to antimisting kerosene without disturbing the rig operating conditions. This feature permitted operating the rig on Jet A fuel while inlet conditions were being set and stabilized, and permitted switching to the antimisting kerosene and operating on this fuel while acquiring data. The antimisting kerosene was consumed only during stabilization time after switching and during the data acquisition process itself. The antimisting kerosene supply system consisted of a 950 liter supply tank pressurized with nitrogen. Fuel flow rates were determined with turbine and mass meters in the supply lines. The fuel supply system instrumentation also included fuel temperature thermocouples and measured the fuel pressure in the primary and secondary systems at the entrance to the fuel injector support.

All test conditions were run with both the bill-of-material and low emissions combustor cans described in Section 3.0. Three fuels were used for each of the configurations; Jet A, 1-pass and 3-pass JT8D fuel pump degraded antimisting kerosene. In all cases ambient fuel temperatures were maintained and samples periodically analyzed for filter ratio value.

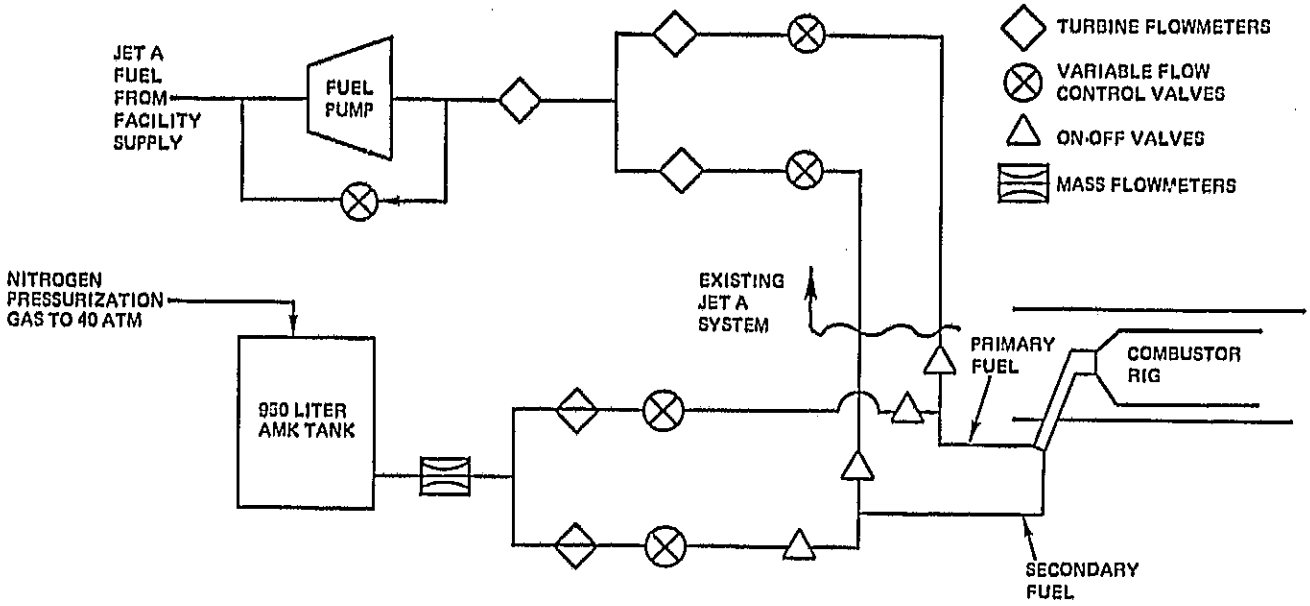

Figure 96 Modifications to Fuel System in X-904 Test Stand for Evaluation of Antimist Fuel

12.2 Ignition and Stability Tests

The altitude relight and sea level ignition tests were conducted in X-306 stand located at the Rentschlaer Airport Laboratory in East Hartford.

The rig contains nine JT8D-17 can-annular combustors. In addition, provisions were made for extracting OD and ID bleeds in amounts representative of the turbine cooling air requirements of the JT8D-17 engine. This allowed a more precise simulation of the JT8D-17 engine operating conditions. Operating airflow conditions in the facility were established with an orifice in the inlet duct and the rig inlet total pressure and total temperature rakes. Fuel flow rate, fuel manifold pressure, igniter current pulse and the output from thermocouple probes at the combustor exit were input to transient recorders to document ignition. The filter ratio of antimisting kerosene fuel samples was periodically checked throughout the test. The antimisting kerosene fuel feed systems and measuring devices are the same as described in the last section.

The relight tests were conducted by operating the rig along four different constant airflow lines covering the extent of the JT8D engine altitude relight envelope as shown in Figure 97. As the effective altitude is increased along these lines, the air inlet total pressure and total temperature progressively decrease. The tests were conducted by operating the rig at a fixed airflow and by progressively increasing the effective altitude until an altitude condition was defined at which ignition was no longer possible after a 30 sec. attempt. The altitude ignition boundary was defined by these points on the airflow lines. The ignition total fuel flow was fixed at 0.065 kg/sec which was consistent with the altitude starting fuel schedule of the JT8D engine and at ambient fuel temperature.

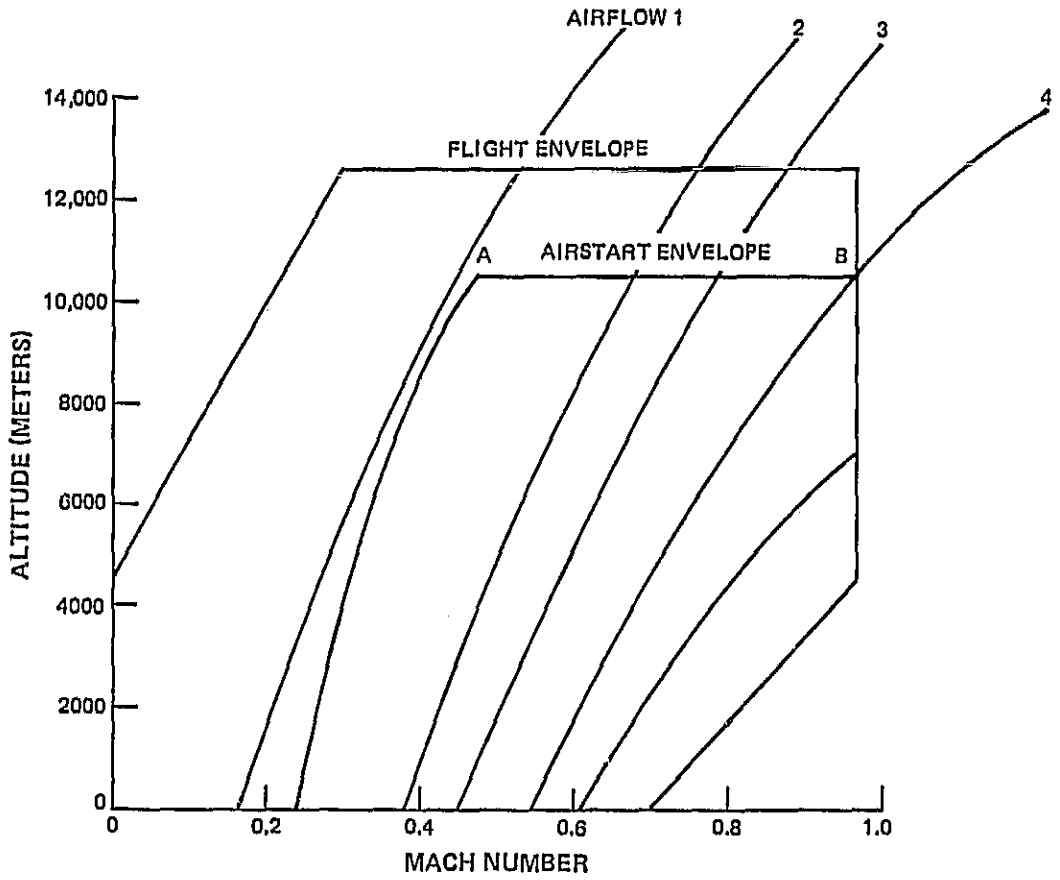

Figure 97 JT8D-17 Airstart Envelope

The combustor was also evaluated for cold fuel sea level starting capability. For these tests the rig was operated at a slightly subatmospheric pressure and at an inlet Mach number and temperature representative of JT8D engine cranking at -29°C and 17°C ambient temperature. The test fuel was at the same temperature as the inlet air. Ignition was attempted over a range of fuel flow rates with the time to ignition being recorded.

12.3 Emission Data Calculation Procedure

The raw emissions data generated at each test condition were transmitted directly to an online computer for processing. The voltage response of the gaseous constituent analyzers was first converted to an emission concentration based on the calibration curves of each instrument, and then used to calculate emission indices, carbon balance fuel-air ratio, and combustion efficiency. Since the instrumented vane pack allowed extraction of a single representative gas sample acquisition time was minimized and the processed emissions data were usually available within a few minutes of setting a test condition.

While every effort was made to set exact design conditions for the test runs, it was rarely possible to set test conditions to precisely match the design condition by interpolation, using plots of emissions as functions of the metered fuel-air ratio. The data for oxides of nitrogen have been corrected for humidity effects at all operating conditions. These corrections were small, generally not exceeding 5 percent.

12.4 Combustor Performance Data Calculation Procedure

The combustor performance parameters presented in this report were either measured directly or calculated from measured data. Table XLI contains a summary of these performance parameters and indicates whether they were measured or calculated.

TABLE XLI

SUMMARY OF REPORTED COMBUSTOR PERFORMANCE PARAMETERS

Parameter	Symbol	Units	Measured	Calculated
Total Airflow	W_{a4}	kg/s	X	--
Total Combustor Airflow	W_{ab}	kg/s		X
Primary Fuel Flow	W_{fp}	kg/s	X	--
Secondary Fuel Flow	W_{fp}	kg/s	X	--
Inlet Total Temperature	T_{t4}	K	X	--
Inlet Total Pressure	P_{tr}	atm	X	--
Reference Velocity	V_{ref}	m/s	--	X
Inlet Air Humidity	h	g H_2O/kg air	X	--
Fuel-Air Ratio	f/a	--	--	X
Pressure Loss	P_t/P_t	--	--	X
Combustion Efficiency	η_c	%	--	X

12.5 Combustor Test Results

The emissions, high altitude relight, and sea level ignition of the bill-of-material and low emission combustors using Jet A and antimisting kerosene are presented in this section.

12.5.1 Emissions and Performance

High pressure rig tests were utilized to determine the effect various levels of degraded antimisting kerosene have on performance and emission parameters as compared to Jet A. In addition, differences between the bill-of-material and low emission combustors using antimisting kerosene were of interest. Measurements of emissions, liner cold side temperatures, lean blow out limits and observations of nozzle and combustor deposits were made.

Emission results for the Jet A fuel were consistent with results obtained previously at Pratt & Whitney Aircraft for the same configurations. The antimisting kerosene emissions can therefore be conveniently compared to a well established Jet A emission baseline.

Emission differences between Jet A and antimisting kerosene occurred at idle. No differences were observed at high power. Under all conditions, the smoke numbers and NO_x levels were not affected by the use of antimisting kerosene.

The effect of fuel on emissions and combustion efficiency (η_c) can be seen in Figures 98a, b, and c. Plotted are η_c, CO_{EI} and THC_{EI} at nominal idle versus type of fuel.*

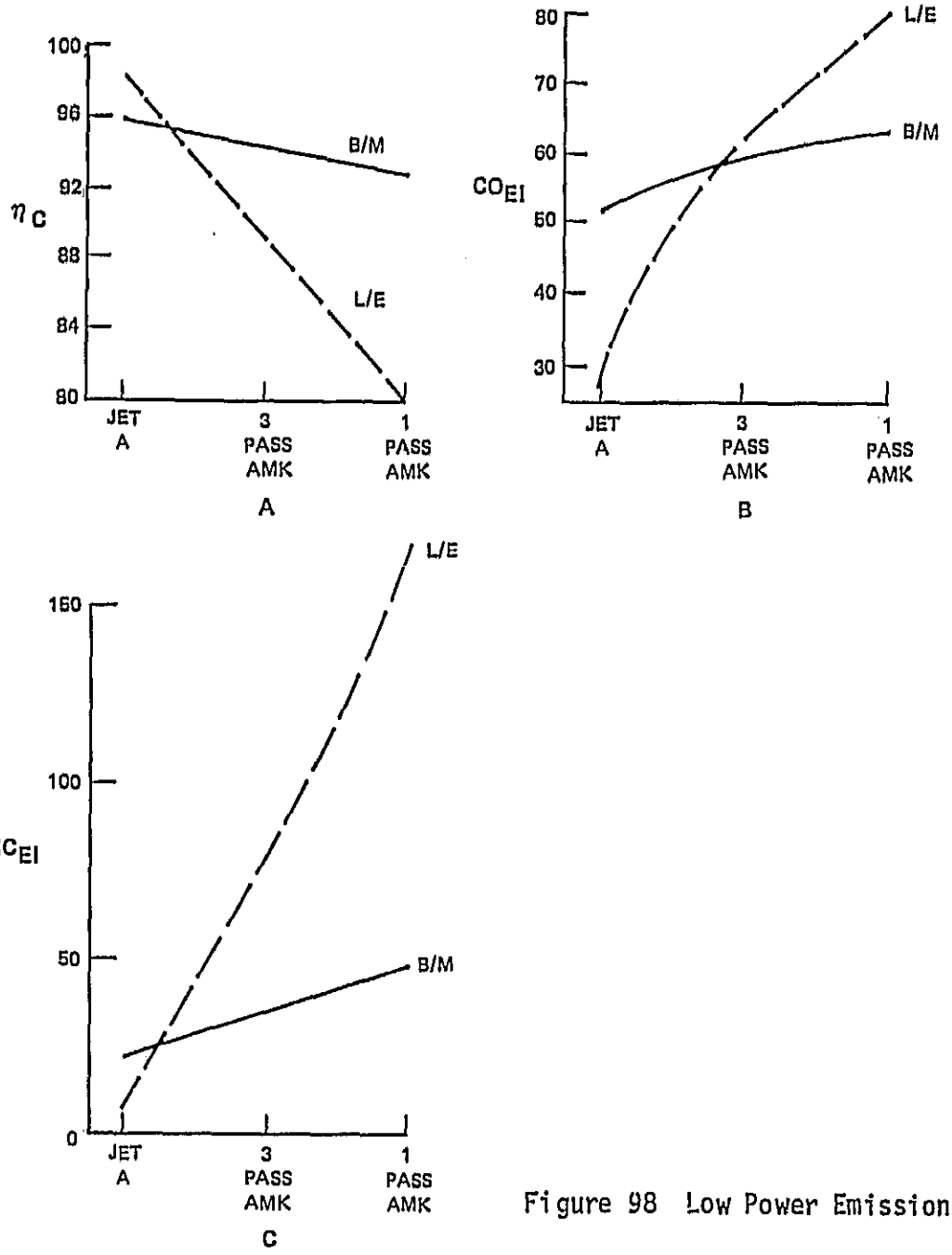

Figure 98 Low Power Emissions (Idle)

---

* Emissions at lean idle are, in some cases, considerably higher than at nominal idle.

In all cases Jet A fuel yielded lower emissions and higher η_c than any tested level of degraded antimisting kerosene. Going from Jet A to 3-pass to 1-pass, the emissions became progressively worse for both combustor configurations. From Jet A to 3-pass the carbon monoxide went up by 20 percent for the bill-of-material and more than doubled for the low emission combustor. From 3-pass to 1-pass the increase was 5 percent for the bill-of-material and 30 percent for the low emission combustor. The total hydrocarbons, Figure 98c, showed similar trends, though the low emission combustor increase in total hydrocarbons from Jet A to 1-pass was much higher than for carbon monoxide.

12.5.2 Ignition and Stability

o Lean Blow Out

Lean blow out is defined as the minimum fuel air ratio at idle that will support combustion. The lean blow out for both the bill-of-material and low emission combustor is shown in Figure 99. The antimisting kerosene required higher fuel air ratio for lean blow out than the Jet A. The low emission combustor's fuel air ratio was very similar to the bill-of-material up to 3-pass, but increased rapidly at 1-pass.

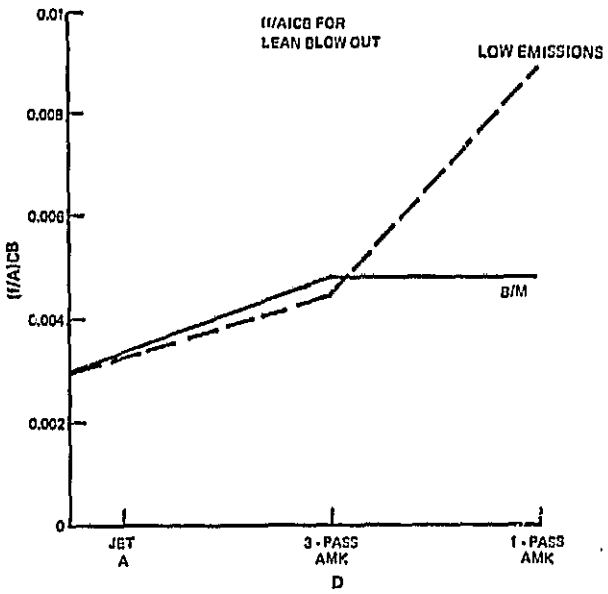

Figure 99 Lean Blowout Test Results

o Relight

The altitude relight results for the bill-of-material and low emissions combustors operating with Jet A and 3-pass (fuel pump) antimisting kerosene are shown in Figures 100 through 103. Plotted is simulated altitude versus flight Mach number with station 4 (burner plus turbine bleeds) airflow as a parameter. The open symbols indicate a light (5 or more of the burner cans lit signifies engine will accelerate) and the closed symbols a no light (4 or less of the burner cans lit). The 3-pass antimisting kerosene consistently exhibited poorer relight characteristics than the Jet A. Figures 100 and 101 are for the bill-of-material combustor, Jet A and 3-pass antimisting kerosene respectively. For the 3-pass antimisting kerosene, the only light achieved was for the 2.27 kg/sec airflow at an altitude of 6000m. Figures 102 and 103 show the relight characteristics for the low emission combustor Jet A and 3-pass respectively. The 3-pass in the low emission combustor appeared better than it did in the bill-of- material, but still was not as good as the Jet A. At an airflow of 2.27 kg/sec for the low emission combustor the 3-pass and Jet A were about equal in their relight capability. For the other airflow, the Jet A was superior.

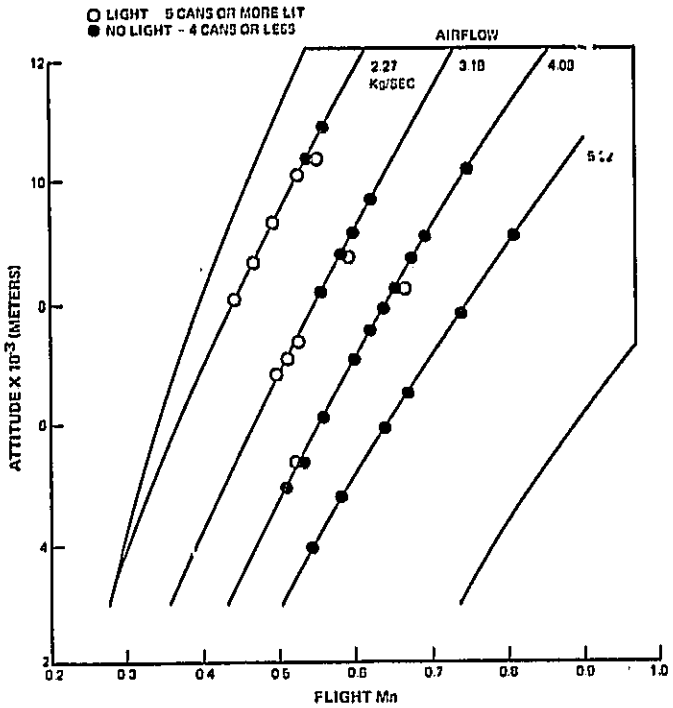

Figure 100 JT8D-17 Airstart Envelope - Bill-of-Material Combustor, Jet A

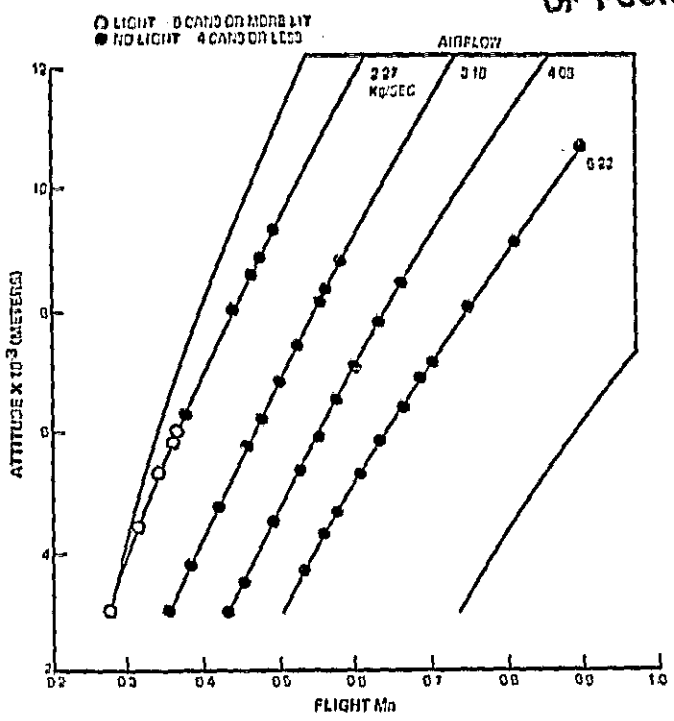

Figure 101 JT8D-17 Airstart Envelope - Bill-of-Material Combustor, 3-Pass AMK

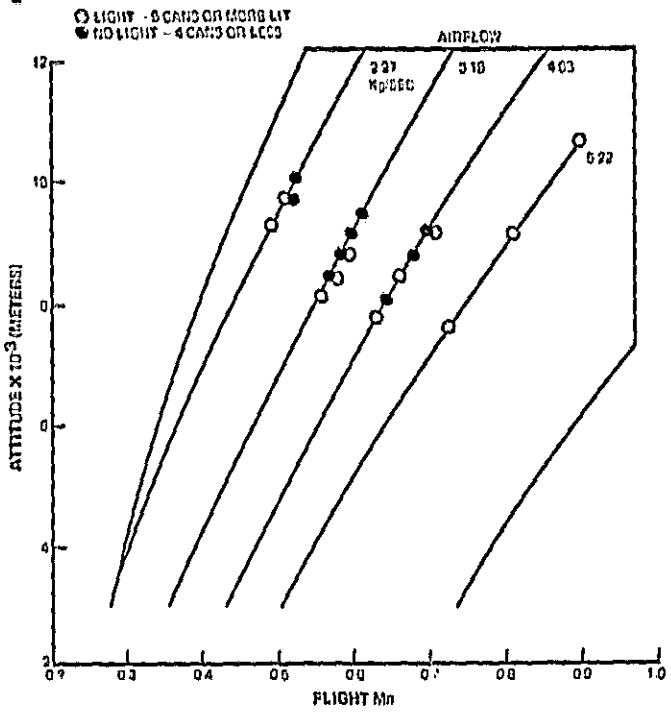

Figure 102 JT8D-17 Airstart Envelope - Low Emissions Combustor, Jet A

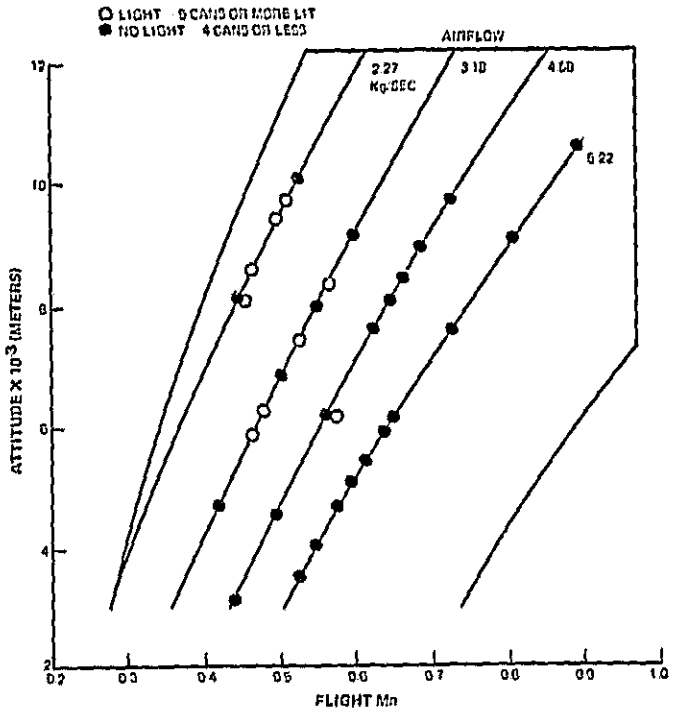

Figure 103 Airstart Envelope - Low Emissions Combustor, 3-Pass AMK

o Sea Level Ignition

In this section, the sea level ignition with antimisting kerosene is compared to Jet A for the bill-of-material and low emission combustors. Both -29°C and 17°C inlet temperatures were used.

In Figures 104 through 107 the fuel flow rate, with Jet A and 3-pass antimisting kerosene, versus number of burner can lights for a fixed airflow and fuel temperature is plotted. In general, the Jet A had better ignition characteristics than the 3-pass antimisting kerosene. Also, fuel at 17°C was better than fuel at -29°C for the bill-of-material combustor, while temperature had no effect on the 3-pass antimisting kerosene with the low emission combustor. In Figure 104 the bill-of-material combustor with a fuel temperature of 17°C is shown. For Jet A, a 9 can light was achieved with a fuel flow rate down to 295 kg/hr. The 3-pass never achieved a full 9 can light with the fuel flow rate as high as 365 kg/hr. In Figure 105, the low emission combustor with a fuel temperature of 17°C is shown. For Jet A, a full 9 can light was achieved with a fuel flow rate down to 230 kg/hr while the 3-pass antimisting kerosene required 340 kg/hr for a full 9 can light. In Figure 106, the bill-of-material combustor with fuel at 244K required at least 340 kg/hr for a full 9 can light while the 3-pass antimisting kerosene could, at best, achieve a 1 can light at 365 kg/hr. In Figure 107, the low emission combustor with 244K 3-pass antimisting kerosene is shown. Jet A was not run. A full 9 can light was achieved with a fuel flow rate down to 295 kg/hr. Comparing this to Figure 105 for a 3-pass, it is seen that no performance penalty was incurred for the low emission combustor at -29°C.

12.5.3 Combustion Test Summary

A summary of the test results is given in Table XLII. These results indicate the emission levels produced from 1 and 3-pass antimisting kerosene are unacceptable. Furthermore lean blow out, relight and starting characteristics are somewhat inferior.

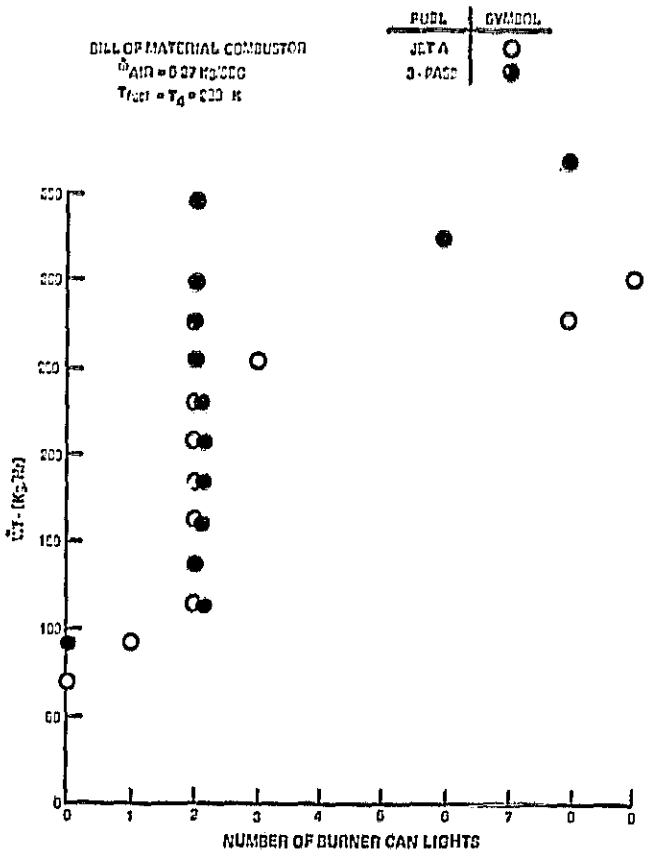

Figure 104 Sea Level Ignition
Bill-of-Material Combustor

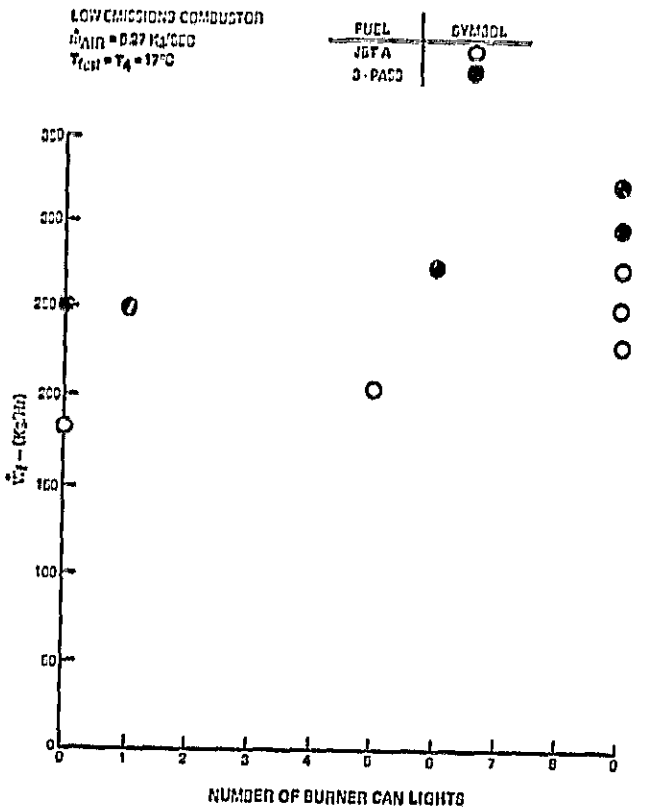

Figure 105 Sea Level Ignition
Low Emissions Combustor

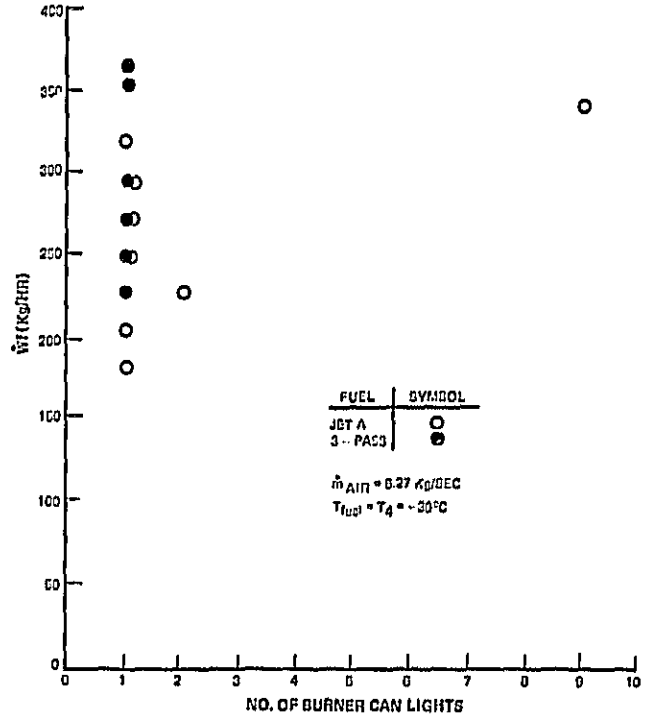

Figure 106 Sea Level Ignition-
Bill-of-Material Combustor

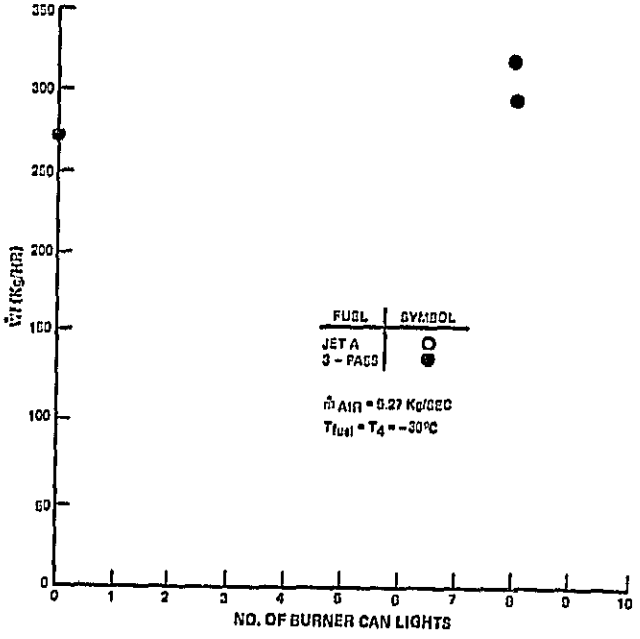

Figure 107 Sea Level Ignition -
Low Emissions Combustor

TABLE XLII
COMBUSTOR PERFORMANCE TEST QUALITATIVE
COMPARISON OF DEGRADED ANTIMISTING KEROSENE TO JET A

	Bill-of-Material		Low Emissions	
	1-Pass	3-Pass	1-Pass	3-Pass
NO_x	0	0	0	0
Smoke	0	0	0	0
CO	-	-	--	-
Total Unburned Hydrocarbon	-	-	--	-
Lean Blow Out	-	-	--	-
Relight	Not Run	-	Not Run	-
Sea Level Ignition	Not Run	-	Not Run	-

0 = Same
- = Worse
-- = Much Worse

Although Gaulin processed antimisting fuels began to approach Jet A in terms of flow characteristics (transitional velocity) and spray quality and distribution during the latter stages of this program, it was not feasible to test it in the combustor rigs due to scheduling constraints. It is the intent of this section to discuss and assess the effect of the most recent fuel injector spray evaluations in Section 11.0 on combustor performance.

The early combustor rig data was obtained at several engine simulated conditions, i.e., idle, cruise and sea level takeoff. In general, there were no adverse emissions or combustion efficiency effects at the cruise or sea level takeoff conditions using the 3 or 1-pass antimisting kerosene fuels and the only effects were at the idle condition. The combustor rig idle tests results indicated that for bill-of-material and low emission injectors the use of Jet A fuel yielded low emissions, higher combustion efficiency and lower blowoff limits than any tested level of degraded antimisting kerosene. This trend was consistent with the distribution data for variations in degradation levels which was similar at SLTO but very different at idle conditions. The combustor tests also indicated a more significant deterioration in the emission and combustion efficiency for the low emission injector when compared to the bill-of-material injector. The droplet data alone indicated the

reverse, the droplet size of the bill-of-material injector deteriorates more rapidly than the low emission injector at idle when AMK fuel is sprayed. However, the idle patternator data indicates that the low emission injector fuel distribution changed from a hollow cone Jet A spray with no fuel in the center to a semi-hollow spray cone using 3 and 1-pass antimisting kerosene and this change could disrupt the primary zone recirculation pattern.

The most recent fuel injector data was recorded for levels of degradation identified by a transitional velocity much like that of Jet (V_T = 8-10). Spray droplet data at SLTO cold fuel conditions follows this trend as can be seen in Figure 108 where SMD is plotted vs. various degraded fuel types. Perhaps even more important is the distribution data at idle where the highly degraded fuels are almost indistinguishable from Jet A. Based on the early combustion results and the more recent spray quality and distribution results, it is implied that low power emissions might be very close to Jet A.

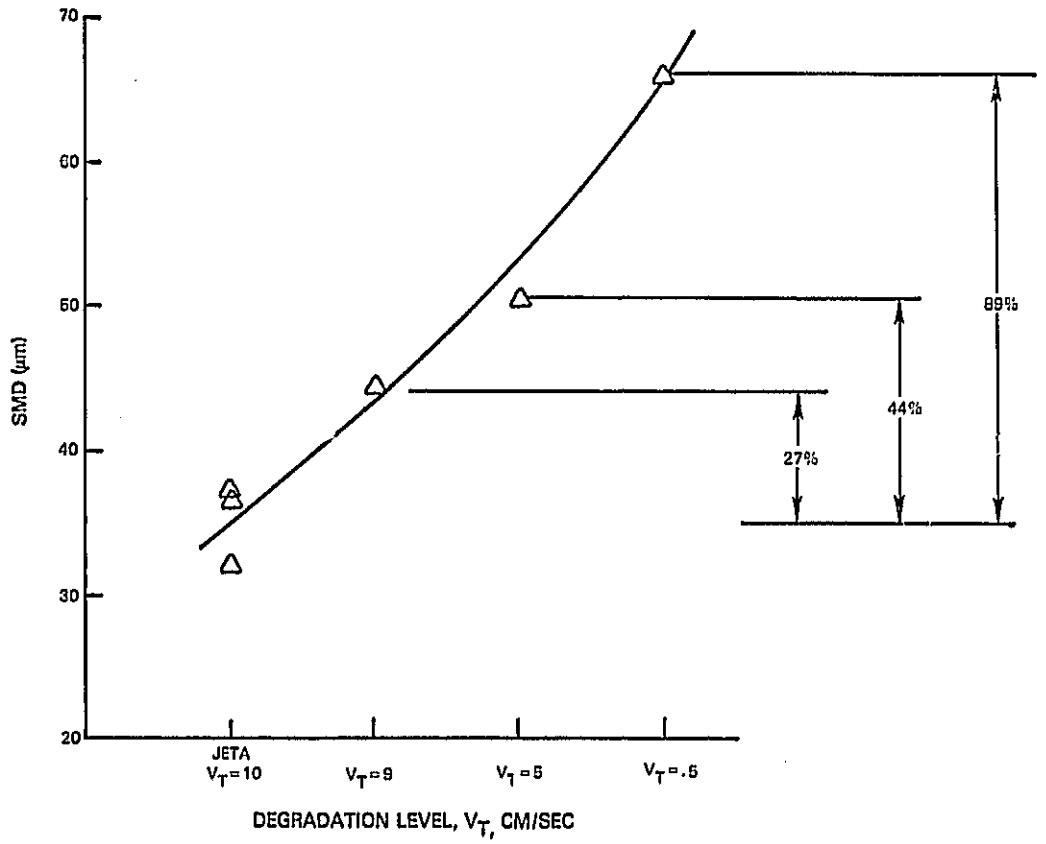

Figure 108 SMD Variation for Various Degraded Fuels at SLTO Condition and -20°C

13.0 CONCLUSIONS

The major results of this program are summarized in Table XLIII. A comparison of transition velocity, filter ratio, number of JT8D pump passes and antimist kerosene molecular weight is shown in the first four columns. The effects of AMK on filtration, atomization and emissions and performance are tabulated as a function of these fuel degradation levels. It can be seen that while engine emissions and performance may be acceptable at a transition velocity of 5 cm/sec, fuel system clogging problems would be expected at cold operating temperatures. A transition velocity of at least 8 cm/sec is necessary in the control for satisfactory operation at reduced fuel temperatures for P&WA JT8D and JT9D current engine components.

TABLE XLIII

MAJOR PROGRAM RESULTS

Transition Velocity	Filter Ratio	# of Passes Thru JT8D Fuel Pump	Mol. Weight	Filtration	Atomization	Emissions and Performance (Relative to Jet A)
10				No Filter Clogging -29°C		
8				Filter Clogging -29°C JT9D No Filter Clogging -29°C JT8D	Drop Size High Power 25% >Jet A Drop Size Low Power = Jet A	
5.7			0.25M			
5				No Filter Clogging Ambient JT8D	Drop Size High Power 40% >Jet A Drop Size Low Power 5% >Jet A	Should Approach That of Jet A
3		16		Filter Clogging -16°C Both Engines		
2.1			0.65M			
1.5	1.2	7		Filter Clogging 4°C Both Engines		
0.5	3	3			Drop Size 50% >Jet A 50% Jet A	NO_x and Smoke No Change CO and THC - Excessive Relight, Ignition and LBO Deficient

The specific conclusions drawn from a series of laboratory and bench scale experiments, and full scale components tests for the two year technical effort are outlined in the following paragraphs.

Quality Control

Fuel analyses and quality control were conducted to monitor the physical and chemical properties of the antimisting kerosene and its parent fuel to ensure consistent quality. Although properties of the parent fuels in all batches received appeared typical of Jet A fuel used for most commercial jet aviation, samples of the antimisting kerosene revealed unexpectedly high sodium levels which could accelerate corrosion of the engine hot section.

Filter ratio measurements made on some as-received, undegraded antimisting fuel samples produced high and non-reproducible values. Additional testing of the batches suggested that the storage temperatures and times at these temperatures may markedly affect the subsequent filter ratio of the fuel.

Fuel Degradation Measurements

The transition velocity method was improved and standardized as the primary degradation measurement technique. Gel Permeation Chromatography, was successfully applied which, together with the transition velocity method, quantified the degradation levels of antimisting kerosene.

The filter ratio method loses resolution at the higher levels of degradation required for JT8D fuel system components (FR $\leq$ 2). Transition velocity and Gel Permeation Chromatography are viable tools for monitoring the degradation process and Gel Permeation Chromatography offers the additional benefit of graphically displaying the distribution of apparent molecular weights of degraded fuel. Furthermore, Gel Permeation Chromatography is capable of analyzing gel residue deposited on fuel system components which allows a direct comparison with the original test fuel.

Peripheral Fuel System Requirements

Laboratory tests made with both undegraded and degraded antimisting fuels indicated that the thermal stability of antimisting kerosene is at least as good if not better than the parent Jet A.

Heat transfer measurements show a marked reduction in the heat transfer with undegraded antimisting kerosene in the turbulent flow range. Degrading antimisting kerosene to a filter ratio less than three would achieve acceptable operation in the JT8D fuel-oil heat exchanger.

Static six month ambient and elevated temperature soak tests made with elastomer seal materials normally employed in gas turbine engine fuel systems resulted in only minor swelling which was within tolerable limits.

Although a copper corrosion test indicated more reaction with AMK than Jet A, bronze materials in a fuel pump that accumulated more than 100 hours during this test program were not adversely effected by antimisting kerosene.

Filterability Tests

The onset of filter clogging by AMK is dependent on degradation level of the fuel, pore size of the filter, temperature and flow velocity. As AMK is degraded to higher levels or as fuel system velocities are decreased clogging is less likely to be encountered. The clogging behavior of filters is approximated by the degradation level and true velocity of the fuel and not the material, pore size or type of construction of the filter.

Filter clogging occurred from gel formation of the FM-9 polymer from the fuel mixture. At low flow velocities, only the largest polymer species with the highest molecular weights are affected; however, as the fluid velocity is increased progressively, smaller molecular species are brought out of suspension to collect on the filter downstream surface. This results in an exponential increase in clogging rate with increasing flow rate due to the normal distribution of apparent AMK molecular weights after degradation.

At the onset of clogging, the rate of clogging may be very slow and require an extended test for detection. Care should be exercised in interpreting the results of long term tests with recirculating antimisting kerosene as Gel Permeation Chromatography results have shown some tendency for modification of molecular weight distribution with circulation.

Filterability properties, indicative of the antimisting kerosene degradation level required to meet the most demanding flow requirements in either the JT8D or JT9D engines, approaches those of Jet A. Extended filter tests at reduced temperatures indicate a transition velocity above 8 cm/sec in the current JT9D fuel control (neat Jet A = 9 - 11 cm/sec) is necessary to prevent long term clogging at cold temperatures (T_F < - 29°C).

Water Compatibility

Free water is incompatible with FM-9 AMK and causes destabilization and precipitation of a polymer at the water-fuel interface. The precipitation occurs regardless of the ratio of water to fuel as long as free water is present. The presence of water induced precipitate results in paper filter clogging which is not reversible during the deicing Process. The volume of precipitate and the potential for clogging filters depends on the manner the water is introduced to the fuel. Water introduced by condensation of water vapor into cold fuel exists as small droplets with high surface area and results in a greater volume of precipitate than that caused by free water introduction. The amount of water that can be dissolved in FM-9 AMK with no phase separation was no greater in antimisting fuel than in Jet A fuel. Reported increases in water solubility in FM-9 AMK result from the ability of AMK to form relatively stable, milky appearing suspensions of fuel water droplets.

Additional Studies

An evaluation of the compatibility of antimisting kerosene with several approved Jet A additives indicated that only the anti-icing additive (Ethylene Glycol Monomethyl Ether) was chemically incompatible, producing a lacy deposit. Rheological effects (filter ratio changes) were recorded for the various additives.

Fuel Shearing Design Study

This study has indicated that a cavitating device (vortex venturi) can theoretically achieve a transition velocity level of 8 cm/sec with considerably less energy consumption than that required by the JT8D fuel pump or by the commercial devices that were tested. A staged pump venturi system would only achieve on the order of 6 cm/sec and it would require upwards of 48.5 KW at JT8D SLTO conditions. This device requires upwards of 17 KW at JT8D cruise conditions which relates to a TSFC penalty of 0.4%.

It may be possible to reduce the horsepower requirement by an improved vortex venturi or by the proposed alternative device. Further analytical and experimental work will be required to develop a practical degrader that is airworthy and satisfies the entire flight spectrum of the aircraft.

Fuel Injector Performance Tests

Droplet size and distribution data need to be assessed together and at all simulated power levels to determine acceptable fuel spray quality for combustion. The more degradation performed on the antimisting fuel, the closer the fuel spray quality resembled Jet A. Fuel processed to a filter ratio of approximately 3 produced a reasonably well atomized spray with slight patternator variations from Jet A. Fuel processed to transition velocities of 5 cm/sec and above produced sprays almost indistinguishable from Jet A.

Combustor Performance Tests

Combustor performance tests conducted with JT8D bill-of-material and low emission combustors while burning AMK degraded to filter ratios of 8 and 3 respectively, resulted in emission levels that were excessive and lean blowout, relight and starting characteristics that were somewhat deficient.

Based on the spray quality and distribution data produced by more highly degraded AMK (V_T = 5 cm/sec) the combustor performance will definitely be improved and approach that of Jet A.

Based on a careful assessment of the aforementioned conclusions and additional test results and analytical projections generated by this program, three additional conclusions are made.

- o Although it is technically feasible to operate a JT8D engine with 0.3% FM-9 antimisting additive, commercial engine application is not justified until several problem areas discussed in this report are addressed and subsequently solved. Furthermore, there is additional research and development required before practical considerations are satisfied.

- o The application of the results from this program can be applied to similar components from other aircraft jet engines.

- o One of the major engine modifications projected to be required at this time for the successful use of an antimisting fuel is the need for a practical energy effective degrading device upstream of the engine to provide the necessary processed fuel.

SUMMARY OF CONCLUSIONS

- o Highly degraded antimisting kerosene is necessary for satisfactory operation at reduced fuel temperatures for P&WA current JT8D and JT9D engine components.

- o The antimisting kerosene revealed unexpectedly high sodium levels which could accelerate corrosion of the engine hot section.

- o Filter ratio measurements made on some as-received, undegraded antimisting fuel samples produced high and non-reproducible values.

- The transition velocity method was improved and standardized as the primary degradation measurement technique. Gel Permeation Chromatography, was successfully applied which, together with the transition velocity method, quantified the degradation levels of antimisting kerosene.

- The filter ratio method loses resolution at the higher levels of degradation required for JT8D fuel system components (FR ≤ 2). Transition velocity and Gel Permeation Chromatography are viable tools for monitoring the degradation process and Gel Permeation Chromatography offers the additional benefit of graphically displaying the distribution of apparent molecular weights of degraded fuel. Furthermore, Gel Permeation Chromatography is capable of analyzing gel residue deposited on fuel system components which allows a direct comparison with the original test fuel.

- Thermal stability of antimisting kerosene is at least as good if not better than the parent Jet A.

- Static six month ambient and elevated temperature soak tests made with elastomer seal materials normally employed in gas turbine engine fuel systems resulted in only minor swelling which was within tolerable limits.

- Although a copper corrosion test indicated more reaction with AMK than Jet A, bronze materials in a fuel pump that accumulated more than 100 hours during this test program were not adversely effected by antimisting kerosene.

- Filter clogging occurred from gel formation of the FM-9 polymer from the fuel mixture. At low flow velocities, only the largest polymer species with the highest molecular weights are affected; however, as the fluid velocity is increased progressively, smaller molecular species are brought out of suspension to collect on the filter downstream surface. This results in an exponential increase in clogging rate with increasing flow rate due to the normal distribution of apparent AMK molecular weights after degradation.

- Free water is incompatible with FM-9 AMK and causes destabilization and precipitation of a polymer at the water-fuel interface. The precipitation occurs regardless of the ratio of water to fuel as long as free water is present. The presence of water induced precipitate results in paper filter clogging which is not reversible during the deicing Process.

- Based on the combustor results and fuel injector spray data, AMK degraded to a $V_t \geq 5$ cm/sec should achieve satisfactory combustor performance.

- Although it is technically feasible to operate a JT8D engine with 0.3% FM-9 antimisting additive, commercial engine application is not justified until several problem areas discussed in this report are addressed and subsequently solved.

14.0 CONCLUDING REMARKS

Laboratory and full scale component tests, and analytical projections conducted during the course of this program revealed problem areas requiring additional technology improvement before serious consideration can be given to commercial engine use.

- The AMK evaluated in this program must be improved or an alternative fuel developed with rheological and chemical properties more comparable to Jet A. Specifically, the fuel must be more tolerant to free water, be more easily degraded to minimize the parasitic power loss, and be less susceptible to the formation of velocity induced gelling.

- The effects of storage times and temperatures should be further investigated to better quantify discrepancies in filter ratios between different batches of fuel as well as between the as received samples and the original samples tested at the source of blending.

- A considerable amount of further analytical and experimental work will be required to develop a practical degrader. Efforts should be directed in the following areas:

  - Continue the venturi investigation to obtain continuous area reduction, improved degrader performance, and system durability information.

  - Conduct a design study of a compact venturi/pump combination to determine: volume and location, pintle and pump control requirements, and to investigate the startup and restart capability of the system.

  - Evaluate the ultrasonic generator by reviewing improved designs and conducting demonstration tests of an improved version.

- The impact of the chemical and rheological effects documented during this program with the addition of additives currently approved for use in Jet A (anti-icing, anti-corrosion, bioxide, etc.) must be more fully assessed.

- Filter ratio and transition velocity should be used in conjunction with Gel Permeation Chromatography to completely define the flow characteristics of degraded AMK.

- The formulation of antimisting kerosene with FM-9 additive must be accomplished with at least an order of magnitude reduction in sodium.

REFERENCES

1. Bednarski, J.R., Georgiou, C., "Performance Evaluation of a TF30-P-408 Turbofan Engine Using AM-1 Anti-Misting Fuel Additive in JP-5 at sea level Static Conditions", Naval Air Propulsion Test Center Report NAPTC- PE-111, July 1977.Figure 1 Antimisting Kerosene Program Flow Chart

2. Bird, R.B., Stewart, W.E., and Lightfoot, E.N., Transport Phenomena ; John Wiley & Sons, Inc; New York; 1960.

3. Medani, M.S. and Hayes, K.G., "Heat Transfer to Aviation Fuels", Journal of Eng. Sci., Vol. 4, No. 1, 1978.

4. Baselow, A.M. and Ebert, K.H.: Ultrasonic Degradation of Polymers in Solution. Advances in Polymer Science, 1976.

5. Hammit, F.G.. Cavitation and Multiphase Flow Phonomena. McGraw-Hill. 1980

6. Knapp, R.T., Daily, J.W., and Hammitt, F.G.: Cavitation. McGraw Hill, 197010.1 Fixed Area Vortex Venturi

7. Doulak, M.S., Journal of Applied Polymer Science 22, 1735 (1978)

8. Niezette, J., and Linkens, A., Polymer 19, 939 (1978)

APPENDIX A

Procedure for Determining the Transition Velocity A Measure of AMK Degradation Level (1)

1. Assemble the apparatus shown in Figure A-1. The device is basically a millipore filtration apparatus with a ball valve added between the vacuum flask and the filter support. In addition, the fine wire mesh filter support is replaced with a 16 mesh wire screen.

2. Place a 47 mm diameter, 8 m pore size Nuclepore filter (2) on the support and close the valve to the flask.

3. Add 300 ml of the test fuel to the reservoir. Turn the vacuum pump on and adjust the vacuum level to 2 inches mercury with the valve closed.

4. Simultaneously open the valve and start the timer. Rapidly make any fine adjustment necessary to keep the vacuum at the desired level. Record the time to the nearest tenth of a second for all the fuel to pass through the filter.

5. Using the same filter, repeat steps 3 and 4 at vacuum levels of 3, 4, 10, 15, 17.5, and 20 in Hg vacuum.

6. Prepare a plot of flow rate in cc/sec-cm^2 versus vacuum level. Plot a straight line through the first three points and another straight line through the top three points (3). The flow rate where the two lines intersect should be reported as the transition velocity in cc/sec-cm^2.

7. Replace the filter for each additional fuel tested.

Notes:

(1) This test is not suitable for fuels with filter ratios greater than two. For those fuels the filter ration is an adequate measure of degradation. Solid debris in the fuel will give a biased result.

(2) Nuclepore polycarbonate membrane filters manufactured by Nuclepore Corporation, 7035 Commerce Circle, Pleasanton, CA., 94566, are available from most scientific supply sources.

93) The transition point should occur at a vacuum level of 5 ± 2 in. Hg. Jet A fuel should give a transition velocity of 9 ± 2 cc/sec-cm^2.

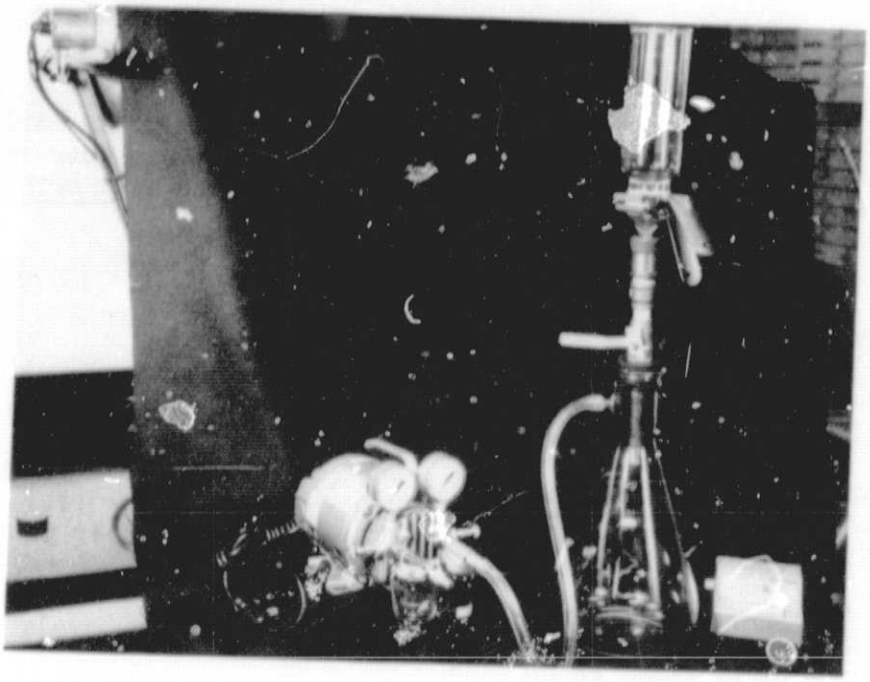

Figure A-1 Transition Velocity Apparatus

APPENDIX B

Determination of Water Content of Antimisting Kerosene (AMK) Fuel

Water was determined in AMK fuel by a semi-automated Karl Fischer titrametric procedure. A coulometric titrameter, the Aqua Test II manufactured by the Photovolt Corporation of New York, N.Y., was used for all water determinations. After conditioning the titrator as described in the instrument operations manual, an aliquot of AMK fuel was added to the titration vessel by hypodermic syringe. The quantity of current required to complete the Karl Fischer reaction with water was recorded directily from the instrument digital readout in total micrograms of water in the injected sample. The instrument was calibrated prior to injecting the sample with injections of pure water. While precision was good for the determination of water in degraded AMK, poor precision resulted from direct injection of undegraded AMK. It was found that precision could be greatly improved by placing the undegraded AMK contained in a closed 50 ml volumetric in a laboratory ultrasonic both for 10 minutes prior to measurement in the Aqua Test II instrument.